CELLULAR STUDIES ON THE ORAL-FACIAL-DIGITAL SYNDROME TYPE 1 DISEASE PROTEIN

Thesis submitted for the degree of

Doctor of Philosophy

at the University of Leicester

by

Carla A. M. Lopes

Department of Biochemistry

University of Leicester

September 2010

DECLARATION

The accompanying thesis submitted for the degree of Doctor of Philosophy, entitled *"Cellular studies on the oral-facial-digital syndrome type 1 disease protein"* is based on work conducted by the author in the Department of Biochemistry at the University of Leicester during the period October 2006 and September 2010. All of the work recorded in this thesis is original unless otherwise acknowledged in the text or by references. None of the work has been submitted for another degree in this or any other University.

Signed:

Date:

Department of Biochemistry
University of Leicester
Lancaster Road
Leicester
LE1 9HN

CELLULAR STUDIES ON THE ORAL-FACIAL-DIGITAL SYNDROME TYPE 1 DISEASE PROTEIN

Carla A. M. Lopes

SUMMARY

Primary cilia were once considered vestigial structures with no obvious function. However, it is now clear that they have important roles in the control of cell proliferation and signalling during development. Indeed, defects in primary cilia are the major cause of many human diseases, collectively known as ciliopathies, that affect diverse organ systems. The growing list of ciliopathies includes oral-facial-digital syndrome type 1, a developmental disorder that features malformations of the face, oral cavity and digits, and is often associated with polycystic kidney disease. The aim of this thesis was to determine the cellular function of OFD1, the protein product of the gene mutated in this disease. Here, we show that OFD1, together with BBS4 and CEP290, proteins encoded by other ciliopathy disease genes, is primarily a component of centriolar satellites, PCM-1-containing particles that surround centrosomes and basal bodies. RNAi depletion experiments reveal that localization of all four of these proteins to centriolar satellites is mutually dependent. Intriguingly, upon satellite dispersal, either through depolymerization of the microtubule network or progression through mitosis, OFD1 and CEP290 remain associated with the centrosome, whereas BBS4 and PCM-1 do not. While others have shown that both CEP290 and BBS4 can physically interact with PCM-1, we show that OFD1 interacts via its fifth coiled-coil motif with the N-terminal coiled-coil domain of PCM-1, and that localization of OFD1 to satellites requires its N-terminal region encompassing the LisH motif. Furthermore, we also show that expression of C-terminal constructs of OFD1 causes mislocalization of PCM-1 and CEP290, while OFD1 and BBS4 functionally synergize in terms of determining organ laterality and body axis integrity in zebrafish. Together, these data highlight centriolar satellites as critical assembly points for proteins implicated in clinically distinct human diseases and that defects in one of these subunits affect the integrity of the whole complex. This work supports a model whereby centriolar satellites play a crucial role in regulating delivery of ciliopathy disease proteins to the basal body and primary cilium, thus extending our understanding as to why such different diseases show considerable phenotypic overlap.

ACKNOWLEDGEMENTS

First and foremost, I would like to thank Prof. Andrew Fry for the opportunity to work on this project. He has made available his support in a number of ways – I cannot express enough how valuable it has been to have the door always open to his guidance, help, and expertise. His enthusiasm and insight into this work over the years have been an inspiration to me.

Thank you to all members of the Fry Lab, past and present, for their help. I would like to especially thank Nav, Joëlle, Dan, Bec, Sam, Jo, Laura, Suzy, Xavier, Magali and Guojie, who not only supported and helped me, but have also become great friends. I also wish to thank Barbara and Liz for all their help and cheerfulness. I take this opportunity to thank Dr. Sue Shackleton, Dr. Raj Patel and Dr. Kayoko Tanaka for their support and encouragement.

I wish to express my gratitude to Prof. Edgar da Cruz e Silva for his guidance and encouragement and for creating the opportunity for me to work on this project. R.I.P.

I am also grateful to Prof. Chris O'Callaghan and Dr. Robert Hirst who very kindly provided me with nasal multiciliated epithelial cells samples; to Prof. Adrian Woolf and Dr. Leila Romio for their collaboration and for carrying out the zebrafish experiments; and to Dr. Suzanna Prosser for performing the centrosome overduplication assay. This thesis would not have been possible without the financial support provided by Fundação para a Ciência e a Tecnologia, Portugal, and the facilities provided by the Department of Biochemistry.

Finally, I wish to thank my family and friends for always being there for me. Gabi, Tiago, António and especially João, I thank you for keeping me sane and happy in Leicester and for being much more than 'acquaintances' in my life. Nav, I thank you for your constant support, encouragement and cheerfulness, and most of all, for being a friend. I could never thank you enough and I am deeply grateful we shared this journey together. Sara, Ana, Ricardo M., Mariana, Ricardo, Manuel, Jorge, Carina, Tânia, Filipe and João, I thank you for your support through every step of the way. Your friendship means the world to me. Thank you to my mum, my dad and my sister. You always inspire me to do my best, and constantly encourage and support me. You are my compass.

Obrigada!

TABLE OF CONTENTS

ABBREVIATIONS

A	absorbance
aa	amino acid
ab	antibody
ADPKD	Autosomal dominant polycystic kidney disease
ALI	air-liquid interface
ALMS	Alström syndrome
ATP	adenosine triphosphate
APS	ammonium persulphate
ARPKD	Autosomal recessive polycystic kidney disease
bp	base pairs
BBS	Bardet-Biedl syndrome
BCA	biciochoic acid
BEGM	Bronchial Epithelial Growth Media
BSA	Bovine Serum Albumin
BCIP	5-bromo-4-chloro-3-indolyl phosphate
C-	carboxy
CC	coiled-coil
Cdk	cyclin-dependent kinase
cDNA	complementary deoxyribonucleic acid
CE	convergent extension
CEP/Cep	centrosomal protein
C-Nap1	centrosomal Nek2-associated protein 1
cm	centimetre
CNS	central nervous system
DMEM	Dulbecco's modified eagle's medium
DMSO	dimethylsulfoxide
DNA	deoxyribonucleic acid
dNTPs	deoxynucleotide triphosphates
DTT	dithiothreitol
EDTA	ethylene diamine tetraacetic acid
EGTA	ethylene glycol tetraacetic acid
FACS	fluorescence activated chromosome sorter

FL	full-length
FBS	foetal bovine serum
GFP	green fluorescent protein
GL2	firefly luciferase
GST	glutathione-S-transferase
HEK293	human embryonic kidney
Hh	Hedgehog
HRP	horseradish peroxidase
hFF	human foreskin fibroblasts
hTERT-RPE1	telomerase-immortalized human retinal pigment epithelial
HU	hydroxyurea
Hz	hertz
IF	immunofluorescence
IFT	Intraflagellar transport
IMCD3	renal inner medullary collecting duct
IPTG	β-D-isopropyl-thiogalactopyranoside
JATD	Jeune asphyxiating thoracid syndrome
JBTS	Joubert syndrome
kDa	kilo Daltons
LB	Luria Bertani
LCA	Leber congenital amaurosis
LisH	Lissencephaly-1 homology
LMB	Leptomycin-B
mRNA	messenger ribonucleic acid
ml	millilitre
mg	milligram
MKS	Meckel-Gruber syndrome
mM	millimolar
MT	microtubule
MTOC	microtubule organizing center
min	minutes
N-	amino
NBT	nitroblue tetrazolium
Nek	NIMA-related kinase
NIMA	never in mitosis A

ng	nanogram
nM	nanomolar
NP-40	nonidet P-40
NPHP	Nephronophthisis
OD	optical density
OFD1	oral-facial-digital syndrome type 1
Pen/Strep	penicillin/streptomycin
PBS	phosphate buffered saline
PC1	polycystin 1
PC2	polycystin 2
PCD	Primary cilia dyskinesia
PCP	planar cell polarity
PCR	polymerase chain reaction
PCM	pericentriolar material
PCM-1	pericentriolar material protein 1
PDGFRα	Platelet-derived growth factor receptor α
PMSF	phenylmethylsulphonyl fluoride
PKD	Polycystic kidney disease
Ptc	Patched
rpm	revolutions per minute
RNA	ribonucleic acid
RNAi	ribonucleic acid interference
dsRNA	double stranded ribonucleic acid
siRNA	small interfering ribonucleic acid interference
RP	Retinitis pigmentosa
RPGR	Retinitis pigmentosa GTPase regulator
RPTEC	Renal proximal tubule epithelial cells
SDS	sodium dodecyl sulphate
SDS-PAGE	sodium dodecyl sulphate polyacrylamide gel electrophoresis
sec	seconds
SGBS2	Simpson-Golabi-Behmel syndrome type 2
Smo	Smoothened
SNLS	Senior-Løken syndrome
Shh	Sonic hedgehog
TEMED	N, N, N, N,-tetramethylethyleneediamine

TBS	tris-buffered saline
Tris	Tris (hydroxymethyl) aminomethane
U	unit
U2OS	human osteosarcoma
µg	micrograms
µM	micromolar
µl	microlitre
UV	Ultraviolet
V	Volts
v/v	volume per volume ratio
w/v	weight per volume ratio
WT	wild-type

TABLE OF FIGURES

CHAPTER 1

INTRODUCTION

CHAPTER 1 INTRODUCTION

1.1 CILIA: ORGANIZATION AND GENERATION

Cilia are tiny hair-like projections that extend from the cell surface into the extracellular space. These evolutionary conserved organelles can be found on most eukaryotic cells, with the exception of higher plants and fungi (Baker & Beales 2009; Bloodgood 2010). Although the biological function of cilia in cell motility and fluid transport, and its roles in sight, smell and mechanosensation have long been recognized, recent discoveries have revealed that cilia also have crucial roles in cell signalling pathways (Singla & Reiter 2006; Marshall & Nonaka 2006). Furthermore, the discovery that defects in the formation or function of these antennae-like projections lead to a wide range of human disorders has led to renewed and explosive interest in cilia. In this section, I aim to provide a general introduction to the cell biology of cilia.

1.1.1 Structure and classification of cilia

Structurally, the cilium is a projection from the cell surface that contains a microtubule-based cytoskeleton, the axoneme, covered by a specialized membrane, which is both structurally and functionally distinct from the cell membrane (Figure 1.1A). This is made possible by the presence of a selective barrier at the base of the cilium, which is known as the ciliary necklace or transition zone. At the distal end of the cilium is a cap structure that links the axonemal microtubules to the ciliary membrane and is the major site of ciliary subunit addition and subtraction (Marshall & Nonaka 2006; Bisgrove & Yost 2006; Satir & Christensen 2007). The axoneme is a highly organized structure of nine peripheral microtubule doublets arranged around a central core that may or may not contain a pair of singlet microtubules (9+2 or 9+0 axoneme, respectively), and serves as scaffolding to organize associated protein complexes and as binding sites for microtubule-based molecular motors. The axonemal doublet microtubules polymerize from $\alpha\beta$ tubulin heterodimers and are connected by filaments of a protein called nexin. They initiate

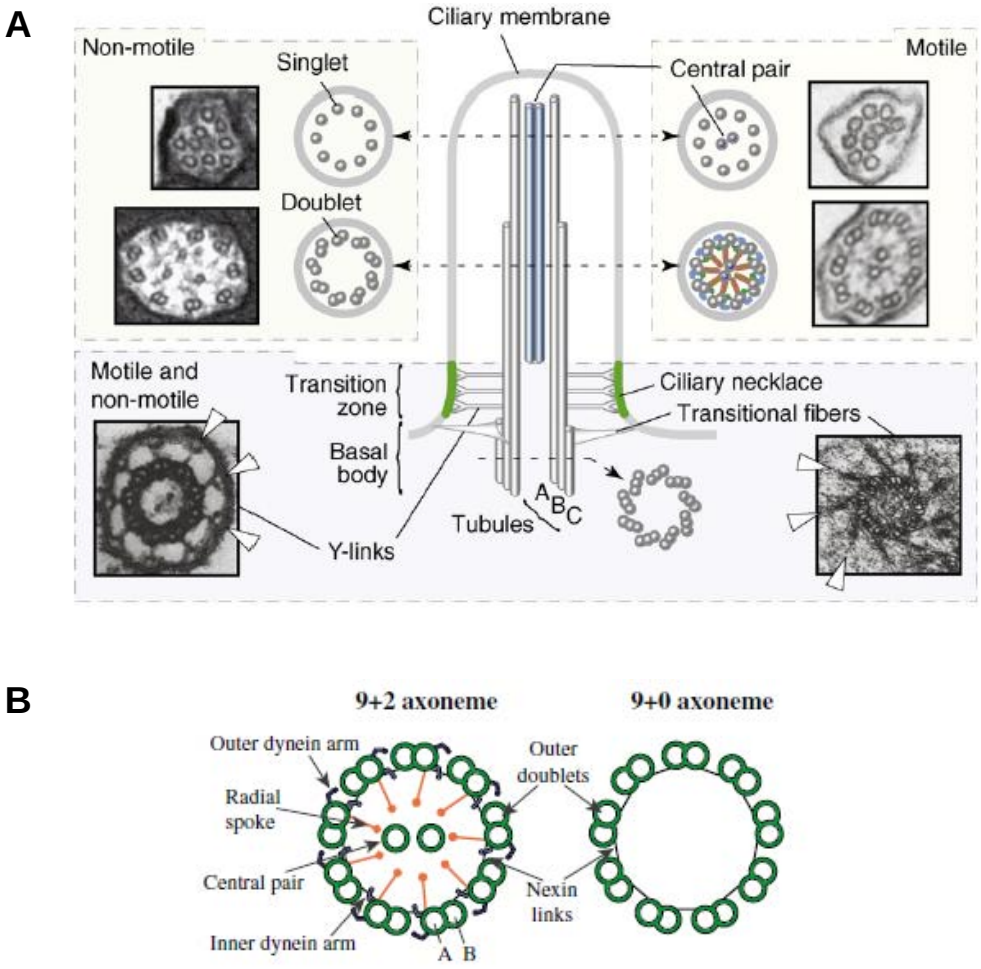

Figure 1.1 General structure of cilia

(A) The basal body, which is built from triplet microtubules, labelled A, B and C, nucleate the axonemal microtubules which extend from microtubules A and B. Transitional fibers, which emanate from the distal end of the basal body and contact the ciliary membrane, are shown schematically and in a transmission electron micrograph (TEM) cross-section of an *Elliptio* (mussel) cilium. Just above, the transition zone region is characterized by Y-shaped links that emanate from the microtubule axoneme and also contact the membrane. These are shown schematically and in a TEM cross-section of a monkey oviduct cilium. Some transitional fibers and Y-links are shown by arrowheads in the TEM micrographs. Microtubule axonemal doublets are depicted with or without central pair microtubules. Representative cross-section TEM micrographs from non-motile (*C. elegans*) or motile (*Tetrahymena*) cilia are also shown on the left and right, respectively. **(B)** Schematic of a transverse section through the motile 9+2 axoneme and the immotile 9+0 axoneme with the structures typically found in non-motile, motile or both cilia types are indicated. This figure is adapted from Silverman et al. (2008) and Dawe et al. (2007).

at the transition zone, extending from the A and B tubules of the triplet microtubules of the basal body. In addition, the distal end of the transition zone is where the central pair microtubules of 9+2 cilia are nucleated (Figure 1.1B) (Marshall & Nonaka 2006; Satir & Christensen 2007). Microtubules from ciliary axonemes are highly stable and show several types of post-translational modifications on α- and β-tubulin, notably acetylation and polyglutamylation (Hagiwara et al. 2004; Hoyer-Fender 2010).

Distinct from bacterial flagella, eukaryotic flagella and cilia are ultrastructurally similar structures and these two terms are often used interchangeably. However, the term cilia was originally used when a cell had numerous relatively short ciliary structures that serve for the transport of fluids (e.g. transport of mucus in the trachea), or for locomotion in an aqueous environment (e.g. Paramecium), whereas the term flagella was applied to the tail-like, usually single, and long structure that serve for propulsion of single cells (e.g. swimming of protozoa and spermatozoa) (Marshall & Nonaka 2006; Bloodgood 2010). Thus, cilia were originally defined by their motility and, for a long time, this was thought to be the only function of these organelles. Over a century ago, Zimmermann (1898) described a class of non-motile, solitary cilia in mammalian cells and suggested a sensory function for them. Yet, these ubiquitous and evolutionary conserved organelles were long considered rudimentary, a vestigial remnant of its motile counterpart, and were overlooked until recently, when a series of studies demonstrated their sensory role and their clinical relevance (Cardenas-Rodriguez & Badano 2009; Baker & Beales 2009; Bloodgood 2010).

Cilia have been classified in two main types according to their ultrastructure and their capacity to move: motile cilia with a 9+2 axoneme, and immotile/primary cilia with a 9+0 axoneme. A third class of motile cilia with a 9+0 axoneme known as nodal cilia, and a fourth class of immotile 9+2 cilia, the kinocilium, have also been described.

1.1.1.1 Motile Cilia

Motile cilia have been the most studied of all cilia and are generally found on the epithelial cells of the trachea, ependymal cells in ventricles of the brain, and on cells lining the oviduct and epididymis of the reproductive tracts. Normally concentrated in large numbers on the apical cell surface, motile cilia beat in an orchestrated wave-like fashion and are involved in fluid and cell movement such as mucociliary clearance in the lung, cerebrospinal fluid movement in the brain, and ovum and sperm transport along the respective reproductive tracts (Figure 1.2A) (Satir & Christensen 2007; Baker & Beales 2009).

These ~10-15 µm-long cilia are constructed on what is referred to as a 9+2 microtubule pattern, where nine sets of doublet microtubules arranged in nine-fold symmetry surround a central pair of singlet microtubules. The axoneme provides a structure on which mechanical movement is generated. The characteristic rhythmic beating of motile cilia is created by the exquisite coordination of the action of key protein complexes that attach to the outer doublet microtubules. Radial spokes project from each outer doublet toward the central pair which is itself enclosed in a sheath of proteins that form projections that interact with each of the spoke heads. Inner and outer dynein arms, motor complexes found on the peripheral doublet microtubules, provide the ATP-hydrolysis-driven mechanical movement that causes adjacent microtubule doublets to slide past each other (Marshall & Nonaka 2006; Satir & Christensen 2007; Baker & Beales 2009; Lindemann & Lesich 2010; Roy 2009). This sliding is converted to bending through the restraining action of the inter-doublet nexin links, and is coordinated by the interaction between the radial spokes and the central-pair projections, with an effective stroke and a recovery stroke. In mammalian motile cilia, the orientation of the effective stroke is fixed, and the central pair sits perpendicular to that direction. Because the inner and outer dynein arms are unidirectional vectorial force producers, the direction of the sliding is uniform around the axoneme, effectively resulting in its division into two operational halves.

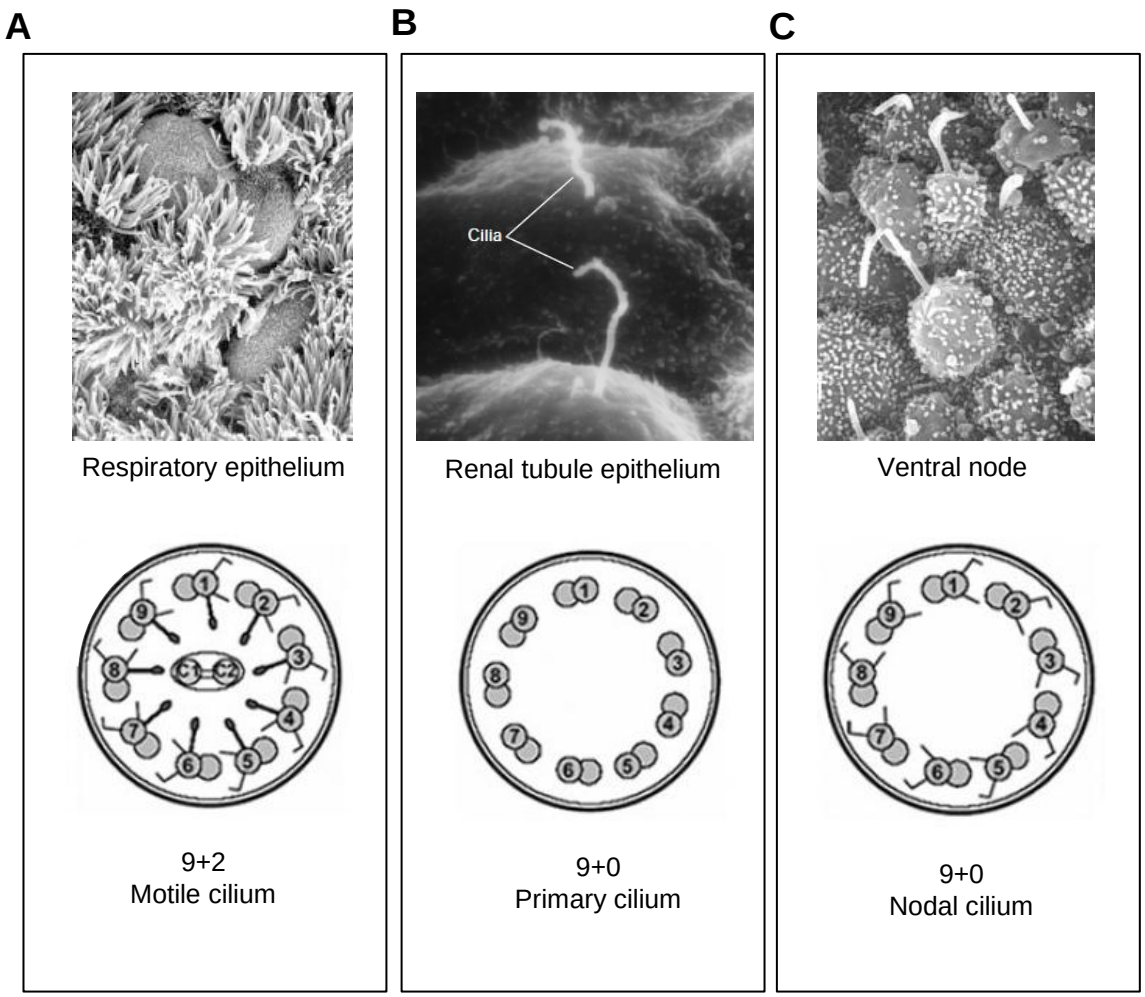

Figure 1.2 Types of Cilia
Images and schematic representation demonstrating cilia and ciliary axoneme diversity, respectively. **(A)** Scanning electron microscopy of respiratory cilia showing that there are multiple cilia per cell. The non-ciliated cells in this image are mucus-secreting goblet cells. Cross-section of the 9+2 motile cilium. **(B)** Scanning electron micrograph of primary cilium located on the apical surface of the renal tubule epithelium. Cross-section of the 9+0 immotile primary cilium. **(B)** Scanning electron micrograph of nodal cilia. Cross-section of the 9+0 motile nodal cilium. This figure is adapted from Zhang et al. (2005), Eley et al. (2005) and Leigh et al. (2009).

When active, the dyneins on one side of the axoneme are responsible for the generation of the effective stroke, while the dyneins on the opposite side generate the recovery stroke. When groups of cilia become activated, they stimulate adjacent cilia, initiating metachronal waves that travel along the epithelium (Satir & Christensen 2007; Lindemann & Lesich 2010). Most mammalian ciliary beat frequencies range from 10-20 Hz. In fact, the efficient mucus clearance from the upper and lower respiratory tract is a major component of our defensive mechanisms against respiratory pathogens, toxins, and particulate matter, and it relies on the coordinate beating of cilia with a normal beat pattern and frequency. Infections, toxins and genetic disorders such as primary ciliary dyskinesia and cystic fibrosis, can disrupt these defences result in reduced or absent mucus clearance from the lungs, leading to susceptibility to chronic recurrent respiratory infections (Chilvers & O'Callaghan 2000; Satir & Christensen 2007; Stannard et al. 2010).

1.1.1.2 Primary cilia

The primary cilium is a ~3-10 µm-long solitary, non-motile, highly conserved sensory organelle found on most vertebrate cells. The term 'primary cilia' was first applied to the initial single cilium (thus called 'primary') that precedes the formation of large numbers of additional cilia (called 'secondary') during differentiation in airway epithelial cells. By analogy, the single cilium observed on most cells of the body is now generally called primary cilium (Marshall & Nonaka 2006).

Primary cilia were long dismissed as unimportant because they do not show the typical wave motion and they lack several structural features characteristic of motile cilia and flagella. Unlike motile cilia, primary cilia have a 9+0 axonemal structure, lacking the central pair of microtubules and the dynein arms normally associated with the axonemal outer doublets (Figure 1.2B). Therefore, like defective motile cilia that lack these structures, they do not actively beat. However, they do retain receptors and channels on its specialized ciliary membrane, comparable with and sometimes identical to those found in motile cilia. Thus, cilia, in particular primary

cilia, are predominantly sensory organelles (Marshall & Nonaka 2006; Satir & Christensen 2007; Bloodgood 2010). The best known examples are those of the specialized primary cilia in the retina and olfactory neuron. Our ability to see and smell depend, respectively, on the continuous transport of new protein through the connecting cilium required by the fast turnover of the photoreceptors, and on the odorant receptors localized on cilia extending from the sensory neuron dendritic knob (Figure 1.3 A and B) (Singla & Reiter 2006; Jenkins et al. 2009).

Because they protrude from the cell surface, primary cilia act as antennae sensing a wide variety of extracellular signaling molecules that otherwise may not be detected by receptors sitting on the cell membrane. Moreover, the high surface to volume ratio of the cilium allows a more effective concentration of receptors and signaling components, making the primary cilium an ideal compartment to convert environmental cues into signaling cascades that are initiated within the cilium and then transduced into the rest of the cell. In addition to their roles as chemical and osmotic sensors, primary cilia also play important roles as mechanosensors, as is the case for renal primary cilia that detect fluid flow through the lumen of the tubule (Zhang et al. 2004; Marshall & Nonaka 2006; Fliegauf et al. 2007; Baker & Beales 2009).

1.1.1.3 Nodal and kinocilia

Nodal cilia, like primary cilia, are solitary organelles with 9+0 microtubule architecture. However, as they possess unique outer dynein arm isoforms, they are able to move in a propeller-like fashion. These cilia are localized to the ventral side of the ‘node’, a transient midline structure formed during embryonic gastrulation, and their posterior tilt and clockwise rotation generate a nodal flow, an autonomous symmetry-breaking process (Figure 1.2C). Indeed, mutations that disrupt nodal cilia in mice indicate that they play essential roles in establishing signalling events required for specification of the left-right body axis in mammals (Hirokawa et al. 2006; Satir & Christensen 2007; Fliegauf et al. 2007; Hashimoto et al. 2010). Two

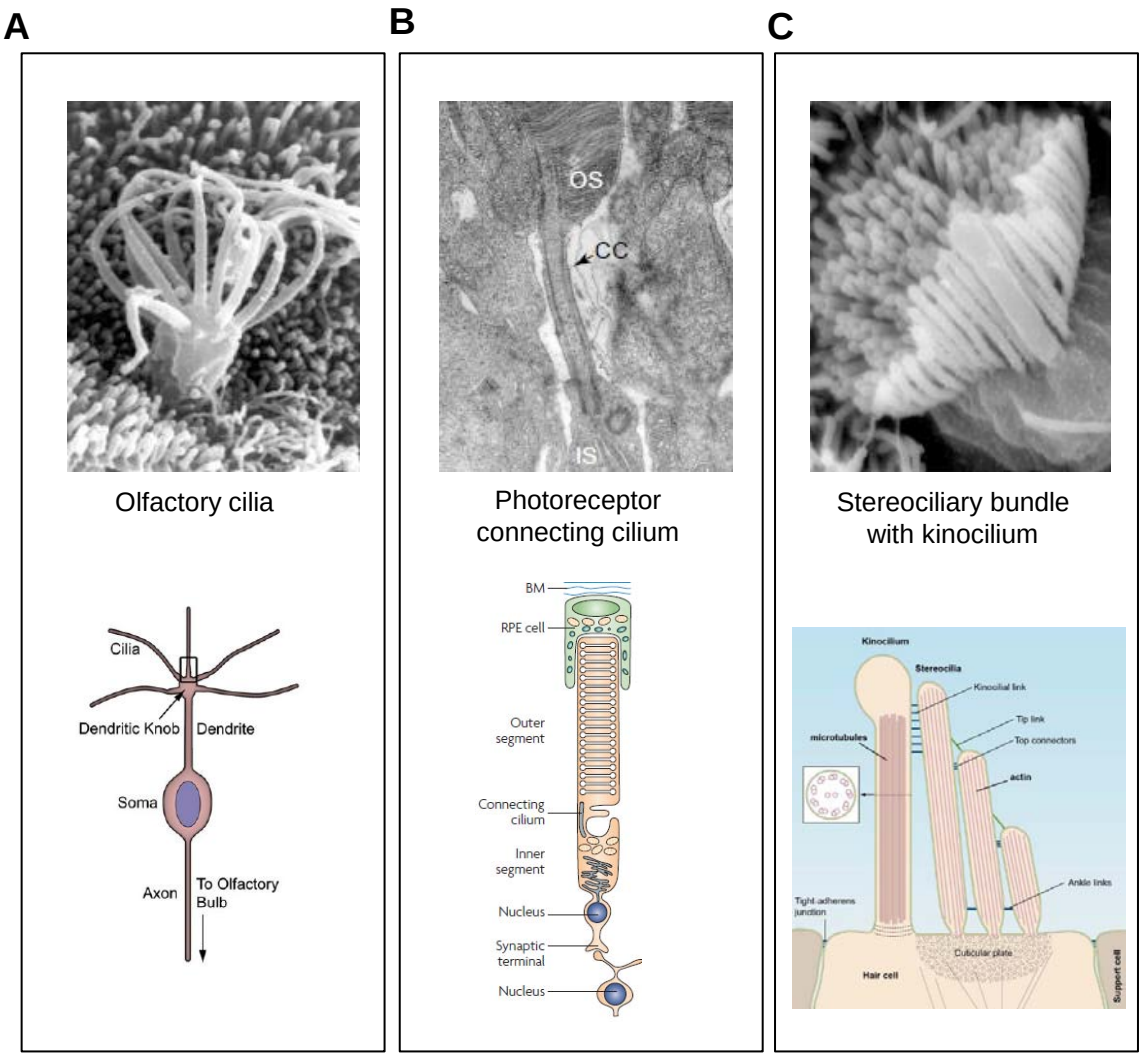

Figure 1.3 Sensory Cilia
(A) Scanning electron micrograph of olfactory cilia. Diagram of a single olfactory sensory neuron. **(B)** Transmission electron micrograph of the longitudinal section through the connecting cilium of a mouse rod photoreceptor cell. CC, connecting cilium; IS, inner segment; OS, outer segment. Diagram of the photoreceptor cell and its substructures. The outer segment, an elaborate array of membrane discs in which light detection takes place, is connected to the photoreceptor cell by a connecting cilium. The light detecting protein machinery must pass through the connecting cilium on its way to the outer segment. **(C)** Scanning electron micrograph stereociliary bundle with kinocilium. Cross-section through a hair bundle and apical hair cell surface indicating the kinocilium, stereocilia, and cuticular plate. Some of the linkages in hair bundles are highlighted. This figure is adapted from Eley et al. (2005), Jenkins et al. (2009), Fliegauf (2007) and Schwander et al. (2010).

models have been proposed for how the nodal flow might contribute to the determination of left-right asymmetry. One model predicts that nodal flow generated by motile cilia is sensed by non-motile mechanosensory cilia. The second model predicts that nodal flow results in a leftward gradient of morphogens produced in membrane parcels in the node. Both models reported an asymmetric Ca^{2+} release that is thought to be involved in the subsequent events of asymmetric expression of signalling molecules and transcription factors (Fliegauf et al. 2007; Satir & Christensen 2008).

In vertebrates, hearing and balance require sensory hair cells in the inner ear. These are specialized mechanosensory cells that carry at their apical surface a staircase array of 50-200 actin-based modified microvilli, stereocilia, that are densely packed to form a bundle, and a single true tubulin-based cilium, the kinocilium (Fliegauf et al. 2007; Nayak et al. 2007; Müller 2009). Although its specific axonemal structure had been a matter of some debate, it is suggested that mature kinocilia have a 9+2 arrangement, while immature cilia have the 9+0 (Dabdoub & Kelley 2005). The stereocilia bundle is highly organized to form a polarized staircase of decreasing height. The kinocilium is located adjacent to, and central with respect to, the tallest row, and in some hair cells, it degenerates once the hair bundle has matured. Hence, it has been suggested that this specialized cilium, though not required for mechanotransduction, is likely important for bundle development and polarity (Figure 1.3C) (Nayak et al. 2007; Müller 2009).

1.1.2 Centrosomes and Cilia organization

All cilia are assembled as an extension of a basal body, a structure derived from the older centriole of the centrosome. Centrioles are therefore the defining unit of both centrosomes and basal bodies. However, despite similarities in overall organisation, centrioles and basal bodies differ in their subcellular localization and functions.

1.1.2.1 Centrosome structure and function

The term ‘centrosome’ was postulated by Theodor Boveri in 1888 to describe a ‘single extremely minute body, or more commonly a pair of bodies, staining intensely with haematoxylin and surrounded by a cytoplasmic radiating aster’. Since the poles that define the bipolar nature of the spindle each contain a centrosome, this organelle was initially coined the ‘especial organ of cell division’. More than a century of research has revealed that the centrosome functions as the major microtubule organizing centre (MTOC) in the animal cell throughout the cell cycle, thus having a key role in numerous cellular functions, including cell motility, adhesion, polarity, maintenance of cell shape, progression through the cell cycle, cell division, transport of vesicles and targeting of many signalling molecules (Bettencourt-Dias & Glover 2007; Lüders & Stearns 2007; Moser et al. 2009; Debec et al. 2010).

Centrosomes are relatively small (1 μm in diameter) but complex non-membranous organelles found in the cytoplasm, usually in the proximity of the nucleus. A centrosome comprises a pair of centrioles that are surrounded by an electron-dense matrix called the pericentriolar material (PCM). The centriole is a very stable and complex structure consisting of a symmetrical barrel-shaped cylinder of nine triplet microtubules, is ~0.5 μm in length and 0.2 μm in diameter, and is polarized along the proximo-distal axis. The two centrioles within a centrosome are held together by linkers, and differ from one another in that one of them, the older or mother centriole, has two sets of nine appendages, subdistal and distal appendages close to its distal end. Moreover, only the mother centriole can anchor microtubules through its subdistal appendages (Figure 1.4) (Bettencourt-Dias & Glover 2007; Schatten 2008; Debec et al. 2010). Increasing evidence indicates that the PCM is a scaffold for anchoring of over 100 proteins, including components required for microtubule nucleation, notably γ-tubulin, and for the organization of multiprotein complexes involved in pathways for cellular regulation (Doxsey 2001; Nigg 2007). Lacking a clear boundary, such as membrane, with the cytoplasm, the extent of the

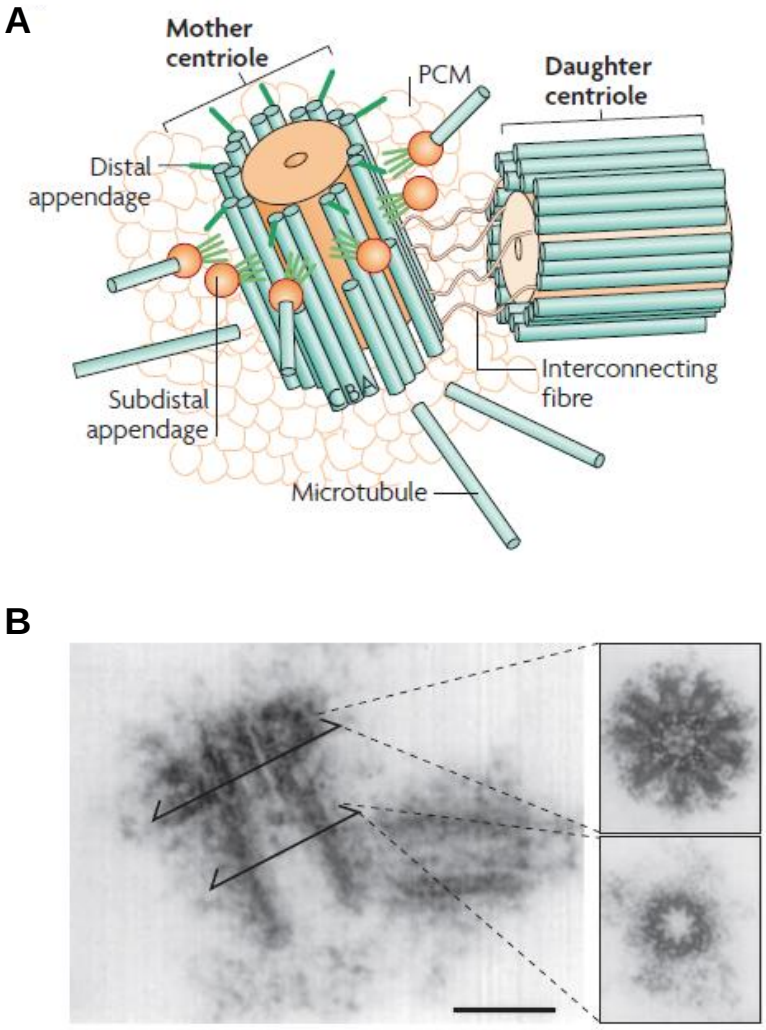

Figure 1.4 Centrosome structure
(A) Schematic representation of the centrosome. In each triplet, the most internal tubule is called the A-tubule; the one following it is the B-tubule; and this is followed by the most external one, the C-tubule. At its distal end, the centriole consists of doublets. **(B)** Electron micrograph of the centrosome. The top inset indicates a cross-section of subdistal appendages; the bottom inset indicates a cross-section of the proximal part of the centriole. Note the triplet microtubules (MTs). Scale bar, 0.2 µm. This figure is adapted from Bettencourt-Dias & Glover (2007).

PCM, and thus the extent of the centrosome, is difficult to establish. As a result, the PCM is a dynamic region and many components transit to and from the centrosome via microtubules or by diffusion, and the centrosome's architecture is maintained through specific protein-protein interactions. Many proteins may use the centrosome as a structural platform to enhance the efficiency of reactions that are crucial for cell-cycle progression or as a way to increase local protein concentration. As a result, some proteins appear only at a particular time and then leave the centrosome or are degraded. Most centrosomal components are in relatively low abundance and it is likely that active mechanisms ensure their delivery to the centrosome at the correct rate and time. The amount of PCM also changes with the cell cycle (Urbani & Stearns 1999; Schatten 2008).

1.1.2.2 Centrosome duplication and the cell cycle

The centrosome undergoes remarkable changes in its organization during the cell cycle. To organize an effective bipolar mitotic spindle, a centrosome must duplicate once per cell cycle. This semi-conservative duplication, with each new centrosome receiving one old centriole and one new centriole, is traditionally subdivided into discrete steps, notably centriole disengagement, centriole duplication, centrosome disjunction and centrosome separation (Bettencourt-Dias & Glover 2007; Nigg 2007; Nigg & Raff 2009). At late G_1/S-phase of the cell cycle, a new centriole (procentriole) forms at the proximal end of each parental centriole at an orthogonal angle, establishing a tight 'base-to-base' linker between parental and progeny centrioles. The two procentrioles then elongate throughout the remainder of S and G_2 phases, until they reach their full length in late G_2. At this stage, the younger of the two parental centrioles acquires distal and subdistal appendages thereby reaching full maturity. At the G_2/M transition, the two centrosomes recruit numerous proteins in preparation for mitosis and lose physical adhesion in processes termed centrosome maturation and disjunction, respectively (Bettencourt-Dias & Glover 2007; Schatten 2008; Nigg & Raff 2009; Debec et al. 2010). Microtubule-based motor proteins then drive the spatial separation of the two centrosomes, each one migrating to one of

the poles of the spindle. Upon exit from M phase, or during early G_1, the tight link between the two centrioles, and therefore their orthogonal configuration, is lost in a process referred to as centriole disengagement. Subsequently, the disengaged centrioles become connected by a 'base-to-base' highly dynamic structure composed of centrosome cohesion proteins, including C-Nap1 and rootletin. Centriole disengagement is thought to be a prerequisite for a new round of duplication (Piel et al. 2000; Nigg & Raff 2009). At the end of mitosis, each of the two resulting daughter cells has a single centrosome containing two centrioles: one newly formed centriole in the previous cycle, and an older centriole generated at least two cycles prior (Figure 1.5) (Nigg 2007; Nigg & Raff 2009).

In normal divisions, the centrosome cycle is coupled with the replication and the chromosomal DNA, and the fidelity and timing of these events is critical. Uncoupling of these events can result in the formation of monopolar or multipolar spindles, with terrible consequences for the accuracy of chromosome segregation. Accordingly, centrosome abnormalities have long been related to aneuploidy and are linked to cell cycle misregulation and the development of cancer. Therefore, in addition to its regular function as an MTOC, the centrosome orchestrates several major cell cycle events including entry into mitosis, anaphase onset, cytokinesis, G_1/S transition, and monitoring of DNA damage (Badano et al. 2005; Nigg 2007; Schatten 2008; Zyss & Gergely 2009).

1.1.2.3 Centrioles and basal bodies

At specific cell cycle or developmental stages, the mother centriole migrates to the cell surface and becomes a basal body nucleating the microtubules that form the primary cilium. In multiciliated epithelia, ciliogenesis begins with the generation of several hundred basal bodies that migrate to the apical cell surface, and acquire accessory structures to dock to the cell membrane. Once a centriole has docked with the cell membrane, it is known as a basal body (Bettencourt-Dias & Glover 2007; Dawe et al. 2007; Debec et al. 2010).

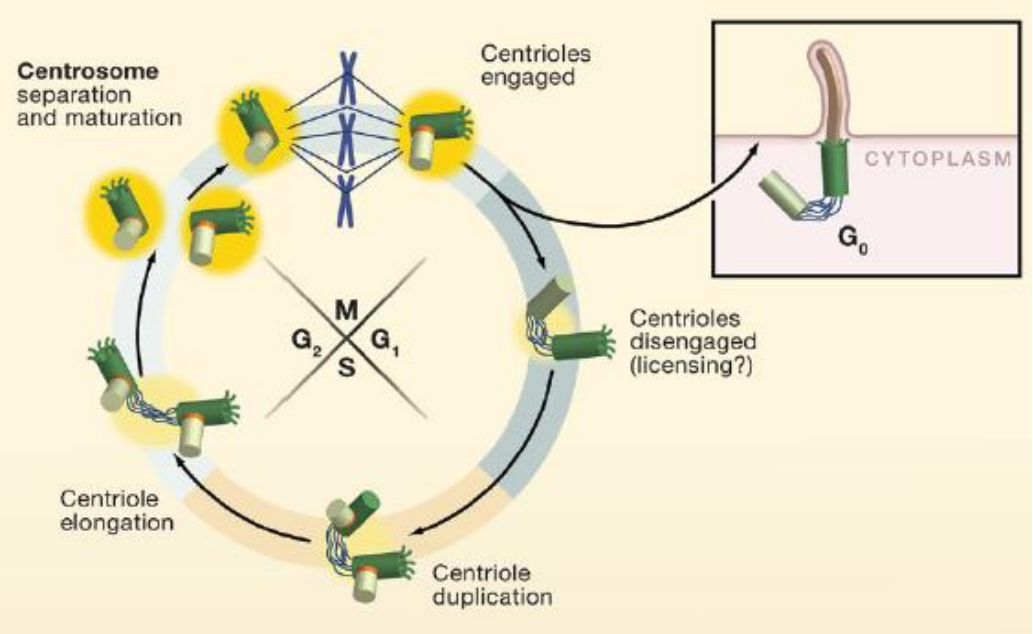

Figure 1.5 Centrosome duplication and the cell cycle
Schematic representation of centriole behavior during the cell cycle. At the end of mitosis each new daughter cell inherits a single pair of 'disengaged' centrioles. Cells then progress into G_1-phase or enter a quiescent state (G_0), during which the cell may form a cilium. In cycling cells the centrioles duplicate in S-phase, with newly born procentrioles (light green) remaining tightly engaged with their mother centrioles (dark green) in an orthogonal arrangement and gradually elongating throughout S- and G_2-phase. At the G_2/M transition, the centrioles accumulate more pericentriolar material (PCM, yellow) and the two centrosomes start to separate from one another, eventually forming the poles of the spindle in mitosis. This figure is adapted from Nigg & Raff (2009).

The structure of the centriole and the basal body is remarkably conserved in eukaryotes, either as centrioles within a centrosome and/or a basal body tethered to the membrane, and, in most studied organisms, the centriole/basal body comprises microtubule triplets that display nine-fold symmetry. In vertebrates, only the mature mother centriole can nucleate primary cilia, whereas the daughter centriole becomes competent for ciliary assembly only in the following cell cycle. Thus, the maturation process takes 1.5 cell cycles, and is characterized by the acquisition of appendages and new proteins. This specific subset of features harboured by the mother centriole is therefore important for ciliogenesis (Bettencourt-Dias & Glover 2007; Dawe et al. 2007; Hoyer-Fender 2010; Carvalho-Santos et al. 2010). Moreover, the distal end of the mother centriole is not associated with proteins that are found at other surfaces of this structure or the PCM. It has been suggested that this difference is an accommodation to ciliogenesis, allowing the formation of a cilium without perturbing PCM organization or function, and containing proteins essential for the initiation of ciliogenesis (Moser et al. 2009). The basal body of a primary cilium remains associated with its daughter centriole through filamentous bundles, called the striated connector. Basal bodies acquire additional accessory structures including transitional fibers, basal feet, and striated rootlets (Hagiwara et al. 2004; Dawe et al. 2007; Hoyer-Fender 2010; Debec et al. 2010).

1.1.3 Pathways of Ciliogenesis

Together, cilia and basal bodies with their associated structures are called the ciliary apparatus, and its formation is known as ciliogenesis. There are several mechanisms of ciliogenesis, enabling the formation of different types of cilia or flagella that can be transient or permanent. Nevertheless, electron microscopy studies of ciliogenesis in cells from a variety of sources have shown that despite some variations, the course of ciliogenesis is similar among different animals. Thus, it can be generally subdivided in four stages: generation of centrioles, migration of centrioles, formation of the basal-body associated structures, and elongation of cilia. Most differences between ciliogenesis of a primary cilium and the multiple cilia of

multiciliated epithelia are observed in the centriole generation stage. Whereas the primary cilium is extended from a pre-existing mature centriole, the generation of several hundred cilia in epithelial cells requires the formation of hundreds of centrioles (Figure 1.6A) (Hagiwara et al. 2004; Dawe et al. 2007; Hoyer-Fender 2010).

1.1.3.1 Centriole production: duplication and multiplication

Basal bodies are attached to the cell membrane and provide a nine-fold symmetric template from which the ciliary axoneme extends. A primary cilium can be assembled in quiescent somatic cells or in interphase in proliferating cells that make a primary cilium in G_1-phase. At such specific stages or developmental cycles, the mature centriole of the pair that makes up the centrosome migrates to the cell surface and is converted into a basal body. The assembly of a primary cilium is therefore tightly coupled to the cell cycle. Centrioles that are converted into a basal body to form a primary cilium are generated through the semi-conservative centriole duplication cycle, where pre-existing centrioles functions as templates for the formation of one daughter centriole each (Bettencourt-Dias & Glover 2007; Dawe et al. 2007).

Terminally differentiated multiciliated epithelial cells, such as those in vertebrate respiratory and reproductive tracts, can have 200-300 cilia per cell. The generation of the multiple centrioles required for the assembly of each of these cilia can be achieved by either using the pre-existing centriole as a template, the centriolar pathway, or via a non-templated method where centrioles are produced de novo, the acentriolar pathway. In contrast to the centriole duplication during the cell cycle, these pathways where multiple procentrioles are produced simultaneously are linked with differentiation, rather than proliferation (Hagiwara et al. 2004; Dawe et al. 2007). In the centriolar pathway, new centrioles are produced around an existing centriole. Unlike cell-cycle-dependent centriole duplication, where only one daughter centriole buds from the lateral side of each mother centriole, as many as ten

A

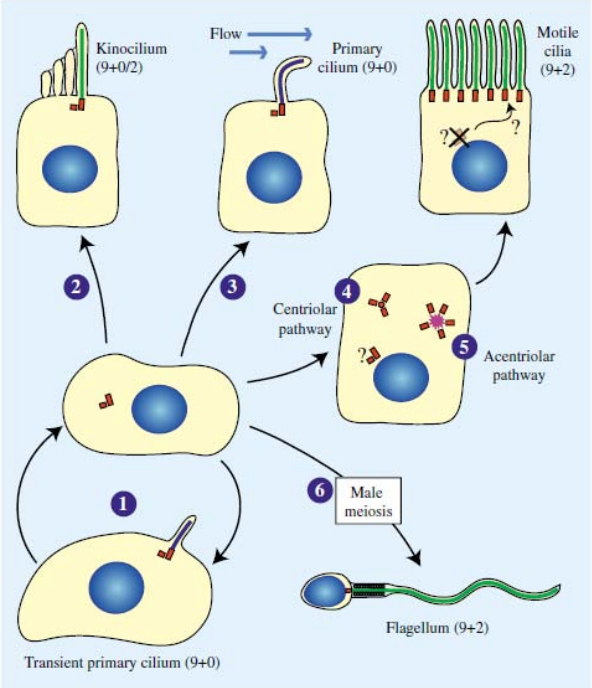

B

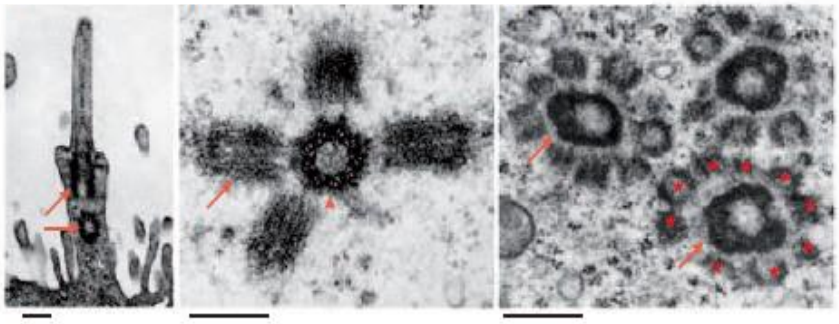

Figure 1.6 Pathways of Ciliogenesis

(A) Diagram representing multiple pathways of ciliogenesis. Quiescent somatic cells use a single pre-existing mature centriole to subtend a transient primary cilium (1) lacking central pair microtubules, which is lost as the cell re-enters the cell cycle. In differentiated cells, single cilia can be produced from a mature centriole, such as the temporary (9+2 or 9+0) kinocilium (2), or the primary (9+0) cilium produced on the luminal epithelium of kidney tubules (3). Epithelial cells in the mammalian airway have several hundred cilia. Here, hundreds of centrioles are produced, either using the pre-existing centriole as a template (4), or formed via a non-templated method (5). The sperm flagellum produced in male meiosis is depicted at 6. Green denotes 9+2 axonemes; dark blue denotes 9+0 axonemes; centrioles are shown in red; the deuterosome is shown in purple. **(B)** Electron micrographs showing the formation of cilia in a monkey oviduct. Left hand panel: note the two basal bodies at the base of the cilia (red arrows). Middle panel: nearly mature basal bodies (arrow) associate with a centriole (arrowhead). Right hand panel: three deuterosomes (red arrow) with several nascent centrioles (asterisks). Scale bars, 0.25 µm. This figure is adapted from Dawe et al. (2007) and Bettencourt-Dias & Glover (2007).

centrioles can develop simultaneously around a single centriole during ciliogenesis, with the daughter centrioles being released into the cytoplasm to mature. In the acentriolar pathway, the major pathway for centriole production, centrioles form around intermediary structures rather than an existing centriole (Hagiwara et al. 2004; Bettencourt-Dias & Glover 2007; Dawe et al. 2007). Fibrous granules are the first recognizable structures in this pathway. They are 70-100 nm structures that appear first in low numbers, but then increase in number and finally form aggregates. The detection of PCM-1 (pericentriolar material protein 1), a known centriolar satellite protein, in fibrous granules indicated that they are equivalent structures to those electron-dense centriolar satellites scattered around the centrosome in proliferating mammalian cells (Kubo et al. 1999; Hagiwara et al. 2004). In the next step, large globular bodies called deuterosomes appear in the area of the fibrous granule aggregates and, although PCM-1 was not detected to localize to deuterosomes, it is thought that these might be the result of the aggregation and clustering of fibrous granules. Deuterosomes then serve as organizing centres for the formation of new centrioles. The number of procentrioles around a deuterosome correlates with its size (Figure 1.6B) (Hagiwara et al. 2004; Bettencourt-Dias & Glover 2007; Dawe et al. 2007).

1.1.3.2 Centriole morphogenesis: basal body generation

Once formed, centrioles migrate to the cell surface, acquire accessory structures, and attach to the cell membrane, thus converting into basal bodies for ciliary elongation. Ultrastructural analysis has revealed alar sheets/transitional fibres, striated rootlets and basal feet as accessory structures associated both with primary cilia and multiciliated epithelia (Figure 1.7A) (Hagiwara et al. 2004; Dawe et al. 2007).

Basal bodies dock to the cell membrane via alar sheets, also known as transitional fibres because the attachment point of the membrane likely corresponds to the region known as the ciliary necklace, the proposed barrier between the ciliary

A

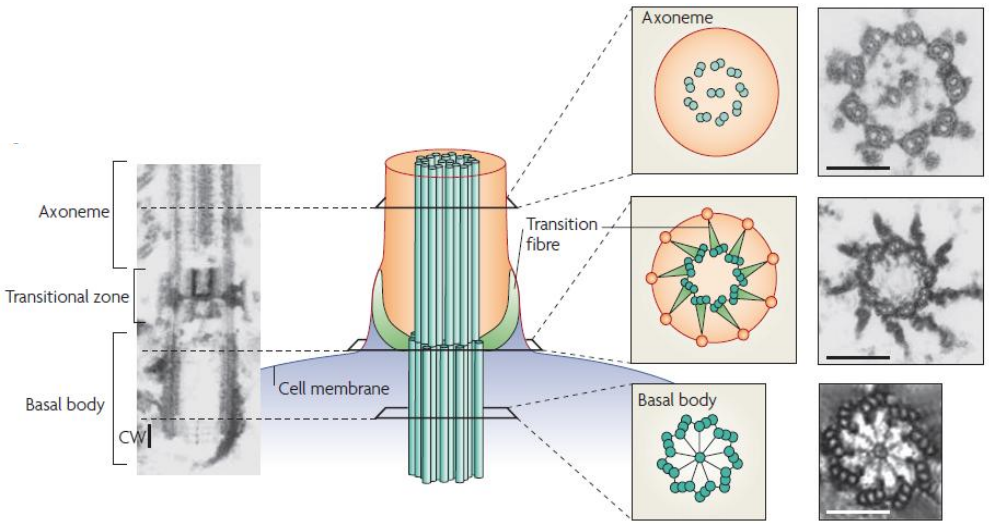

B

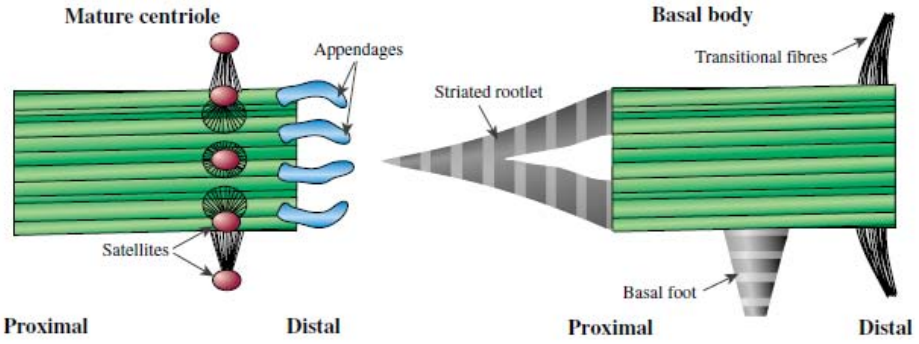

Figure 1.7 Centriole/basal body accessory structures
(A) Electron micrographs and schematic representation of the flagella of green algae. The transition fibers extend from the distal end of the basal body to the cell membrane. Scale bar, 0.25 µm. **(B)** Schematic of a longitudinal view of the mature centriole, showing the appendages, and a basal body with accessory structures. This figure is adapted from Dawe et al. (2007) and Bettencourt-Dias & Glover (2007).

membrane and the general cell membrane. Together with the ciliary necklace, the transitional fibres are thought to be part of a 'ciliary pore complex', allowing passage of only selected proteins into the ciliary compartment (Seeley & Nachury 2010; Satir et al. 2010). The docking of the basal bodies is achieved either by attaching directly to the apical membrane, or by first docking with the membrane of ciliary vesicles that fuse secondarily with the apical membrane. These wing-like trapezoidal sheets extend from the lateral side of each triplet microtubule of the basal body to the cytoplasmic face of the plasma membrane tethering it to the apical cell surface. For the basal body that nucleates the primary cilium, transitional fibres originate from the distal appendages of the mother centriole (Hagiwara et al. 2004; Pedersen et al. 2008; Seeley & Nachury 2010; Satir et al. 2010). The basal foot is a cross-banded structure, formed by fibrous granules, that originates laterally from the midregion of the basal body and, in monociliated cells, basal feet are modified centriolar subdistal appendages. In normal multiciliated cells, basal feet are all oriented in the same direction, and this corresponds to the direction of the effective stroke of ciliary beat. The striated or ciliary rootlets are composed of longitudinally aligned filaments and extend from the proximal end of the basal bodies toward the interior of ciliated cells. Evidence suggests that these structures are not essential to cilia formation or function, but rather provide mechanical support to cilia in certain specialized settings (Figure 1.7B) (Hagiwara et al. 2004; Seeley & Nachury 2010).

1.1.3.3 Cilia formation and intraflagellar transport

Assembly and maintenance of cilia and flagella are dependent on intraflagellar transport (IFT), an evolutionarily conserved process first described by Kozminski et al. (1993) in the biflagellate green alga, *Chlamydomonas*, as the bidirectional movement of discrete granule-like particles (rafts) between the base and the distal tips of flagella. IFT was first observed by differential interference contrast (DIC) microscopy in *Chlamydomonas* flagella, and electron microscopy analysis has revealed that the IFT rafts correspond to linear arrays of single non-vesicular electron dense particles (IFT particles), which exist in the shallow space between

the outer doublet microtubules of the axoneme, and the membrane of the cilium. IFT particle movement has also been observed in the nematode worm, *Caenorhabditis elegans*, as well as in primary cilia of cultured mouse kidney cells using GFP-tagged IFT particle proteins and/or motor subunits. Genes encoding IFT components are remarkably conserved among ciliated eukaryotes, but absent from non-ciliated organisms (Pedersen et al. 2008; Vlacque et al. 2008; Satir et al. 2010).

Since cilia do not contain any protein biosynthetic machinery, all of its components are synthesized in the cell body and transported into the cilium by means of IFT. The IFT machinery comprises at least two molecular motors, kinesin-II and dynein, and large protein complexes of at least 16 proteins, known as IFT particles, that associate with the IFT motors and serve as potential docking sites for IFT cargos, the 'delivered' proteins that include many different structural and functional ciliary components. Initial biochemical analysis of IFT particles from *Chlamydomonas* flagella using sucrose density gradient has revealed the presence of two complexes, A and B, which collectively comprise 16-17 different proteins. The IFT particle proteins range from 20 to 172 kDa being consequently designated IFT20 through IFT172. The process of assembling these particles occurs at the base of the cilia near the transition fibres, the region containing the selective filter or pore that allows only a selective subset of cellular proteins to enter the ciliary compartment (Pedersen et al. 2008; Vlacque et al. 2008). The axonemal doublet microtubules initiate at the transition zone, extending from the A and B tubules of the triplet microtubules of the basal body. IFT complexes A and B, inactive dynein, and axonemal precursors are transported by active kinesin-II in an anterograde manner, from the base to the tip of the cilium, along the outer doublet microtubule B. Once the kinesin-II reaches the tip of the cilia axoneme, cargo proteins and IFT particles are released into the ciliary tip compartment and complexes A and B dissociate from each other. Modifications at the tip of the axoneme result in the inactivation of the kinesin and facilitate the retrograde return of the raft to the base of the cilium via dynein. This raft contains complexes A and B, inactive kinesin-II and possibly

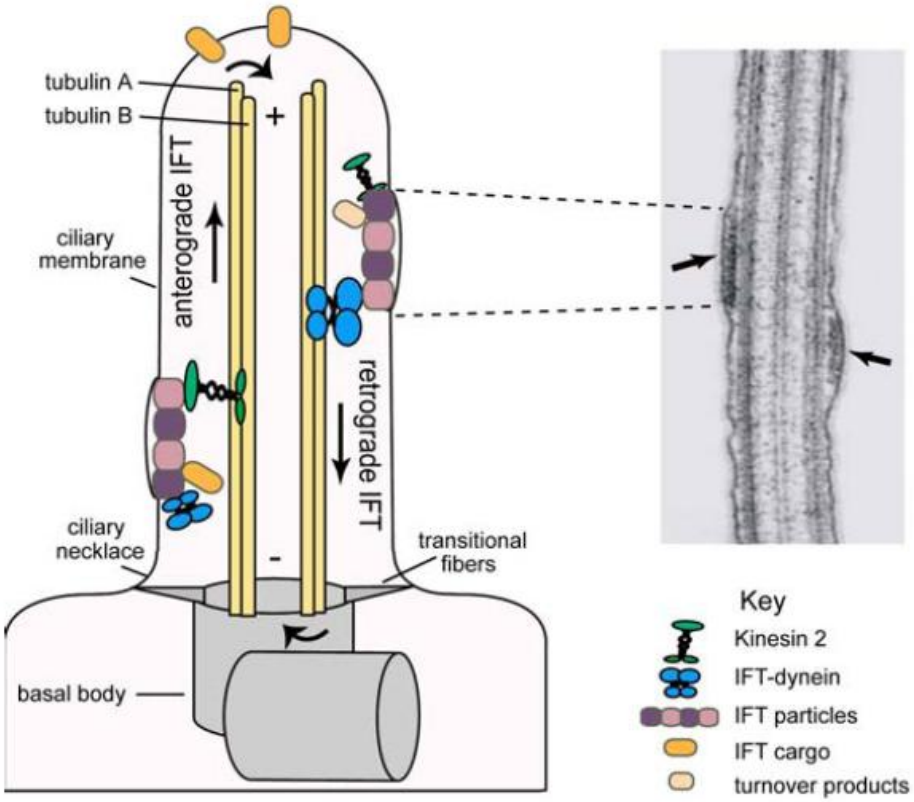

Figure 1.8 Intraflagellar transport
Schematic representation of intraflagellar transport, depicting kinesin 2 (towards the microtubule plus end) and dynein (towards the microtubule minus end) driven IFT along the outer doublet microtubules of ciliary axonemes (for simplicity, only two of the nine outer doublets are shown). Also indicated is the anchoring basal body, the transitional fibers and the position of the membrane-associated ciliary necklace, all of which may form a pore that regulates entry of ciliary proteins into the organelle. The electron micrograph of a *Chlamydomonas* flagellum shows the linear arrangement of electron dense IFT granules between the outer doublet microtubules and the ciliary membrane. Kinesin 2 drives anterograde transport (ciliary base to tip; towards the microtubule plus end) of IFT particles (and presumed cargo), whereas dynein recycles the IFT machinery (and potentially ciliary turnover products) back to the ciliary base. Remodelling of IFT assemblies occurs at the turnaround phases at the tip and base of cilia (denoted by curved arrows). This figure is adapted from Vlacque et al. (2008).

axonemal turnover products. Evidence suggests that complexes A and B have physiologically distinct roles. It is thought that whereas complex B proteins are generally required for entry of IFT proteins into the ciliary axoneme via kinesin-II-mediated anterograde transport, complex A proteins facilitate the removal/recycling of IFT proteins from cilia via retrograde dynein-driven IFT. The IFT cycle is completed when IFT components are returned to the cytoplasm for recycling (Figure 1.8) (Satir & Christensen 2007; Pedersen et al. 2008; Vlacque et al. 2008).

1.1.3.4 Cilia assembly and disassembly

In normal proliferating cells, a transient cilium is commonly observed in G_0 or G_1-phase. In these cells, entry into the cell cycle is preceded by ciliary disassembly, possibly to free the ciliary centriole to allow the centrosome to form the mitotic spindle. However, little is known about the molecular mechanisms governing the switch from a centriole to a basal body and vice versa. Spektor et al. (2007) have shown that two centrosomal proteins, CEP97 and CP110, coordinately suppress the assembly of the ciliary axoneme. Evidence from this study suggests that removal of CP110 from the mother centriole is a prerequisite for axoneme elongation. Moreover, this protein may function as a cap to limit the length of centriolar microtubule triplets in proliferating cells thus preventing aberrant cilium assembly (Spektor et al. 2007; Seeley & Nachury 2010).

Two mechanisms have been proposed to be involved in the disassembly of cilia: resorption or deflagellation/deciliation. Resorption consists in the gradual retraction of the cilium into the cell and usually occurs ahead of cell division, freeing centrioles to undergo duplication and segregation to the poles of the mitotic spindle, and possibly so that the axonemal tubulin can be reutilized during mitosis. Deflagellation consists in the abscission of the flagellum in the transition zone, in response to a wide range of stimuli, perhaps to free the basal body to perform other roles in mitosis and cell division. In *Chlamydomonas*, the transition zone is not resorbed, as its associated fibres and plasma membrane and cell wall connections are not easily

disassembled for recycling of component molecules. However, because not all transition zones are as structurally elaborate as those in *Chlamydomonas*, it is not clear if this severing event to release the basal bodies prior to mitosis is required (Quarmby & Parker 2005; Parker et al. 2010). Pugacheva et al. (2007) have shown that primary cilium disassembly might be triggered by Aurora A, a centrosomal kinase that regulates cell cycle progression and is activated in many cancers characterized by centrosomal amplification and genomic instability. On the basis of their studies on the effects of Aurora A kinase activity and the nature of its interactions with the histone deacetylase 6 (HDAC6) and the enhancer of filamentation 1 (HEF1), a model of cilium disassembly was proposed whereby Aurora A, activated by HEF1, phosphorylates ciliary HDAC6, which in turn deacetylates axonemal microtubules, resulting in the collapse of the primary cilium. IFT has also been implicated in cilium shortening. It is possible that cilium disassembly involves a decrease in the rate of delivery of axoneme subunits to the tip of the cilium, and an increase in the rate of retrograde trafficking of disassembled cilium components (Pugacheva et al. 2007; Pan & Snell 2007; Seeley & Nachury 2010). Studies in *Chlamydomonas* deflagellation have revealed that a member of the NIMA family of cell cycle kinases, Fa2, is essential for calcium-activated axonemal microtubule severing during flagellar detachment. Interestingly, this protein also has a role during cell cycle progression (Quarmby & Parker 2005; Pan & Snell 2007).

1.1.3.5 Cilia and the cell cycle

Accumulating evidence suggests that cilia disassembly/assembly and cell cycle entry/exit are coordinately regulated. Studies in *Chlamydomonas* and in vertebrate cells have revealed dual functions of proteins that regulate both the formation and maintenance of the primary cilium and cell division. This relationship may reflect the duality of the centriole, as a basal body that nucleates axonemes and as a core component of the centrosome that organizes the spindle formation (Quarmby & Parker 2005; Vlacque et al. 2008; Debec et al. 2010).

Consistent with this notion of duality of roles, the presence of cilia depends on cell cycle proteins. As mentioned above, a non-mitotic function of Aurora A was documented, being necessary and sufficient for ciliary shortening. Another centrosomal protein, EB1, a small microtubule-binding protein required for centrosomal microtubule anchoring and organization of the microtubule network, is also found at the basal body and is required for primary cilia assembly. NIMA-related kinases (Nek) are a family of known cell cycle kinases, and have also been linked to cilia in mammalian cells. Nek1 and Nek8 have been found to localize within the basal body/centrosomal region and along ciliary axonemes, and mutations in the genes coding for these proteins cause cystic kidney disease in mice, zebrafish and humans. The Nek family may provide an important general connection between cilia and the regulation of the cell cycle progression (Mahjoub et al. 2005; Schrøder et al. 2007; Pan & Snell 2007; Fliegauf et al. 2007; Vlacque et al. 2008).

Conversely, it has been shown that factors that control the formation or loss of cilia also influence the cell cycle. Notably, IFT components have been found to also function in the cell cycle. For example, reduced levels of IFT27, a Rab-like small G protein, results in cell growth inhibition and incomplete or symmetrical cytokenesis; overexpression of IFT88/polaris prevents G_1/S transition, and depletion of IFT88 leads to loss of cilia and promotes cell cycle progression (Pan & Snell 2007; Robert et al. 2007; Plotnikova et al. 2008). In fact, given their role in the detection and transmission of extracellular signals, it is not surprising that the regulated formation, shortening or disassembly of primary cilia may play important roles in the execution of cell developmental programs, such as maintenance of the differentiated state, cellular growth control, and suppression of cyst formation or oncogenesis.

1.2 CILIARY SIGNALLING

Sensory modalities to which the primary cilium responds include mechanical stimulation and chemosensation. In the mammalian retina, photoreceptors sense light through a modified primary cilium, and the light detecting protein machinery is

highly dependent on the correct functioning of IFT along the connecting cilium. In the nose, specialized olfactory cilia house G-protein-coupled receptor signalling cascade for detection and transduction of odorant signals. Defects in these cilia-mediated signalling pathways are associated with blindness and anosmia (Berbari et al. 2009; Kiefer 2010; Satir et al. 2010).

The presence of a variety of receptors, ion channels and transporter proteins, as well as some of their downstream effector molecules at the cilium set it up for several different types of signalling, being able to respond to mechanical stress as well as to distinct morphogens, hormones or growth factors. Indeed, signalling in the cilium coordinates key processes during development and in tissue homeostasis, including cell migration, differentiation and/or re-entry into the cell cycle, specification of the plane of the cell division, and apoptosis. In this section, I will present a brief overview of some of the signal transduction pathways coordinated by the primary cilium.

1.2.1 Hedgehog signalling pathway

The Hedgehog (Hh) family of secreted proteins controls a wide variety of processes during embryonic development and adult tissue homeostasis. It was initially identified nearly 30 years ago by Nüsslein-Volhard and Wieschaus as the 'segment polarity gene', controlling the embryonic cuticle pattern and adult appendages in *Drosophila*. The stubby and "spiked" phenotype of *Hh* mutant larvae inspired the name 'hedgehog'. Subsequent studies have revealed the importance of Hh signalling in the regulation of cell growth, survival, and fate, and pattern of almost every aspect of the vertebrate body plan (Jiang & Hui 2008; Varjosalo & Taipale 2008).

Whereas flies possess a single *Hh* gene, mammals have three: the *Desert Hegdehog* (*Dhh*) (closely related to the *Drosophila Hh*), *Indian Hedgehog* (*Ihh*), and *Sonic Hedgehog* (*Shh*), the best studied of the three. Ihh and Dhh participate in

bone development and spermatogenesis, respectively, whereas Shh, the most broadly expressed mammalian Hh signalling molecule, controls patterning of the left-right and dorso-ventral axes of the embryo and the distal elements of the limb in early embryogenesis, and in later development, Shh is important for the correct morphogenesis of organs such as the skin, eye, lung, muscle and pancreas (Jiang & Hui 2008; Varjosalo & Taipale 2008; Wong & Reiter 2008).

1.2.1.1 Mechanism of Hedgehog signalling pathway

After translation, Hh undergoes multiple processing steps required for generation and release of the active ligand from the producing cell. Dispatched (Disp) is the transmembrane protein responsible for this release. The Hh reception system consists of two separate transmembrane proteins, Patched (Ptc) and Smoothened (Smo), and downstream effectors, the Gli zinc-finger transcription factors, Gli1, Gli2, and Gli3. In the absence of Hh, Ptc localizes on the cilia membrane and inhibits ciliary Smo accumulation. As a result, Glis, and predominantly Gli3, are proteolytically processed to repressor forms (Gli_R) that actively repress the transcription of a subset of Hh target genes. By contrast, when Hh is present, Ptc binds the ligand and exits from the cilia membrane, allowing for Smo accumulation. Activated Smo then triggers a signal transduction cascade that blocks Gli_R production and promotes Gli_A activation, which, in turn, promotes target gene activation (Jiang & Hui 2008; Berbari et al. 2009). Analysis of mutations in mouse mutants that showed morphological and patterning phenotypes consistent with altered Hh signalling revealed that genes disrupted in these mutants encode several components of the IFT machinery and basal body proteins. The Hh pathway and cilia are clearly intertwined and all key components of the Hh pathway are enriched in cilia, including the suppressor of fused (SuFu), an important negative regulator of mammalian Hh signalling (Figure 1.9) (Kiefer 2010; Goetz & Anderson 2010).

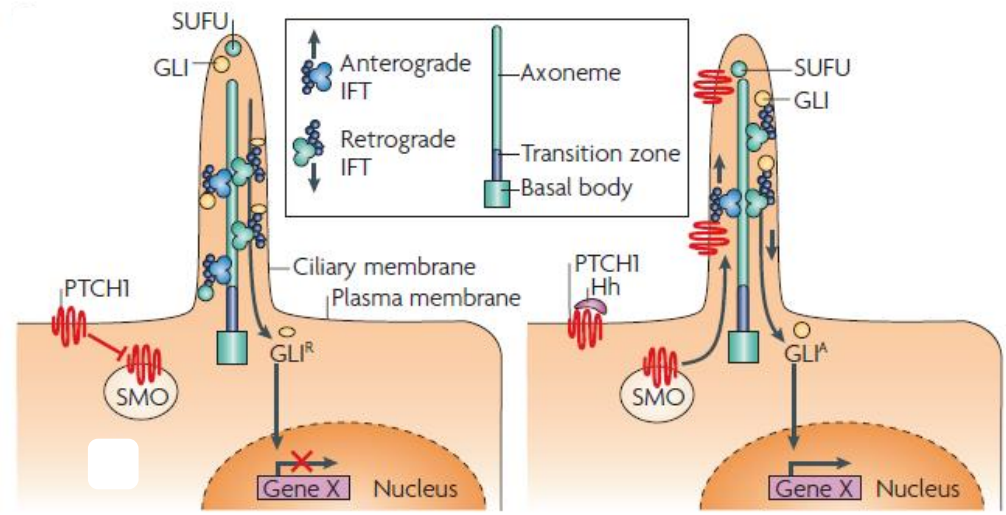

Figure 1.9 Model of Hedgehog signalling mechanism
Hedgehog (Hh) signalling in cilia involves the intraflagellar transport machinery, which moves components of the Hh signalling pathway to their functional sites. The transcription factors GLI and suppressor of fused (SUFU) are transported to the ciliary tip. GLI is processed to create a transcriptional repressor, which is transported back to the cell body (left panel). On Hh ligand binding to its receptor patched-1 (PTCH1), smoothened (SMO) is released and transported to the ciliary tip, where it turns off GLI processing by interacting with SUFU. The activator form of the GLI transcription factor is transported to the cell body and enters the nucleus where it induces the expression of genes. This figure is adapted from Fliegauf (2007).

1.2.1.2 Hedgehog signalling and cilia

A possible explanation for the successful relationship between cilia and the Hh pathway is that cilia provide a defined space in which signalling components are enriched, thereby facilitating a rapid, efficient response. Furthermore, the dynamic relocalization of pathway components in response to ligands suggests that trafficking of Hh pathway proteins is crucial for pathway activation, and it is likely that IFT proteins are important in this trafficking. Indeed, genetic studies showed that IFT proteins act downstream of the membrane proteins Patched 1 and Smoothened, and upstream of the Gli transcription factors that implement the Hh pathway. Moreover, mutations in IFT proteins required for ciliary assembly results in dysfunctional Hh signalling and severe developmental disorders in mammals. Mutations disrupting IFT in mice alter the Gli3 activator-to-repressor ratio and result in severe polydactyly; mutant mouse embryos lacking Kif3a subunit of kinesin-II anterograde motor, and embryos lacking *Ift88* or *Ift172* display an open neural tube, and loss of ventral cell types in the neural tube (Wong & Reiter 2008; Goetz & Anderson 2010; Kiefer 2010).

Using a single morphogen, Hh signalling is able to control distinct cell fates as a function of Hh concentration. In other words, signalling strength and duration, together with the type of responding cell, are important factors that shape developmental outcomes. In adulthood, Hh signalling maintains normal tissue homeostasis and has been implicated as essential for stem cell maintenance. Not surprisingly, malfunction of Hh signalling contributes to numerous human disorders. While germline mutations that affect the Hh pathway activity are associated with developmental disorders, somatic mutations that improperly activate the pathway have been linked to several forms of human cancer, playing a causative role in basal cell carcinoma and medullobastoma (Jiang & Hui 2008; Varjosalo & Taipale 2008; Wong & Reiter 2008).

1.2.2 Wnt signalling pathway

The Wnt family of secreted growth factors is important in cell proliferation and differentiation during development. Wnt ligands trigger two intracellular signalling cascades: the canonical Wnt/β-catenin pathway, which controls the stability of the transcription co-activator β-catenin, and the non-canonical Wnt/planar cell polarity (PCP) pathway, which is primarily involved in the organization of cytoskeletal architectures associated with cell polarity, migration and mitotic spindle orientation. Both signalling pathways are initiated by binding of a ligand of the Wnt family to a transmembrane receptor called Frizzled (Fz) (He 2008; Veland et al. 2009; Berbari et al. 2009).

1.2.2.1 Mechanism of Canonical and Non-canonical Wnt signalling pathways

The downstream effects of the canonical Wnt pathway are mediated by β-catenin, which serves as a transcriptional co-activator, inducing cell cycle progression, proliferation, differentiation, and growth in addition to migration and regulation of embryonic development. In the absence of Wnt ligands, β-catenin is marked for degradation by phosphorylation by a cytoplasmic 'destruction complex'. This multiprotein complex contains the scaffold protein axin, the adenomatous polyposis coli (APC) tumour suppressor gene product, glycogen synthase kinase 3β (GSK3β), casein kinase I (CKI), and protein phosphatase 2A (PP2A). In the absence of β-catenin, degraded by the proteasome, the nuclear transcription factors T cell factor (TCF) and lymphocyte enhancer factor (LEF) are associated with transcriptional suppressors to keep the canonical Wnt pathways inactive. In the presence of Wnts, Dishevelled (Dvl) blocks β-catenin degradation by displacing GSK3β from axin. Stabilised β-catenin then enters the nucleus and associates with the LEF/TCF transcription factors activating transcription (Figure 1.10) (Huelsken 2002; Mosimann et al. 2009; Veland et al. 2009; Berbari et al. 2009).

The non-canonical branch of Wnt signalling is β-catenin independent and mediates its effects through various factors including RhoA, Rock, Jun N-terminal kinase

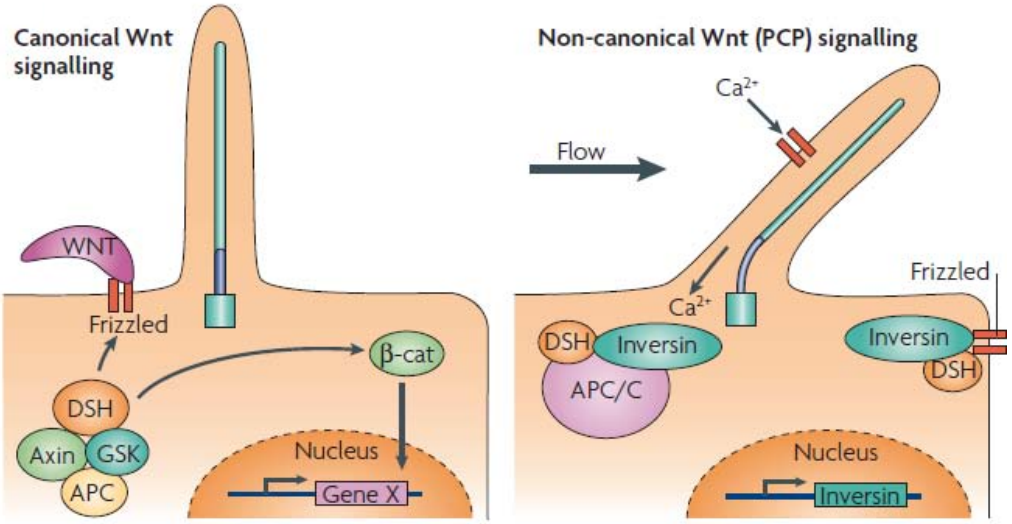

Figure 1.10 Model of Wnt signalling mechanism
Cilia-mediated signalling acts as a switch between canonical and non-canonical Wnt signalling pathways. In the absence of fluid flow, canonical Wnt signalling predominates. Wnt binds to the receptor frizzled, dishevelled (Dsh) is recruited to frizzled, and glycogen synthase kinase-3β (GSK3β) is inactivated. β-catenin (β-cat) translocates to the nucleus where it acts as a transcriptional co-activator with members of the lymphoid enhancer binding factor (LEF)–T-cell-specific transcription factor (TCF) family and induces transcription of Wnt target genes. On mechanosensation of fluid flow, intracellular Ca^{2+} release causes increased inversin expression. Inversin targets cytoplasmic Dsh for APC/C (anaphase-promoting complex/cyclosome)-dependent ubiquitylation and degradation, thus making it unavailable for canonical Wnt signalling. Inversin does not affect Dsh recruitment to the plasma membrane, where Dsh is available for non-canonical Wnt signalling. This figure is adapted from Fliegauf (2007).

(JNK), calcineurin, protein kinase C (PKC) and casein kinase II (CKII). Notably, Dvl is positioned at a crucial crossroads between the two branches of the Wnt pathway. Upon binding of a Wnt ligand to Fz, Dvl determines whether canonical Wnt (e.g. Wnt3a) or non-canonical Wnt (e.g. Wnt5a) signalling is initiated (Germino 2005; Mans et al. 2008; Berbari et al. 2009). Activation of the non-canonical Wnt signalling pathway directs asymmetric cytoskeletal organization and coordinated polarization of cells within the plane of epithelial sheets. Most cell types require polarization to function. In addition to the ubiquitous epithelial cell polarity along the apical-basal axis, most epithelial cells are also polarized within the plane of the epithelium. This polarization is called planar cell polarity (PCP). In vertebrates, PCP has also been found in mesenchymal cells and neural tube cells, where it regulates cell migration and cell intercalation (convergent-extension movements) during gastrulation and neurulation, respectively. Furthermore, PCP signalling factors have recently been found to be associated with the orientation or formation of cilia (Figure 1.10) (Huelsken 2002; Simons & Mlodzik 2008; Wu & Mlodzik 2009; Veland et al. 2009).

1.2.2.2 Wnt signalling and cilia

Localization of PCP proteins, such as Inversin (Inv) and Van Gogh 2 (Vangl2), as well as members of the degradation complex, GSK3β and APC, to the ciliary apparatus suggested a role for this structure in the regulation of both the canonical and the non-canonical Wnt signalling pathways. Furthermore, following the observation that knockdown of cilia-associated proteins in cultured cells or zebrafish or mouse embryos elevates canonical/β-catenin signalling and/or disrupts processes that depend on non-canonical Wnt/PCP signalling such as convergent extension movements, the primary cilium was proposed to function as a switch between the two signalling cascades (Berbari et al. 2009; Veland et al. 2009; Goetz & Anderson 2010).

Inversin (Inv), the gene product mutated in nephronophthisis type 2 (NPHP2), an autosomal recessive cystic kidney disease characterized by extensive renal cysts

and situs inversus (reversal of left-right asymmetry of organs of the body), was found to inhibit the canonical/β-catenin Wnt pathway and to activate the non-canonical/PCP Wnt signalling. Moreover, since Inv promotes degradation of cytosolic but not membrane-associated Dvl, a critical component of both canonical/β-catenin and non-canonical/PCP pathways, it has been proposed that it may function as a molecular switch between the two signalling pathways (Simons et al. 2005; He 2008; Berbari et al. 2009). Mice with mutations in genes involved in Bardet-Biedl syndrome (BBS), a disorder associated with ciliary dysfunction, share phenotypes with PCP mutants, including neural tube defects and disrupted cochlear stereociliary bundles. Furthermore, BBS genes genetically interact with the PCP gene, Vangl2, indicating that cilia are intrinsically involved in PCP processes. However, because Inversin and BBS proteins are found both at the cilium and elsewhere in the cell, the role of the cilium in Wnt signalling is not entirely clear (Ross et al. 2005; Huang et al. 2009; Berbari et al. 2009). Studies have also reported that in the absence of proteins essential for cilia formation, such as Kif3a, Ift88/polaris or Ofd1, Wnt/β-catenin signalling is enhanced. Therefore, regardless of how cilia formation is perturbed, an upregulation of Wnt responsiveness is observed, thus confirming a role of cilia in restraining Wnt/β-catenin signalling. In contrast to its role in promoting Hedgehog (Hh) signalling, the cilium restrains canonical/β-catenin Wnt signalling (Corbit et al. 2008; He 2008). Furthermore, the posterior positioning of the basal body that provides the posterior tilt to nodal cilia, which then generates the leftward fluid flow responsible for the breaking of left-right symmetry in the mouse embryo, is determined by PCP mediated by non-canonical Wnt signalling. Another connection between PCP signalling and cilia positioning is found in the hairs cells in the cochlea. The position of the kinocilium, which determines the polarity of the stereocilia bundles on the hair cell, is dependent on core components of the non-canonical/PCP Wnt signalling pathway. Components of the PCP pathway have also been reported to be necessary for the apical docking of basal bodies, and therefore the ability to form cilia. Thus, components of the planar cell polarity

pathway may be important for both formation and polarity of cilia (Rida & Chen 2009; Hashimoto et al. 2010; Goetz & Anderson 2010).

1.2.3 Other cilia-based signalling cascades

Cilia have been found to be important for signalling by platelet-derived growth factor receptor α (PDGFRα) in mouse embryonic fibroblasts, as well as for PDGF-dependent migration in these cells. Fibroblasts in tissues are usually in a state of growth arrest, but if stimulated they can enter the cell cycle for proliferation and migrate throughout the extracellular matrix in events such as wound healing and tissue reorganization (Satir & Christensen 2007; Goetz & Anderson 2010). Binding of PDGFs to their receptors, PDGFRs, which are located along the cilium, induces cellular responses through downstream signalling pathways such as the MEK/ERK pathway. Signalling via PDGFs and PDGFRs plays an essential role in cell survival, growth control and cell migration during gastrulation, fetal development and in maintenance of tissues in the adult. Defects in this signalling pathway can lead to cancer, vascular disorders and fibrosis (Figure 1.11) (Mans et al. 2008; Veland et al. 2009).

Mechanotransduction is the process by which cells convert mechanical forces into biochemical signals. Primary cilia have been shown to be essential for mechanosensation, sensing and initiating important signalling cascades in different tissue types such as liver, kidney and bone. Renal primary cilia act as mechanosensors, bending in response to fluid flow and consequently activating intracellular Ca^{2+} channels. The induced Ca^{2+} increase occurs through the polycystin 1/2 receptor-ion channel complex, composed of polycystin 1 (PC1) and polycystin 2 (PC2), found on the primary cilium. The subsequent increase in cellular Ca^{2+} is thought to influence several subcellular activities required for tissue morphogenesis. In fact, defects in mechanosensory cilia in the kidney result in abnormal renal cell proliferation and cyst formation, a hallmark of polycystic kidney disease (PKD). In liver cholangiocytes, primary cilia acts as mechanosensors that monitor and transmit

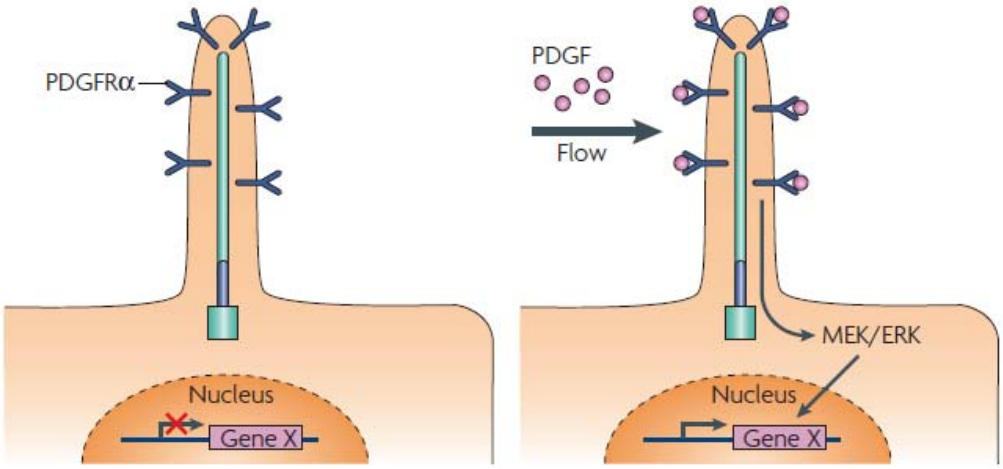

Figure 1.11 Model of the chemosensation receptor based signalling mechanism
Receptors such as platelet-derived growth factor-α (PDGRFα) are located within the axonemal membrane. Ligands in the tubular flow bind to their receptors, inducing cellular responses through downstream signalling pathways such as the MEK/ERK cascade. This figure is adapted from Fliegauf (2007).

luminal bile flow stimuli into integrated intracellular Ca^{2+} and cyclic adenosine monophosphate (cAMP) signalling. Recent studies suggest that primary cilia also act as mechanosensors in bone, being important for maintaining adult bone health and homeostasis. The osteocyte primary cilium mediates mechanically induced responses independent of intracellular Ca^{2+} release, which suggests that the mechanotransduction signalling pathway in bone differs from the kidney and liver (Figure 1.12) (Onori et al. 2010; Satir et al. 2010; Temiyasathit & Jacobs 2010).

1.3 CILIA IN DISEASE: HUMAN CILIOPATHIES

Collectively, human disorders linked to mutations in ciliary genes are known as ciliopathies. The clinical features associated with ciliopathies are extremely diverse and include randomization of the left-right body axis, abnormalities in neural tube closure and patterning, polydactyly, kidney, hepatic and pancreatic cyst formation, retinal degeneration, anosmia, cognitive defects and obesity. Interestingly, a specific mutation in one cilia gene may present as one clinical disorder while a different mutation in the same gene will give a different outcome, suggesting that the positioning and severity of the mutations may have important implications for clinical presentation. Ciliopathies form a group of genetic diseases whose origin may not lie in the dysfunction in a single gene product, but rather in an integrated aspect of cellular physiology. Although ciliopathies are generally rare, their clinical features offer important opportunities to glean insights into more common disease processes (Adams et al. 2008; Baker & Beales 2009; Berbari et al. 2009; Leigh et al. 2009). In this section, I will introduce some of these cilia-related human disorders and their pathomechanisms.

1.3.1 Disorders of motile cilia

A link between ciliary dysfunction and human disease was first discovered in 1976, when Afzelius observed defects in ciliary structure and function in patients with symptoms including respiratory problems and male infertility (primary cilia dyskinesia or PCD). Another hallmark feature of ciliary dysfunction is situs inversus,

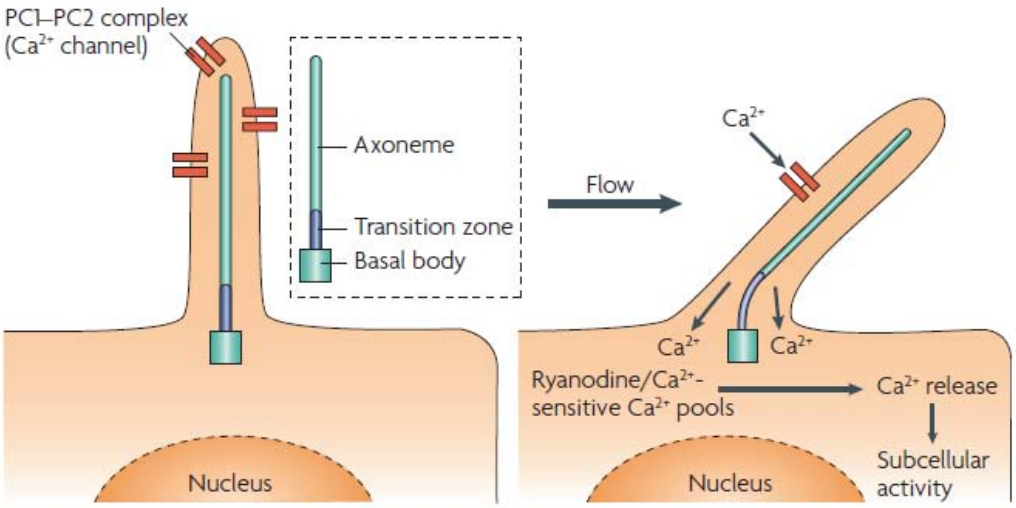

Figure 1.12 Model of the mechanosensation-based cilia signalling
The polycystin 1/polycystin 2 complex (PC1/PC2), which is sensitive to shear stress, is localized within the ciliary membrane. Fluid-induced ciliary bending activates this Ca^{2+} channel. The Ca^{2+} influx causes Ca^{2+} stores and subsequent downstream responses. Mutations in PC1 or PC2 might disable cilia-mediated mechanosensation, which is normally required for tissue morphogenesis, and thus can cause polycystic kidney disease. This figure is adapted from Fliegauf (2007).

the defective left-right symmetry axis determination, which, together with the symptoms that characterize PCD, defines the triad of symptoms of Kartagener syndrome. Hydrocephalus, a symptom occasionally observed in PCD patients, is also associated with defects in motile cilia (Satir 2008; Toriello 2009b; Leigh et al. 2009).

1.3.1.1 Primary cilia dyskinesia, situs inversus and hydrocephalus

Ciliated cells that line the lower respiratory tract coordinately move to sweep the periciliary fluid and overlying mucus in an exterior direction, thereby providing the primary defence mechanism of the airways. Primary cilia dyskinesia (PCD) is a genetically heterogeneous disorder, typically autosomal recessive, affecting 1 in 60,000 individuals. It is characterized by ciliary dysfunction and impaired mucociliary clearance, resulting in an array of clinical manifestations. The ciliary structural defects observed in PCD patients include abnormal or missing dynein arms, radial spokes and central microtubule doublets, and the clinical symptoms reflect the distribution of motile cilia in affected tissues and organs. Thus far, mutations in genes encoding different components of the complex machinery that generates and coordinates ciliary movement have been found to cause this condition. Mutations in genes encoding for dynein axonemal intermediate, heavy and light chains, such as *DNAI1*, *DNAH5*, *DNAH11*, *DNAI2* and *TXNDC3*, and genes encoding for radial spoke head proteins, such as *RSPH9* and *RSPH4A*, have been found in PCD patients. Respiratory manifestations of primary cilia dyskinesia, such as chronic bronchitis leading to bronchiectasis, chronic rhino-sinusitis, and chronic otitis media, result from impaired mucociliary clearance caused by defective axonemal structure. Male infertility is common and results from defects in sperm tail axonemes (Chilvers & O'Callaghan 2000; Marshall 2008; Satir & Christensen 2008; Leigh et al. 2009). Diagnosis of PCD has traditionally been done through microscopic ultrastructural analysis of respiratory cilia obtained by nasal scrape or bronchial brush biopsy. Immunofluorescence staining, ciliary beat assessment and nasal nitric oxide

measurements are other diagnostic tests available (O'Callaghan et al. 2007; Zariwala et al. 2007; Leigh et al. 2009).

PCD patients can also have laterality defects, including complete reversal (situs inversus) or partial mispositioning (heterotaxy) of organs. This reflects dysfunction of embryonic nodal cilia, whose activity is key in the establishment of left-right body axis asymmetry early in the developing embryo (Fliegauf et al. 2007; Satir & Christensen 2008). Other clinical manifestations such as sensory hearing defects and hydrocephalus have also been linked to some forms of PCD. Hydrocephalus, which is characterized by dilation of the inner brain, results from impaired ciliary beating in the ependymal cells lining the brain ventricles which normally generate a flow of cerebrospinal fluid that is necessary to maintain an open aqueduct between the third and the fourth ventricle. It seems to be typically associated with defects in the central pair of axonemal microtubules (Marshall 2008; Cardenas-Rodriguez & Badano 2009).

PCD has been reported to cosegregate with other genetic conditions whose causative genes primarily do not affect motile cilia. For example, a novel X-linked recessive mental retardation syndrome (Simpson-Golabi-Behmel syndrome type 2) comprising macrocephaly and dyskinetic cilia cosegregates with a frameshift mutation in the *OFD1* gene, associated with the ciliopathy oral-facial-digital syndrome type 1 (OFD1). Also, the X-linked form of retinitis pigmentosa (xLRP), a group of genetic disorders characterized by defects in the photoreceptors that lead to progressive loss of vision, has been reported to be associated with symptoms consistent with PCD (Budny et al. 2006; Fliegauf et al. 2007; Leigh et al. 2009).

1.3.2 Primary cilia-related disorders

The realization that mutations that interfere with primary cilia formation in specific tissues were linked to important human diseases or developmental defects changed the prevailing view that these organelles were vestigial with no known function.

Indeed, it was only ten years ago that the significance of primary cilia in signalling became clear with the discovery that the gene whose function was disrupted in the Oak Ridge Polycystic kidney mouse hypomorphic mutant (ORPK mouse, *ift88*^{orpk}, or *ift88*^{Tg737NRpw}) encoded an ortholog of *Chlamydomonas* IFT88, a protein required for assembly of flagella. ORPK mouse had kidney and liver defects that were very similar to those seen in humans with autosomal recessive polycystic kidney disease (ADPKD), thus providing a direct link between primary cilia and human disease (Pazour et al. 2000; Satir et al. 2010).

Furthermore, the phenotype of the ORPK mouse, a model for ADPKD, includes scruffy fur, preaxial polydactyly, hepatic and pancreatic ductal cysts, retinal degeneration, skeletal defects, cerebellar hypoplasia, hydrocephalus, growth retardation, and late-onset obesity. This plurality of symptoms is in accordance with the fact that ciliopathies are typically multisystemic disorders. Indeed, ciliopathies display common clinical features that can be used to identify new ciliopathy syndromes. The kidney and liver are the most commonly affected organs in ciliopathies. Second in prevalence is situs inversus, followed by a triad of features that tend to manifest together: polydactyly, agenesis of the corpus callosum, and mental retardation. Numerous ciliopathies are characterized by retinal degeneration and, less commonly, by skeletal defects, obesity, anosmia, ataxia, liver fibrosis, cardiac defects, infertility, and central nervous system (CNS) abnormalities. Moreover, the ciliary theory of cystic kidney disorders provides an explanation for the pathogenic basis of extrarenal organ involvement (Toriello 2009b; Baker & Beales 2009; Zhou 2009; Tobin & Beales 2009).

1.3.2.1 Polycystic kidney disease

Cystic kidney diseases are a group of human genetic disorders characterized by the development of fluid filled cysts in the kidney, gradually leading to end-stage renal failure, either in adulthood or in childhood, as in autosomal dominant (ADPKD) or recessive (ARPKD) polycystic kidney disease, respectively. ADPKD is the most

common monogenic disorder of the kidney, with a frequency of 1:400 to 1:1000. Mutations in the *PKD1* or *PKD2* genes, encoding for the primary cilium membrane proteins, polycystin 1 (PC1) and polycystin 2 (PC2), respectively, result in ADPKD in humans and mice. PC1 is an integral membrane protein that senses nephron and collecting duct urine flow and that interacts directly with PC2, a Ca^{2+}-selective channel that responds to this stimulus by generating a Ca^{2+} influx through the cilium and into the renal epithelial cells. In addition to their ciliary localization, PC1 and PC2 are also found in other subcellular compartments and membrane domains: PC1 has been detected in the apical membranes and in the adherent and desmosomal junctions, whereas PC2 is found in the cytoplasm and in the apical and basolateral membranes (Figure 1.13). ARPKD is a rare (1:20,000 newborns) and severe disorder characterized by large cystic kidneys, hepatic fibrosis and systemic hypertension. ARPKD results from mutations in the *PKHD1* gene, and its phenotypic variability can be explained by the alternative splicing of its 85 exons which results in a variable number of transcripts, with the longest being fibrocystin/polyductin. In renal epithelial cells, fibrocystin/polyductin localizes to the renal primary cilium and the centrosome, and it has been proposed that it functions through its interaction with polycystins (Cardenas-Rodriguez & Badano 2009; Zhou 2009; Deltas & Papagregoriou 2010).

1.3.2.2 Bardet-Biedl Syndrome

Bardet-Biedl syndrome (BBS) was the first disease to be studied in detail whose origin lay in primary cilia dysfunction, thus becoming a model ciliopathy. BBS is characterized by retinal dystrophy (retinitis pigmentosa), renal dysplasia, obesity, cognitive impairment, hearing loss, and polydactyly. Situs inversus and congenital cardiovascular disease also occur in some patients. To date, 12 genes have been identified (*BBS1* through *12*). These encode for proteins that are mostly associated with the centrosome and/or basal body. BBS can segregate in a classical autosomal recessive manner or in some cases as a complex trait whereby mutations at more than one BBS locus contribute to the penetrance and/or expressivity of the

phenotype. In addition, mutations in three other ciliopathy-related genes have been associated with BBS: *MKS1* and *MKS3*, mutated in Meckel-Gruber syndrome (MKS), and *CEP290*, mutated in Joubert syndrome (JBTS) (Tobin & Beales 2009; May-Simera et al. 2009).

Protein-protein interaction motifs are found in BBS1/BBS2/BBS7 (β-propeller repeats) and BBS4/BBS8 (TPR motifs). *BBS3* encodes the ARF-like GTPase ARL6, BBS11 is identical to the E3 ubiquitin-ligase TRIM32, and BBS6/BBS10/BBS12 are likely chaperonins which may facilitate protein folding. Despite the variety of putative functions for BBS proteins, a few studies have proposed some of these to be involved in the regulation of intraflagellar transport (IFT) processes, and also to participate in processes mediated by the PCP. BBS4 has been found to interact with PCM-1, a core component of centriolar satellites, and with the p150Glued subunit of the minus-end-directed microtubule motor, dynein/dynactin. BBS4 has therefore been proposed to act a bridging factor between PCM-1 and dynein to transport proteins such as centrin, pericentrin, Nek2 and ninein to the centrosome (Dammermann & Merdes 2002; Kim et al. 2004; Hames et al. 2005; Kim et al. 2008; May-Simera et al. 2009). Proteomic evidence for a complex comprising seven highly conserved BBS proteins (BBS1, BBS2, BBS4, BBS5, BBS7, BBS8 and BBS9) has been reported by Nachury et al. (2007). BBS6 and PCM-1 also transiently associate with this interactome. This stable complex, known as the BBSome, localizes to centriolar satellites and to the membrane of the cilium, and it has been proposed to function in membrane trafficking to the primary cilium (Figure 1.13). The Rab family of Ras-like small GTPases is a key regulator of vesicle trafficking, and Rabin8, a GDP/GTP exchange factor specific for Rab8, has been found to localize to the basal body and to bind BBS1. A current model suggests that the BBSome may direct Rabin8 to the base of the cilium, thus mediating a localized activation of Rab8, which then targets vesicles to the cilium to promote ciliary membrane elongation. Moreover, a recent study by Kim et al. (2008) reported a physical interaction between PCM-1 and CEP290, and the requirement of both proteins for the ciliary

localization of Rab8. This proposed involvement of CEP290 in the BBS4 pathways provides a clue to understand the underlying mechanisms of the genetic link between JBTS and BBS (Nachury et al. 2007; Kim et al. 2008; Loktev et al. 2008; May-Simera et al. 2009). The participation of BBS proteins in multiple large complexes may also explain the genetic heterogeneity, the lack of phenotype-genotype correlations, and the oligogenic nature of BBS.

1.3.2.3 Alström syndrome

The Alström syndrome (ALMS) is a rare recessive disorder that shows strong resemblance to BBS. It is characterized by retinitis pigmentosa, deafness, early-onset obesity and insulin resistance leading to diabetes type 2. Polydactyly, dilated cardiomyopathy, hepatic and renal dysfunction, short stature, and male hypogonadism may also be present. Mutations in the recessive gene, *ALMS1*, account for all cases of this syndrome, and its gene product localizes to the centrosome and basal body, thus suggesting a ciliary role and a possible explanation for the phenotypic overlap with BBS. Studies in mutant and knockout mice have suggested a role for ALMS1 in intracellular trafficking (Hildebrandt et al. 2009; Tobin & Beales 2009).

1.3.2.4 Nephronophthisis

Nephronophthisis (NPHP) is a complex of autosomal recessive kidney diseases that currently comprises nine different types that correspond to nine different genes (*NPHP1* through *9*). Unlike PKD, where large kidney cysts, and therefore enlarged kidneys, are a common diagnostic feature, NPHP cysts are usually small and the overall size of the kidney is normal or diminished. Phenotypic characteristics include corticomedullary cysts, degradation of tubular basement membranes, tubular collapse, and interstitial fibrosis. Nephronophthisis literally means ‘disappearance of nephrons’ and, in fact, loss of normal tissue rather than abnormal cell proliferation is thought to be responsible for cyst development. NPHP is the main cause of end-stage renal failure within the first three decades of life, and is traditionally classified

in three groups according to the time of onset of end-stage renal disease: infantile, juvenile, and adolescent (Simms et al. 2009; Veland et al. 2009; Tobin & Beales 2009; Deltas & Papagregoriou 2010).

Nephronophthisis is characterized by extensive genetic heterogeneity and results from mutations in nine genes identified by positional cloning: *NPHP1*, *NPHP2/inversin*, *NPHP3*, *NPHP4*, *NPHP5*, *NPHP6/CEP290*, *NPHP7/GLIS2*, *NPHP8/RPGRIP1L*, and *NPHP9/Nek8*. Collectively, the proteins encoded by these genes are referred to as nephrocystins and localize to the cilium or the basal body. About 10% of NPHP cases are combined with extrarenal manifestations such as retinitis pigmentosa, described as Senior-Løken syndrome (SLSN), cerebellar vermis hypoplasia known as Joubert syndrome (JBTS), congenital ocular motor apraxia type Cogan, cognitive impairment, hepatic fibrosis, phalangeal cone-shaped epiphyses in Mainzer-Saldino, and situs inversus. NPHP has also been described in cases of Bardet-Biedl syndrome (BBS), Ellis-van Creveld syndrome (EVC), Jeune asphyxiating thoracic dystrophy (JATD), Alström syndrome (ALMS), and Meckel-Gruber syndrome (MKS) (Hildebrandt & Zhou 2007; Yoder 2007; Adams et al. 2008; Cardenas-Rodriguez & Badano 2009; Baker & Beales 2009; Hildebrandt et al. 2009).

NPHP1 mutations account for 20-25% of cases of NPHP, and these can be associated with congenital ocular motor apraxia type Cogan and SLSN and also give rise to JBTS phenotypes. The *NPHP1* gene encodes for nephrocystin-1, which has been localized to the transition zone of primary cilia in renal and respiratory epithelia and to the connecting cilia in photoreceptor cells, and to epithelial cell adherens junctions. Nephrocystin-1 also interacts with products of other NPHP genes such as nephrocystin-2/inversin, nephrocystin-3, and nephrocystin-4, and Jouberin. *NPHP2* encodes nephrocystin-2/Inversin protein, which has a dynamic distribution during the cell cycle and is expressed in renal primary cilia. *NPHP2* gene mutations are responsible for the infantile type of NPHP, and may cause situs

inversus in affected patients. Retinitis pigmentosa is an uncommon but reported association with NPHP2. Furthermore, Inversin has been shown to play important roles in Wnt signalling, possibly acting as a switch between the canonical/β-catenin and the non-canonical/PCP Wnt signalling pathways, and as discussed earlier required for convergent extension movements. Indeed, Inversin has a crucial role in PCP, and its disruption may underlie the pathophysiology of cyst development. Mutations in *NPHP3* have been associated with hepatic fibrosis and retinal degeneration. Truncating mutations of *NPHP3* in humans cause a broad clinical spectrum of early embryonic patterning defects that resembles MKS. Nephrocystin-3 interacts with nephrocystin-1 and Inversin, and can inhibit canonical Wnt signalling. Mutations in the murine ortholog *Nphp3* cause the renal cystic mouse model mutant *pcy*, which responds to treatment with the vasopressin-2-receptor antagonists. *NPHP4* mutations may cause isolated NPHP, SLSN, and NPHP associated with ocular motor apraxia type Cogan. Its gene product, the highly conserved protein nephrocystin-4, also known as nephroretinin, interacts with nephrocystin-1 and RPGRIP1L (retinitis pigmentosa GTPase regulator interacting protein 1-like). The clinical phenotype of *NPHP5* mutations is always associated with severe retinal degeneration (early onset SLSN). Mutations in *NPHP6/CEP290* account for a growing spectrum of clinical phenotypes that include isolated NPHP, SLSN, JBTS, MKS and BBS. Its gene product nephrocystin-6/CEP290 is part of the centrosomal proteome. The *NPHP7/GLIS2* gene encodes the Kruppel-like zinc-finger transcription factor, GLIS2, that localizes both to the primary cilia and the nucleus. There are no reports of extrarenal manifestations in patients with this rare genetic cause of NPHP. Mutations in the *NPHP8/RPGRIP1L* gene have been identified as the cause of a JBTS-like phenotype (cerebro-oculo-renal syndrome) and MKS. Its gene product, RPGRIP1L colocalizes at the centrosome and basal body with neprocystin-4 and nephrocystin-6. *NPHP9/Nek8* gene encodes the Nek8 protein (never in mitosis A-related kinase 8). Mutations in this gene are rare, and they might contribute to the oligogenicity in patients with NPHP. Nek8 has been shown to form a complex with polycystin-2, supporting a common mechanism for NPHP and

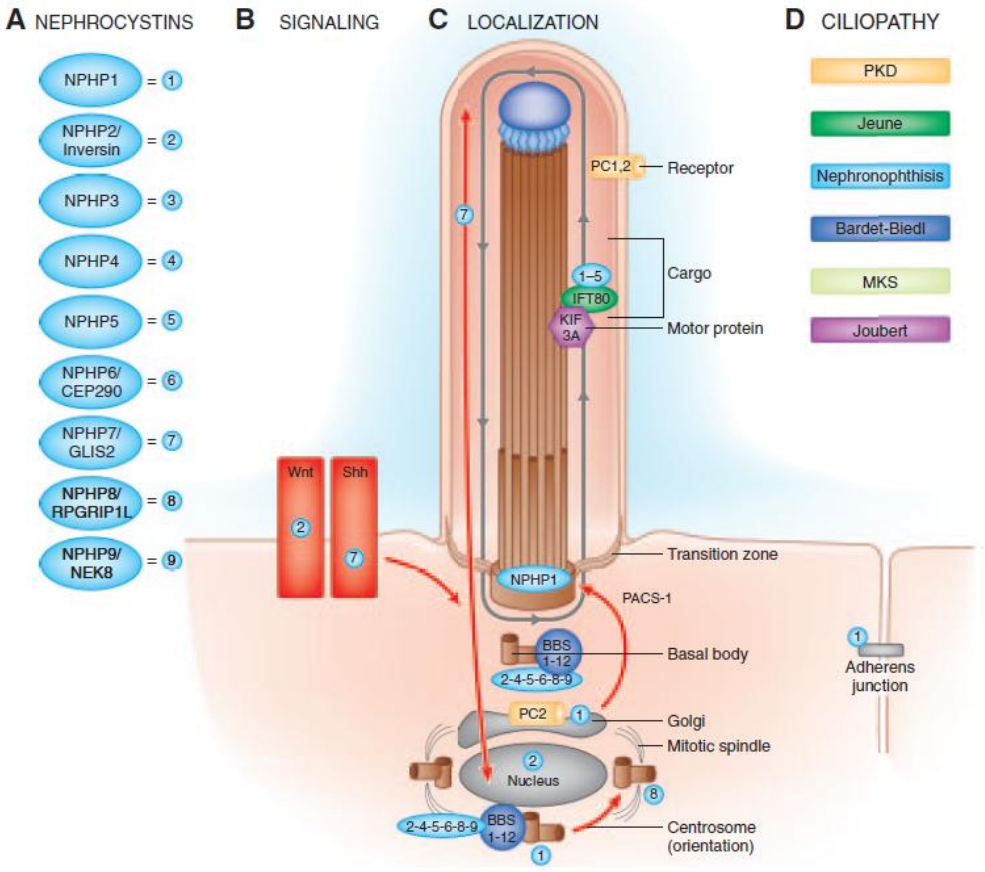

Figure 1.13 Primary cilia related disorders
Subcellular localization of nephrocystins to primary cilia, basal bodies, the mitotic spindle, focal adhesions and adherens junctions, and functional interaction with other proteins mutated in ciliopathies. Depending on cell-cycle stage, these proteins are localized at different subcellular organelles (shown in grey or brown). Arrows in the primary cilium indicate the direction of anterograde transport along the microtubule system mediated by kinesin-2 and retrograde transport by cytoplasmic dynein 1b. **(A)** Most nephrocystins (blue) are located at cilia, the basal body, and centrosome in a cell cycle–dependent manner. **(B)** Sensory cilia perceive and process cell external signals, and ciliopathy proteins are involved in signaling mechanisms downstream of ciliary signal recognition. Downstream of cilia (pink), Wnt signaling and hedgehog signaling play a role in planar cell polarity, which is mediated **(C)** partially through orientation of centrosomes and the mitotic spindle poles. **(D)** Cilia-dependent mechanisms of planar cell polarity seem to be central to the pathogenesis of the ciliopathies, the most prominent of which are listed on the right. This figure is adapted from Hildebrandt et al. (2009).

ADPDK (Figure 1.13). Just like it has been shown for BBS proteins, the genetic heterogeneity of NPHP suggests that the encoded NPHP proteins may be components of either a common pathway or a multisubunit complex (Hildebrandt et al. 2009; Simms et al. 2009; Deltas & Papagregoriou 2010).

1.3.2.5 Senior-Løken Syndrome

When NPHP presents with retinitis pigmentosa (RP), it is called Senior-Løken Syndrome (SNLS). RP is a group of genetically heterogeneous disorders in which abnormalities of the photoreceptors on the retinal pigment epithelium lead to progressive loss of vision, and can be inherited as an autosomal dominant, autosomal recessive, or X-linked trait. Patients with X-linked retinitis pigmentosa (xlRP) have mutations in *RPGR* (retinitis pigmentosa GTPase regulator) gene, whose protein product localizes to the photoreceptor connecting cilium and is essential for photoreceptor maintenance and viability. RPGRIP1 (retinitis pigmentosa GTPase regulator interacting protein 1), another structural component of the connecting cilium axoneme, interacts with RPGR at the connecting cilium to restrict its localization to the axoneme (Boylan & Wright 2000; Zariwala et al. 2007; Ramamurthy & Cayouette 2009).

Retinitis pigmentosa has been observed in association with mutations in most *NPHP* genes (except *NPHP7*). However, whereas RP is always present and severe in patients with *NPHP5* and *NPHP6* mutations, the symptoms are generally mild in patients with mutations in the other *NPHP* genes. Nephrocystins encoded by *NPHP4*, *5*, *6* and *8* genes have been shown to localize to the connecting cilia between the inner and outer segments of the photoreceptors. Mutations in *NPHP4*, a gene encoding for nephrocystin-4, were found in SLSN type 4 patients. Nephrocystin-4 and RPGRIP1L have been shown to interact, forming a complex that is thought to regulate ciliogenesis (Hildebrandt & Zhou 2007; Simms et al. 2009; Salomon et al. 2009; Deltas & Papagregoriou 2010). Mutations in *NPHP5*, the gene encoding for nephrocystin-5, lead to early-onset retinitis pigmentosa, a form of

Leber's congenital amaurosis (*SLSN type 5*). Nephrocystin-5 contains an IQ domain, which directly interacts with calmodulin, and is in a complex with RPGR. Nephrocystin-5 and RPGR colocalize at photoreceptor connecting cilia and primary cilia of renal epithelial cells. The fact that these two ciliary structures are equivalent elucidates the retinal involvement in the retina-renal syndrome Senior-Løken Syndrome. Mutations in *NPHP6/CEP290* represent one of the most frequent causes of isolated Leber's congenital amaurosis (LCA), a severe retinal dystrophy, without associated cerebellar abnormalities (den Hollander et al. 2006; Friedhelm Hildebrandt et al. 2009; Simms et al. 2009; Ramamurthy & Cayouette 2009; Deltas & Papagregoriou 2010).

1.3.2.6 Joubert Syndrome

Joubert syndrome (JBTS) is an autosomal recessive neurological disorder that associates congenital hypotonia evolving into cerebellar ataxia, severe psycomotor delay, oculomotor apraxia, and episodes of rapid breathing. It is characterized by a complex cerebellar and brainstem malformation, the so-called 'molar tooth sign' observed by magnetic resonance imaging. This has greatly enhanced the diagnosis of JBTS and has allowed the identification of JBTS-related disorders with involvement of other organs (Tobin & Beales 2009; Salomon et al. 2009).

Other conditions associated with JBTS include central nervous system (CNS) abnormalities, ocular coloboma, retinal dystrophy, skeletal defects such as polydactyly, hepatic fibrosis and NPHP. Six of eight JBTS loci have been described, and there is a clear genetic overlap with other ciliopathies. In patients with the association of JBTS and NPHP, mutations have been described in four different genes, *NPHP1* (JBTS type 4), *AHI1* (JBTS type 3), *NPHP6/CEP290* (JBTS type 5), and *NPHP8/RPGRIP1L* (JBTS type 7). Some JBTS patients with mutations in *NPHP1* have ocular motor apraxia type Cogan, defined as the transient inability of horizontal eye movements in the first few years of life (JBTS type 4). JBTS type 3 has been shown to be caused by mutations in the *AHI1* (Abelson helper integration

site) gene. Its gene product, Jouberin, is localized to adherens junctions, basal bodies and primary cilia, and interacts with nephrocystin-1. JBTS type 5 is characterized by mutations in *NPHP6* gene, which encodes for CEP290, a centrosomal protein known to interact with and activate the cAMP transcription factor, CREB2/ATF4. Both JBTS type 7 and Meckel-Gruber syndrome (MKS) type 5 are ascribed to mutations in the *NPHP8/RPGRIP1L* gene, encoding a protein primarily localized to the base and axoneme of cilia in the kidney, brain, and retina. These mutations are thought to interfere with the protein's normal interaction with nephrocystin-4. JBTS type 8 has been shown to be caused by mutations in *ARL13B* gene, encoding for ARL13B which belongs to the Ras GTPase family and in other species is required for ciliogenesis, body axis formation, and renal function. The underlying gene mutations for JBTS type 1 and JBTS type 2 loci are yet to be identified (Hildebrandt & Zhou 2007; Simms et al. 2009; Ramamurthy & Cayouette 2009; Tobin & Beales 2009; Deltas & Papagregoriou 2010).

1.3.2.7 Meckel-Gruber Syndrome

The Meckel-Gruber syndrome (MKS) is a lethal autosomal recessive disorder characterized by renal cystic dysplasia with fibrotic changes in the liver, occipital encephalocoele or some other central nervous system malformation. Polydactyly is frequently reported, and some patients have cleft palate, cardiac abnormalities, and incomplete development of genitalia and gonads. Patients that survive to term invariably die of respiratory and/or renal failure. Six loci have been linked to MKS, and five genes have been identified thus far (*MKS1*, *MKS3* through *6*). All identified gene products are associated with ciliary functions. MKS1 interacts with MKS3/meckelin, which is predicted to be a multi-pass transmembrane protein. MKS phenotype has also been described for mutations of *NPHP3*, *NPHP6/CEP290*, and *NPHP8/RPGRIP1L*, and mutations in three BBS genes (*BBS2*, *BBS4* and *BBS6*) have been shown to cause MKS-like phenotypes (Kim et al. 2008; Hildebrandt et al. 2009; Simms et al. 2009; Tobin & Beales 2009).

1.3.2.8 Jeune asphyxiating thoracic Syndrome

The Jeune asphyxiating thoracic syndrome (JATD) is a rare autosomal recessive chondrodysplasia. Patients have a small rib cage and narrow chest, which obstructs the lungs and can cause death by asphyxiation in affected children. In addition, the long bones, such as the femur, are short, as are bones of the hands and feet, and up to 50% of all cases have postaxial polydactyly. Biliary dysgenesis with portal fibrosis and bile duct proliferation, renal cytogenesis and failure, situs inversus and cardiac malformations, and retinal degeneration can occur. Recessive mutations of *IFT80*, which encodes a component of the intraflagellar transport machinery, have been found to underlie a subset of JATD cases (Figure 1.13). To date, JATD is the only human ciliopathy that is associated with mutations in an IFT protein. Mutations in *DYNCH2H1*, encoding a dynein complex subunit, have also been identified (Beales et al. 2007; Tobin & Beales 2009; Lehman et al. 2010).

1.3.3 Mechanisms of Disease

The presence of primary cilia on nearly every cell of the human body, together with the multiple signalling pathways controlled through the primary cilia, provides an explanation for the extensive pleiotropy that characterizes ciliopathies. In addition, observations that mutations in a single gene can lead to a broad array of phenotypes in ciliopathies has blurred the boundaries between these diseases, and led to an emerging concept of a spectrum disease. Most ciliopathies are genetically heterogeneous, where mutations in different genes can cause the same disease. Moreover, these diseases can have complex non-Mendelian patterns of inheritance, such as oligogenic inheritance, whereby mutations in more than one locus segregate with the disease in families, potentially collaborating to modulate the penetrance and expressivity of the disorder, as in the case of BBS and NPHP. Another possibility is that mutations in a given gene might be related to distinct clinical entities as a causal or modifying factor. For instance, *RPGRIP1L* contributes alleles to the pathogenesis of NPHP, JBTS and MKS, mutations in *NPHP6/CEP290*

are associated with NPHP, MKS and BBS, and mutations in *MKS3* have also been found in JBTS patients (Cardenas-Rodriguez & Badano 2009; Lee & Gleeson 2010).

Although ciliopathies can be recognized as distinct clinical entities, it is becoming apparent that these are determined by not only the specific gene that is mutated, its biological role and pattern of expression, but also by the type and effect of the mutation on protein function and the total mutational load across different ciliary genes. As a result, it is likely that many ciliary proteins are components of large multi-subunit complexes. The absence or dysfunction of one of these components affects the function of the whole, thus resulting in a range of phenotypic severity (Adams et al. 2008; Cardenas-Rodriguez & Badano 2009; Deltas & Papagregoriou 2010).

1.3.3.1 Kidney cyst formation

Cystic pathology is proposed to be the result of abnormal cell proliferation and deregulated apoptosis, increased secretion of fluids into the tubular lumen, irregular cell-matrix interactions, and defective cellular polarity. Fisher et al. (2006) have shown that lengthening of renal tubules is associated with the mitotic orientation of cells along the tubule axis, an intrinsic planar cell polarization (PCP) process. Moreover, their studies in mutant rodent models for ADPKD suggest that defects in PCP are responsible for cyst development. In a flow gradient, as in the kidney tubule, all primary cilia align in a single direction, determining the direction in which the cilia bend. As a result, the flow, and therefore the bend, is always in the anterior-posterior direction so that the gradient of Ca^{2+} concentration or other signalling molecules along the cellular axes should be uniform from cell to cell. It has been proposed that cilia may sense the direction of primary urinary flow and provide a vectorial cue for the observed PCP and oriented cell division. By determining a consistent anterior-posterior orientation of the mitotic spindle for cell division, primary cilia, together with PCP signalling, provide renal tubules with the capacity to maintain a constant diameter, despite the intense proliferative phase that

accompanies tubular lengthening. Thus, deregulated PCP disrupts the normal cell division and tubule lengthening leading instead to cystic dilation (Fischer et al. 2006; Zhou 2009; Veland et al. 2009; Deltas & Papagregoriou 2010; Satir et al. 2010).

NPHP2/Inversin also implicates cilia and PCP in cystogenesis. *NPHP2/Inversin* mutations are the cause of infantile NPHP whose renal cystic changes combine clinical features of NPHP and PKD. Inversin has been shown to inhibit the canonical Wnt pathway, concomitantly inducing PCP activity necessary to maintain normal tubular development and morphology. Furthermore, fluid flow in renal cells was shown to increase the levels of Inversin in cultured kidney cells, suggesting that, in developing renal tubule, urine flow terminates canonical Wnt signalling in favour of PCP which will pattern the tubule. Consequently, when inversin in defective (as in the case of NPHP type 2), canonical Wnt pathway will prevail and disrupt the apical-basolateral polarity of renal epithelium (Simons et al. 2005; Hildebrandt et al. 2009; Tobin & Beales 2009). BBS proteins have also been reported to modulate the balance between canonical and non-canonical Wnt signalling. Loss of BBS function leads to PCP defects and the concomitant upregulation of canonical Wnt through the stabilization of β-catenin (Gerdes et al. 2007; Cardenas-Rodriguez & Badano 2009). These studies suggest that in ciliopathy mutants, kidney cyst formation may arise from unopposed canonical Wnt signaling that suppresses terminal differentiation of tubular cells. Because cilia are proposed to act to inhibit Wnt signaling, the absence or dysfunction of proteins necessary for its correct assembly and function relieves this brake, causing excess canonical Wnt pathway-dependent proliferation, combined with concomitant defects in planar cell polarization. On the other hand, a recent study using mice lacking Jouberin protein, the product of the *AHI1* gene which is mutated in Joubert syndrome, identified a role for canonical Wnt signaling in adult mammalian homeostasis, and found that abrogation of this signaling can lead to cystic kidney pathogenesis. These seemingly contradictory results suggest a unique balance of Wnt signaling regulation modulating renal development and homeostasis (Lancaster et al. 2009).

Polycystin 1 (PC1) has also been shown to regulate activity of mammalian target of rapamycin (mTOR), a serine/threonine protein kinase with essential roles in protein translation, cell growth, and proliferation. The dysregulation of the mTOR pathway is implicated in various types of cancer. In cystic epithelium, mTOR activity is elevated, and treatment of rodent PKD models with rapamycin, an inhibitor of mTOR, has been shown to alleviate the cystic phenotype in these animal models. The disruption of cilia or mutations in PC1 are proposed to result in loss of a PC1/mTOR inhibitory complex in the cilium, which in turns leads to increased proliferation and cyst development (Zhou 2009; Tobin & Beales 2009).

1.3.3.2 Retinal-renal involvement

Photoreceptor cells rely on IFT for transport of proteins and lipids between the inner and outer segments along the connecting cilium. The involvement of multiple organs, a prominent feature of ciliopathies, suggests the disruption of global ciliogenesis and/or transport mechanisms. Thus, it is not surprising that defects in intersegmental transport in photoreceptors, due to dysfunction or absence of ciliary or basal body proteins, can give rise to retinitis pigmentosa (RP) or blindness due to retinal degeneration in many ciliopathies, including BBS, JBTS and SLSN. For example, although mutations in RPGR account for approximately 20% of all RP cases, RPGR is not specific to photoreceptors and some mutations in RPGR also lead to systemic manifestations. Also, mutations in RPGRIP, another component of the connecting cilium, have been associated with ciliopathies like SLSN and JBTS. Indeed, the retinal-renal involvement in SLSN can be explained by the fact that the connecting cilium of the photoreceptor cells in the retina and the primary cilium of renal epithelial cells are structurally equivalent, and the expression of proteins such as nephrocystin-5, nephrocystin-6 and RPGRIP proteins in both structures. The localization of the BBSome proteins to the base of the connecting cilium, together with results showing that the inactivation of Rab8 in photoreceptor cells leads to photoreceptor degeneration, provides a potential mechanism for the retinal

degeneration observed in BBS (Hildebrandt & Zhou 2007; Ramamurthy & Cayouette 2009; Wright et al. 2010).

1.3.3.3 Neuronal function

In contrast to motile cilia, primary cilia are present on most cells in the brain and, surprisingly, all neurons display a primary cilium. Since Shh has a central role in proliferation of cerebellar granule neurons, and cilia are critical for the transduction of Shh signals, it has been suggested that the cerebellar hypoplasia observed in Joubert syndrome (JBTS) and other ciliopathies may arise from defective Shh signalling. Mechanotransport along microtubules is important for intraciliary and axonal transport. Indeed, the subunit of IFT motor kinesin-II, KIF3A, which is mutated in a cystic mouse model, also plays a role in axonal transport. Because malformations of the cerebellum observed in JBTS consist of abnormal decussating (crossing) of neurons, defective axonal outgrowth and axon guidance may explain neurological defects such as the ocular motor apraxia type Cogan (associated with *NPHP1* and *NPHP4* mutations), cerebellar vermis hypoplasia (in JBTS), and mental retardation (in *NPHP6*) (Hildebrandt & Zhou 2007; Han & Alvarez-Buylla 2010; Lee & Gleeson 2010).

Bardet-Biedl syndrome (BBS) and Alström syndrome (AS) patients frequently display hyperphagia-induced obesity. Specific hormone receptors associated with feeding behaviour localize to the cilia of the hypothalamus. Studies on some of these proteins have revealed their mislocalization in neurons of mice that have mutations in *Bbs2*, *Bbs4* or *Bbs6* genes that correspond to those observed in individuals with BBS and the obesity condition. Thus, ciliary receptors in the hypothalamic neurons regulate the feeling of satiety and hunger, controlling feeding behaviour accordingly (Tobin & Beales 2009; Han & Alvarez-Buylla 2010; Satir et al. 2010; Lee & Gleeson 2010).

1.3.3.4 Situs inversus

Situs inversus, the complete reversal of organ laterality, is one of the most prominent features of ciliopathies. *NPHP2* encodes for Inversin, which has been shown to be necessary to position cilia in cells of the ventral node by Okada et al (1999). In the mouse model, inversion of embryonic turning (inv) where Inversin is disrupted, nodal cilia present defective orientation, which results in abnormal movement and decreased nodal flow explaining the characteristic left-right specification defects of these animals (Simons et al. 2005; Hildebrandt et al. 2009; Simms et al. 2009; Tobin & Beales 2009).

1.3.3.5 Skeletal abnormalities

The presence of several Shh-associated phenotypes in patients with ciliopathy, including polydactyly, external genitalia anomalies, and craniofacial defects suggests a potential Shh signalling defect in these ciliopathy mutants. Postaxial polydactyly is a common feature of ciliopathies, present in BBS, JATD, MKS and JBTS. Moreover, BBS4 has been shown to be necessary for responsiveness to Shh signalling and activation of downstream targets (Cardenas-Rodriguez & Badano 2009; Tobin & Beales 2009; Goetz & Anderson 2010).

1.4 ORAL-FACIAL-DIGITAL SYNDROME TYPE 1

Oral-facial-digital syndromes (OFD) are a group of developmental disorders that feature malformations of the face, oral cavity, and digits. Other organ systems can be involved, and current classification systems have identified at least thirteen different forms of OFD. OFD1, the most common type, occurs in 1:50,000 births, and its X-linked dominant transmission with prenatal lethality in affected males and the occurrence of cystic kidney disease distinguish it from other types of OFD (Feather et al. 1997; Toriello 2009a).

With the exception of OFD1 and OFD2, there are only a few reports of the other types of OFD. These conditions are therefore less well-defined, and distinction

among them is based on one or more unusual findings. Also, there are many reports of individuals with conditions that are difficult to classify, and several other reports of children with a phenotype that appears to be either an overlap of several OFD, or an overlap of an OFD with some other condition. Since other than OFD1, the causative genes for these conditions are unknown, and chromosome studies have generally been found to be normal, there are no clues yet to explain these other forms of OFD. It is possible that, as with other ciliopathies, a potential explanation for this heterogeneous group of conditions may lie in the fact that different phenotypes can result from mutations in the same gene (Toriello 2009a; Thauvin-Robinet et al. 2009).

1.4.1 Clinical spectrum of OFD1 syndrome

Dysmorphic features affecting the head, observed in about 87% of cases of OFD1 syndrome, include facial asymmetry, hypertelorism, micrognathia, broadened nasal ridge, facial milia, telecanthus, flat face, and sparse hair or alopecia. Oral cavity lesions have been reported in about 97% of cases, and include pseudoclefting of the upper lip, clefts of the palate and tongue, oral frenulae, alveolar ridge notching and dental abnormalities. The digital abnormalities (which affect the hands more often than the feet) are also quite common (about 88% of cases) and include syndactyly, brachydactyly, clinodactyly, and, more rarely, pre- or postaxial polydactyly. Short stature is observed in about 7% of cases. Central nervous system abnormalities are reported in about 50% of the cases, and include cerebellar hypoplasia, agenesis of the corpus callosum, hydrocephaly, arachnoid cysts, and mental retardation and/or selective cognitive impairment. Decreased hearing acuity has also been reported in a few cases. Polycystic kidney disease (PKD) is found in about one-third of patients, and although cysts resulting in early renal failure have been described in children, the age of onset of cystic kidneys is most often adulthood. Indeed, the probability to develop renal failure has been estimated to be more than 50% after the age of 36 years, and renal involvement has been reported to completely dominate the clinical course of the disease in some patients. Additional findings include pancreatic,

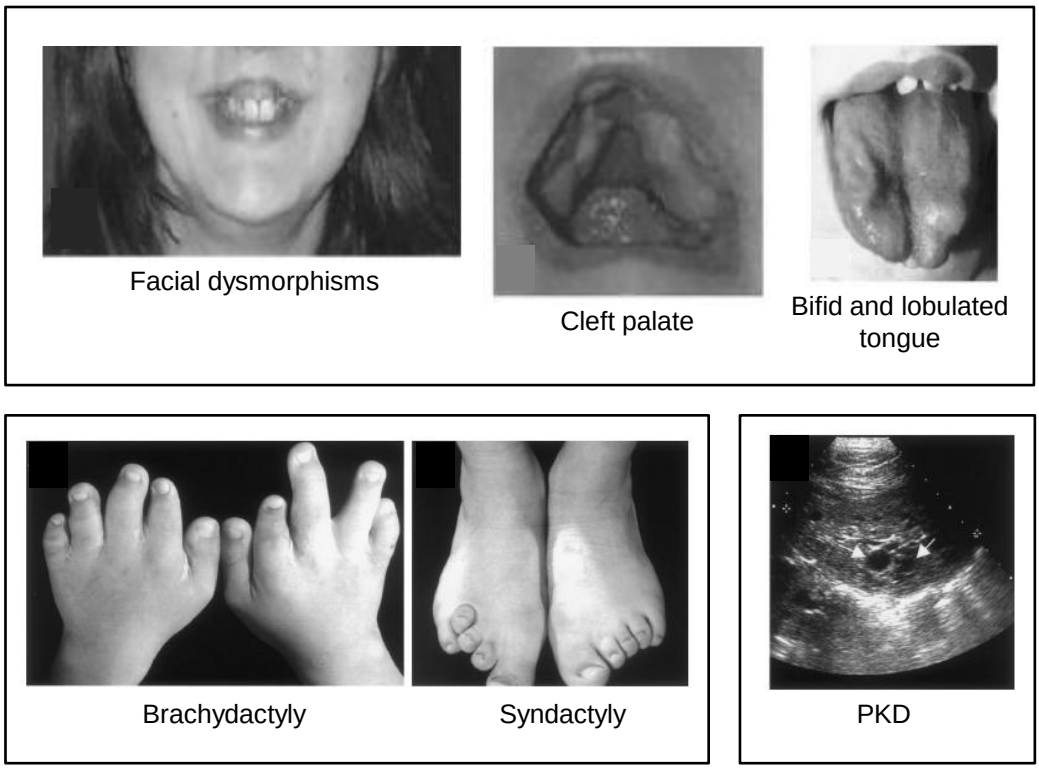

Figure 1.14 Oral-facial-digital syndrome type 1
Examples of the oral-facial-digital findings observed in OFD1 patients. Top panel: facial dysmorphisms, cleft palate, and bifid and lobulated tongue. Bottom left panel: limb abnormalities are also frequent. Upper- and lower-digit abnormalities in a 12-year-old girl with OFD1. Bottom right panel: ultrasound scan of kidney of the same individual who is depicted in the left hand panel. The patient had chronic renal excretory failure and polycystic kidneys: note the cysts (white arrows), up to 1 cm in diameter, located in the parenchyma of the organ. This figure is adapted from Ferrante et al. (2001) and Prattichizzo et al. (2008).

hepatic, and/or ovarian cysts in about 5% of cases (Figure 1.14) (Ferrante et al. 2001; Macca & Franco 2009; Toriello 2009a; Saal et al. 2009).

1.4.2 Molecular basis of OFD1 syndrome

OFD syndrome type 1 (OFD1) was first identified in 1954 and named orodigitofacial dysostosis or Papillon-League-Psaume syndrome, and later renamed oral-facial-digital syndrome type 1. In 2001, Ferrante et al. discovered that the syndrome is caused by mutations in the *OFD1* gene (formerly named *Cxorf5/71-7A*). The locus for this gene had been previously mapped by linkage analysis in the Xp22 region (Xp22.2-p22.3) by Feather et al. (1997), being the first gene for an X-linked dominant male lethal disorder found to escape X inactivation by de Concillis et al. (1998) (Feather et al. 1997; de Conciliis et al. 1998; Ferrante et al. 2001). The *OFD1* gene has an open reading frame of 3033 base pairs (bp) over 23 exons. Due to alternative splicing, *OFD1* has at least two transcripts. *OFD1a* encodes for a 1012-amino acid protein (hereafter called OFD1) which contains a Lis1 homology (LisH) motif in its N-terminal region and six predicted coiled-coil (CC) domains distributed along the C-terminal region. Based on analysis of other LisH-containing proteins as well as OFD1, the LisH motif may play roles in protein interactions, protein stability and intracellular localization, regulation of microtubule dynamics, cell migration, nucleokinesis and chromosome segregation. The coiled-coil domains are thought to mediate subunit oligomerization and protein-protein interactions. An alternative 3´ splice site in intron 9 (created by the insertion of additional 663 bp) introduces an in-frame stop codon in exon 10, generating *OFD1b* encoding a 367 amino acid protein containing the first 353 residues of OFD1 and an alternative C-terminal region (de Conciliis et al. 1998; Emes & Ponting 2001; Romio et al. 2003; Gerlitz et al. 2005; SMART (http://smart.embl-heidelberg.de)).

To date 99 different mutations have been identified in individuals with OFD1. Mutation analysis has revealed that 7 are genomic deletions and 92 are point mutations, which include 14 missense (12%), 13 nonsense (11%), 14 splice site

mutations (12%), 1 in-frame deletion, and 67 frameshifts, which account for the vast majority of mutations (58%). These are scattered along the first 17 exons of OFD1 and the majority of mutations occur in exons 3, 8, 9, 12, 13 and 16. Genomic deletions account for 23% of OFD1 cases negative for DNA sequencing, and the ones identified thus far include deletions of exon 5, exon1-8, exons 1-14, exons 10-11, exons 13-23, exon 17, and one case of a double deletion encompassing exons 7 to intron 9 and a 14 bp deletion in intron 9 (Ferrante et al. 2001; Rakkolainen et al. 2002; Romio et al. 2003; Thauvin-Robinet et al. 2006; Prattichizzo et al. 2008; Thauvin-Robinet et al. 2008). Most mutations occur in the first half of the gene, generally causing a truncated protein, and thus a loss of function mechanism. It is possible that mutations in other parts of the gene or those affecting function in a different manner could be responsible for other phenotypes. Still, mutations have been identified in about 85% of OFD1 patients. Interestingly, a frameshift mutation in exon 16 of the *OFD1* gene has been identified in male members of a family with the X-linked recessive Simpson-Golabi-Behmel syndrome type 2 (SGBS2), a mental retardation syndrome comprising macrocephaly and ciliary dysfunction. Moreover, two frameshift mutations in exon 21 of *OFD1* have been identified in males with Joubert syndrome (JBTS), presenting with mental retardation accompanied by postaxial polydactyly and retinitis pigmentosa. These observations offer a potential explanation for the phenotypic spectrum observed for *OFD1* mutations, which now includes OFD1, SGBS2 and JBTS (Figure 1.15) (Budny et al. 2006; Macca & Brunella Franco 2009; Coene et al. 2009; Toriello 2009a).

1.4.3 Functional studies on OFD1

The *OFD1* gene is ubiquitously expressed in human adult tissues. Moreover, consistent with previous RNA *in situ* studies in mice embryonic tissues, Northern blot analysis of organs from normal human embryos revealed the presence of OFD1 transcript in all the organs affected in this syndrome (de Conciliis et al. 1998; Ferrante et al. 2001; Romio et al. 2003). Thus, OFD1 is also expressed during development.

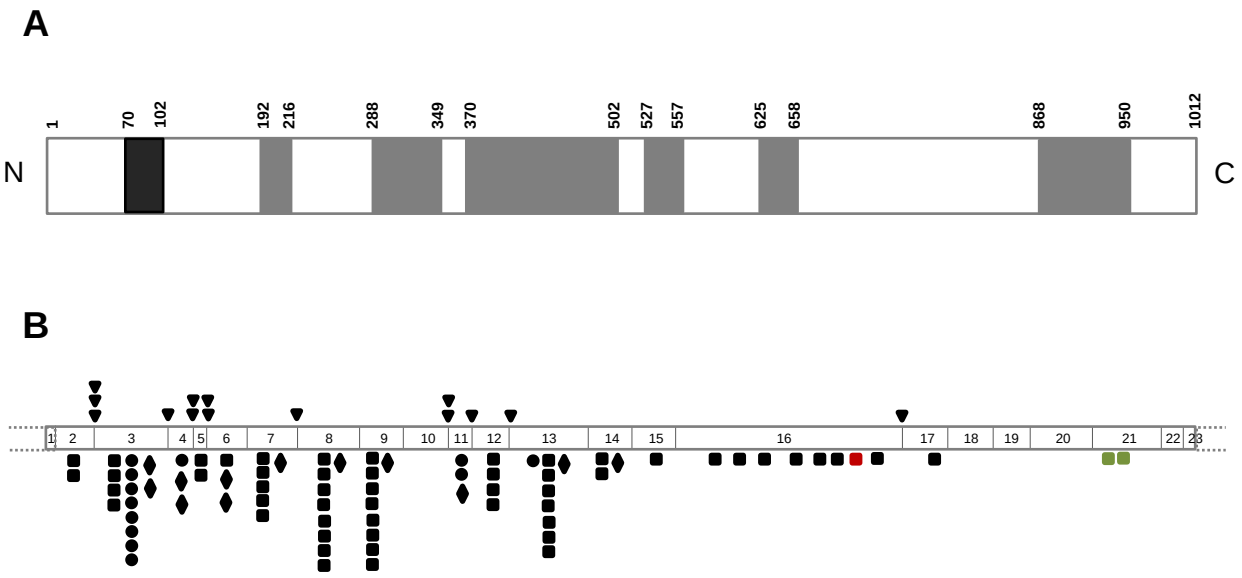

Figure 1.15 Molecular basis of OFD1
(A) Schematic representation of OFD1 protein. LisH (black) and coiled-coil (grey) motifs, as well as amino acid numbers, are indicated. **(B)** Schematic representation of OFD1 gene. The diagram depicts the 23 exons of OFD1 gene, and the positions of intron/exon boundaries are indicated by vertical bars. This is in scale so that the OFD1 protein domains shown above are aligned with their coding sequence below. All the point mutations identified to date in the literature are also shown (Ferrante et al. 2001; Rakkolainen et al. 2002; Romio et al. 2003; Thauvin-Robinet et al. 2006; Prattichizzo et al 2008; Budney et al. 2006; Coene et al. 2009). Point mutations are reported as frameshift (square); splice-site (triangle); nonsense (diamond); and missense (circle). The frameshift mutation in exon 16 depicted in red has been described in X-linked Simpson-Golabi-Behmed-like syndrome (Budney et al. 2006) and the frameshift mutations in exon 21 (green) have been described in X-linked Joubert syndrome (Coene et al. 2009). This diagram is adapted from Macca et al. (2009). Full description of mutations can be found in Macca et al. (2009).

Previous studies have demonstrated that OFD1 is a core component of the human centrosome throughout the cell cycle, is detected at the basal body and, in rare cases, along the primary cilium, thus confirming that OFD1 syndrome is a ciliopathy (Romio et al. 2003; Romio et al. 2004). More specifically, OFD1 has very recently been shown to localize to the distal regions of centrioles. Here, it appears to be important in the control of centriole length, centriole distal appendage formation and centriolar recruitment of the intraflagellar transport protein Ift88 (Singla et al. 2010). Another study has also reported OFD1 in the nucleus. Consistent with this finding, OFD1 was found to interact with RuvBl1, a protein belonging to the AAA^{+}-family of ATPases and a component of the multiprotein nuclear complex TIP60, raising the possibility that it may play direct roles in regulation of gene expression (Giorgio et al. 2007). Notably, OFD1 has been identified as an interacting partner of lebercilin, a protein encoded by a gene whose mutations cause Leber congenital amaurosis (LCA), another ciliopathy condition (Coene et al. 2009).

Animal models for OFD1 have been generated in mouse and zebrafish. The mouse model reproduced the main features observed in the human condition, with an increased severity possibly due to the differences of X-inactivation patterns observed between human and mouse. Mutant male embryos exhibited lack of cilia in the embryonic node, and displayed left-right axis specification defects, suggesting that Ofd1 is required for primary cilia formation and left-right axis specification. Moreover, defective cilia formation was observed in heterozygous females, exhibiting cystic kidneys and lack of cilia on the surface of epithelial cells lining the cysts. Heterozygous females also displayed severe craniofacial abnormalities, and limb and skeletal defects (Ferrante et al. 2006). Further supporting that Ofd1 is required for normal biology of cilia, Ofd1 inactivation in zebrafish resulted in a typical ciliary phenotype with bent body, laterality defects, and oedema (Ferrante et al. 2009). In agreement with this, OFD1 is required for primary cilia formation in cultured cells (Graser et al. 2007; Corbit et al. 2008; Singla et al. 2010). Furthermore, while mutant male mouse embryos showed altered expression of

Sonic hedgehog (Shh) signaling pathway genes, zebrafish mutant embryos exhibited convergent extension (CE) defects during gastrulation, which were accentuated by loss of PCP pathways genes. These findings demonstrate that Ofd1 inactivation is associated with defective Shh and Wnt signaling pathways, possibly through disruption of ciliogenesis (Ferrante et al. 2006; Ferrante et al. 2009; Macca & Franco 2009).

1.5 AIMS AND OBJECTIVES OF THIS PROJECT

Unquestionably, the ciliary hypothesis of cystic kidney disease has revolutionized studies into the pathogenesis of many genetic diseases. Studies linking cilia/basal body/centrosome proteins to human genetic disorders (collectively now known as ciliopathies) have clearly shown that compromised ciliary function have profound consequences in the development and cellular homeostasis.

The fact that mutations in the *OFD1* gene lead to polycystic kidney disease, together with the reported centrosomal/basal body location of its protein product, led us to speculate that OFD1 may be involved in the biogenesis, maintenance or signalling function of primary cilia. Progress over the past years, has led to a better understanding of the role of primary cilia in normal mammalian development. However, despite advances in the characterization of OFD1 at the molecular level, the biological function and importance of OFD1 for centrosome and cilia activity remain unknown. In this project, we set out to test the hypothesis that the *OFD1* gene encodes a protein critical to the organization and function of cilia through its molecular role at the centrosome. This would be achieved through examination of OFD1 protein localization and dynamics, the functional analysis of OFD1 through RNA-mediated interference, the identification of interacting partners of OFD1, and the consequences of expression of truncated versions of OFD1.

CHAPTER 2

MATERIAL AND METHODS

CHAPTER 2 MATERIAL AND METHODS

2.1 MATERIALS

2.1.1 Chemicals suppliers

All chemicals were of analytical grade purity or higher and supplied by Sigma (Poole, UK), Roche (Lewes, UK), or as stated below.

Reagent	Supplier
OFD1 and BBS4 siRNA oligoribonucleotides	Dharmacon (Lafayette Colorado, USA)
Poly-prep columns	Bio-Rad (Hemel Hempstead, UK)
Precision Plus all blue protein standards	
Hoechst 33258	Calbiochem (Nottingham, UK)
Leptomycin-B	
Roscovitine	
EDTA; EGTA; NaCl; KCl; Na_2HPO_4; KH_2PO_4	Fisher Scientific (Loughborough, UK)
Ethanol	
Glacial acetic acid	
Methanol	
Super RX X-Ray film	Fuji Photo Film (Tokyo, Japan)
Bovine serum albumin (fraction V)	Fluka (Gilligham, UK)
Protogel liquid acrylamide (30% w/v)	Flowgen Bioscience (Nottingham, UK)
BCA protein assay reagent	Pierce (Rockford, USA)
Slide-A-Lyzer dialysis cassettes	
Yeast extract	Oxoid (Rockford, USA)
Bacto-agar	
Bacto-tryptone	
GeneRuler 1 kb DNA ladder	Fermentas (York, UK)

NI-NTA agarose	Invitrogen/Gibco (Paisley, UK)
Oligonucleotide primers	
Penicillin/streptomycin	
0.05% Trypsin-EDTA	
D-MEM with Glutamax	
D-MEM:F12 (1:1)	
Opti-MEM	
Lipofectamine 2000	
QIAfilter plasmid miniprep spin kit	Qiagen (Hilden, Germany)
QIAfilter plasmid maxiprep kit	
QIAfilter PCR purification/nucleotide removal kit	
PCM-1 siRNA oligoribonucleotides	
jetPRIME	Polyplus Transfection (New York, USA)
3MM chromatography paper	Whatman International (Maidstone, UK)
Nitrocellulose transfer membrane	Schleider & Schuell (Dassel, Germany)
Coverslips 22mm/13mm diameter, No. 1.5	VWR International (Lutterworth, UK)
Glass slides	

2.1.2 Vectors and constructs

Vector	Application	Supplier
pCMV-Tag-3c	Eukaryotic protein expression	Stratgene (Stockport, UK)
pGEX-4T-1	Bacterial protein expression	GE Healthcare (Chalfont St Giles, UK)
pETM-11	Bacterial protein expression	EMBL

Plasmid and tag	Vector	From
Myc-dynamitin	pCMV-myc	gift from Dr. Richard Vallee (New York, USA)
GFP-BBS4	pEGFP	gift from Dr. Phil Beales (London, UK)

PCM-1-FL-GFP	pEGFP	gift from Dr. Andreas Merdes (Toulouse, France)
PCM-1-NTD-GFP		
PCM-1-CTD-GFP		

2.1.3 Antibodies

2.1.3.1 Primary antibodies

Primary Antibodies	Dilution ([ab])*	Supplier
Anti-GFP (mouse)	1:500 (0.25 µg/ml)	Abcam (Cambridge, UK)
Anti-GFP (rabbit)	1:1000 (0.1 µg/ml)	
Anti-CEP290 (rabbit)	1:200	
Anti-pericentrin (rabbit)	1:1000 (0.5 µg/ml)	
Anti-GST	1:5000	Santa Cruz (Heildelber, Germany)
Anti-centrin2 (N17;rabbit)	1:100 (2 µg/ml)	
Anti-Myc (mouse)	1:1000	Cell Signalling (Hitchin, UK)
Anti-α-tubulin (mouse)	1:2000 (0.3 µg/ml)	Sigma (Poole, UK)
Anti-γ-tubulin (mouse)	1:500	
Anti-γ-tubulin (rabbit)	1:500	
Anti-acetylated tubulin (mouse)	1:1000 (1 µg/ml)	
Anti-OFD1 (rabbit) (Ab1)	1:100	Gift from Prof. Adrian Woolf (Manchester, UK)
Anti-OFD1 (rabbit) (Ab2)	1:100 (2.7 µg/ml)	This study
Anti-BBS4 (rabbit)	1:250	
Anti-PCM-1 (rabbit)	1:1000	Gift from Dr. Andreas Merdes (Toulouse, France)
Anti-C-Nap1 (rabbit)	1:1000 (1 µg/ml)	Prof. Andrew Fry (Leicester, UK)

* Where known, final antibody concentrations are stated in brackets after the working dilution

2.1.3.2 Secondary antibodies

Secondary Antibodies	Dilution ([ab])*	Supplier
Anti-mouse alkaline phosphatese conjugate	1:7500 (0.1 µg/ml)	Promega (Southampton, UK)
Anti-rabbit alkaline phosphatase conjugate	1:7500 (0.1 µg/ml)	
Anti-mouse horseradish peroxidase conjugate	1:1000	Sigma (Poole, UK)
Anti-rabbit horseradish peroxidase conjugate	1:1000	
Anti-mouse Alexa 488 nm	1:200 (10 µg/ml)	Invitrogen (Paisley, UK)
Anti-rabbit Alexa 488 nm	1:200 (10 µg/ml)	
Anti-mouse Alexa 594 nm	1:200 (10 µg/ml)	
Anti-rabbit Alexa 594 nm	1:200 (10 µg/ml)	

* Where known, final antibody concentrations are stated in brackets after the working dilution

2.1.4 Bacterial strains

Bacterial strain	Supplier
DH5a-T1R competent bacteria	Invitrogen/Gibco (Paisley, UK)
Rosetta 2(DE3) *E. coli* competent cells	Novagen (Nottingham, UK)

2.2 MOLECULAR BIOLOGY TECHNIQUES

2.2.1 Cloning

The standard cloning procedure involved amplification of insert DNA by polymerase chain reaction (PCR), followed by restriction digestion of purified PCR products and of the destination vector, which was subject to dephosphorylation, before ligation of the two under appropriate conditions. Selected colonies were used to prepare bacterial cultures from which DNA was prepared and verified by DNA sequencing. Each of these steps is described in more detail below. OFD1 fragments were amplified by PCR using full-length human OFD1 cDNA as the template (Romio et al.

2004). Amplified fragments were subcloned into the mammalian expression vector pCMV-Tag3C (Stratagene) and bacterial expression vectors pGEX-4T-1 (GE Healthcare) and pETM-11 (EMBL) providing N-terminal myc, GST or His tags, respectively.

2.2.1.1 Oligonucleotide design

Oligonucleotides designed for PCR-based cloning were between 20-25 bp in length with an AT:GC ratio of approximately 50% to ensure an annealing temperature of around 50-60ºC. To incorporate appropriate restriction enzyme sites for cloning, additional bases were added to the 5' end of the oligonucleotide sequences with additional bases added to ensure maintenance of the correct reading frame upon insertion into the vector, as necessary.

2.2.1.2 Polymerase chain reaction

PCR amplification was carried out to obtain insert DNA for cloning. A standard reaction mixture was 50 µl in volume and typically contained 0.1-1 µg template DNA, 0.4 µM forward primer, 0.4 µM reverse primer, 0.1-0.5 mM $MgCl_2$, 0.2 mM dNTPs, 1 U Expand high fidelity proof-reading DNA polymerase, 1x PCR amplification buffer and the appropriate volume of sterile water to complete the reaction volume. The basic PCR reaction consisted of one cycle of denaturation at 94ºC for 2 min, followed by 25 cycles of denaturation at 94ºC for 30 sec, annealing at the appropriate temperature for 30 sec and elongation at 72ºC for the appropriate extension time (1 min per kb), followed by one cycle of extension at 72ºC for 7 min. Annealing temperatures and elongation times suitable for each set of primers and template, respectively, were employed as appropriate. PCR products were then analysed by agarose gel electrophoresis to assess yield.

2.2.1.3 Agarose gel electrophoresis

DNA was combined with loading buffer (50% v/v glycerol, 100 mM EDTA, 0.3% v/v bromophenol blue) in a 1:5 ratio and resolved by electrophoresis on a 1% (w/v)

agarose gel made by dissolving agarose in 1x TBE (89 mM Tris-HCl, 89 mM Boric acid, 1 mM EDTA pH 8.0) supplemented with ethidium bromide (0.5 µg/ml). 2 µl of 1 kb markers were added to a separate well and electrophoresis was carried out at 80 V for 45 min. DNA was analysed then by UV transillumination and images captured using a Gene Genius CDC gel documentation system (Syngene, Cambridge, UK).

2.2.1.4 Purification of PCR products for cloning

Upon verification that sufficient levels of a PCR product of the appropriate size were obtained, PCR products were purified for cloning using a PCR purification kit (Qiagen) according to the manufacturer's instructions. Purified DNA was eluted in 50 µl of sterile water and product yield and DNA concentration was assessed by comparison to known DNA concentrations on a DNA agarose gel or by UV light at OD_{260} (BioPhotometer plus, Eppendorf).

2.2.1.5 Restriction enzyme digest

Purified insert DNA and destination vector were digested with the appropriate restriction enzymes using suitable buffer conditions and temperature, as specified by the manufacturer. Typically, restriction digest was performed by incubating 10 U restriction endonucleases and appropriate buffer with approximately 5 µg DNA at 37ºC for 2 hours. Double digestions were performed by the addition of the second enzyme to the reaction or a separate experiment performed after removal of the first enzyme using a nucleotide removal kit (Qiagen). The total reaction volume of the digested insert DNA was purified using a nucleotide removal kit (Qiagen) and eluted in 30 µl of sterile water. The total reaction volume of the digested vector was incubated at 65ºC for 15 min to inactivate enzyme activity before dephosphorylation.

2.2.1.6 Vector dephosphorylation

Dephosphorylation of the linear vector DNA was performed by incubating the total reaction volume of digested vector with approximately 3 U shrimp alkaline phosphatase and appropriate buffer at 37ºC for 15 min. The total reaction volume

was then purified using a nucleotide removal kit (Qiagen) and DNA was eluted in 30 µl of sterile water.

2.2.1.7 DNA ligation

Before ligation, the yield of purified DNA fragments was assessed by agarose gel electrophoresis in order to assess DNA concentrations for ligation. Ligation reactions were carried out using a rapid DNA ligation kit (Roche). Typically, vector:insert molar ration of 1:3 was employed in a standard reaction mix of 50 ng vector DNA, 150 ng insert DNA and 5 U DNA ligase diluted in the appropriate volume of ligation buffer. Reactions were incubated for 5-15 min at room temperature.

2.2.1.8 Transformation of competent bacteria

For cloning, 100 ng of ligated DNA was added to 100 µl of chemically competent DH5α, which had been defrosted on ice, and the slurry was mixed by gently tapping the side of the tube. The mix was incubated on ice for 30 min, heat shocked at 42ºC for 1 min to induce plasmid DNA uptake, and returned to the ice for a further 2 min. 500 µl of pre-warmed Luria Bertani (LB) media (10 g/l tryptone, 5 g/l yeast extract, 5 g/l NaCl, pH 7.0) was added to the cells and the transformation mix was incubated at 37ºC, 225 rpm for 1 hour. Following incubation, the transformation mix was briefly spun down to pellet transformed cells. These were then gently resuspended in approximately 200 µl of remaining supernatant and cell suspension was spread onto LB agar plates containing the appropriate antibiotic for selection (10 g/l tryptone, 5 g/l yeast extract, 5 g/l NaCl, agar 2% w/v, pH 7.0, plus ampicillin 100 µg/ml or kanamycin 50 µg/ml, as appropriate). Plates were incubated for 12-14 hours at 37ºC. Colonies were then picked for plasmid preparation.

2.2.1.9 Isolation of plasmid DNA by DNA miniprep

Individual bacterial colonies were picked off LB agar plates, inoculated into 5 ml LB containing the appropriate antibiotic and incubated at 37ºC, 225 rpm for 12-16

hours. Following incubation, cells were recovered by centrifugation (2500 g, 10 min) and DNA was isolated using a QIAfilter plasmid miniprep kit (Qiagen) according to the manufacturer's instructions. DNA was eluted in 50 µl of sterile water.

2.2.1.10 DNA sequencing

Automated DNA sequencing was employed to verify the presence of the appropriate insert and the correct reading frame. This was carried out by PNACL (The Protein Nucleic Acid Chemistry Laboratory), Leicester.

2.2.2 Isolation of plasmid DNA by DNA maxiprep

For isolation of large quantities of high quality, pure plasmid DNA for transfection, DNA plasmid maxipreps were used. Starter cultures were made by inoculating 5 ml LB containing the appropriate antibiotic and incubating for 8 hours at 37ºC, 225 rpm. These were used to inoculate 100 ml LB containing the appropriate antibiotic at a dilution of 1:500 which were then grown at 37ºC, 225 rpm for 12-16 hours. Cells were then harvested by centrifugation at 6000 g for 15 min at 4ºC before plasmid DNA was isolated using a QIAfilter plasmid Maxiprep kit (Qiagen) according to the manufacturer's instructions. Isolated plasmid DNA was resuspended in 200 µl of sterile water and DNA concentration was determined by measuring OD_{260} (BioPhotometer plus, Eppendorf) after which DNA was diluted to a final concentration of 1 µg/µl.

2.3 PROTEIN ANALYSIS TECHNIQUES

2.3.1 SDS-PAGE

Protein gels were resolved using the Mini Protean 2 polyacrylamide gel electrophoresis (PAGE) system (Bio-Rad) with a discontinuous Tris-HCl buffer system. This comprised a stacking gel (1.5 M Tris-HCl pH 6.8, 0.4% SDS (w/v), 3.9% (v/v) acrylamide) and a resolving gel (1.5 M Tris-HCl pH 8.8, 0.4% SDS (w/v), 5-18% (v/v) acrylamide) with an SDS running buffer (0.1% SDS (w/v), 0.3% Tris

(w/v), 1.44% glycine (w/v)). Gel polymerization was brought about by addition of 0.8% or 2.4% (v/v) TEMED and 0.015% or 0.045% (v/v) APS for stacking and resolving gels, respectively. The percentage of acrylamide in the resolving gel varied between 5-18% according to the size of the proteins to be resolved. The appropriate volume of samples to be resolved were mixed with 3x Laemmli buffer (62.5 mM Tris-HCl pH 6.8, 2% (w/v) SDS, 5% (v/v) β-mercaptoethanol, 10% (v/v) glycerol, 0.01% (v/v) bromophenol blue) and boiled for 1-10 min before being loaded into the gel. Precision plus protein standards (BioRad) were added to a separate well for indication of protein size. Proteins were separated by electrophoresis by the application of 120-180 V for the appropriate time.

2.3.2 Analysis of SDS-PAGE gels

2.3.2.1 Coomasie Blue staining

To directly visualize protein content following electrophoresis, the resolving gel was removed from the apparatus and the stacking gel was discarded. The resolving gel was soaked in Coomasie Blue solution (0.25% (w/v) Coomasie Brilliant Blue, 40% (v/v) IMS, 10% (v/v) acetic acid) for a minimum of 15 min. The Coomasie Blue solution was then removed and protein bands were visualized by repeated washes in destain solution (25% (v/v) IMS, 7.5% (v/v) acetic acid) to remove background gel staining, until gel bands become clearly visible. Gels were dried onto 3MM paper (Whatmann) under a vaccum at 80ºC as appropriate.

2.3.2.2 Western blotting

For immunodetection of proteins, the stacking gel was discarded and the resolved proteins were transferred to nitrocellulose membrane by semi-dry electrophoretic blotting. Briefly, the resolving gel, ProTran nitrocellulose membrane (Schleicher and Schuell), and 3MM chromatography paper were soaked in Western blotting transfer buffer (25 mM Tris, 192 mM glycine, 5-10% (v/v) methanol) before the gel was placed on the membrane and in turn sandwiched between the buffer-soaked blotting

paper. Transfer was carried out in a TE 77 semi-dry transfer unit (Amersham) for 1 hour at 1 mA/cm^2 membrane. Following transfer, equality of loading was visualized by ponceau red stain solution (0.1% (w/v) Ponceau S, 5% (v/v) acetic acid) and the position of size markers and lanes marked. Prior to immunoblotting, membranes were incubated in 5% (w/v) non-fat milk powder in 1x PBS-Tween (PBST) (137 mM NaCl, 26.8 mM KCl, 2.7 mM Na_2HPO_4, 1.4 mM KH_2PO_4, 0.1% (v/v) Tween-20) for 30 min to block non-specific antibody binding. The blocked membrane was then incubated with primary antibody at the appropriate dilution in 5% non-fat milk powder/PBST for 1 hour at room temperature or overnight at 4ºC. Membranes were then washed three times in PBST to remove unbound antibody before being incubated with the alkaline phosphatase- or horseradish peroxidase-conjugated secondary antibody for a further 1 hour at room temperature. Membranes were then washed a further three times to remove unbound secondary antibody and membranes were either washed and developed in alkaline phosphate buffer (100 mM NaCl, 5 mM $MgCl_2$, 100 mM Tris-HCl pH 9.5) containing 33% NBT (50 mg/ml in DMSF) and 66% BCIP (50 mg/ml in 70% DMF) and proteins visualized directly or in enhanced chemiluminescence (ECL) Western blotting detection solution (Thermo Scientific), and proteins visualized on X-ray film.

2.3.3 Immunoprecipitation

Immunoprecipitation experiments were carried out on whole cell lysates (see section 2.5.6 for preparation of cell protein extracts) using the appropriate mouse monoclonal antibody bound to protein G sepharose beads (Sigma). Briefly, 4 mg of cell lysate in Lysis Buffer (50 mM Hepes-KOH pH 8.0, 100 mM KCl, 100 mM EDTA, 0.1% NP-40, 10 mM NaF, 50 mM β-glycerophosphate, 2 mM DTT, 1x Protease Inhibitor Cocktail, 10% glycerol) was incubated with 10 µl of washed beads rotating at 4ºC for 1 hour to pre-clear the lysate of any proteins that non-specifically bound to the beads. The pre-cleared supernatant was removed and incubated on ice for 1 hour with the appropriate antibody and then rotating at 4ºC for 1 hour with 40 µl

washed beads. Beads were then washed 4 times with Lysis Buffer, resuspended with 3x Laemmli buffer and analysed by SDS-PAGE and Western blotting.

2.3.4 In vitro pull-down assays

In vitro protein-protein interactions were tested using purified GST-tagged protein constructs (see section 2.4 for recombinant protein expression and purification) and whole cell lysates. In this case, extracts of transfected mammalian cells were prepared by lysis with NETN buffer (200 mM Tris.HCl pH 8.0, 200 mM NaCl, 0.5% NP-40, 1 mM EDTA) and processed as detailed in section 2.5.6. 50 µl of glutathione sepharose 4B beads (GE Healthcare) were washed three times with NETN buffer + 0.5% milk. 100 µg of purified GST-tagged protein was added to the pre-washed beads and allowed to bind for 1 h rotating at 4ºC. Beads were consequently washed 4 times with NETN buffer, before being resuspended in NETN buffer plus inhibitors (1 mM PMSF, 1 mM DTT, 1x Protease Inhibitors Cocktail) and incubated with 1 mg of cell lysate overnight rotating at 4ºC. Beads were washed 4 times with NETN buffer and resuspended with 3x Laemmli buffer. Binding was determined by SDS-PAGE and Western blotting.

2.4 RECOMBINANT PROTEIN EXPRESSION AND PURIFICATION

2.4.1 Recombinant protein expression in *E. coli*

For recombinant protein expression, OFD1 DNA fragments were amplified by PCR and inserted into pGEX-4T-1 bacterial expression vector as described in section 2.2.1. Plasmids were transformed into *E. coli* Rosetta 2(DE3) (Novagen) competent cells. 1 µg DNA was added to 50 µl of chemically competent Rosetta cells, which had been defrosted on ice, and the slurry was mixed by gently tapping the side of the tube. The mix was incubated on ice for 5 min, heat shocked at 42ºC for 30sec to induce plasmid DNA uptake, and returned to the ice for a further 2 min. 250 µl of pre-warmed LB media was added to the cells and the transformation mix was incubated at 37ºC, 225 rpm for 1 hour. Following incubation, 100 µl of the cell

suspension was spread onto LB agar plates containing the appropriate antibiotic for selection (chloramphenicol, 34 µg/ml, and ampicillin, 100 µg/ml). Plates were incubated for 12-14 hours at 37ºC. Individual colonies were used to inoculate cultures of LB supplemented with the appropriate antibiotics (chloramphenicol, 34 µg/ml, and ampicillin, 100 µg/ml). Cultures were grown at 37ºC, 225 rpm until an OD_{600} of ~0.5 was reached. The temperature was then either kept at 37ºC (for GST, GST-OFD1-NTD, GST-OFD1-CC5-6, GST-OFD1-CC6) or adjusted to 22ºC (for GST-OFD1-CT) and expression was induced using 0.1 mM IPTG for 3 hours. Cells were then collected by centrifugation and the recombinant protein purified.

2.4.2 Recombinant protein purification

Following harvesting by centrifugation, bacterial cells were resuspended in lysis buffer (PBS containing 1 mM PSMF, 1 mM EDTA, 5 mM DTT, 200 µg/ml lysozyme) and sonicated on ice (MSE Soniprep 150, 10 mm probe, amplitude 12 µm) using 10 cycles of 10 sec sonication followed by 20 sec cooling. The lysate was then clarified by centrifugation at 15000 g for 30 min at 4ºC. The cleared lysate (supernatant) was stored at -80ºC or immediately mixed with 1 ml of glutathione sepharose 4B beads (GE Healthcare), which had been pre-washed in 1x PBS three times, and rotated at 4ºC for 1 hour. The lysate bead slurry was then loaded onto a column and subjected to two rounds of washing with ice-cold 1x PBS. Bound protein was then eluted in elution buffer (50 mM Tris-HCl pH 8.0, 25 mM reduced glutathione, 100 mM KCl, 1 mM DTT, 1 mM PMSF; pH adjusted to 8.0) in several 1 ml fractions. Protein recovery was determined by SDS-PAGE and Coomasie Blue analysis of aliquots of each fraction and those containing highest protein levels were pooled and dialysed against 1x PBS.

2.4.3 Quantification of protein concentration

Total protein content of solutions was determined using the BCA protein assay (Pierce), which exploits the quantitative colorimetric interaction of reduced copper sulphate, bicinchoninic acid and peptide bonds. Typically, 5 µl of the protein solution

(or appropriate dilutions of the protein solution) were incubated with 1 ml of BCA assay reagent at 37ºC for 30 min. Following a cooling period, A_{562} was measured. A serial dilution of BSA standards was prepared and analysed alongside the protein samples to allow construction of a standard curve from which the protein concentration of the samples could be determined.

2.5 MAMMALIAN CELL CULTURE TECHNIQUES

2.5.1 Maintenance of human cell lines

All cell lines were maintained in a humidified 5% CO_2 atmosphere at 37ºC and passaged upon reaching ~80% confluency. To passage, growth media was aspirated off adherent cell populations, cells were washed with 1x PBS and harvested either by incubation in 1x PBS supplemented with 0.5 mM EDTA, or by incubation in Trypsin/EDTA (Invitrogen), according to the appropriate cell line. Cells were cultured in the following media: hTERT-RPE1 cells in Dulbecco's modified Eagle's medium (DMEM)/Ham's F12 (1:1) supplemented with 0.348% sodium bicarbonate solution; IMCD3 cells in DMEM/Ham's F12 (1:1); hFF and HEK293, cells in DMEM; CHO cells in Ham's F12. All cells were supplemented with 10% (v/v) fetal calf serum, 100 IU/ml penicillin (Pen), and 100 µg/ml streptomycin (Strep).

2.5.2 Storage of human cell lines

For long term storage, cell lines were cryopreserved in liquid nitrogen. Briefly, cells were washed and harvested before being collected by centrifugation (1100 rpm, 5 min). After a second wash, cells were resuspended in FBS supplemented with 10% (v/v) DMSO and transferred to cryotubes for freezing in steps (-20ºC overnight; -80ºC overnight; liquid nitrogen).

2.5.3 Transient transfection of mammalian cells

Transient transfection of cultured mammalian cells to induce expression of appropriate recombinant proteins was achieved using Lipofectamine 2000

(Invitrogen), Fugene HD (Roche) or jetPRIME (Polyplus Transfection) according to the manufacturer's instructions.

2.5.3.1 Lipofectamine 2000

Cells were seeded 24 hours prior to transfection to reach 80% confluency on the day of transfection. Plasmid DNA and lipofectamine were mixed in a 1:3 ratio in Opti-MEM, according to the manufacturer's instructions, and added dropwise to cells whose normal growth media has been replaced with medium without FBS or Pen/Strep. Following a 4 hours incubation period (5% CO_2, 37ºC), transfection media was replaced with the appropriate complete media and cells were allowed to express recombinant protein for the appropriate length of time before transfected cells were processed as required.

2.5.3.2 jetPRIME

Cells were seeded 24 hours prior to transfection to reach 60-80% confluency on the day of transfection. Plasmid DNA and jetPRIME transfection reagent were diluted in jetPRIME buffer according to the manufacturer's instructions. The mixture was added dropwise to cells whose normal growth media has been replaced with medium without FBS or Pen/Strep. Following a 4 hours incubation period (5% CO_2, 37ºC), transfection media was replaced with the appropriate complete media and cells were allowed to express recombinant protein for 24 hours to allow expression before being used in subsequent assays.

2.5.3.3 Fugene HD

Unlike with Lipofectamine 2000 and JetPrime, cells were split using complete growth media just before adding the transfection reaction. Plasmid DNA and Fugene HD were mixed in a 1:3 ratio in the appropriate volume of Opti-MEM, according to the manufacturer's instructions. The mixture was added dropwise to cells which were then cultured for a minimum of 16 hours to allow for expression before being used in subsequent assays.

2.5.4 Induction of primary cilia formation

Primary cilia formation was induced by culturing hTERT-RPE1 or hFF cells in serum-free media for at least 48 h.

2.5.5 Centrosome overduplication assay

To monitor centrosome duplication during S-phase arrest upon inhibition of nuclear export or Cdk2 activity, CHO cells were treated as previously described (Prosser et al. 2009). Cells seeded the day before, were washed in 1x PBS and placed in fresh growth media containing 2 mM hydroxyurea. Additional inhibitors were either added concurrently with the hydroxyurea or after 18 hours depending on whether the inhibitor would cause a G_1-phase arrest. Leptomycin-B (LMB) (20 nM, Calbiochem) was used to block nuclear export and roscovitine (180 µM, Calbiochem) was used to inhibit Cdk2 activity. Following the desired assay duration, cells were then fixed and processed for immunofluorescence microscopy. These experiments were carried out by Dr. Suzanna Prosser (Leicester, UK).

2.5.6 Preparation of cell protein extracts

Whole cell lysates were prepared in Lysis Buffer (50 mM Hepes-KOH pH 8.0, 100 mM KCl, 100 mM EDTA, 0.1% NP-40, 10 mM NaF, 50 mM β-glycerophosphate, 2 mM DTT, 1x Protease Inhibitor Cocktail, 10% glycerol). Briefly, cells were washed in 1x PBS, and then harvested by scrapping after adding lysis buffer directly to the plate. Lysis was carried out ice for 30 min after which lysates were passed 10 times through a 27G needle and centrifuged at 13000 rpm for 10 min at 4ºC to remove insoluble material. Supernatants were then either used directly as required or stored at -80ºC.

2.5.7 Microtubule depolymerization/re-growth

Microtubule depolymerization was achieved by treating cells with 6 µg/ml nocodazole for 1 h at 37ºC and then on ice for 30 minutes. To allow microtubule

regrowth, cells were subsequently washed 3 times with 1x PBS and pre-warmed media added.

2.5.8 Cell synchronization

Cells were cultured in the appropriate complete growth medium to a suitable (usually ~60-70%) confluency. M-phase arrested cells were obtained by 16 hours treatment with 500 ng/µl nocodazole; rounded mitotic cells were collected by gently pipetting off the floating population. G_1/S-phase arrested cells were obtained by 16 hours treatment with 1 mM hydroxyurea. Cells were collected as usual.

2.5.9 Flow cytometric analysis

To determine cell cycle distribution, cell populations for analysis were harvested as appropriate (mitotic shake-off for M-phase cells or as usual for all other cell populations), pelleted by centrifugation and washed in 1x PBS before being resuspended in 1 ml 70% ice-cold ethanol to fix cells. Cells were maintained on ethanol at 4ºC for a minimum of 30 min before being stained with propidium iodide. Briefly, cells were washed twice in 1x PBS supplemented with 200 µg/ml RNase A and 20 µg/ml propidium iodide. Cells were stained in the dark at 4ºC for a minimum of 4 hours. Cells were then analyzed via flow cytometry, using a BD FACSCanto II analyzer and BD FACSDiva software.

2.5.10 RNA interference

Cells were seeded into a 24-well or a 6-well dish the day before transfection so as to reach a confluency of ~30% for transfection. 100 mM siRNAs and Oligofectamine (Invitrogen) transfection reagent were mixed according to the manufacturer's instructions and added dropwise to cells whose normal growth media has been replaced with medium without FBS or Pen/Strep. Following a 4 hour incubation period (5% CO_2, 37ºC), antibiotic free media containing 30% FBS (v/v) was added and cells incubated (5% CO_2, 37ºC) for 72 hours before being processed as required. OFD1 was depleted using two different siRNA duplex oligonucleotides (5'-

GCUCAUAGCUAUUAAUUCA-3' and 5'-GAUCGAUCGUUCUGUCAAU-3') with dTdT overhangs at the 3' termini (Dharmacon). PCM-1 siRNA duplex oligonucleotides were obtained from QIAGEN (Dammermann and Merdes 2002). BBS4 was depleted using a pool of four oligonucleotides (5'-GGAUAAGUGUAACCCUUUA-3'; 5'-CUGCAAGGCUGUUAUCAAA-3'; 5'-CAUUAUAUCCGGAAAGAUU-3' and 5'-GCAAUGCACUGACUUAUGA-3') with dTdT overhangs at the 3' termini (Dharmacon). Control depletions were performed with GL2 siRNAs that target luciferase (Dharmacon).

2.6 INDIRECT IMMUNOFLUORESCENCE MICROSCOPY

Cells grown on acid-etched coverslips were fixed and permeabilised using ice-cold methanol before processing for immunofluorescence microscopy. Briefly, cells were maintained at -20ºC in methanol for a minimum of 6 minutes before being rehydrated by three 5 min washes in 1x PBS. Non-specific antibody binding was blocked by incubation for 15 min in 1x PBS supplemented with 1% (w/v) bovine serum albumin (BSA), followed by three 5 min washes in 1x PBS. Coverslips were incubated with an appropriate volume (50-100 µl) of primary antibody solution diluted to a suitable concentration in 1x PBS supplemented with 3% (w/v) BSA. Incubation with primary antibodies was for a minimum of 1 hour at room temperature. Coverslips were then subjected to three 5 min washes in 1x PBS to remove unbound antibody before incubation with appropriate secondary antibodies diluted in 1x PBS supplemented with 3% (w/v) BSA and 0.3 µg/ml Hoechst 33258 in the dark for 1 hour at room temperature. Coverslips were then subjected to a final round of washes before being mounted on glass microscope slides in mountant (80% (v/v) glycerol, 35% (w/v) n-propyl gallate). Images were obtained using either a TE300 inverted microscope (Nikon), using an ORCA ER CCD camera (Hamamutsu) and Openlab software, or a Leica TCS SP5 confocal microscope equipped with a Leica DMI 6000B inverted microscope using a 63x oil objective (numerical aperture, 1.4). Images were processed using Adobe Photoshop 7.

2.6.1 Data analysis and quantification techniques

The relative abundance of protein at the centrosome area was quantified using the relevant immunofluorescence images, captured and processed as described above using Openlab sofware (Improvision). All images to be measured for a given experiment were captured under identical conditions and processed identically. Briefly, a region of interest of the appropriate size was selected and saved. Total pixel intensity within this region was calculated and background intensity subtracted for each image to be analysed.

2.7 ANTIBODY GENERATION AND PURIFICATION

2.7.1 Antigen generation

For production of antibodies against OFD1, rabbits were immunised with a His-tagged C-terminal fragment of OFD1 spanning amino acids 145 to 1012. This fragment was expressed in *E. coli* strain Rosetta 2 (DE3) and individual colonies were used to inoculate cultures of LB supplemented with the appropriate antibiotics (chloramphenicol, 34 µg/ml, and kanamycin, 50 µg/ml). Cultures were grown at 37ºC, 225 rpm until an OD_{600} of ~0.5 was reached. The temperature was then adjusted to 22ºC and expression was induced using 0.1 mM IPTG for 6 hours. Cells were then collected by centrifugation and bacterial cells were resuspended in denaturing lysis buffer (100 mM NaH_2PO_4, 10 mM Tris, 8 M urea) adjusted pH to 8.0, and lysed by rotating for 15-60 min at room temperature until solution became translucent. The lysate was then centrifuged at 10000g for 30 min at room temperature to pellet the cellular debris, and the cleared lysate was mixed with 50% Ni-NTA slurry and rotated at room temperature for 1 hour. The lysate-resin mixture was then loaded onto a column and subjected to two rounds of washing with lysis buffer with pH adjusted to 6.3. Bound protein was then eluted in lysis buffer with pH adjusted to 5.9 in four 500 µl fractions, followed by elution in lysis buffer with pH adjusted to 4.5 in an additional four 500 µl fractions. Protein recovery was

determined by SDS-PAGE and Coomasie Blue analysis of aliquots of each fraction and those containing highest protein levels were pooled.

For production of antibodies against BBS4, rabbits were immunised with the GST-tagged BBS4 C-terminal fragment (residues 235-519) following expression in *E. coli* strain Rosetta 2 (DE3) (Novagen). Individual colonies were used to inoculate cultures of LB supplemented with the appropriate antibiotics (chloramphenicol, 34 µg/ml and ampicillin, 100 µg/ml). Cultures were grown at 37ºC, 225 rpm until an OD_{600} of ~0.5 was reached. The temperature was then adjusted to 22ºC and expression was induced using 0.1 mM IPTG for 6 hours. Cells were then collected by centrifugation and the recombinant protein purified according to standard protocols (see section 2.4.2). Protein recovery after elution was determined by SDS-PAGE and Coomasie Blue analysis of aliquots of each fraction and those containing highest protein levels were pooled.

For each purified recombinant protein, the pooled purified protein fractions were analysed on SDS-PAGE and Coomasie Blue analysis and total concentration was determined by comparison against BSA standards.

2.7.2 Antibody generation and affinity purification

Immunizations and affinity purification of antibodies were performed by Cambridge Research Biochemicals.

2.8 MISCELLANEOUS TECHNIQUES

2.8.1 Zebrafish morpholino experiments

Breeding zebrafish (*Danio rerio*) were maintained at 28°C on 14 hours light/10 hours dark cycle. Morpholino antisense oligonucleotides for Ofd1 and Bbs4 were generated and stated amounts were injected in one to two cell stage embryos using needles pulled from glass capillary tubes as previously described (Gerdes et al.

2007; Ferrante et al. 2009). In whole embryos, the heart rudiment was visualized by direct inspection and the frequency of deviation from the normal leftward displacement of the heart cone, or cardiac 'jogging', was recorded as a laterality readout (Ferrante et al. 2009). Comparison between groups was undertaken using Fisher's Exact Test. In addition, whether the bodies of embryos were straight or displayed abnormal curvature characteristic of ciliary defects was noted (Ferrante et al. 2009). These experiments were carried out by Dr. Leila Romio and Prof. Adrian Woolf (London, UK).

2.8.2 Nasal respiratory cell culture

Human nasal epithelial cells were obtained with ethical approval from healthy volunteers and cultured and induced to differentiate in ALI (air-liquid interface)-cell culture as previously described (Hirst et al. 2010). Nasal brush biopsy samples were grown on Collagen coated tissue culture trays in Bronchial Epithelial Growth Media (BEGM) for 2-7 days until they reached confluency. The confluent unciliated basal cells were expanded into collagen coated flasks and the BEGM was replaced every 2-3 days. The basal cells were then seeded on a collagen coated 12 mm diameter transwell clear insert under BEGM for 2 days. Once confluency was reached the basal cell monolayer was fed on the basolateral side only with ALI-media (50% BEGM and 50% Hi-glucose minimal essential medium containing 100 nM retinoic acid) and this media was exchanged every 2-4 days. These experiments were carried out by Dr. Robert Hirst and Prof. Chris O'Callaghan (Leicester, UK). Samples of unciliated cells (day 10 post ALI) and fully differentiated ciliated epithelial cells (day 28 post ALI) were fixed and processed for immunofluorescence microscopy.

CHAPTER 3

GENERATION OF OFD1 AND BBS4 ANTIBODIES

CHAPTER 3 GENERATION OF OFD1 AND BBS4 ANTIBODIES

3.1 INTRODUCTION

Antibodies are essential tools for almost every area of cell biology research as they allow the identification and characterization of proteins of interest. Through applications such as immunofluorescence microscopy, Western blotting and immunoprecipitation, antibodies enable us to locate proteins within cells, identify protein separated by electrophoresis, and separate proteins and associated complexes from other molecules in a cell lysate. Antibodies are produced by injecting an antigen into an animal, such as a rabbit, which induces the B-lymphocytes to produce immunoglobulins specific for the antigen. This animal's blood will then contain polyclonal antibodies that can be purified from the serum.

For the reasons mentioned above, it was of great importance to have a good source of antibodies, especially against OFD1, the focus of this study. Because all of our experiments relied on a limited source of OFD1 antibodies provided by our collaborator (Prof. Adrian Woolf), we decided to generate our own specific antibody against OFD1. Furthermore, given the close association of OFD1 with another ciliopathy associated protein, BBS4, suggested by our early studies (see Chapter 4), we decided to generate an antibody against the BBS4 protein as well.

3.2 RESULTS

3.2.1 Generation of OFD1 and BBS4 antigens for polyclonal antibody generation

For generation of a new antibody against OFD1, we decided to use the coiled-coil rich C-terminal domain as an antigen. We therefore cloned this region of the OFD1 cDNA encoding residues 145-1012 into a His-tagged bacterial expression vector (Figure 3.1A). For BBS4, we chose to use a GST-tagged recombinant protein encoding the C-terminal half of BBS4 (residues 235-519) that had been previously

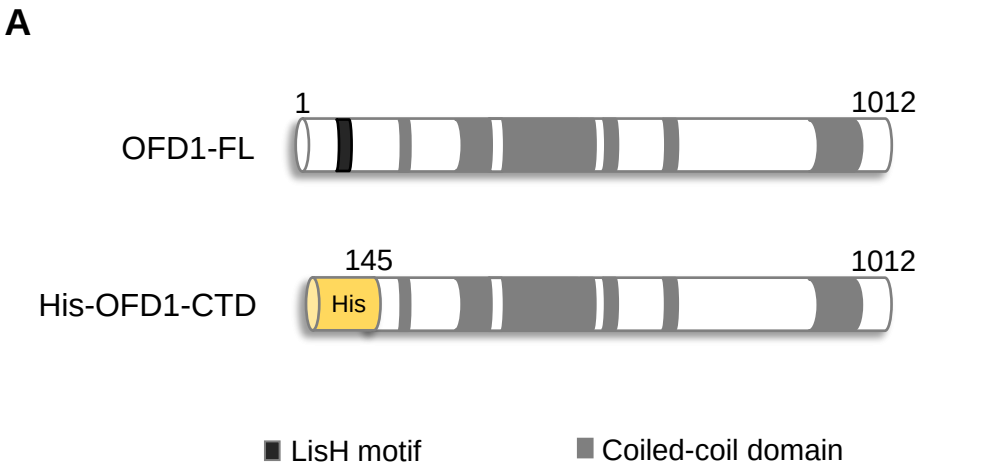

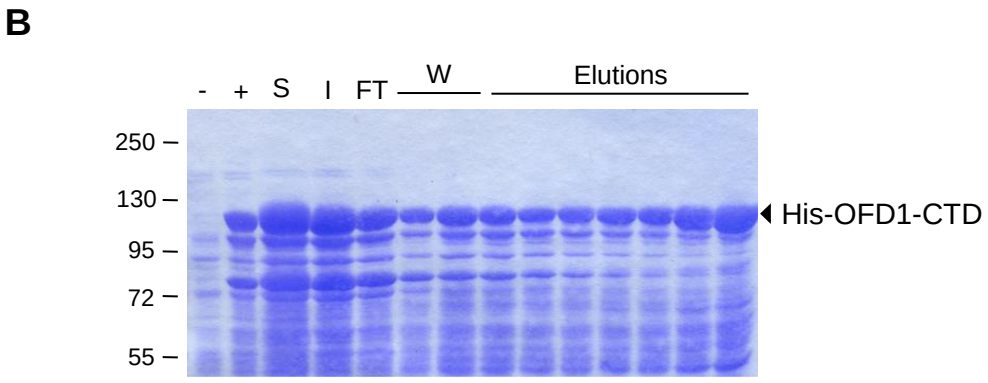

Figure 3.1 Generation of OFD1 antigen for antibody generation
(A) Schematic representation of full-length OFD1 protein (OFD1-FL) and of the region expressed as a His-tagged recombinant protein (OFD1-CTD) and used as an antigen for immunisation of rabbits for antibody generation. The black box indicates the LisH motif and the grey boxes represent the coiled-coil domains. Amino acid numbers are indicated. **(B)** Expression and purification of the His-OFD1-CTD recombinant protein. The non-induced (-), induced (+), soluble (S), insoluble (I), flow-through (FT), washes (W) and elution fractions were analysed by SDS-PAGE with Coomasie Blue staining. Molecular weights (kDa) are indicated on the left. Black arrowhead indicates predicted molecular size of His-OFD1-CTD (100 kDa).

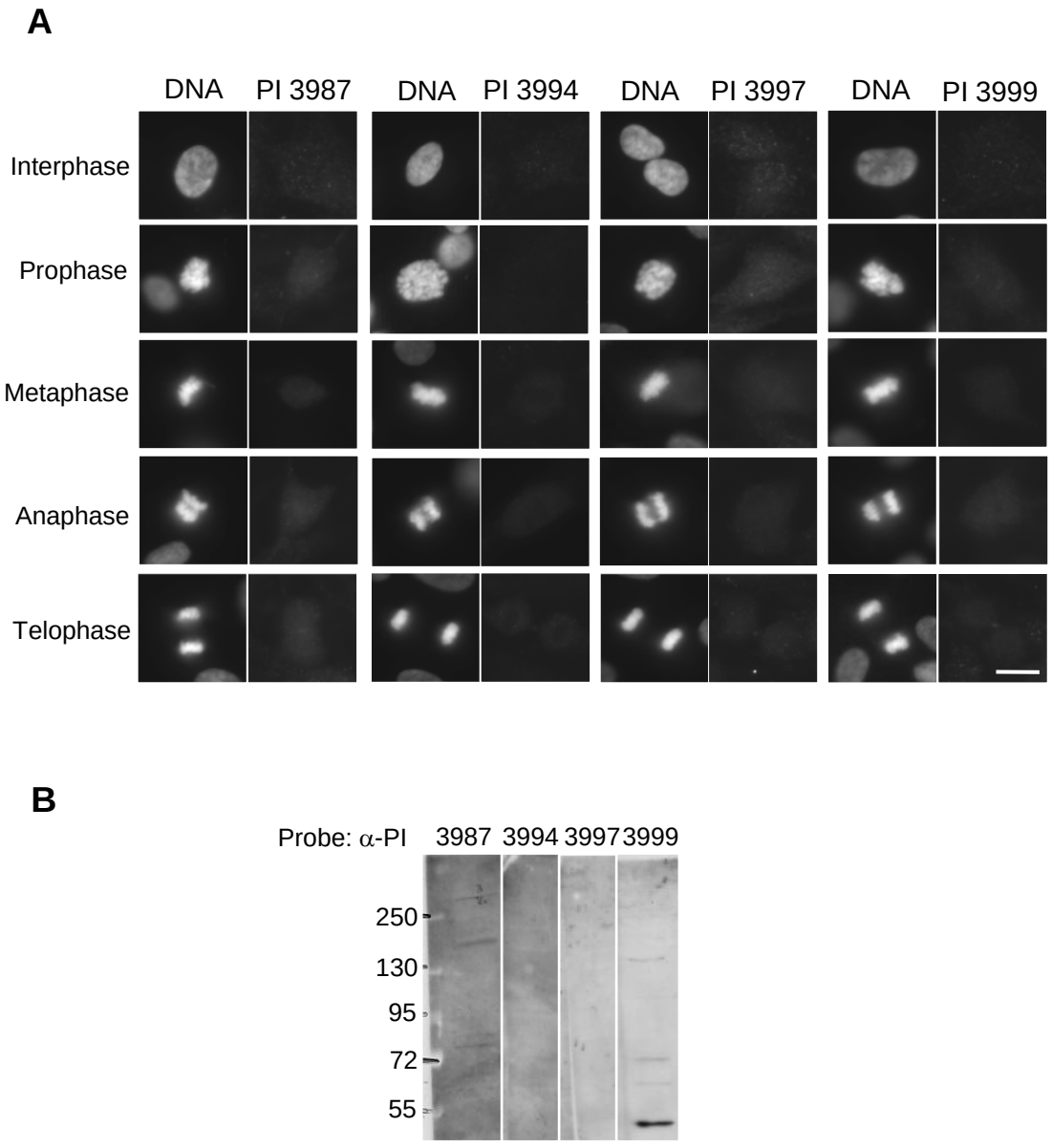

Figure 3.3 Characterisation of pre-immune sera from rabbits
(A) Reactivity of the pre-immune sera from rabbits was characterised by immunofluorescence microscopy in hTERT-RPE1 cells. Cells were processed for immunofluorescence microscopy with the appropriate rabbit sera used at 1:250. DNA was stained with Hoechst 33258. Images show the results obtained for the pre-immune sera (PI) of rabbits 3987, 3997, 3994 and 3999, through different stages of the cell cycle (indicated on the left of the panels). Scale bar, 5 µm. **(B)** Western blot analysis of reactivity of the pre-immune (PI) sera from rabbits 3987, 3994, 3997 and 3999, used at 1:250, against whole cell lysates of hTERT-RPE1 cells. Molecular weights (kDa) are indicated on the left of each panel.

generated in our lab (Figure 3.2A). To determine the optimal conditions of expression and solubilisation of each recombinant protein, we tested different IPTG concentrations (0.1 mM or 0.4 mM), temperature (22ºC to 37ºC), time of induction (3 to 16 hours), and lysis method (sonication/liquid homogenization and lysis buffer). The best protein expression levels were obtained using 0.1 mM IPTG at 22ºC for 6 hours for both recombinant proteins. His-OFD1-CTD was then prepared with denaturing buffer and a sonication, whereas GST-BBS4-CTD was prepared with standard lysis buffer and a French press. Following this process of optimisation of their expression and solubilisation (data not shown), His-OFD1-CTD and GST-BBS4-CTD recombinant proteins were expressed and then purified in large scale using Ni-NTA agarose or glutathione sepharose, respectively, and used as antigens for immunisation of rabbits for antibody generation (Figure 3.1B for His-OFD1-CTD, and Figure 3.2B for GST-BBS4-CTD).

Before immunisation, however, immunofluorescence microscopy analysis of sera from rabbits prior to immunisation was performed to check which pre-immune sera did not naturally cross-react with the centrosomes (Figure 3.3A). This is an important consideration as both OFD1 and BBS4 have been reported to localize to the centrosome and/or its vicinity throughout the cell cycle, and many rabbit sera show reactivity to centrosomes prior to immunisation (Romio et al. 2004; Kim et al. 2004). Western blot analysis was also performed to ensure no reactivity of the pre-immune sera around the predicted molecular weights of OFD1 (110 kDa) and BBS4 (58 kDa) (Figure 3.3B). Based on the combined information from both approaches, two rabbits were selected for immunisation for each antigen: rabbits 3994 and 3999 for OFD1, and rabbits 3987 and 3997 for BBS4. Rabbit immunisation was carried out by Cambridge Research Biochemicals.

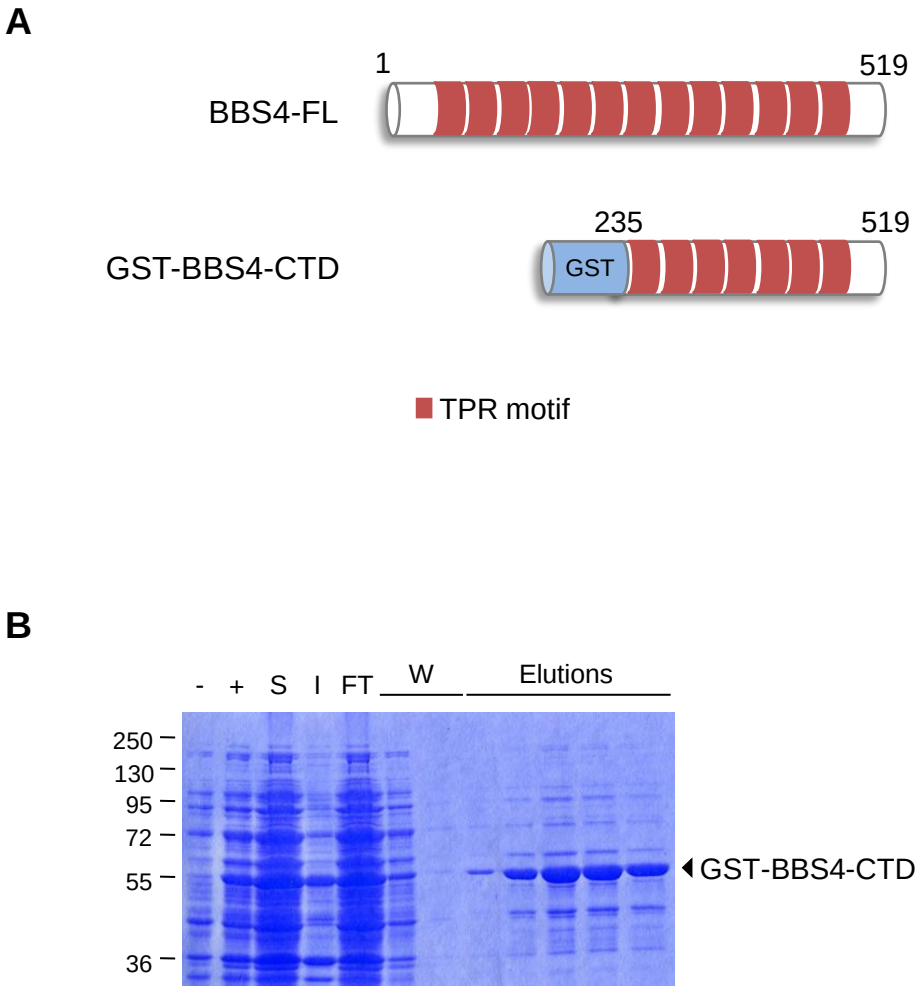

Figure 3.2 Generation of BBS4 antigen for antibody generation
(A) Schematic representation of the full-length BBS4 protein (BBS4-FL) and of the region expressed as a GST-tagged recombinant protein (BBS4-CTD) and used as an antigen for immunisation of rabbits for antibody generation. The red boxes represent TPR motifs. Amino acid numbers are indicated. **(B)** Expression and purification of the GST-BBS4-CTD recombinant protein. The non-induced (-), induced (+), soluble (S), insoluble (I), flow-through (FT), washes (W) and elution fractions were analysed by SDS-PAGE with Coomasie Blue staining. Molecular weights (kDa) are indicated on the left of the panel. Black arrowhead indicates predicted molecular size of GST-BBS4-CTD (56 kDa).

3.2.2 Characterisation of OFD1 and BBS4 antisera from immunised rabbits

Each rabbit was subjected to four cycles of immunisation and bleeding, and reactivity of the rabbits' post-immunisation sera was tested by both Western blot analysis and immunofluorescence microscopy.

By Western blot analysis the antisera from rabbits 3994 (Figure 3.4A) and 3999 (Figure 3.4B) detected a protein in extracts prepared from myc-OFD1-CTD-transfected cells, but not untransfected cells, which corresponded to the expected size of this recombinant protein (100 kDa). Also, this protein was not detected by the pre-immune sera and is equivalent in size to the protein detected by the anti-myc antibody. Importantly, this protein shows increased reactivity from bleed 1 to the final bleed (Figure 3.4A and B). Moreover, a protein of the predicted size of endogenous OFD1 protein (110 kDa) was clearly detected, both in untransfected and myc-OFD1-CTD-transfected cell extracts, by bleed 3 to the final bleed for the sera from rabbit 3999 (Figure 3.4B). Although faint bands of the expected size for endogenous OFD1 protein were also detected by bleed 4 from rabbit 3994 (Figure 3.4A), overall, OFD1 antisera from this rabbit revealed lower reactivity against transfected protein than rabbit 3999. These results suggest a more specific response to the immunisation in rabbit 3999. Consistent with the Western blot analysis, immunofluorescence microscopy performed with the OFD1 antisera from rabbits 3994 and 3999 showed an overall increase in the intensity of the reactivity from bleeds 1 to the final bleed in asynchronous cells (Figure 3.5A and B). Close inspection of cells stained with the final bleed of OFD1 antisera from rabbits 3994 and 3999 revealed the detection of the centrosome in interphase (Figure 3.6A and B), a pattern not detected by the pre-immune sera (Figure 3.3A). Furthermore, in agreement with Romio et al. (2004), both antisera from rabbits 3994 and 3999 detected the centrosome and the spindle pole throughout the cell cycle (Romio et al. 2004). Together, these results indicate that whilst immunisation of both rabbits

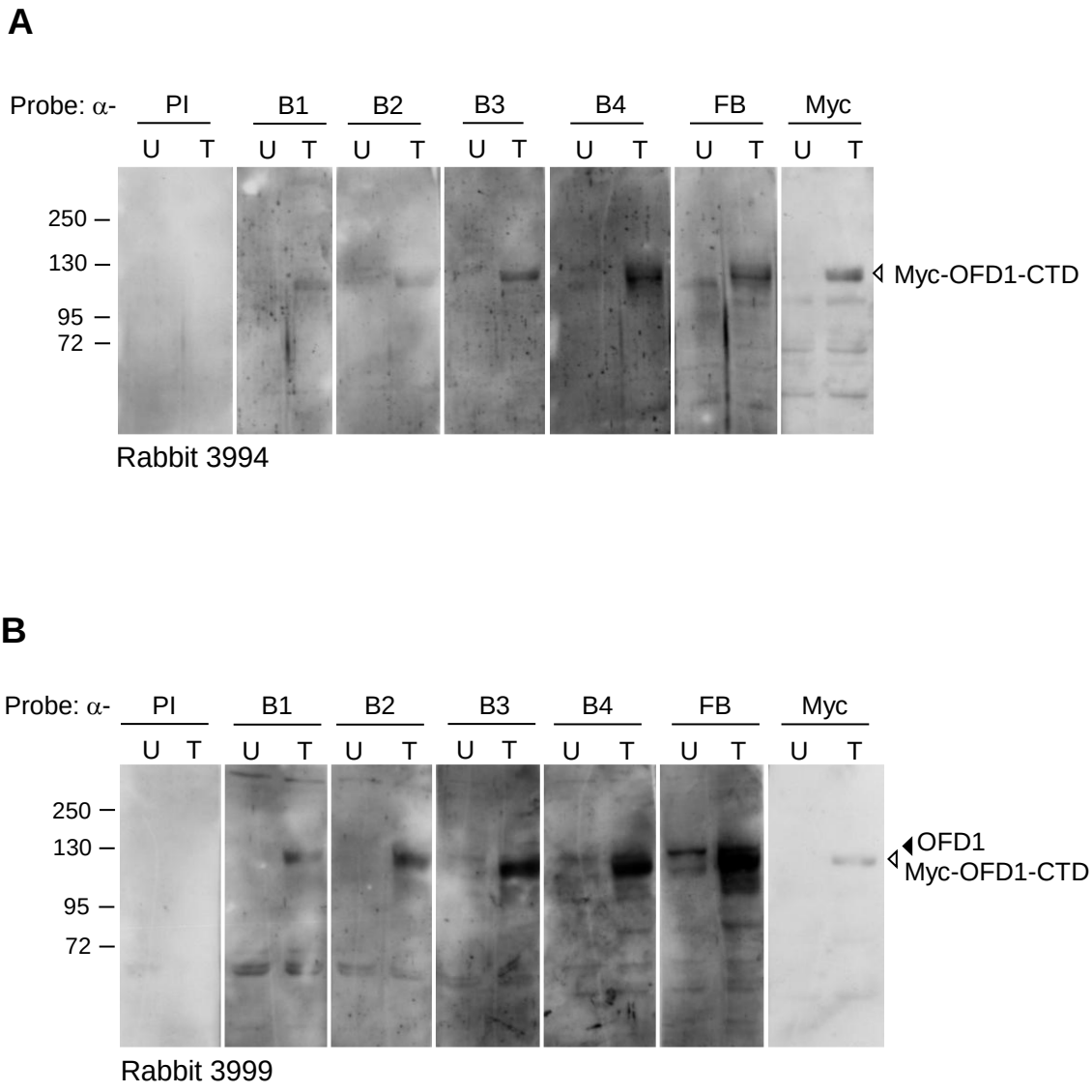

Figure 3.4 Characterisation of OFD1 antisera by Western blot analysis
Reactivity of the OFD1 antisera taken from rabbit 3994 **(A)** and rabbit 3999 **(B)** was tested by Western blot, used at 1:250, against untransfected (U) and Myc-OFD1-CTD-transfected (T) HEK293 whole cell lysates. PI, pre-immune sera; B1 to B4, antisera from bleeds 1 to 4, respectively, FB, final bleed; Myc, anti-Myc antibody. Molecular weights (kDa) are indicated on the left of each panel. Black arrowhead indicates predicted molecular size of endogenous OFD1 (110 kDa), white arrowhead indicates predicted molecular size of Myc-OFD1-CTD (100 kDa).

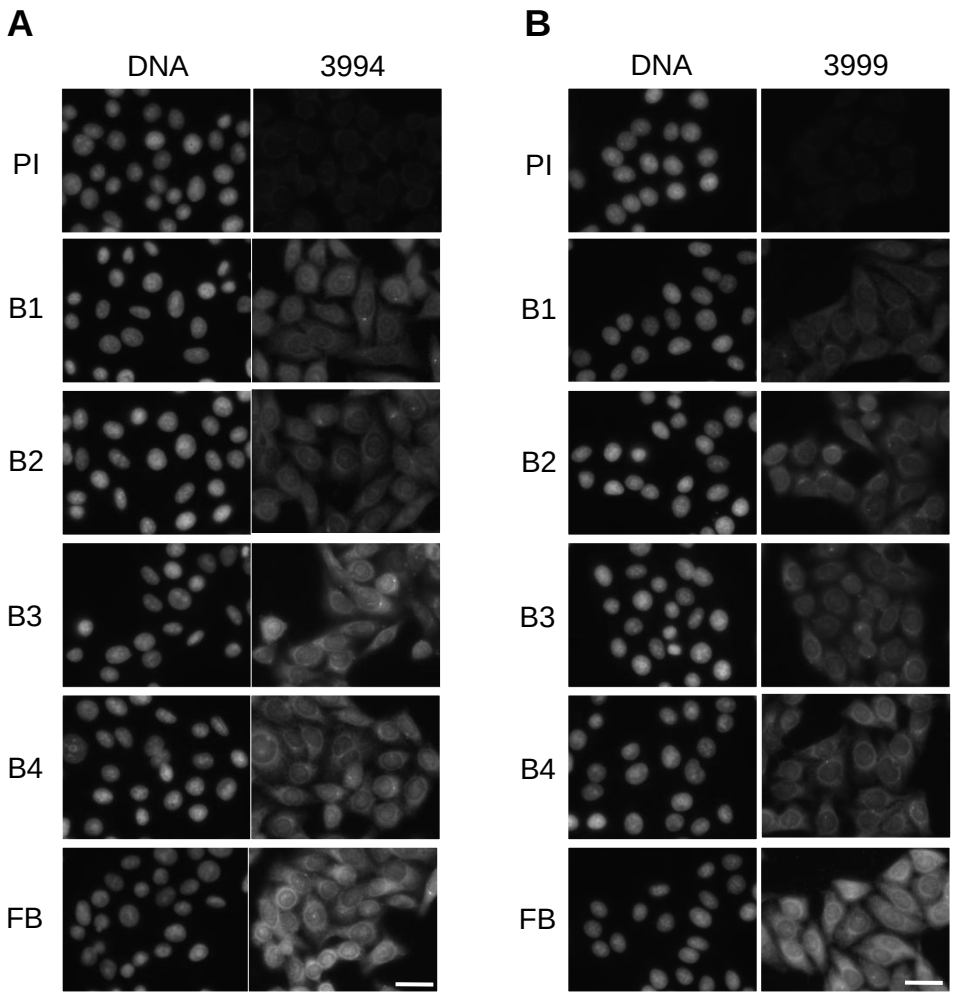

Figure 3.5 Characterisation of OFD1 antisera by immunofluorescence microscopy
Reactivity of the OFD1 antisera taken from rabbit 3994 **(A)** and rabbit 3999 **(B)** was characterised by immunofluorescence microscopy in asynchronous U2OS cells. Cells were processed for immunofluorescence microscopy with the appropriate rabbit antisera, used at 1:250, and DNA was stained with Hoechst 33258. PI, pre-immune sera; B1 to B4, antisera from bleeds 1 to 4, respectively; FB, final bleed. Scale bars, 15 µm.

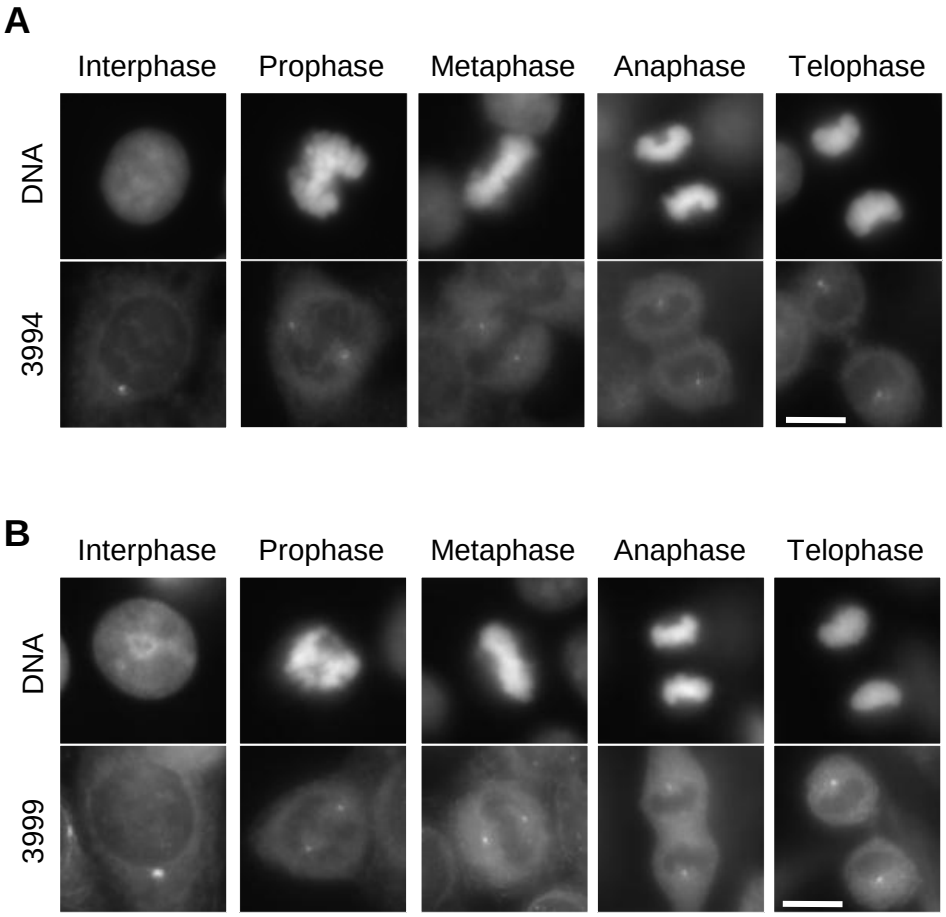

Figure 3.6 Characterisation of OFD1 antisera through the cell cycle by immunofluorescence microscopy
Reactivity of the OFD1 antisera taken from rabbit 3994 **(A)** and rabbit 3999 **(B)** was characterised by immunofluorescence microscopy in U2OS cells at different stages of the cell cycle. Cells were processed for immunofluorescence microscopy with the appropriate rabbit antisera, used at 1:250, and DNA was stained with Hoechst 33258. PI, pre-immune sera; B1 to B4, antisera from bleeds 1 to 4, respectively; FB, final bleed. Cell cycle stages are indicated. Scale bars, 5 µm.

was successful, the response of rabbit 3999 was the strongest. Hence, the final bleed of this antiserum was used for antibody purification.

For BBS4, Western blot analysis of the antisera from rabbits 3987 (Figure 3.7A) and 3997 (Figure 3.7B) revealed a protein in the GFP-BBS4-transfected cell extract, not detected in the untransfected cell extract, that corresponded in size to the transfected GFP-tagged BBS4 (85 kDa), as confirmed with the anti-GFP antibody. Also, this band was not detected by the pre-immune sera and showed increased intensity from bleed 1 to the final bleed (Figure 3.7A and B). Furthermore, this analysis also revealed a band of the predicted size of endogenous BBS4 (58 kDa) in untransfected and GFP-BBS4-transfected cell extracts in the fourth and final bleeds for the antisera from rabbit 3987 (Figure 3.8A), and from the third to the final bleeds for the antisera from rabbit 3997 (Figure 3.8B). Nonetheless, the antisera from rabbit 3997 showed less background cross-reactivity than rabbit 3987, suggesting a more specific response to the immunisation in this rabbit. Immunofluorescence microscopy analysis of the sera from rabbits 3987 and 3997 revealed that these, unlike the pre-immune sera, detected the centrosome in interphase cells with intensity gradually increasing from bleed 1 to the final bleed (Figure 3.8A and B). The final bleed antisera from each rabbit was analysed in more detail specifically by looking at the staining patterns at different stages of the cell cycle (Figure 3.9A and B). In agreement with what had been previously reported (Kim et al. 2004), the final bleed antisera from rabbit 3987 revealed a consistent centrosomal localization throughout the cell cycle. The final bleed antisera from rabbit 3997, on the other hand, despite detecting the centrosome quite clearly in interphase and prophase cells, revealed a stronger stain across the whole cell during all other mitotic stages. This pattern of background staining impeded a clear detection of the centrosome in these cells. In summary, for BBS4, the response of rabbit 3997 was the strongest and, hence, the final bleed of this antiserum was used for antibody purification.

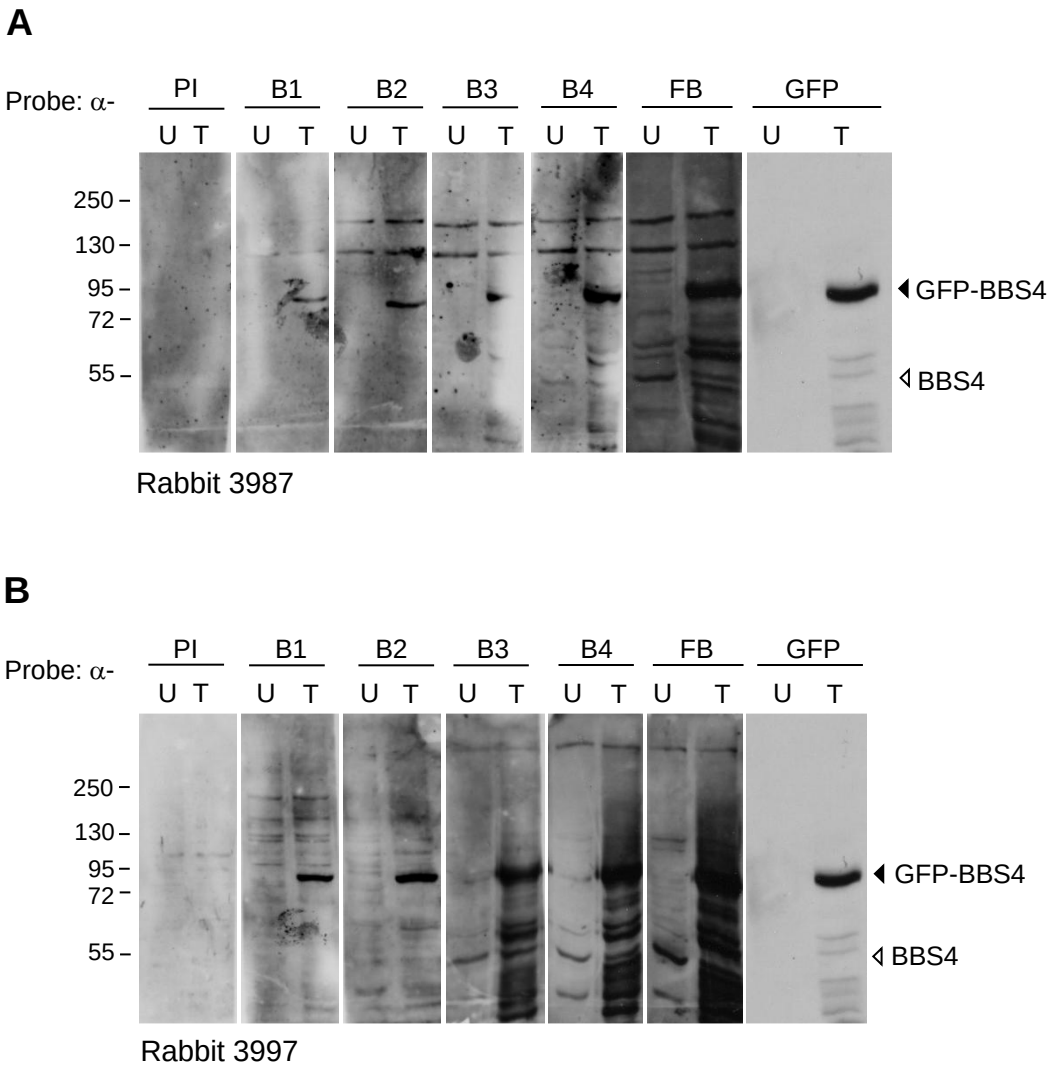

Figure 3.7 Characterisation of BBS4 antisera by Western blot analysis
Reactivity of the BBS4 antisera taken from rabbit 3987 **(A)** and rabbit 3997 **(B)** was tested by Western blot, used at 1:250, against untransfected (U) and GFP-BBS4-transfected (T) HEK293 whole cell lysates. PI, pre-immune sera; B1 to B4, antisera from bleeds 1 to 4, respectively; FB, final bleed; GFP, anti-GFP antibody. Molecular weights (kDa) are indicated on the left of each panel. Black arrowhead indicates predicted molecular size of GFP-BBS4 (85 kDa), white arrowhead indicates predicted molecular size of endogenous BBS4 (58 kDa).

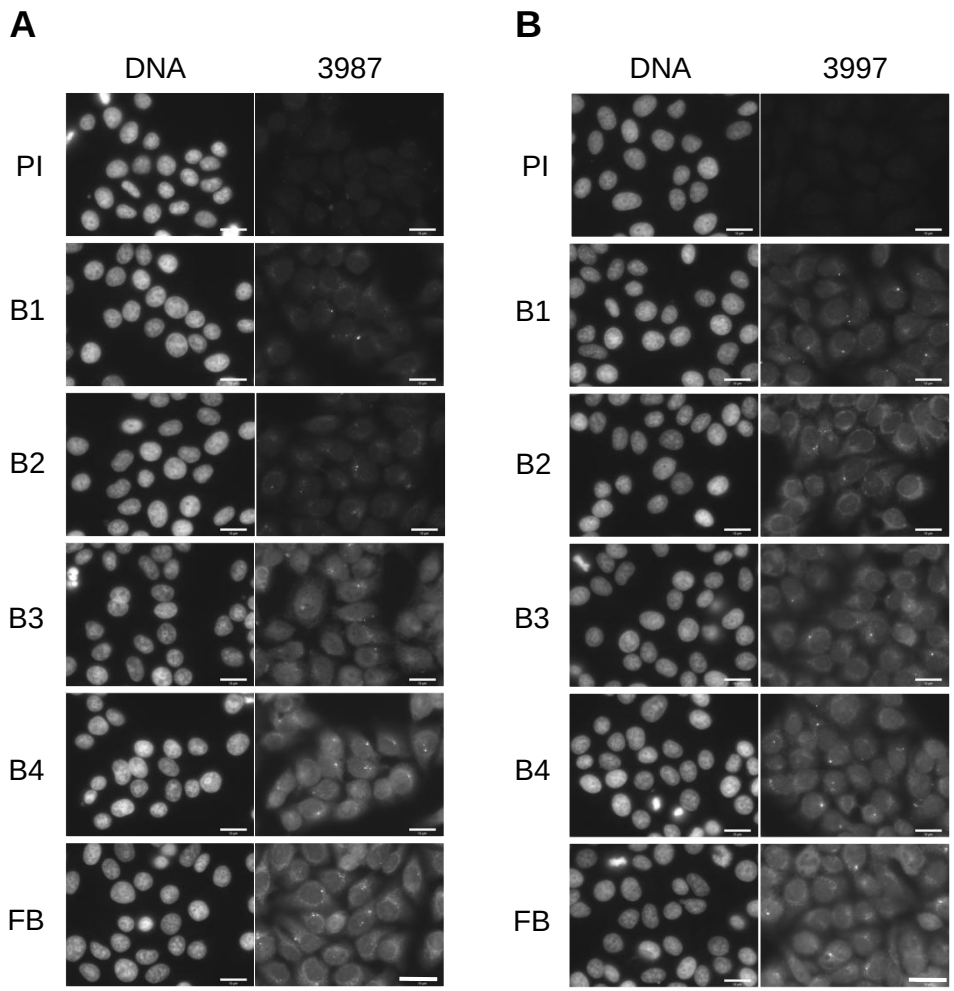

Figure 3.8 Characterisation of BBS4 antisera by immunofluorescence microscopy
Reactivity of the BBS4 antisera taken from rabbit 3987 **(A)** and rabbit 3997 **(B)** was characterised by immunofluorescence microscopy in asynchronous U2OS cells. Cells were processed for immunofluorescence microscopy with the appropriate rabbit antisera, used at 1:250, and DNA was stained with Hoechst 33258. PI, pre-immune sera; B1 to B4, antisera from bleeds 1 to 4, respectively; FB, final bleed. Scale bars, 15 µm.

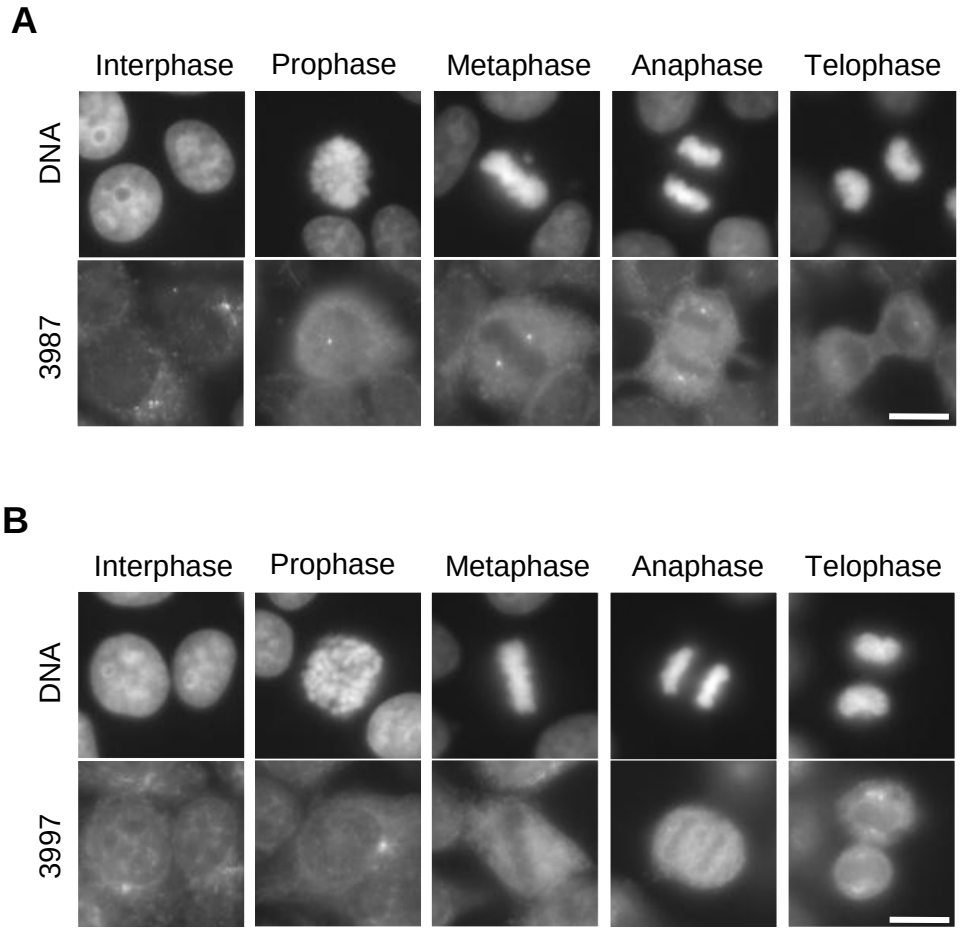

Figure 3.9 Characterisation of BBS4 antisera through the cell cycle by immunofluorescence microscopy
Reactivity of the BBS4 antisera taken from rabbit 3987 **(A)** and rabbit 3997 **(B)** was characterised by immunofluorescence microscopy in U2OS cells at different stages of the cell cycle. Cells were processed for immunofluorescence microscopy with the appropriate rabbit antisera, used at 1:250, and DNA was stained with Hoechst 33258. PI, pre-immune sera; B1 to B4, antisera from bleeds 1 to 4, respectively; FB, final bleed. Cell cycle stages are indicated. Scale bars, 5 µm.

3.2.3 Characterisation of purified OFD1 antibody

Purification of the final bleed antisera from rabbits 3999, for OFD1, and 3997, for BBS4, was then carried out by Cambridge Research Biochemicals using the corresponding antigens. During purification of the final bleed antisera from rabbits 3999 and 3997, OFD1 and BBS4 purified antibodies, respectively, were eluted first with a low pH glycine buffer and then with a high pH triethylamine (TEA) buffer. Purified antibody fractions were rapidly neutralized after elution. Cambridge Research Biochemicals therefore provided us with two distinct elutions of purified antibodies in glycine and TEA buffers. The reactivity of these was tested both by Western blot analysis and immunofluorescence microscopy.

Western blot analysis of both glycine and TEA elutions of OFD1 purified antibodies showed that, although both elutions were able to detected bands of the expected size in extracts of cells expressing myc-OFD1-FL and myc-OFD1-CTD, the TEA elution did not detect endogenous OFD1 (Figure 3.10A). The glycine elution, on the other hand, detected bands of the expected size of endogenous OFD1 protein in untreated and transfected cell extracts. Notably, its reactivity was very similar to that of the unpurified final bleed (Figure 3.10A), suggesting that this elution contains a higher concentration of OFD1 antibodies. Immunofluorescence microscopy analysis of OFD1 purified antibodies confirmed that the glycine elution had a stronger and more specific reactivity, detecting the centrosome in a similar fashion to the final bleed, and with less background than the TEA elution (Figure 3.10B). The glycine elution was therefore chosen as our new OFD1 antibody and used for most of the experiments in this study.

With regard to BBS4, Western blot analysis and immunofluorescence microscopy of both glycine and TEA elutions of purified BBS4 antibodies revealed that the purification of the final bleed antiserum from rabbit 3997 was not successful. Both elutions failed to recognize both transfected GFP-tagged full-length BBS4 and

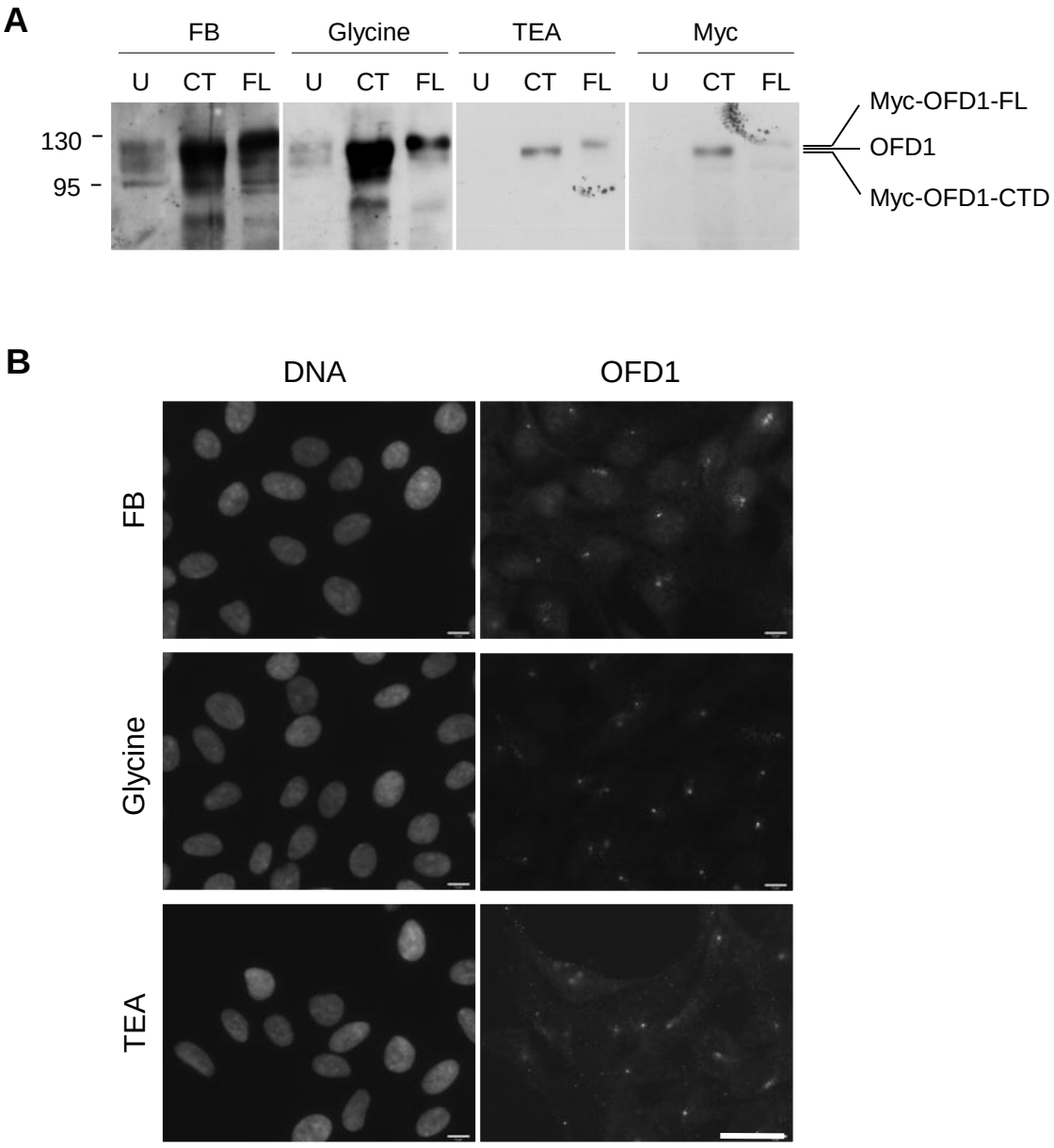

Figure 3.10 Characterisation of OFD1 purified antibody
(A) Reactivity of the OFD1 purified antibody glycine and TEA elutions was tested by Western blot against untransfected (U), Myc-OFD1-CTD- (CT) and Myc-OFD1-FL (FL) transfected HEK293 whole cell lysates. Purified antibodies were used at 1:100 (2.7 µg/µl and 1.1 µg/µl for glycine and TEA elutions, respectively). FB, final bleed (used at 1:250); Myc, anti-Myc antibody. Molecular weights (kDa) are indicated on the left of the panel. The predicted sizes of Myc-OFD1-FL (110 kDa), Myc-OFD1-CTD (100 kDa), and endogenous OFD1 (110 kDa) are indicated. **(B)** Reactivity of the OFD1 purified antibody glycine and TEA elutions was characterised by immunofluorescence microscopy in hTERT-RPE1 cells. Purified antibodies were used at 1:100 (2.7 µg/µl and 1.1 µg/µl for glycine and TEA elutions, respectively), and final bleed was used at 1:250. DNA was stained with Hoechst 33258. FB, final bleed. Scale bar, 15 µm.

endogenous BBS4 (data not shown). We therefore decided to use the final bleed antiserum in all of our experiments.

3.3 DISCUSSION

Antibodies are invaluable tools in research, and are widely used in numerous applications. In cell biology, they are crucial for the detection of specific proteins, either by revealing their specific localization within a cell through immunofluorescence microscopy, or by unveiling their presence in cell extracts by Western blot analysis. Indeed, our results show that the OFD1 and BBS4 antibodies generated are able to detect the endogenous proteins and these are expressed in HEK293 cells, as shown by Western blot analysis, and in U2OS cells, shown by immunofluorescence microscopy. Particularly, in these cells, the proteins are confirmed as centrosomal through the cell cycle, as previously reported (Romio et al. 2004; Kim et al. 2004). The unsuccessful purification of the BBS4 antibodies may result from specific BBS4 antibodies being very tightly bound to the columns, impeding its elution. Alternatively, the elution in low or high pH may have led to denaturation of the specific BBS4 antibodies.

The generation of specific antibodies, particularly against OFD1, has made possible our studies on the localization, dynamics and behaviour of OFD1 protein upon several different treatments, depicted in the following chapters.

CHAPTER 4

OFD1 IS A COMPONENT OF CENTRIOLAR SATELLITES

CHAPTER 4 OFD1 IS A COMPONENT OF CENTRIOLAR SATELLITES

4.1 INTRODUCTION

Proteins associated with ciliopathies, a group of genetic disorders characterized by cilia dysfunction, are found in the cilium, the basal body or the centrosome (Baker & Beales 2009). Consistent with this, the first studies on the intracellular localization of the ciliopathy protein OFD1 showed it to be a core component of the human centrosome throughout the cell cycle (L. Romio et al. 2003; Leila Romio et al. 2004). In addition, in human renal proximal tubule epithelial cells (RPTEC), cultured under conditions that promote ciliogenesis, OFD1 was detected at the basal body and, occasionally, along the primary cilium (Romio et al. 2004). Electron microscopy of a human metanephric mesenchyme cell line with immunogold labeling for OFD1 confirmed this close association with centrosomes and centrioles in particular (Romio et al. 2003; omio et al. 2004). Indeed, OFD1 was recently shown to localize to the distal regions of centrioles in murine embryonic stem cells and also in several cell lines of mouse or human origin (Singla et al. 2010). OFD1 localization to the basal body was confirmed in ciliated murine fibroblasts (NIH-3T3), renal inner medullary collecting duct (IMCD3), human retinal pigmented epithelial cells (hTERT-RPE1) (Singla et al. 2010) and canine kidney epithelial cells (MDCK) (Giorgio et al. 2007).

All ciliopathies arise from defects in cilia. However, different cilia-related genes can lead to distinct diseases where the range of symptoms can vary significantly (Baker & Beales 2009). A possible explanation for this can be that some gene products may have an alternative cilia-unrelated function. Indeed, OFD1 has also been detected in the nucleus of kidney cells of canine (MDCK) and ape (Cos-7) origin and human epithelial cervical cancer cells (HeLa) (Giovanna Giorgio et al. 2007). Indeed, alternatively, different structures of cilia can be affected and therefore only influence a subset of ciliary functions (Marshall 2008). Although localization does not define a protein's function, it gives an important clue as to which cellular processes it

might be involved in. Having this in mind, we set out to examine the function of OFD1 by first revisiting its localization.

4.2 RESULTS

4.2.1 OFD1 localizes to pericentriolar aggregates

We started out to review the localization of OFD1 in telomerase-immortalized human retinal pigment epithelial (hTERT-RPE1) cells. For this we used two different polyclonal antibodies raised against distinct regions of OFD1: Ab1, from Romio et al. (2003), was raised against the peptide containing the amino acids 867-891, and Ab2, from this study (Chapter 3), was raised against the amino acids 145 to 1012. Due to alternative splicing, the *OFD1* gene encodes at least two transcripts. *OFD1a* encodes a 1012-amino acid protein (hereafter designated OFD1) that contains an N-terminal Lis1 homology motif (LisH; residues 70 to 102) and six coiled-coil (CC) domains distributed along the C-terminal region (de Conciliis et al. 1998; Emes & Ponting 2001; Romio et al. 2003). An alternative 3´ splice site in intron 9 (created by the insertion of an additional 663 bp) introduces an in-frame stop codon in exon 10. As a result, *OFD1b* has a shorter open reading frame that encodes a 367 amino acid protein containing the first 353 residues of OFD1 and an alternative C-terminal region; i.e. it contains the LisH and the first two coiled-coil domains (de Conciliis et al. 1998; Romio et al. 2003). Hence, whereas Ab1 would not detect OFD1b, Ab2 should detect both OFD1a and OFD1b isoforms.

Both antibodies revealed that OFD1 not only localized to the centrosome but is also distributed in small aggregates in its vicinity in proliferating hTERT-RPE1 cells (Figure 4.1A). This distribution pattern was also evident in human foreskin fibroblasts (hFF), renal inner medullary collecting duct (IMCD3) and human osteosarcoma (U2OS) cells (Figure 4.1B). However, contrary to what was observed in renal proximal tubule epithelial cells (RPTEC) (Romio et al. 2004), an OFD1 signal was not detected along the stalk of the primary cilium in hTERT-RPE1 or hFF

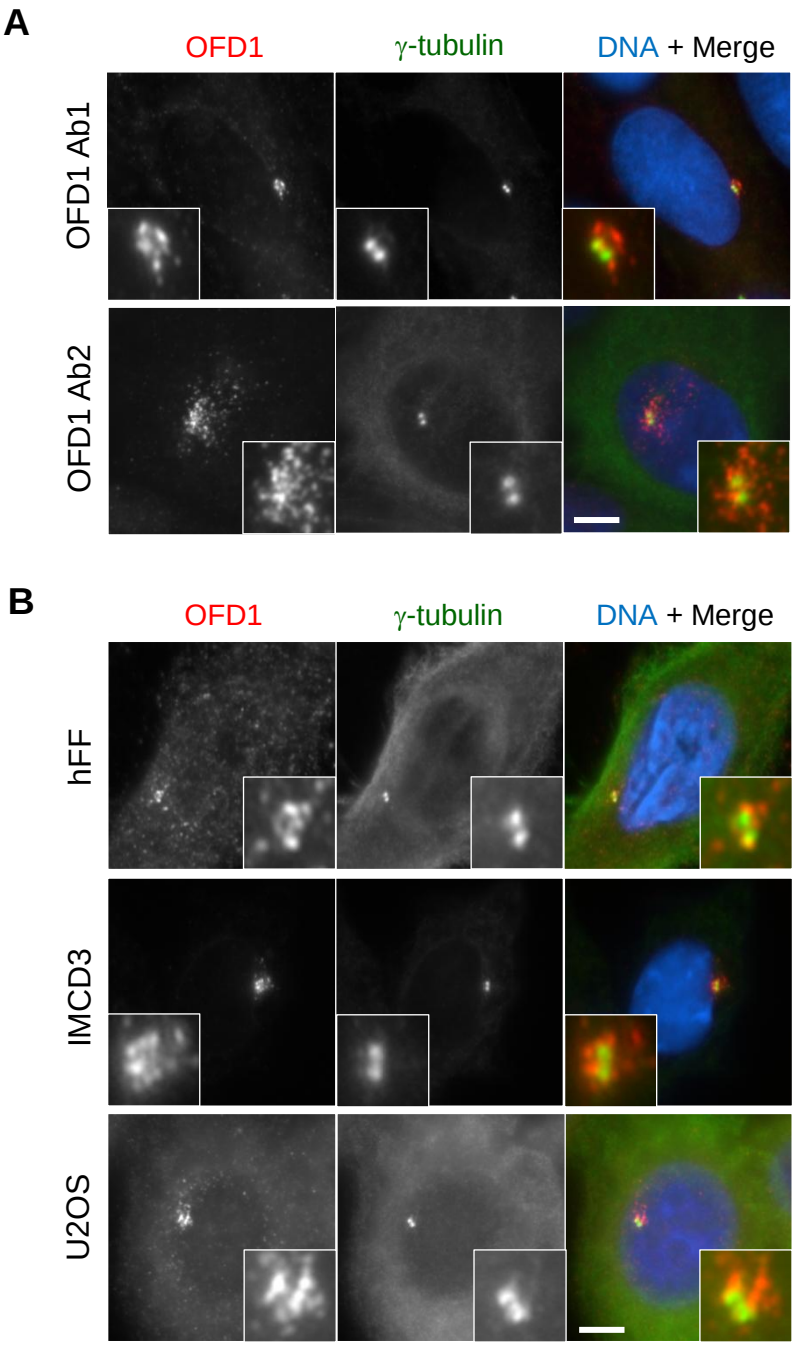

Figure 4.1 OFD1 localizes to small aggregates in the vicinity of the centrosome

(A) hTERT-RPE1 cells were co-stained with antibodies against γ-tubulin to detect the centrosome and with two different antibodies against OFD1 (Ab1 and Ab2; red) and γ-tubulin (green) to detect the centrosome. **(B)** Human foreskin fibroblasts (hFF), inner medullary collecting duct (IMCD3) and human osteosarcoma (U2OS) cells were co-stained with antibodies against OFD1 (red) and γ-tubulin (green). Insets show enlargements of the centrosome. DNA was stained with Hoechst 33258. Scale bars, 5 µm.

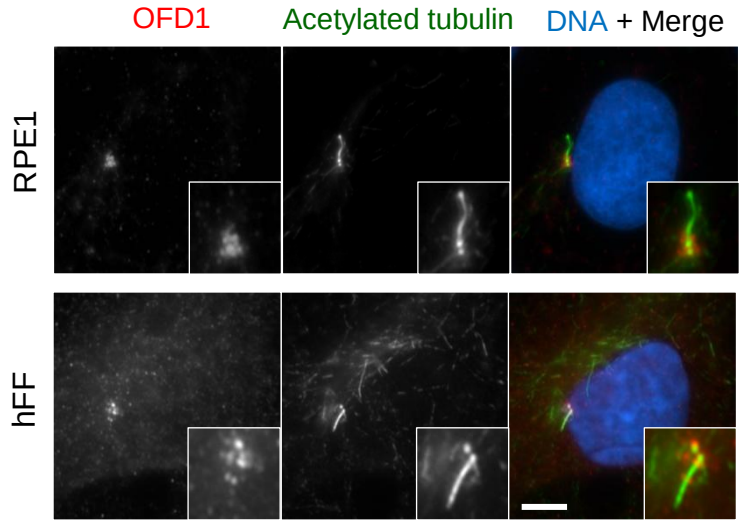

Figure 4.2 OFD1 does not localize to the axoneme of monociliated hTERT-RPE1 or hFF cells

Monociliated hTERT-RPE1 and hFF cells were co-stained with antibodies against acetylated tubulin (green) to detect the axonemal microtubules and OFD1 (red). Insets show enlargements of the primary cilium. DNA was stained with Hoechst 33258. Scale bar, 5 µm.

cells cultured under conditions to promote ciliogenesis (Figure 4.2). Localization to small aggregates was confirmed in hTERT-RPE1 cells by overexpressing GFP- or Myc-tagged constructs of the full-length protein (Figure 4.3A and B). This is consistent with the pericentriolar localization described in cells expressing eCFP-OFD1 (Coene et al. 2009) and with the gold particle labelling detected around the centrioles in immunoelectron microscopy for OFD1 (Romio et al. 2004).

4.2.2 OFD1 localizes to centriolar satellites with other disease proteins

This conspicuous distribution of OFD1 as aggregates in the vicinity of the centrosome reminded us of centriolar satellites, non-membranous 70-100 nm cytoplasmic granules that concentrate around the centrosome and contain PCM-1 protein (Figure 4.4A) (Kubo et al. 1999; Dammermann & Merdes 2002; Kubo & Tsukita 2003). Using antibodies to detect endogenous OFD1 or expressing GFP- or Myc-tagged full-length constructs of the protein, it was clear that OFD1 aggregates specifically colocalize with PCM-1 at centriolar satellites (Figure 4.4A and B).

Intriguingly, BBS4 had also been described to localize to centriolar satellites with PCM-1 (Kim et al. 2004). Moreover, during the course of this study, CEP290 was also localized to PCM-1-containing centriolar satellites (J. Kim et al. 2008). We therefore costained cells expressing a Myc-tagged full-length OFD1 construct with CEP290 or BBS4 antibodies. This revealed significant colocalization of the proteins at centriolar satellites. Thus, the ciliopathy disease proteins OFD1, CEP290 and BBS4 colocalize to centriolar satellites in interphase hTERT-RPE1 cells. However, other reported satellite proteins like pericentrin, Cep135 or centrin (Dammermann & Merdes 2002; Ohta et al. 2002) were not visibly detected at satellites in hTERT-RPE1 cells; these were rather primarily associated with the centrosome, and did not strongly colocalize with OFD1 (Figure 4.5).

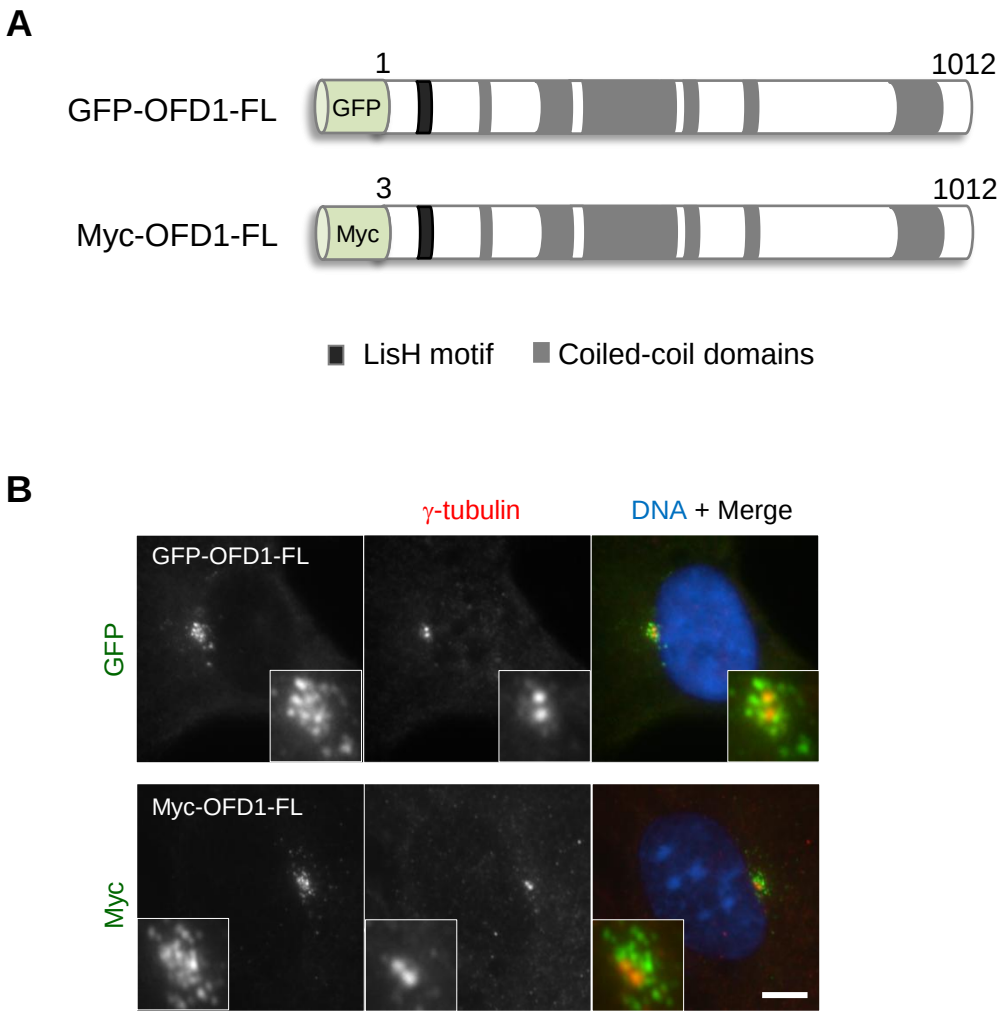

Figure 4.3 Expression of recombinant OFD1 recapitulates endogenous OFD1 localization

(**A**) Schematic representation of GFP- and Myc-tagged fusion proteins of OFD1 (full-length). The black box indicates the LisH motif; grey boxes indicate the coiled-coil domains. (**B**) hTERT-RPE1 cells transiently transfected with GFP- or Myc-tagged OFD1 full-length constructs were co-stained with antibodies to detect the GFP or the Myc tags (green) and with antibodies against γ-tubulin (red). Insets show enlargements of the centrosome. DNA was stained with Hoechst 33258. Scale bar, 5 µm.

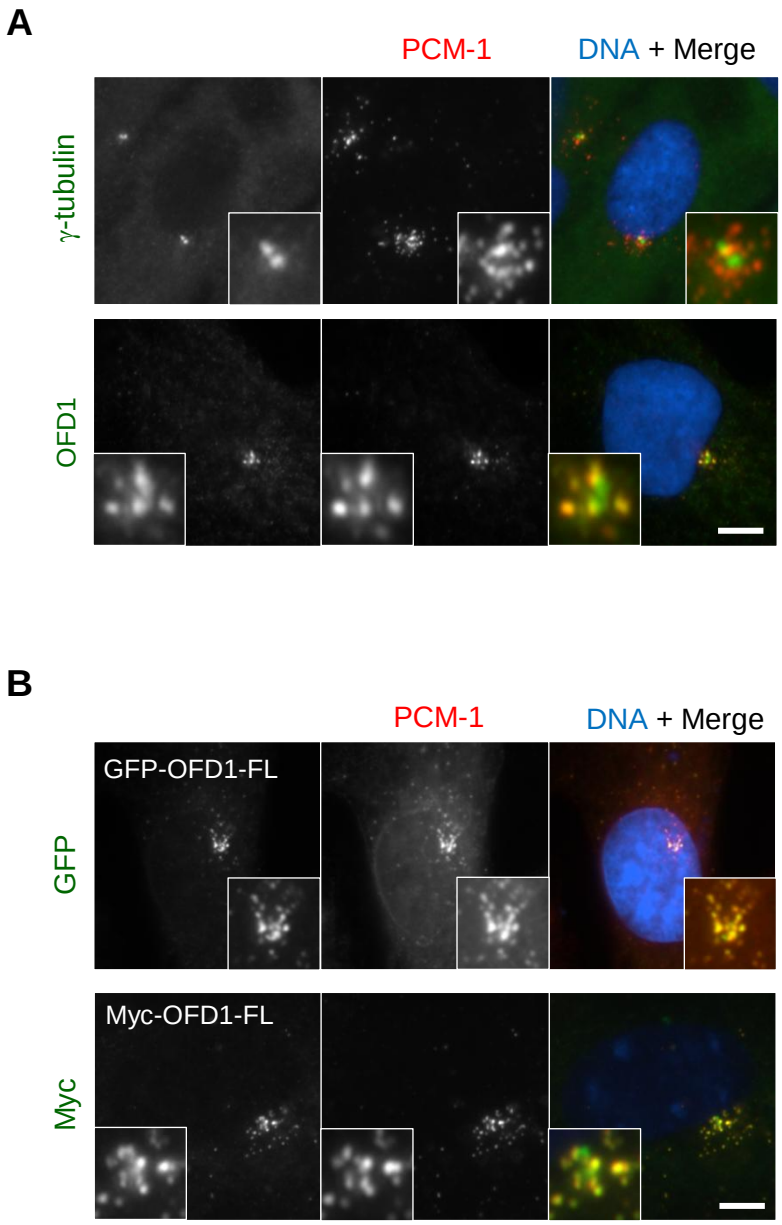

Figure 4.4 OFD1 co-localizes with PCM-1 at centriolar satellites
(A) hTERT-RPE1 cells were co-stained with antibodies against PCM-1 (red) and with antibodies against OFD1 or γ-tubulin (green). **(B)** hTERT-RPE1 cells transiently transfected with GFP- or Myc-tagged OFD1 full-length constructs were co-stained with antibodies to detect the GFP or the Myc tags (green) and with antibodies against PCM-1 (red). Insets show enlargements of the centrosome. DNA was stained with Hoechst 33258. Scale bars, 5 µm.

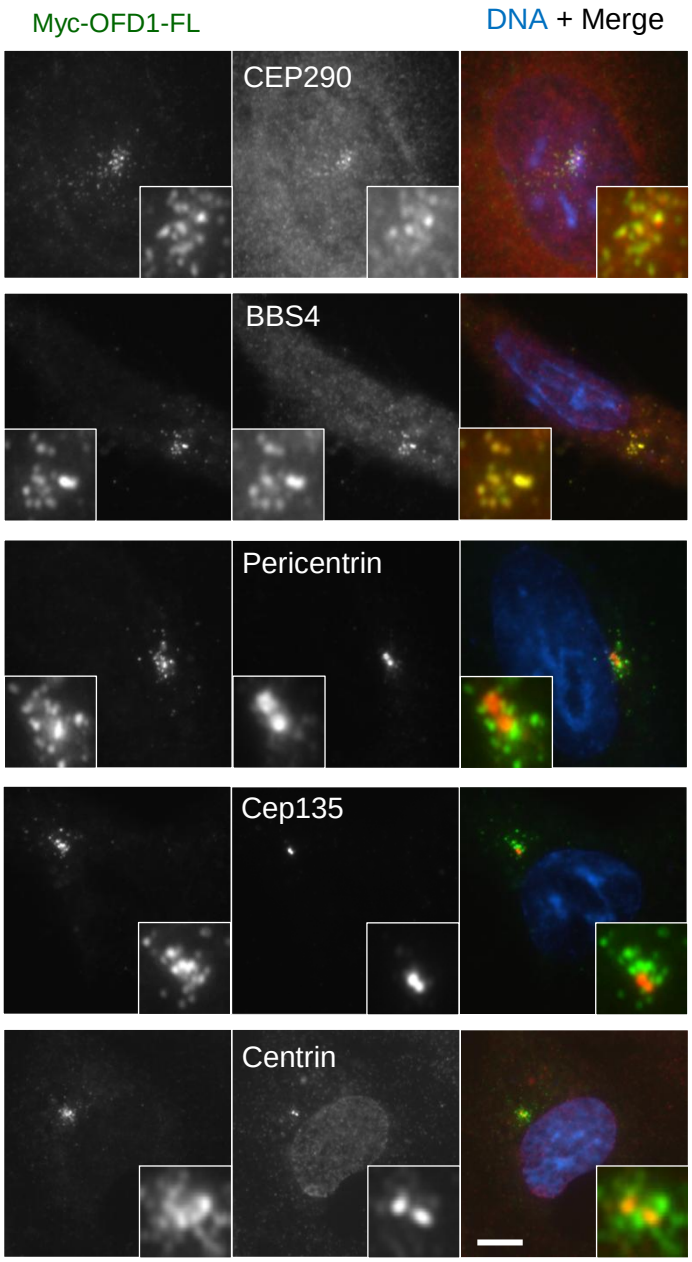

Figure 4.5 Ciliopathy disease proteins are components of centriolar satellites
hTERT-RPE1 cells transiently transfected with a Myc-tagged OFD1 full-length construct were co-stained with antibodies to detect the Myc tag (green) and with antibodies against CEP290, BBS4, pericentrin, Cep135 or centrin2 (red). Insets show enlargements of the centrosome. DNA was stained with Hoechst 33258. Scale bar, 5 µm.

4.2.3 Loss of centriolar satellites disturbs OFD1 localization

The distribution of centriolar satellites is very dynamic and dependent on microtubules and the microtubule-dependent motor dynein-dynactin (Dammermann & Merdes 2002). As a result, PCM-1, CEP290 and BBS4 are dispersed when this system is disrupted (Dammermann & Merdes 2002; Kim et al. 2004; Kim et al. 2008). Given the close association between these proteins and OFD1, it was important to assess if the recruitment of OFD1 to the centriolar satellites was also dependent on the microtubule network and/or the dynein-dynactin molecular motor. In order to depolymerise the microtubule network, hTERT-RPE1 cells were treated with nocodazole. Under these conditions, the OFD1 aggregates that clustered around the centrosome in untreated cells became mislocalized in a similar manner to PCM-1 (Figure 4.6A and C). In contrast, a fraction of OFD1 remained associated with the centrosome, in a similar fashion to the core centrosomal protein γ-tubulin (Figure 4.6A and B). The centrosomal fraction of OFD1 was not clearly detected in untreated cells. However, this could be possibly due to the clustering of aggregates surrounding the centrosome. As a result, we cannot be sure if the centrosomal OFD1 seen upon microtubule depolymerization becomes more easily detected with the dispersal of the aggregates, or if it moves to the centrosome under these conditions. Microtubule regrowth after washout of the nocodazole led to the reappearance of OFD1 aggregates around the centrosome, concomitant with the accumulation of centriolar satellites shown by PCM-1 (Figure 4.6A and C). The potential involvement of the dynein-dynactin molecular motor in OFD1 recruitment was determined by overexpressing p50-dynamitin, which antagonizes the function of this motor *in vivo* (Dammermann & Merdes 2002). Just as observed with PCM-1, overexpression of p50-dynamitin caused the pericentriolar aggregates of OFD1 to mislocalize in hTERT-RPE1 cells. However, as found for γ-tubulin, a fraction of OFD1 was detected at the centrosome (Figure 4.6D).

Furthermore, it has been shown that treatments that block centrosome overduplication in S-phase arrested cells, including inhibiting nuclear export or Cdk

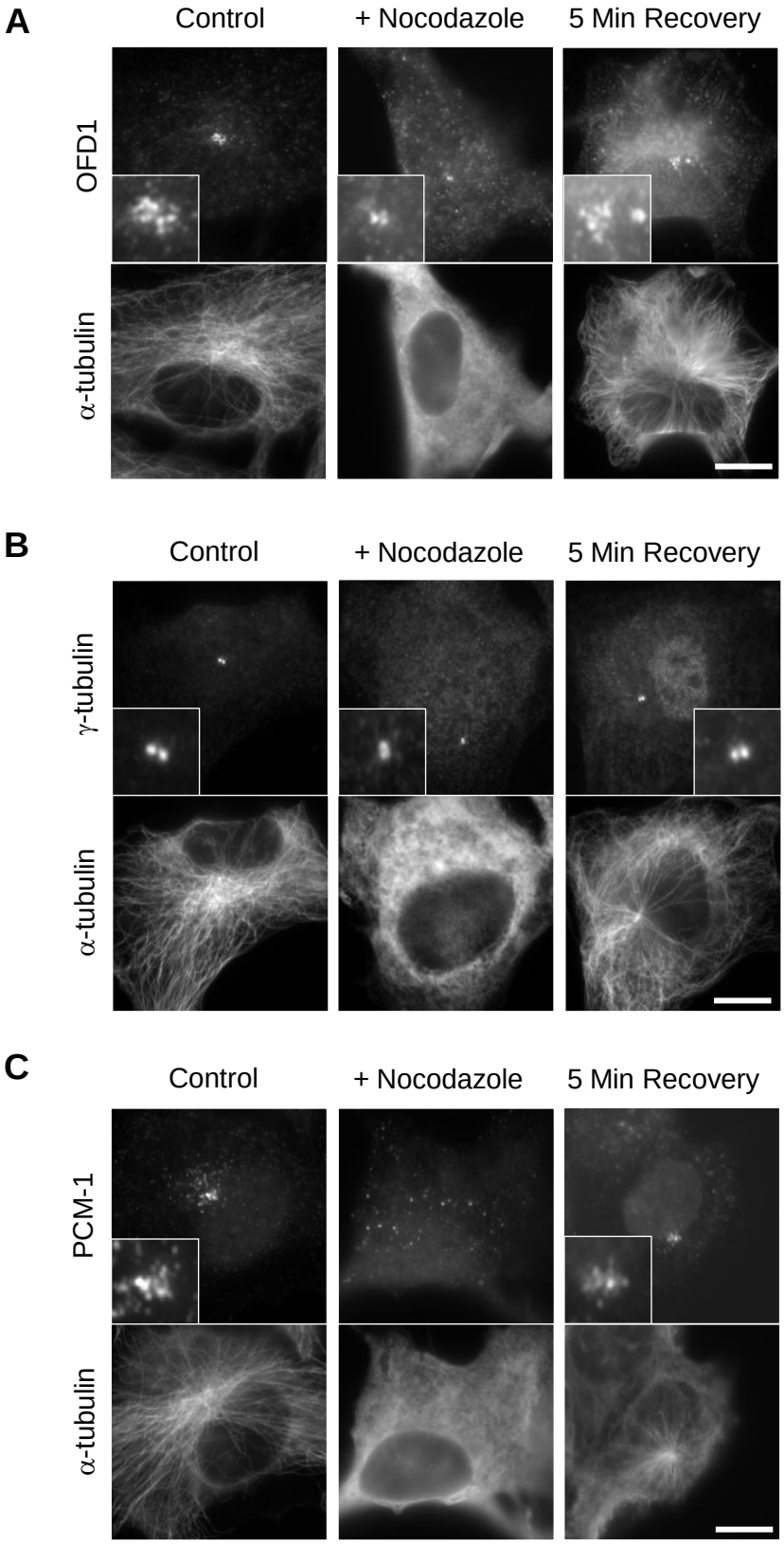
A
Control
+ Nocodazole
5 Min Recovery
OFD1
α-tubulin
B
Control
+ Nocodazole
5 Min Recovery
γ-tubulin
α-tubulin
C
Control
+ Nocodazole
5 Min Recovery
PCM-1
α-tubulin

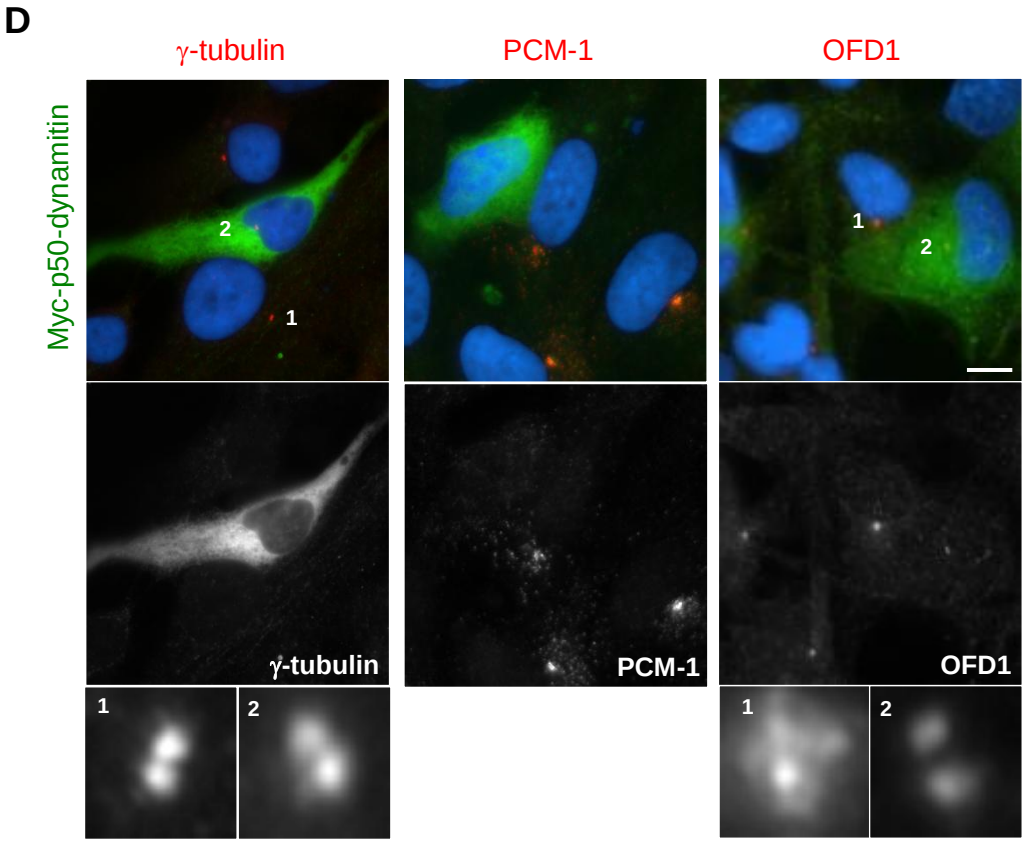

Figure 4.6 Localization of OFD1 to centriolar satellites depends upon microtubule-dependent transport

(A-C) hTERT-RPE1 cells were either mock-treated (Control) or treated with 6 µg/ml nocodazole (+ Nocodazole) to depolymerize the microtubule network, or treated with nocodazole and allowed to recover for 5 minutes (5 Min Recovery). Cells were then costained with antibodies against α-tubulin and OFD1 **(A)**, γ-tubulin **(B)** or PCM-1 **(C)** as indicated. Insets show enlargements of the centrosome. Scale bars, 10 µm. **(D)** hTERT-RPE1 cells were transfected for 24 hours with Myc-tagged p50-dynamitin to disrupt the dynein-dynactin motor function and costained with antibodies against Myc (green) and γ-tubulin, PCM-1 or OFD1 (red). Enlargements of γ-tubulin and OFD1 signals from untransfected (1) or transfected (2) cells are shown. DNA was stained with Hoechst 33258. Scale bar, 10 µm.

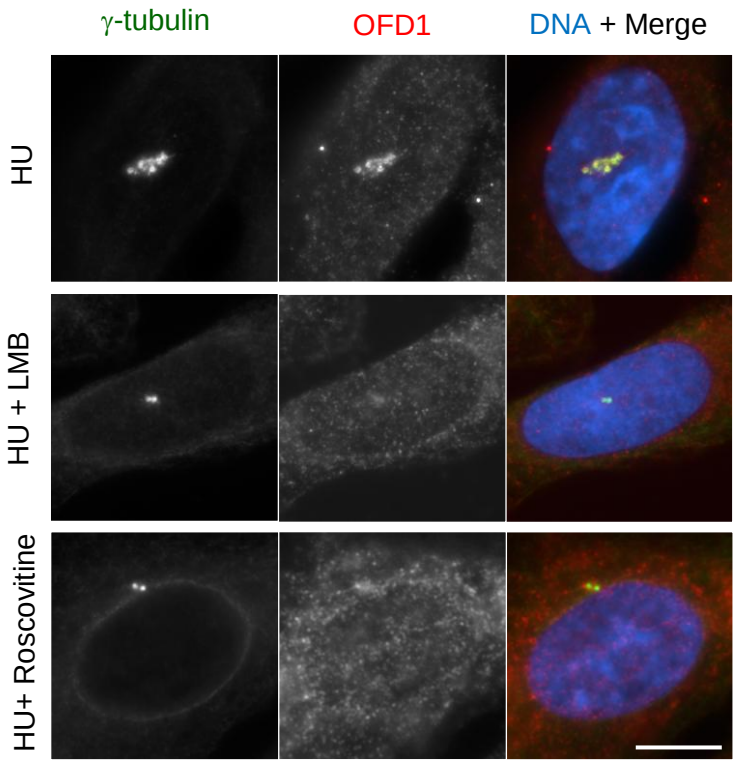

Figure 4.7 OFD1 signal disappears under conditions that lead to loss of centriolar satellites

CHO cells were treated with HU alone for 48 hours, HU for 18 hours followed by HU and LMB for 30 hours, or HU for 18 hours followed by HU and roscovitine for 30 hours. Cells were processed for immunofluorescence microscopy and stained for γ-tubulin (green) and OFD1 (red). DNA was stained with Hoechst 33258. Scale bar, 10 μm. Experiment undertaken by Dr. Suzanna L. Prosser.

activity, also lead to loss of centriolar satellites (Prosser et al. 2009). In this assay, Chinese hamster ovary (CHO) cells treated with hydroxyurea (HU) are blocked in S-phase, but undergo multiple rounds of centrosome duplication over time without DNA replication or cell division (Khodjakov et al. 2002; Prosser et al. 2009). These cells are then treated with roscovitine to specifically inhibit Cdk activity or with Leptomycin-B (LMB) to inhibit nuclear export (Meraldi et al. 1999; Prosser et al. 2009). Centrosome multiplication is monitored by immunofluorescence staining of cells with γ-tubulin antibodies. Similar to what was found for PCM-1 (Prosser et al. 2009), these treatments led to loss of pericentriolar aggregates of OFD1 (Figure 4.7; experiment undertaken by Dr. Suzanna L. Prosser). Together, this data demonstrates that OFD1 is not only a core component of the centrosome as previously reported (Romio et al., 2004; Singla et al 2010) but it also behaves as a *bona fide* centriolar satellite component.

4.2.4 OFD1 associates with basal bodies in cells with motile cilia

Centriolar satellites are most likely equivalent to fibrous granules (Kubo et al. 1999), the first recognizable structures generated during ciliogenesis in multiciliated epithelia of the respiratory tract and the oviduct (Hagiwara et al. 2004). Given the localization of OFD1 to centriolar satellites in monociliated cells, we were interested to examine its localization in cells with multiple cilia. To this end, primary human nasal epithelial cells, collected from a nasal brush biopsy by Prof. Chris O'Callaghan (University of Leicester), were cultured at an air-liquid interface (ALI) to induce differentiation. The cell culture was undertaken by Dr. Robert A. Hirst (University of Leicester) as previously described (Hirst et al. 2010). During this process, which lasts approximately 2-4 weeks, epithelial cells first produce hundreds of centrioles, through both centriolar and acentriolar pathways, which then migrate to the apical surface becoming basal bodies and each generating a motile cilium (Hagiwara et al. 2004; Dawe et al. 2007). Cells at different stages of differentiation were co-stained with antibodies against OFD1 and γ-tubulin. Contrary to what is seen in monociliated cells, prior to differentiation (10 days post ALI) OFD1 localizes to the centrosome

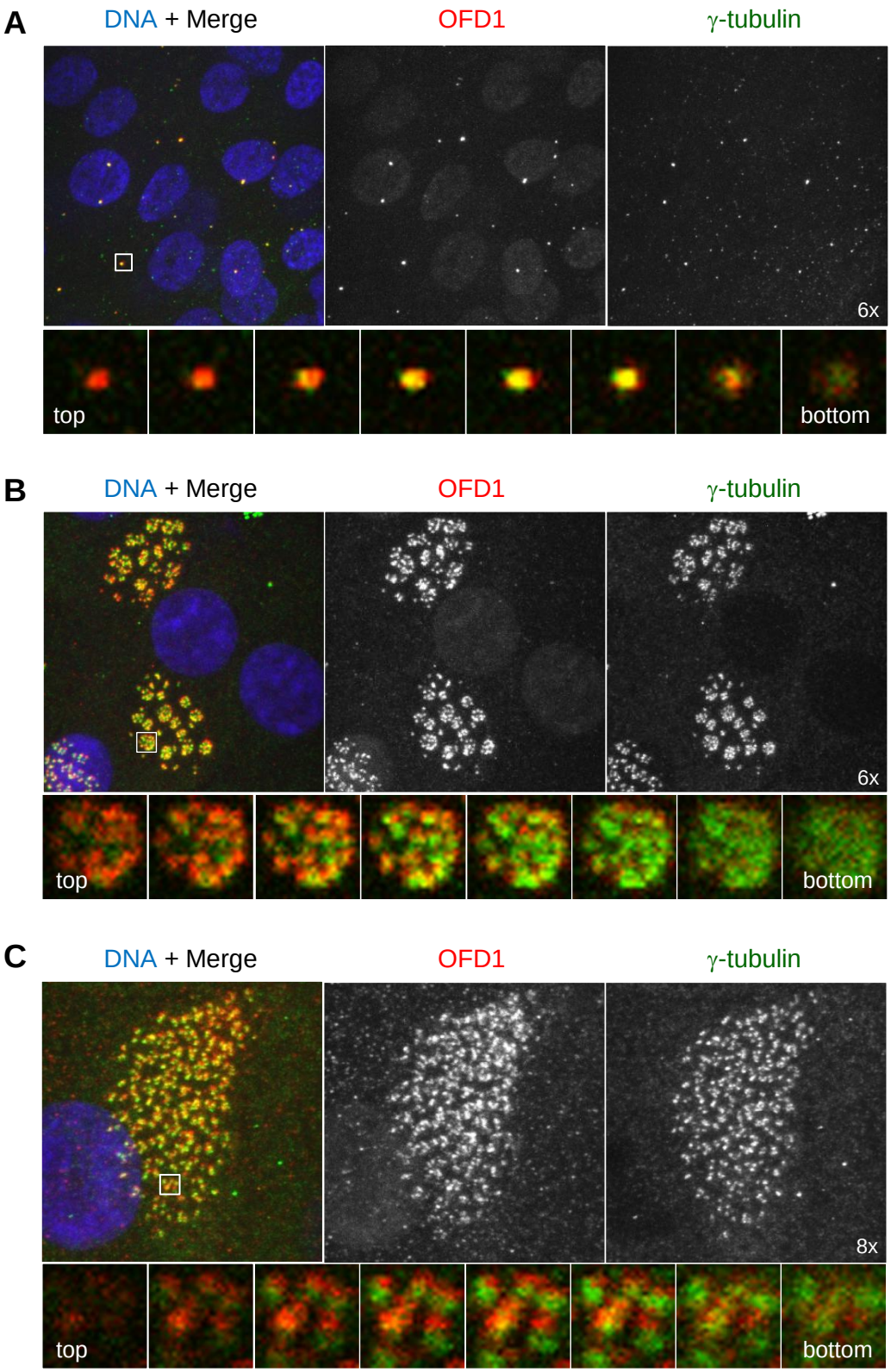
A
DNA + Merge
OFD1
γ-tubulin
6x
top
bottom
B
DNA + Merge
OFD1
γ-tubulin
6x
top
bottom
C
DNA + Merge
OFD1
γ-tubulin
8x
top
bottom

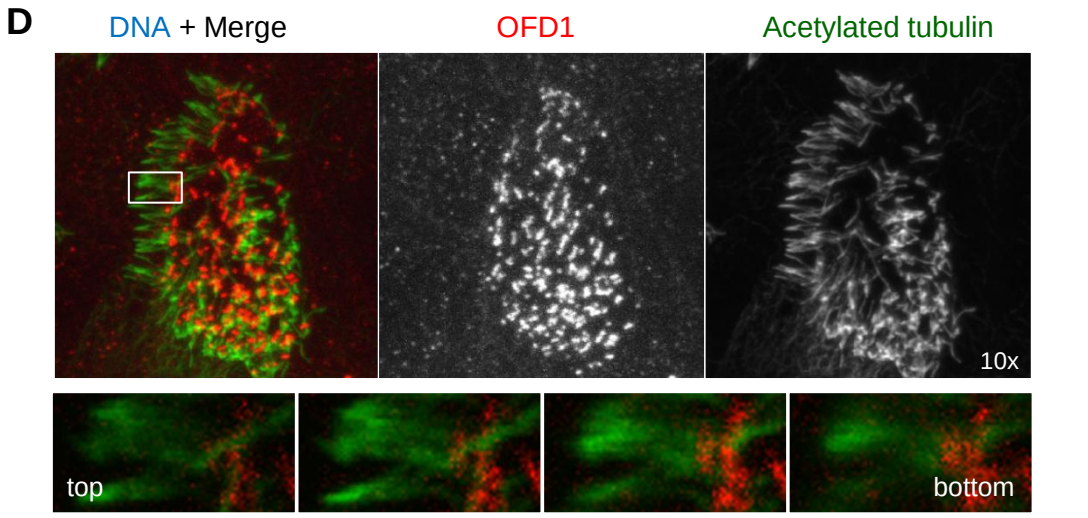

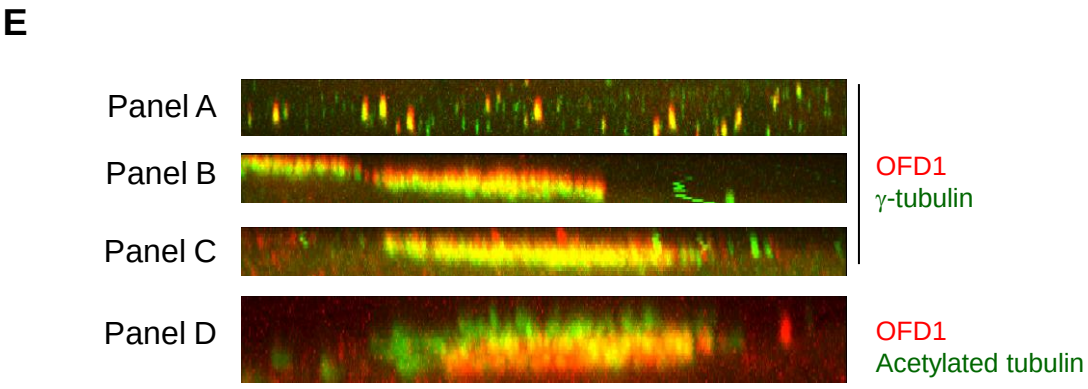

Figure 4.8 OFD1 localizes to sites of basal body assembly in multiciliated epithelia
Primary human nasal epithelial cells were grown to different stages of differentiation by transfer to an air-liquid interface (ALI) before fixation and co-staining with antibodies against OFD1 (red) and γ-tubulin **(A-C)** or acetylated tubulin **(D)** (green). DNA was stained with Hoechst 33258. Cells were imaged by confocal microscopy and maximum intensity projections are shown in the upper panels. The lower panels show enlargements of the boxed areas through sequential z-sections. **(A)** Cells at day 10 post-ALI. **(B-D)** Cells at day 28 post ALI. **(E)** Z-axis projections of panels A-D.

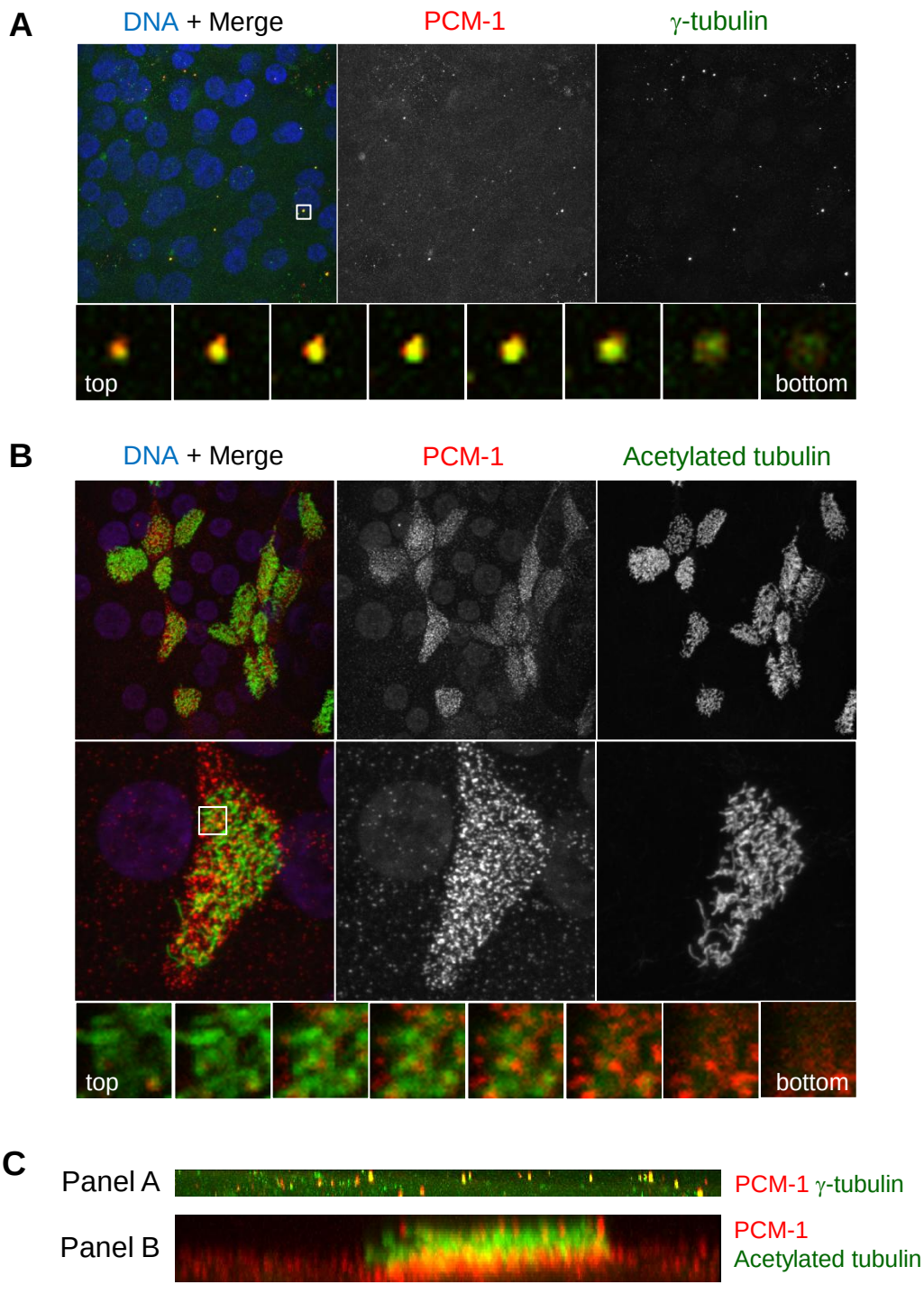

Figure 4.9 PCM-1 localizes to the vicinity of basal bodies in multiciliated epithelia
Primary human nasal epithelial cells were grown to different stages of differentiation by transfer to an air-liquid interface (ALI) before fixation and co-staining with antibodies against PCM-1 (red) and γ-tubulin **(A)** or acetylated tubulin **(B)** (green). DNA was stained with Hoechst 33258. Cells were imaged by confocal microscopy and maximum intensity projections are shown in the upper panels. The lower panels show enlargements of the boxed areas through sequential z-sections. **(A)** Cells at day 10 post-ALI. **(B)** Cells at day 28 post ALI. **(C)** Z-axis projections of panels A and B.

and does not appear to localize as pericentriolar aggregates (Figure 4.8A). In differentiated cells (28 days post ALI) OFD1 reveals a similar localization pattern, being closely associated with each of the multiple basal bodies. This is true both when the basal bodies were arranged in distinct rosette-like clusters (presumably representing a midway point in the differentiation process), and when cells were full of basal bodies (fully differentiated) (Figure 4.8B and C). Costaining of OFD1 with acetylated tubulin revealed that, in accordance to what was observed in monociliated cells, OFD1 was not detected along the axonemal microtubules (Figure 4.8D). Close examination of OFD1, γ-tubulin and acetylated tubulin signals through x-y and z-sections showed that, despite the tight association of OFD1 with the basal bodies, is does not perfectly colocalize with γ-tubulin. In fact, it appears that OFD1 concentrates on the apical side of basal bodies at the foot of the ciliary axoneme (Figure 4.8B-E). A similar distribution pattern was found for PCM-1, both before and after differentiation. Costaining of cells prior to differentiation (10 days post ALI) for PCM-1 and γ-tubulin did not reveal any distinct centriolar satellites (Figure 4.9A). Fully differentiated cells (28 days post ALI) costained for PCM-1 and acetylated tubulin did not reveal PCM-1 along the axonemal microtubules suggesting that it is also restricted to the basal bodies (Figure 4.9B). This was further confirmed by close inspection of *x-y* and *z*-sections (Figure 4.9A-C).

4.2.5 Redistribution of ciliopathy disease proteins during mitotic progression

To study OFD1 behaviour during cell cycle progression, we first analyzed its protein expression levels by Western blot. hTERT-RPE1 cells were either hydroxyurea- or nocodazole-treated to arrest in S and M phases, respectively. Synchronization of the cells was confirmed by flow cytometry analysis (Figure 4.10A). Western blot analysis revealed that OFD1 expression appeared to vary during the cell cycle, being lower in M phase than S phase. PCM-1 levels, however, appear to remain constant during cell cycle progression (Figure 4.10B). We then looked at the behaviour of OFD1 during mitosis in hTERT-RPE1 cells using immunofluorescence microscopy. Using

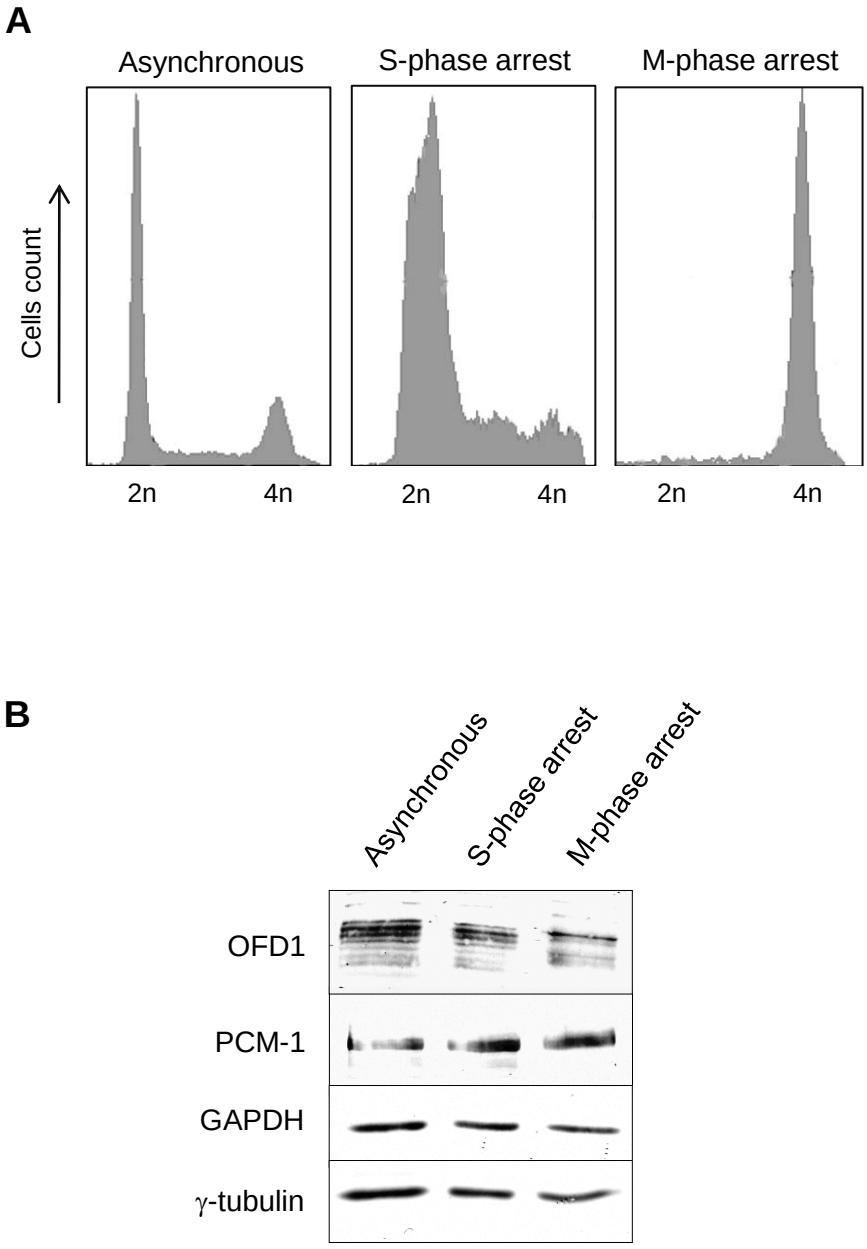

Figure 4.10 Cell cycle expression of OFD1 and PCM-1

Asynchronous and hydroxyurea- (S-phase) or nocodazole- (M-phase) treated hTERT-RPE1 cells were analysed by flow cytometry **(A)** and Western blot **(B)**. **(A)** Flow cytometry profiles indicating 2n (G_1) and 4n (G_2/M) populations. **(B)** Cell lysates were immunoblotted with antibodies against OFD1, PCM-1, GAPDH and γ-tubulin.

antibodies to detect endogenous OFD1 or by expressing recombinant Myc-OFD1, we found that whereas the small aggregates that surround the centrosome in interphase disperse during mitosis, the weakly detectable OFD1 localization to the centrosome in interphase cells became more obvious during metaphase and anaphase (Figure 4.11 and 4.12). This dispersal of OFD1 aggregates is consistent with the previous description of centriolar satellite dispersal during metaphase and anaphase (Dammermann & Merdes 2002). Indeed, we confirmed that PCM-1 and BBS4 are mainly dispersed in the cytoplasm during mitosis (Figure 4.13A and B). In the case of CEP290, although the satellites dispersed during mitotic progression, a centrosomal fraction was retained at the spindle poles, just as for OFD1 (Figure 4.13C). In contrast, pericentrin and Cep135 did not appear to change their localization, remaining associated with the spindle poles in mitosis (Figure 4.14). Using recombinant myc-tagged OFD1 and costaining for centrin, a marker of centriole distal ends (Figure 4.15A), or C-Nap1, a marker of centriole proximal ends (Figure 4.15B), we confirmed that OFD1 associates with the distal ends of centrioles during mitosis. Thus, centriolar satellite proteins do not all exhibit the same behaviour during mitosis. Whilst some are either completely dispersed to the cytoplasm (PCM-1 and BBS4) or not affected at all (pericentrin and Cep135), others not only disperse but also redistribute to the spindle poles (OFD1 and CEP290).

4.3 DISCUSSION

Primary cilia, present on most mammalian cell types, were long considered rudimentary and vestigial organelles. However, recent work has shown that they have important roles in the control of cell proliferation and in signalling pathways during development and, when defective, can cause human disorders – ciliopathies – that affect many organ systems (Fliegauf et al. 2007; Satir et al. 2010). The growing list of ciliopathies includes distinct diseases such as Bardet-Biedl syndrome (BBS), nephronophthisis (NPHP), polycystic kidney disease (PKD), Oral-facial-digital syndrome type 1 (OFD1) and Jourbert syndrome (JBTS), but all result from

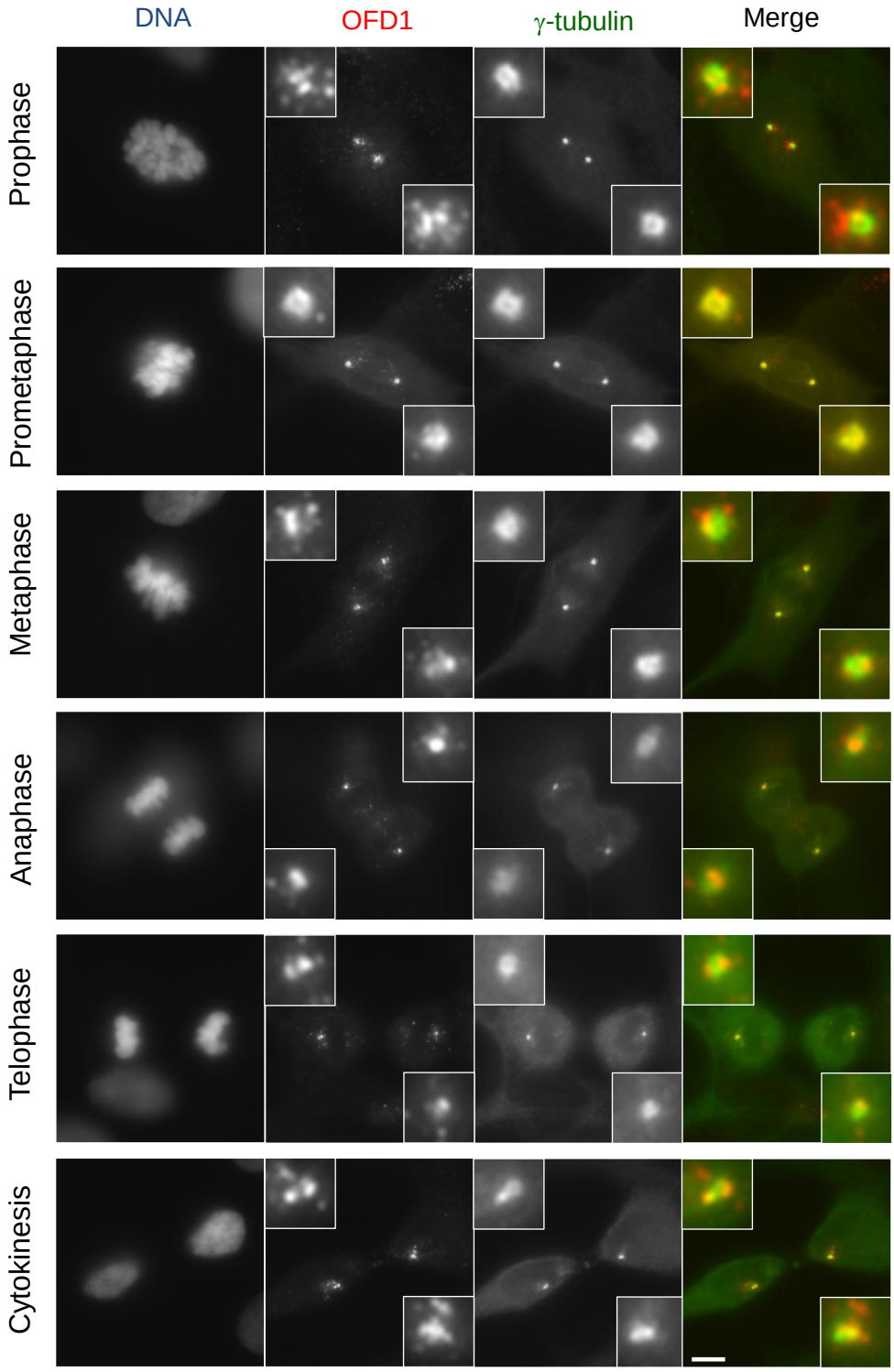

Figure 4.11 OFD1 localizes to spindle poles throughout mitosis
hTERT-RPE1 cells were co-stained with antibodies against OFD1 (red) and with antibodies against γ-tubulin (green). DNA was stained with Hoechst 33258. The cell cycle phase is indicated on the left of each panel. Insets show enlargements of the mitotic spindle poles. Scale bar, 5 µm.

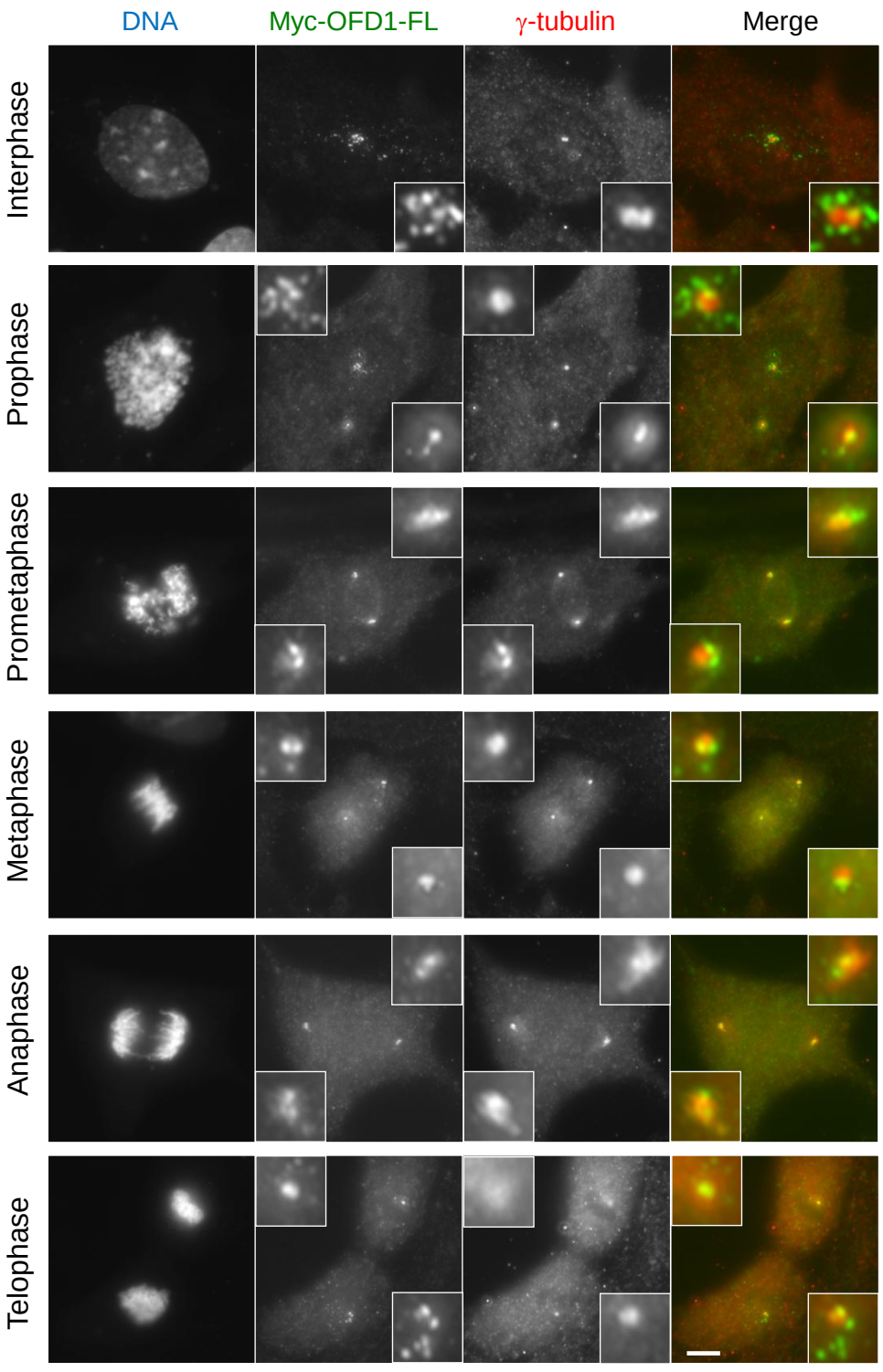

Figure 4.12 Recombinant OFD1 recapitulates endogenous OFD1 localization to the centrosome throughout the cell cycle

hTERT-RPE1 cells transiently transfected with a Myc-tagged full-lengthOFD1 were co-stained with antibodies against the Myc tag (green) and with antibodies against γ-tubulin (red). DNA was stained with Hoechst 33258. The cell cycle phase is indicated on the left of each panel. Insets show enlargements of the centrosome/spindle pole. Scale bar, 5 µm.

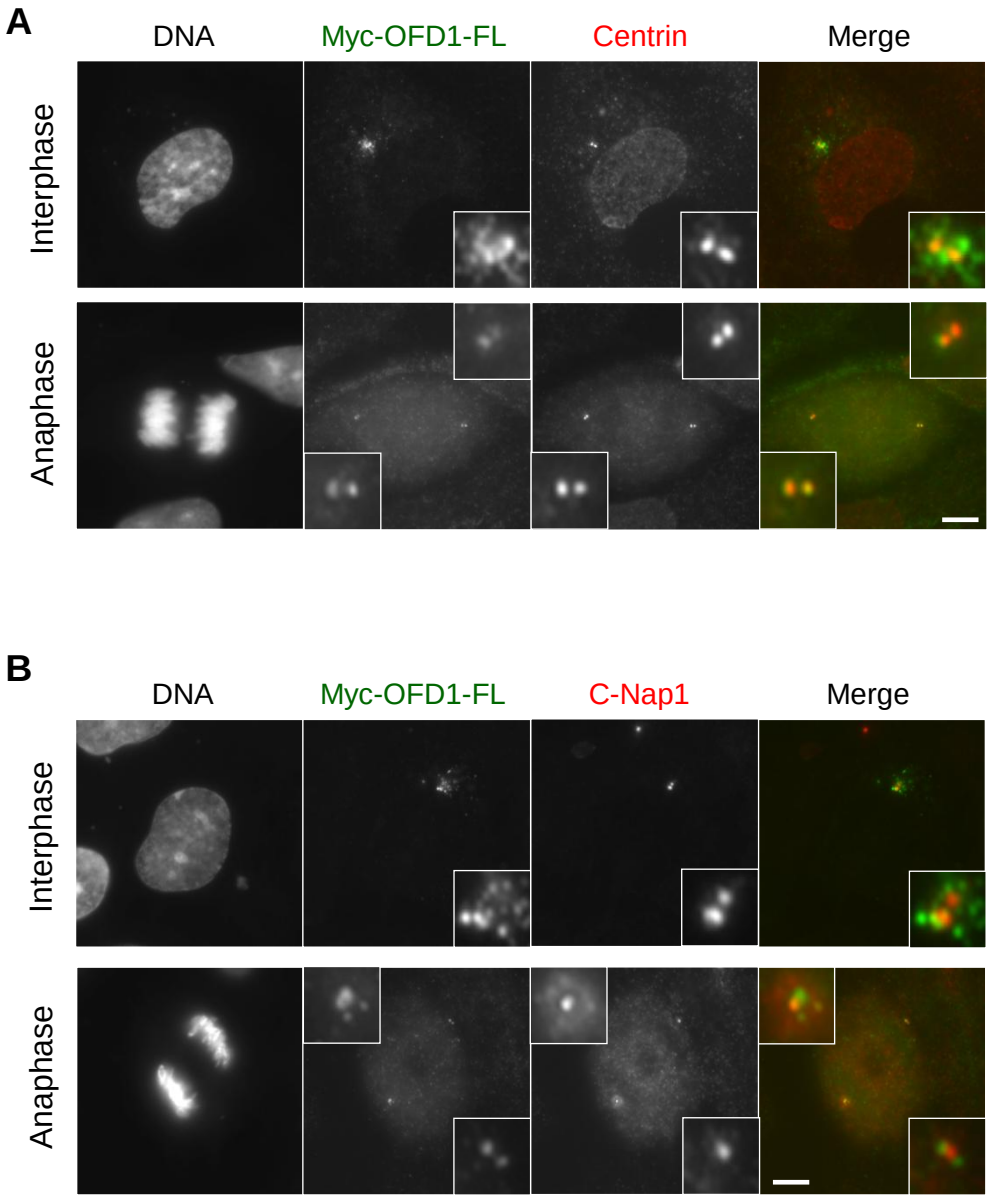

Figure 4.13 OFD1 localizes to the distal end of centrioles during mitosis
hTERT-RPE1 cells transiently transfected with a Myc-tagged full-length construct of OFD1 were co-stained with antibodies against the Myc tag (green) and with antibodies against centrin-2 **(A)** or C-Nap1 **(B)** (red). DNA was stained with Hoechst 33258. The cell cycle phase is indicated on the left of each panel. Insets show enlargements of the centrosome/spindle pole. Scale bar, 5 µm.

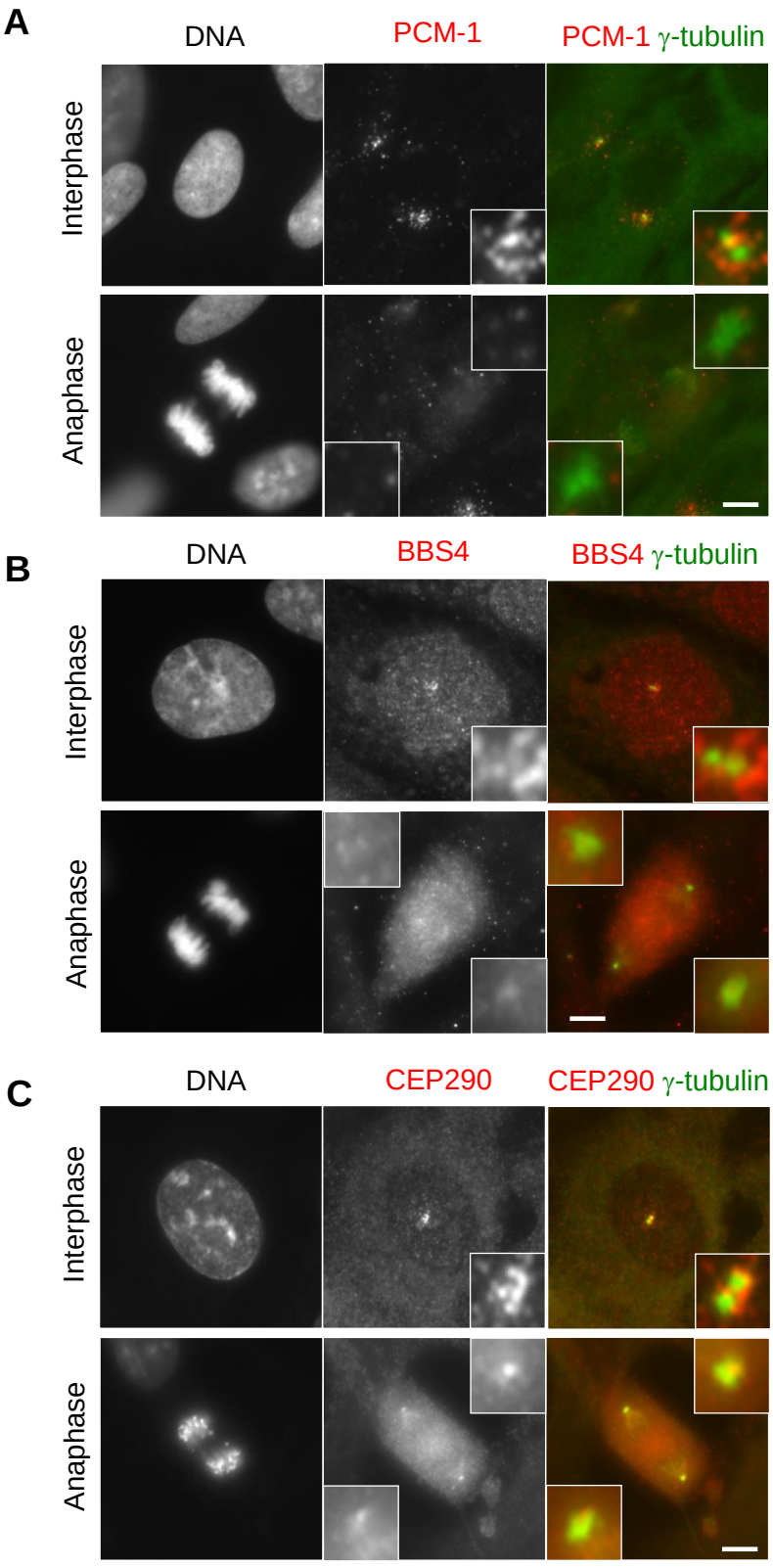

Figure 4.14 Localization of PCM-1, BBS4 and CEP290 during mitosis
hTERT-RPE1 cells were co-stained with antibodies against γ-tubulin (green) and PCM-1 **(A)**, BBS4 **(B)** or CEP290 **(C)** (red). DNA was stained with Hoechst 33258. The cell cycle phase is indicated on the left of each panel. Insets show enlargements of the centrosome/spindle pole. Scale bars, 5 µm.

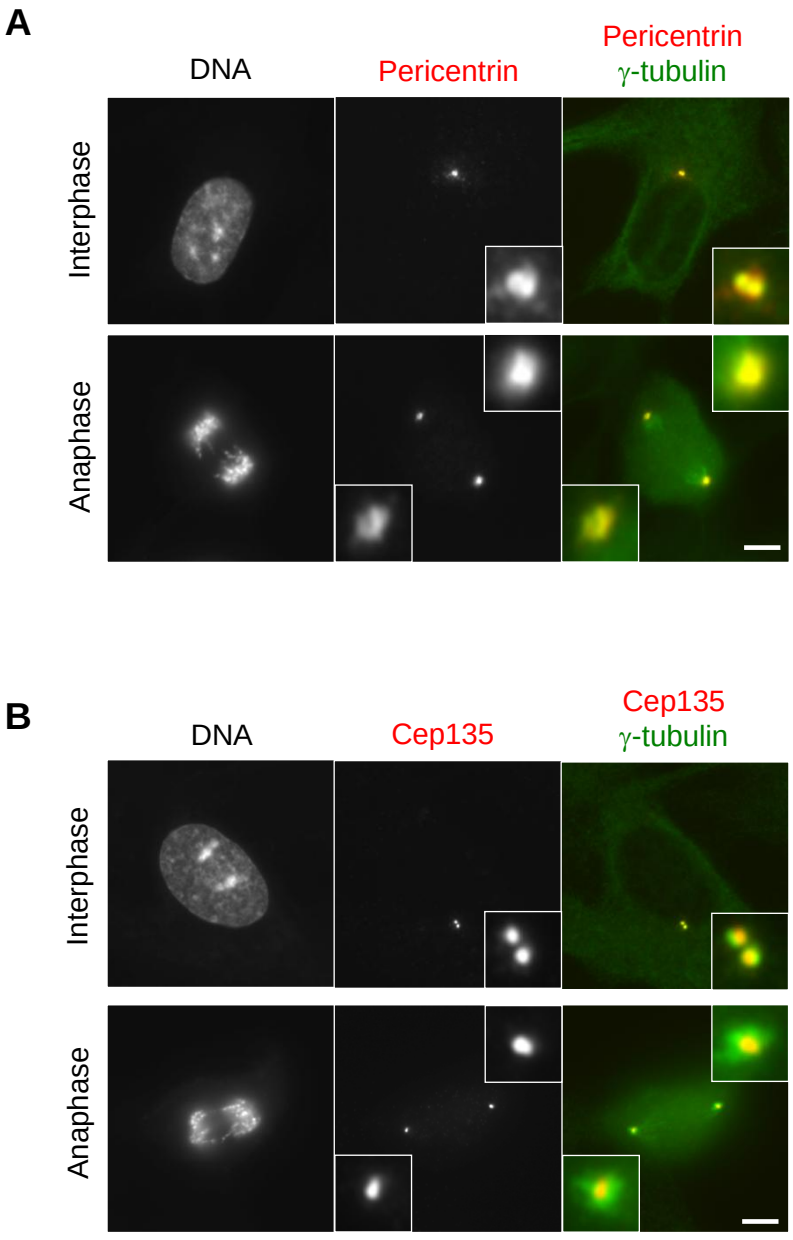

Figure 4.15 Localization of pericentrin and Cep135 during mitosis
hTERT-RPE1 cells were co-stained with antibodies against γ-tubulin (green) and pericentrin **(A)** or Cep135 **(B)** (red). DNA was stained with Hoechst 33258. The cell cycle phase is indicated on the left of each panel. Insets show enlargements of the centrosome/spindle pole. Scale bars, 5 µm.

defects in genes that encode proteins associated with the primary cilium, the basal body or the centrosome (Marshall 2008; Baker & Beales 2009).

Unexpectedly, we found that both endogenous and recombinant OFD1 were mainly detected as small aggregates surrounding the centrosome in different mammalian cell lines in a pattern highly reminiscent of centriolar satellites, non-membranous cytoplasmic granules that concentrate around the centrosome (Kubo et al. 1999). Remarkably, pericentriolar OFD1 perfectly colocalized with PCM-1, a core component of these structures. At the time of our study, of all the ciliopathy disease proteins, only BBS4, one of the twelve known BBS associated proteins, had been described to localize to PCM-1-containing centriolar satellites (Kim et al. 2004). Recently, though, CEP290, a protein associated with a subtype of JBTS, joined this list of ciliopathy disease proteins that primarily localize to centriolar satellites in interphase cells (Kim et al. 2008). Not surprisingly, OFD1, BBS4 and CEP290 pericentriolar aggregates disperse under conditions that are known to disturb these structures, such as interfering with microtubule dynamics, thus behaving as *bona fide* centriolar satellite components (Dammermann & Merdes 2002; Kim et al. 2004; Kim et al. 2008). We therefore speculate that these ciliopathy disease proteins and PCM-1 may cooperate in common molecular pathways.

Centriolar satellites are thought to be equivalent structures to fibrous granules, PCM-1-containing granular structures observed early on during ciliogenesis in multiciliated epithelial cells (Kubo et al. 1999). In differentiating cells undergoing ciliogenesis multiple centrioles are generated by a centriolar pathway, in which several basal bodies form around individual centrioles, or an acentriolar pathway, in which multiple basal bodies are assembled around electron-dense structures. These are formed by fibrous granules, which accumulate in these cells to form clusters and aggregates – deuterosomes – which then serve as organizing centres for the formation of new centrioles. They then separate from deuterosomes, migrate to the cell surface where they dock with the apical plasma membrane, becoming basal

bodies and each elongating a motile cilium (Hagiwara et al. 2004). We studied OFD1 and PCM-1 localization in human nasal epithelial cells cultured at an air-liquid interface (ALI) to trigger ciliation. In differentiated cells (28 days post ALI) we observed distinct rosette-like structures, similar to the ultrastructural observations of Hagiwara et al (2002), which represent the centrioles being assembled from clustered fibrous granules. OFD1 and PCM-1 associated with each of these new centrioles and with every basal body at a later stage when they separated from deuterosomes and presumably migrated to the cell surface. The fact that we did not detect pericentriolar aggregates of OFD1 and PCM-1 prior to generation of multiple centrioles may be because the fibrous granules were very tightly associated with the centrosomes or because they were not present in this cell type at this stage. It is possible that they started to accumulate sometime between 10 and 28 days post ALI; therefore, imaging of nasal epithelial cells between this time would help to confirm whether OFD1 is a component of these structures in cells undergoing ciliogenesis.

Similar to what is observed during ciliogenesis in multiciliated cells, it has been experimentally determined that in proliferating cells, in addition to templated duplication of centrioles, under certain circumstances centrioles can be formed using a *de novo* assembly pathway (Khodjakov et al. 2002; La Terra et al. 2005). Although the presence of pre-existing centrioles suppresses the *de novo* centriole formation in order to maintain genome integrity, this control may be lost in cancer cells. Studies have revealed the presence of centrin- and PCM-1-containing intermediate structures (La Terra et al. 2005; Prosser et al. 2009). Indeed, we showed that OFD1-containing satellites are also intermediate structures in this process. Together, these findings further support that OFD1 is a component of centriolar satellites, and that these structures may be involved in centriole assembly.

Basal bodies docking to the apical surface of epithelial cells are associated with alar sheets (also known as transitional fibers) that attach them to the plasma membrane

with a basal foot, a conical structure that projects from the lateral side in the direction of the effective stroke of ciliary beating, and with striated rootlets, cross-banded structures that extend from the proximal end toward the interior of the cell (Hagiwara et al. 2004). Although the formation and composition of these structures are largely unknown, it's been suggested that some could be formed by fibrous granules (Hagiwara et al. 2004) and, more recently, it was proposed that alar sheets and the basal foot correspond to the distal and subdistal appendages, respectively, of the mother centriole (Hoyer-Fender 2010). In fully differentiated and ciliated nasal epithelial cells, OFD1 was not detected along the axonemal microtubules of multiciliated nasal epithelial cells, consistent with what was observed in monociliated cells. Hence, in multiciliated cells, OFD1 and PCM-1 concentrate on basal bodies at the foot of the ciliary axoneme, possibly at alar sheets or the basal foot. This is consistent with a recent study that detected OFD1 at the distal ends of all centrioles and to the base of the primary cilium in monociliated mammalian cells (Singla et al. 2010).

While respiratory infections are not a symptom present in classical OFD1 syndrome, these are recurrent in male members of a family with the X-linked recessive Simpson-Golabi-Behmel syndrome type 2 that carries a frameshift mutation in the OFD1 gene (Budny et al. 2006). Thus, although the exact roles that ciliopathy disease proteins have in the assembly and function of motile cilia are still unknown, the tight association of OFD1 with basal bodies during ciliogenesis in multiciliated cells is intriguing and supportive of a potential role for OFD1 in these cells.

Previous studies have clearly shown OFD1 is a core centrosomal protein throughout the cell cycle (Romio et al. 2004; Giorgio et al. 2007; Singla et al. 2010). In our study, however, possibly due to the strong staining of OFD1 aggregates, this centrosomal localization was more difficult to establish. The centrosomal fraction of OFD1 became more easily detected when centriolar satellites were dispersed either by interfering with microtubule dynamics or upon progression through mitosis. It is

noteworthy that the loss of OFD1 satellite staining during mitosis can also represent degradation of this fraction rather than dispersal. This would be in agreement with the slight decrease observed in OFD1 protein levels by Western blot analysis. PCM-1, on the other hand, exclusively localized to centriolar satellites, disperses completely during mitosis and a centrosomal fraction is not detected. This is similar to BBS4, whereas CEP290 exhibited similar behaviour to OFD1 as it also remained associated with the spindle poles in mitosis. In the case of OFD1, it became clearly associated with the distal end of centrioles. Whether OFD1 and CEP290 have mitotic functions is not clear, although intriguingly, OFD1 was identified as essential for mitosis in a recent genome-wide study by the Mitocheck consortium (Neumann et al. 2010).

In summary, these findings indicate that there are two fractions of OFD1, one associated with centriolar satellites and one with the centrioles, with distinct dynamics and behaviour throughout the cell cycle, and, thus possibly, distinct functions in the cell.

CHAPTER 5

CILIOPATHY DISEASE PROTEINS ARE MUTUALLY DEPENDENT FOR CENTRIOLAR SATELLITE INTEGRITY

CHAPTER 5 CILIOPATHY DISEASE PROTEINS ARE MUTUALLY DEPENDENT FOR CENTRIOLAR SATELLITE INTEGRITY

5.1 INTRODUCTION

The beginning of this century witnessed the sequencing of the 3 billion chemical base pairs that make up the human DNA and the identification of approximately 20,000-25,000 genes by the Human Genome Project (IHGSC 2001; IHGSC 2004). In the first decade of this post-genomic era, effort has now turned to decipher the function of each of these genes.

Whole animal gene knockdown approaches can be very effective to study the function of a gene by observing the phenotype in the whole animal. For example, given the high homology between the mouse and human genomes, knockout mice can be used as models for human disorders (Lieschke & Currie 2010; Guan et al. 2010). Moreover, despite certain differences between fish and human physiology, zebrafish are also a good model for several human diseases due to the ease of embryological manipulability and the optical clarity of its embryos. Knockdown of specific genes in zebrafish can be achieved by microinjection of early embryos with antisense morpholino oligonucleotides (Lieschke & Currie 2010).

Functional studies on OFD1 have been done in mice and zebrafish (Ferrante et al. 2006; Ferrante et al. 2009). Knockout mice lacking *Ofd1* generated by Ferrante et al. (2006) recapitulated the main features of the disease. Whilst mutant male embryos exhibited left-right axis specification defects concomitant with lack of cilia in the embryonic node, and altered expression of Sonic hedgehog (Shh) signaling pathway genes, heterozygous females showed craniofacial and limb abnormalities, cystic kidneys and lack of cilia on the surface of epithelial cells lining the cysts (Ferrante et al. 2006). Zebrafish embryos injected with antisense morpholinos specifically designed against Ofd1 displayed a bent body, hydrocephalus, oedema, and laterality defects likely due to shorter cilia than normal and disrupted

intravesicular fluid flow in the Kupfer's vesicle (Ferrante et al. 2009). This data shows that OFD1 is required for ciliary motility and function in zebrafish, supporting data showing its importance in primary cilia function in mice (Ferrante et al. 2006). Furthermore, this is in agreement with findings in cultured cells, where OFD1 is clearly required for primary cilia formation (Graser et al. 2007; Corbit et al. 2008; Singla et al. 2010). Zebrafish embryos injected with Ofd1 morpholinos also exhibited convergent extension (CE) defects during gastrulation and these were accentuated by loss of the planar cell polarity (PCP) pathway genes Slb/Wnt11 and Tri/Vangl2 (Ferrante et al. 2009). As CE movements are regulated by non-canonical/PCP Wnt signalling, this data provides evidence for a role for OFD1 in the non-canonical/PCP Wnt signalling pathway.

The phenotypes described in knockout animals are consistent with the clinical presentation of human OFD1 patients, typical of a ciliopathy. Moreover, the intracellular localization of OFD1 correlates well with these phenotypes. However, how the OFD1 protein contributes to ciliogenesis at the cellular level is still unknown. At the time of our study, a new technique to study gene function had been developed: RNA interference (RNAi). This powerful biological technique entails sequence-specific gene silencing mediated by small double-stranded RNA (Campbell & Choy 2005). RNA interference (RNAi) is a naturally occurring and highly conserved pathway in which sequence-specific gene silencing is induced by short double stranded RNAs. RNAi was coined in 1998 by Andrew Fire and Craig Mello when they first reported the specific silencing of a functional gene by exogenous introduction of double stranded RNA (dsRNA) molecules in the nematode *C. elegans* (Fire et al. 1998). Three years later, Elbashir et al. (2001) demonstrated that efficient gene silencing in mammalian cells could be achieved by introducing short, ~21 base pairs (bp) long dsRNAs, circumventing the undesired triggering of the interferon response caused by the introduction of dsRNA >30 bp. These short dsRNAs were termed small interfering RNAs (siRNAs) (Elbashir et al. 2001; Elbashir et al. 2001). Since its inception in 1998, the cellular mechanism of

the RNAi pathway has been unravelled, and the understanding of its selective and robust effect on gene expression has uncovered an outstanding potential not only in loss-of-function studies in cultured cells and in whole animals, but also as a therapeutic agent in infectious disease, cancer and inherited disorders (Campbell & Choy 2005; Grimm 2009). We therefore set out to examine the consequences of OFD1 depletion in mammalian cells using RNAi.

5.2 RESULTS

5.2.1 Depletion of OFD1 through RNAi

To gain insight into the function of OFD1, hTERT-RPE1 cells were transiently transfected with a pool of siRNAs oligonucleotides designed to specifically knockdown OFD1, BBS4 or PCM-1. Non-specific siRNA against firefly luciferase (GL2) was used as a negative control (Elbashir et al. 2001). Western blot analysis of extracts prepared from hTERT-RPE1 cells transfected with these siRNAs for 72 hours confirmed that we were successful in specifically depleting OFD1, PCM-1 and BBS4 (Figure 5.1). Depletion of these proteins was also confirmed by immunofluorescence microscopy (Figures 5.5 to 5.7).

5.2.2 OFD1 is required for efficient primary cilia formation

At the time of this study, defects in the assembly or function of primary cilia were beginning to be suggested as the major contributing factor in cystic kidney disease, a common feature of disorders like autosomal dominant polycystic kidney disease (ADPKD), Oral-facial-digital syndrome type 1 (OFD1), Bardet-Biedl syndrome (BBS) and nephronophthisis (NPHP) (Zhang et al. 2004; Guay-Woodford 2006). Moreover, analysis of a murine knockout model that replicated the main features of OFD1 syndrome, showed primary cilia were absent in kidney cysts, further supporting the role for primary cilia in cyst development (Ferrante et al. 2006). Therefore, it was important to investigate if OFD1 was necessary for primary cilia formation in cultured cells. To test this, hTERT-RPE1 cells treated with siRNA against OFD1 or mock

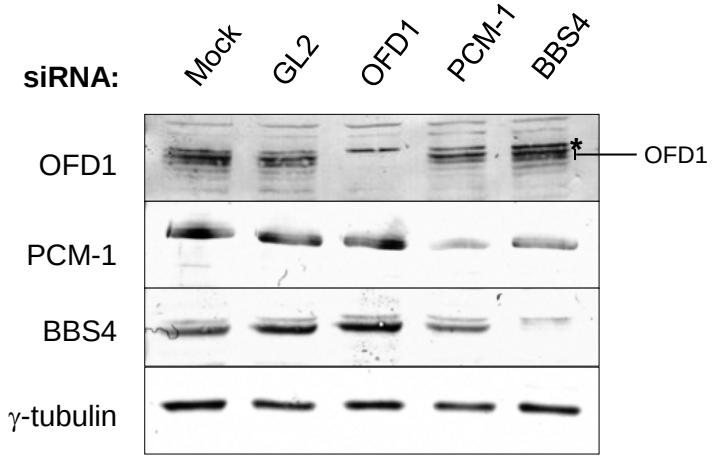

Figure 5.1 siRNA-mediated depletion of OFD1, PCM-1 and BBS4 proteins
hTERT-RPE1 cells were either mock-depleted or depleted with siRNA oligonucleotides against luciferase (GL2), OFD1, PCM-1 or BBS4 for 72 hours and depletion assessed by Western blot with the antibodies indicated. γ-tubulin served as a loading control. OFD1 bands are indicated . The top band indicated by the asterisk, and that does not disappear after OFD1 depletion is non-specific.

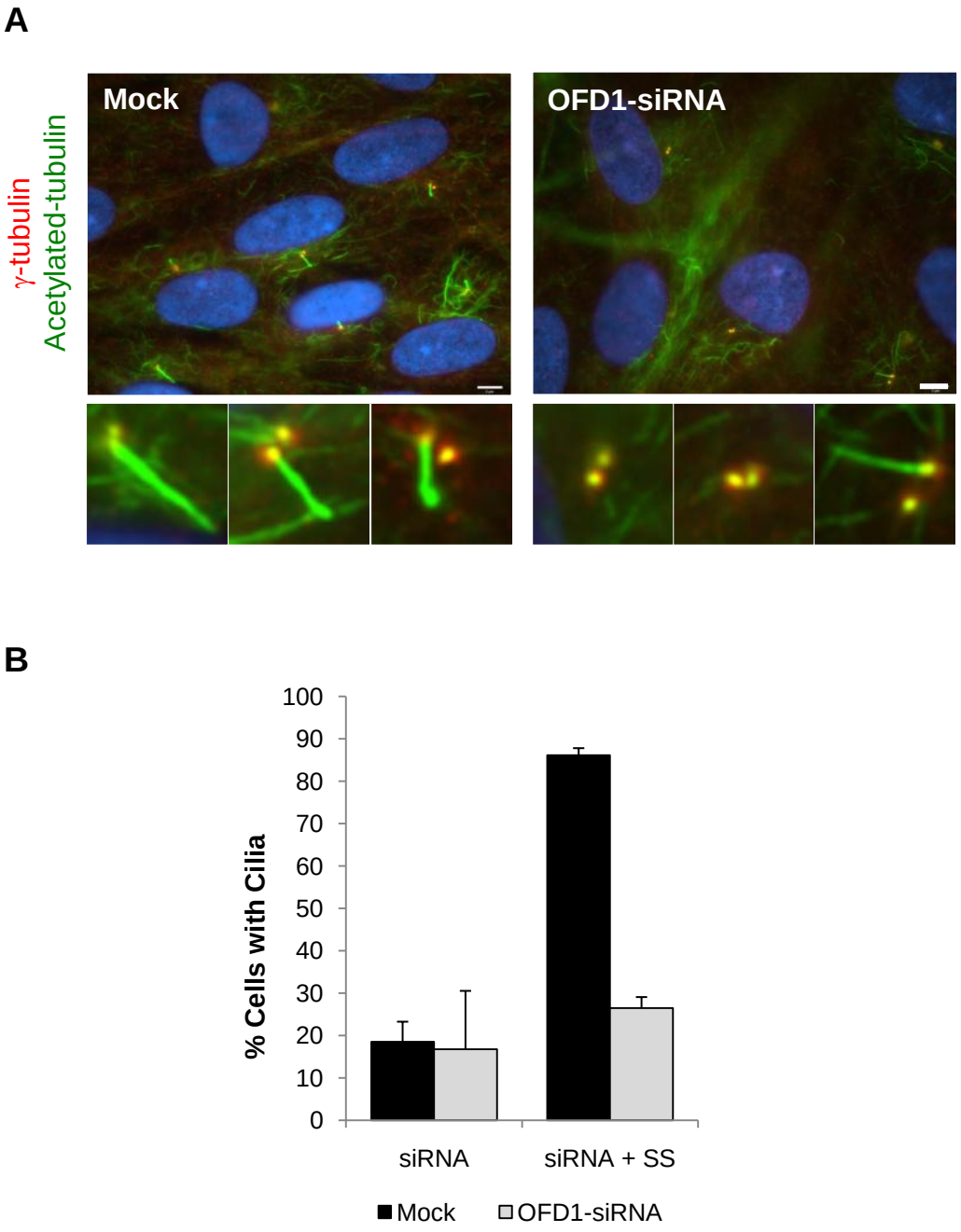

Figure 5.2 OFD1 depletion reduces the efficiency of primary cilia formation
(A) 72 h after transfection, mock or OFD1-siRNA-treated hTERT-RPE1 cells were serum-starved to promote ciliogenesis. Cells were co-stained with antibodies against acetylated tubulin (green) and γ-tubulin (red). DNA was stained with Hoechst 33258 (blue). Enlargements of basal bodies/primary cilia are shown. Scale bars, 5 µm. **(B)** Histogram shows the percentage of mock and OFD1-depleted cells before (siRNA) and after serum-starvation (siRNA + SS) that were ciliated. 200 cells were counted for each condition in three independent experiments. Error bars represent SD.

transfected were then serum starved to promote ciliogenesis. The presence of primary cilia observed by immunofluorescence microscopy in OFD1-depleted cells was significantly reduced when compared to the mock controls (Figure 5.2A and B), indicating that OFD1 is required for efficient primary cilia formation.

5.2.3 OFD1 depletion does not affect cell cycle progression

Mikule et al. (2007) demonstrated that depletion of integral centrosome and/or centriole components induced G_1-phase arrest in hTERT-RPE1 cells. These cells failed to reach confluency, did not progress into S-phase, and flow cytometry analysis showed a small increase in the 2N DNA content and a concomitant decrease in the 4N DNA content, when compared to controls (cells depleted of non-centrosomal proteins). Furthermore, this difference was more evident in cells treated with nocodazole that normally blocks cells in M-phase with 4N DNA content. Contrary to control cells that showed a major G_2/M peak with 4N DNA content almost all centrosomal protein-depleted cells were retained in G_1 with 2N DNA content. In addition, these G_1-arrested cells also exhibited loss of centrosome integrity (loss, separation or fragmentation of centrioles) (Mikule et al. 2007). Given the centrosomal localization of OFD1, it was important to determine if its depletion affected cell cycle progression. Interestingly, PCM-1 was identified in the study mentioned above as one of the proteins whose depletion led to G_1-arrest (Mikule et al. 2007). Depletion of BBS4 had been previously reported to induce arrest in cell division and apoptotic cell death (Kim et al. 2004). On the other hand, depletion of CEP290 did not interfere with G_1-S progression and no evidence of altered centriole structure was found (Kim et al. 2008).

We performed flow cytometry analysis of hTERT-RPE1 cells depleted of OFD1, PCM-1 and BBS4 for 72 hours. This did not show any significant change in the cell cycle profile when compared to controls. Furthermore, when OFD1-, BBS4- or PCM-1-depleted cells were treated with nocodazole for 16 hours to block them in M-

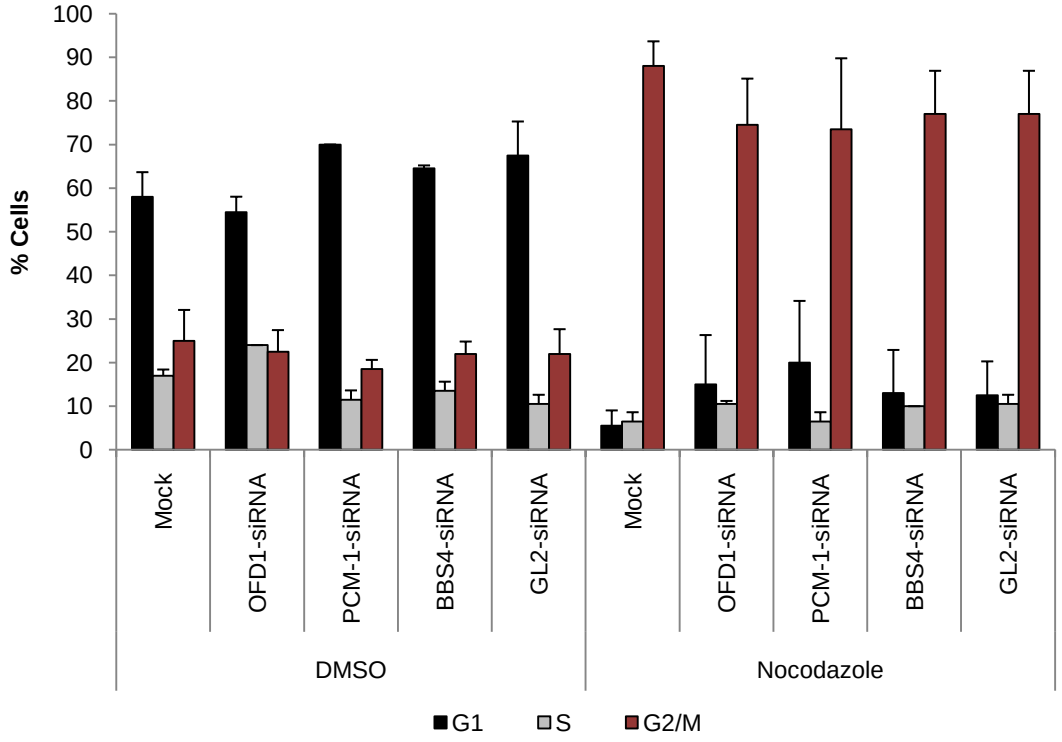

Figure 5.3 Depletion of OFD1, PCM-1 or BBS4 does not affect cell cycle progression

The percentage of cells in different phases of the cell cycle was determined from flow cytometry profiles of hTERT-RPE1 cells treated with indicated siRNAs for 72 h, and treated without (DMSO) or with nocodazole for the final 12 h (10,000 cells were counted in each experiment and histogram represents average of two independent experiments.

phase, similar to controls, these cells shifted to the G_2/M peak with 4N DNA content (Figure 5.3). Hence, contrary to what was previously found (Mikule et al. 2007), our results show that cell cycle progression was not affected by depleting OFD1, BBS4 or PCM-1.

5.2.4 OFD1 depletion does not affect microtubule anchoring or nucleation

Given the localization of OFD1 to centriolar satellites, we wished to examine if its depletion had similar effects on the microtubule network as depletion of other pericentriolar proteins. For example, it has been shown that depletion of PCM-1 results in defective anchoring of the microtubule network at the centrosome, but it does not affect microtubule nucleation (Dammermann & Merdes 2002). Furthermore, depletion of the centriolar satellite proteins, BBS4 and CEP290, has also been found to disrupt the anchoring of the microtubule network (Kim et al. 2004; Kim et al. 2008). By contrast, we found that depletion of OFD1 in hTERT-RPE1 did not obviously disrupt the organization of microtubules. Unexpectedly, PCM-1-depleted cells did not show the previously reported phenotype with no apparent change to the microtubule network (Dammermann & Merdes 2002) (Figure 5.4). To determine if silencing of OFD1 affected microtubule nucleation, OFD1 depleted hTERT-RPE1 cells were then treated with nocodazole to depolymerise the microtubule network, followed by washout of the nocodazole to allow the regrowth of the microtubules. Similar to controls and PCM-1-depleted cells, depletion of OFD1 also did not appear to affect the microtubule nucleation capacity of the centrosome (Figure 5.4). Together, our results show that OFD1 depletion did not affect either the anchoring or nucleation of the microtubule network in hTERT-RPE1 cells. Consistent with this, a recent study also showed that loss of Ofd1 in murine embryonic stem cells did not affect microtubule nucleation or anchoring (Singla et al. 2010).

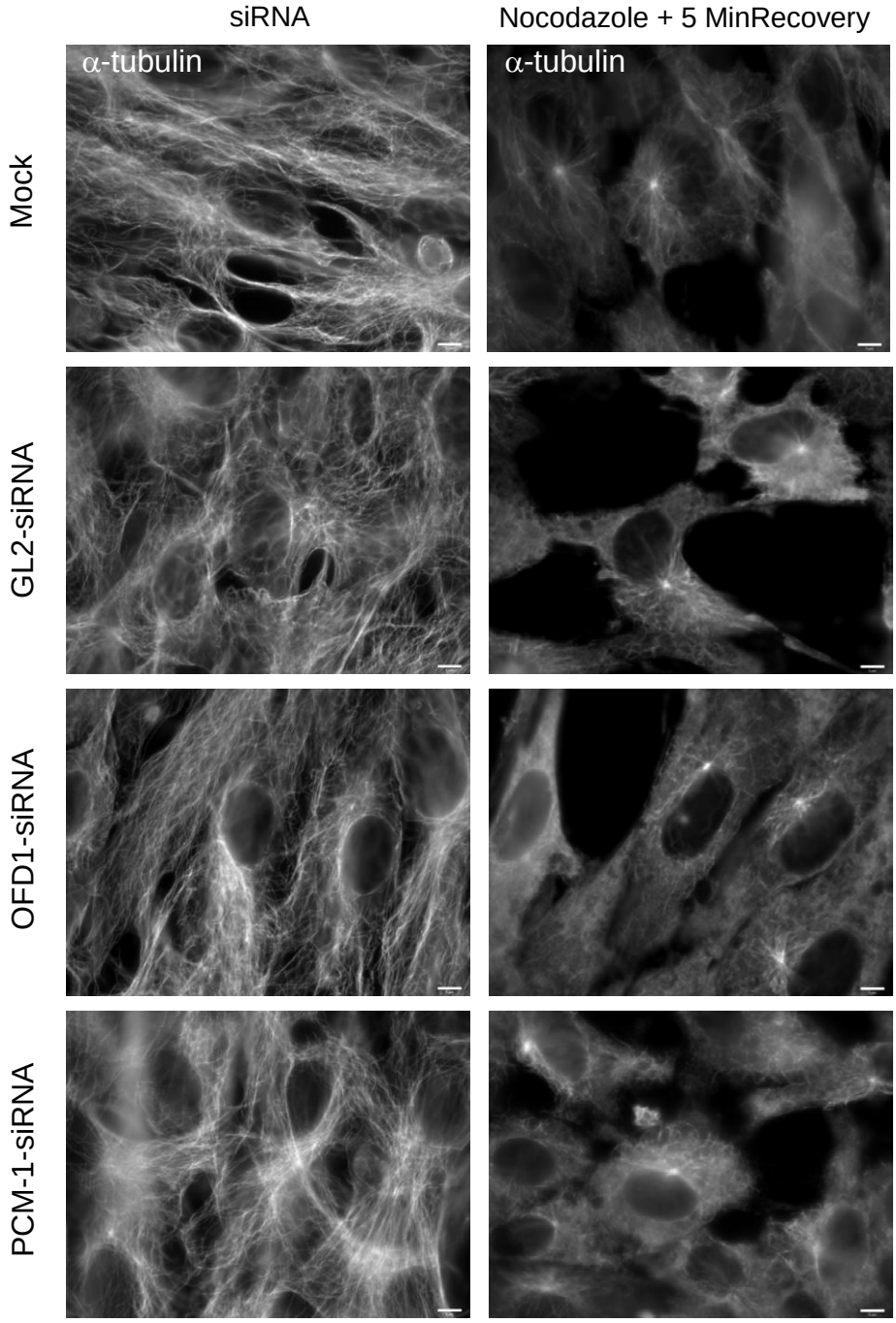

Figure 5.4 OFD1 depletion does not affect the anchoring or nucleation of the microtubule network

hTERT-RPE1 cells were either mock-depleted or depleted with siRNA oligonucleotides against luciferase (GL2), OFD1 or PCM-1 for 72 hours (siRNA) and then treated with 6 µg/µl nocodazole for 1 hour to depolymerize the microtubule network, followed by 5 minute washout of the nocodazole to allow the regrowth of the microtubules (Nocodazole + 5 Min recovery). Cells were stained with antibodies against α-tubulin to detect the microtubule network. Scale bars, 5 µm.

5.2.5 Ciliopathy disease proteins are mutually dependent for centriolar satellite integrity

We then addressed the consequence of depleting OFD1 on centriolar satellite organization and, conversely, how depletion of other known centriolar satellite proteins affected OFD1 localization. Previous studies on the centriolar satellite proteins, PCM-1, BBS4 and CEP290, have shown that depletion of PCM-1 by siRNA reduces centrosomal localization of centrin, pericentrin and ninein, but not γ-tubulin (Dammermann & Merdes 2002). Silencing of BBS4 led to dispersal of PCM-1-containing centriolar satellites (Kim et al. 2004). Interestingly, whilst PCM-1 was found to be necessary for localization of CEP290 to the centriolar satellites, depletion of CEP290 caused PCM-1 to become concentrated on to the centrosome (Kim et al. 2008).

We found that depletion of BBS4 led to complete loss of OFD1 from both centriolar satellites and centrosomes. Strikingly, however, when PCM-1 was depleted, OFD1 disappeared from the pericentriolar satellites but OFD1 could still be detected on the centrosomes (Figure 5.5). While PCM-1 centriolar satellites are lost in OFD1- or BBS4-depleted cells, loss of PCM-1 is more complete in the absence of OFD1 than BBS4. Moreover, it is noteworthy that depletion of either of these two ciliopathy proteins, OFD1 and BBS4, PCM-1 is never detected at the centrosome (Figure 5.6). Similarly, BBS4 pericentriolar satellites are lost in cells where either OFD1 or PCM-1 is absent, and not clearly detected at the centrosome upon depletion of either OFD1 or PCM-1 (Figure 5.7). In the case of CEP290, the protein disappeared from satellites in cells depleted of OFD1, PCM-1 or BBS4, but CEP290 could be detected on the centrosomes (Figure 5.8). Together, these data indicate that the pericentriolar localization of OFD1, PCM-1, BBS4 and CEP290 is interdependent. Remarkably, these proteins exhibit a distinct behaviour with respect to centrosomes. PCM-1 is never detected at the centrosome upon depletion of BBS4 or OFD1 proteins and, similarly, BBS4 is not observed at the centrosome in cells depleted of PCM-1 or OFD1. In contrast, upon depletion of certain centriolar satellite proteins,

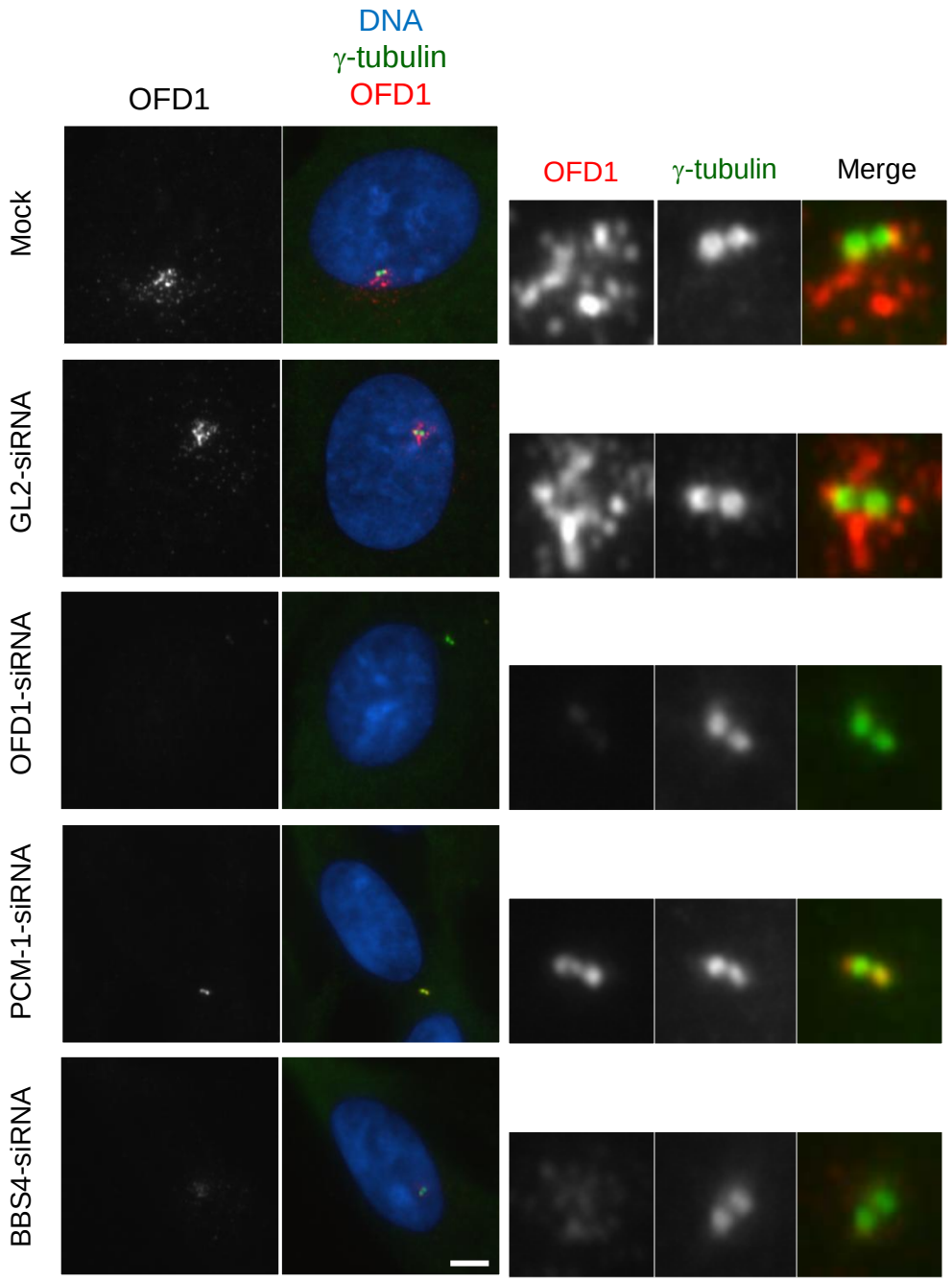

Figure 5.5 OFD1 localization to centriolar satellites is dependent upon PCM-1 and BBS4

Mock, luciferase (GL2), OFD1, PCM-1 and BBS4 depleted hTERT-RPE1 cells were co-stained with antibodies against γ-tubulin (green in merge) and OFD1 (red in merge). DNA was stained with Hoechst 33258 (blue). Enlargements of the centrosome are shown. Scale bar, 5 µm.

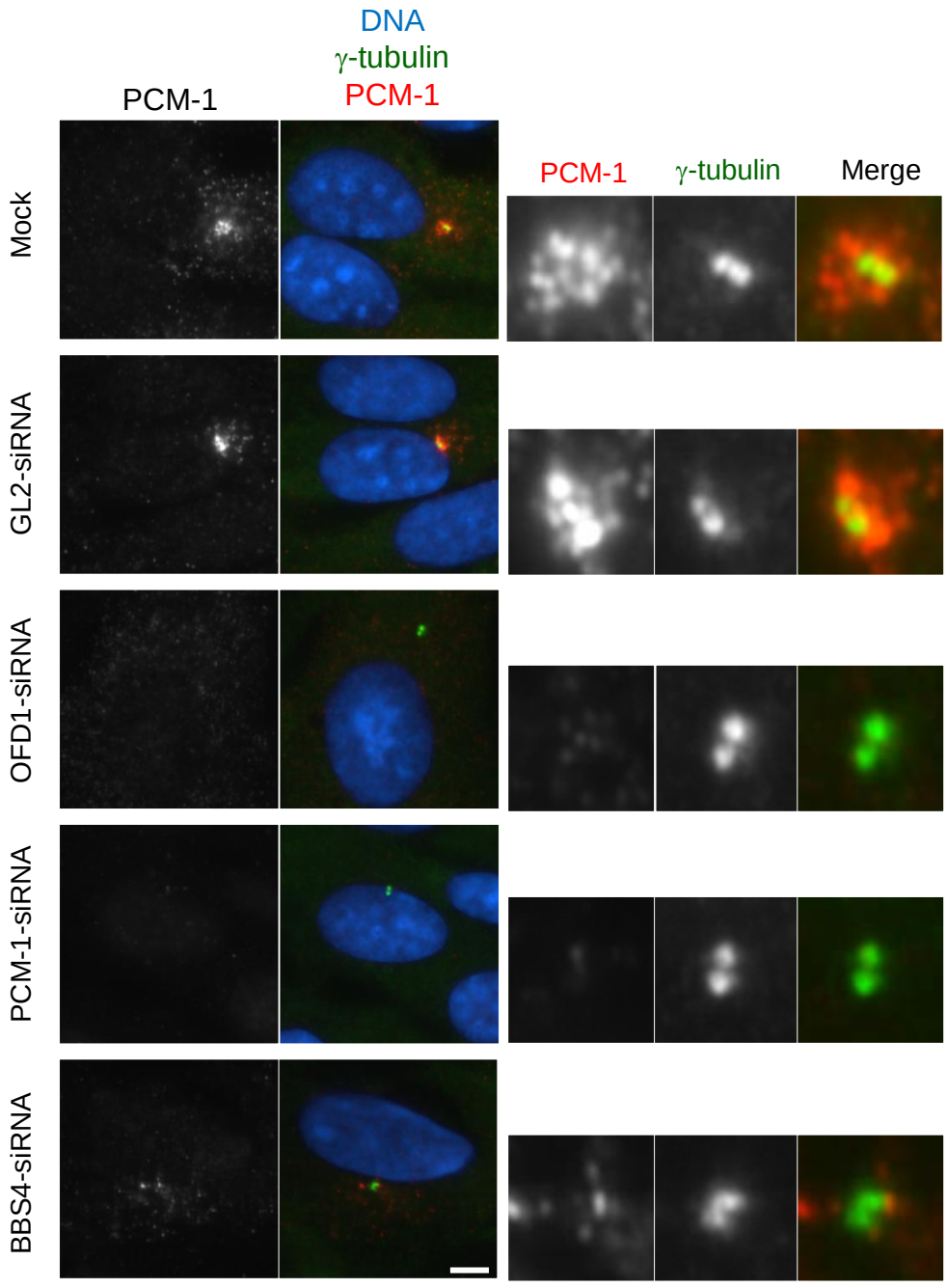

Figure 5.6 PCM-1 localization to centriolar satellites is dependent upon OFD1 and BBS4

Mock, luciferase (GL2), OFD1, PCM-1 and BBS4 depleted hTERT-RPE1 cells were co-stained with antibodies against γ-tubulin (green in merge) and PCM-1 (red in merge). DNA was stained with Hoechst 33258 (blue). Enlargements of the centrosome are shown. Scale bar, 5 µm.

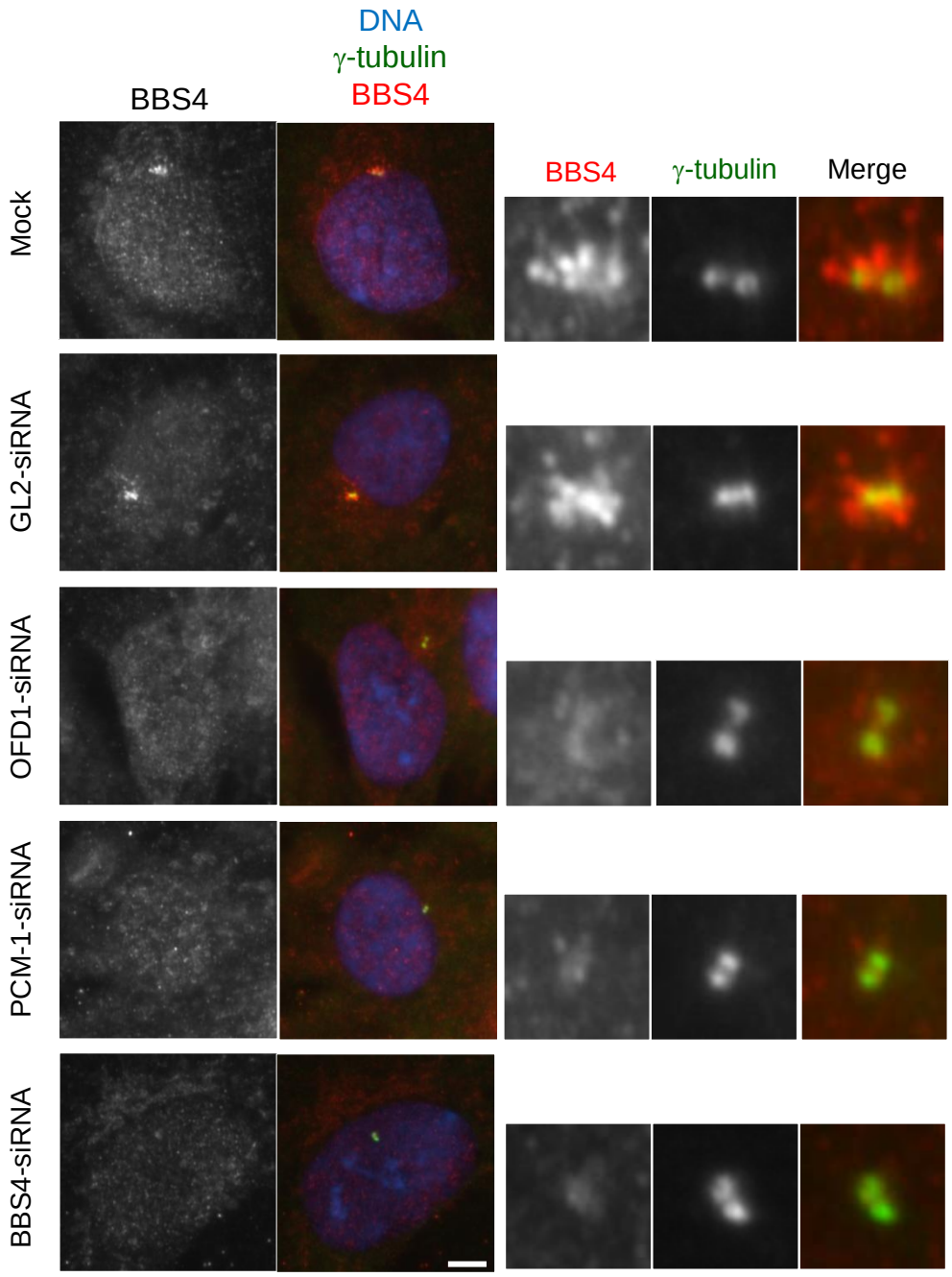

Figure 5.7 BBS4 localization to centriolar satellites is dependent upon OFD1 and PCM-1

Mock, luciferase (GL2), OFD1, PCM-1 and BBS4 depleted hTERT-RPE1 cells were co-stained with antibodies against γ-tubulin (green in merge) and BBS4 (red in merge). DNA was stained with Hoechst 33258 (blue). Enlargements of the centrosome are shown. Scale bar, 5 µm.

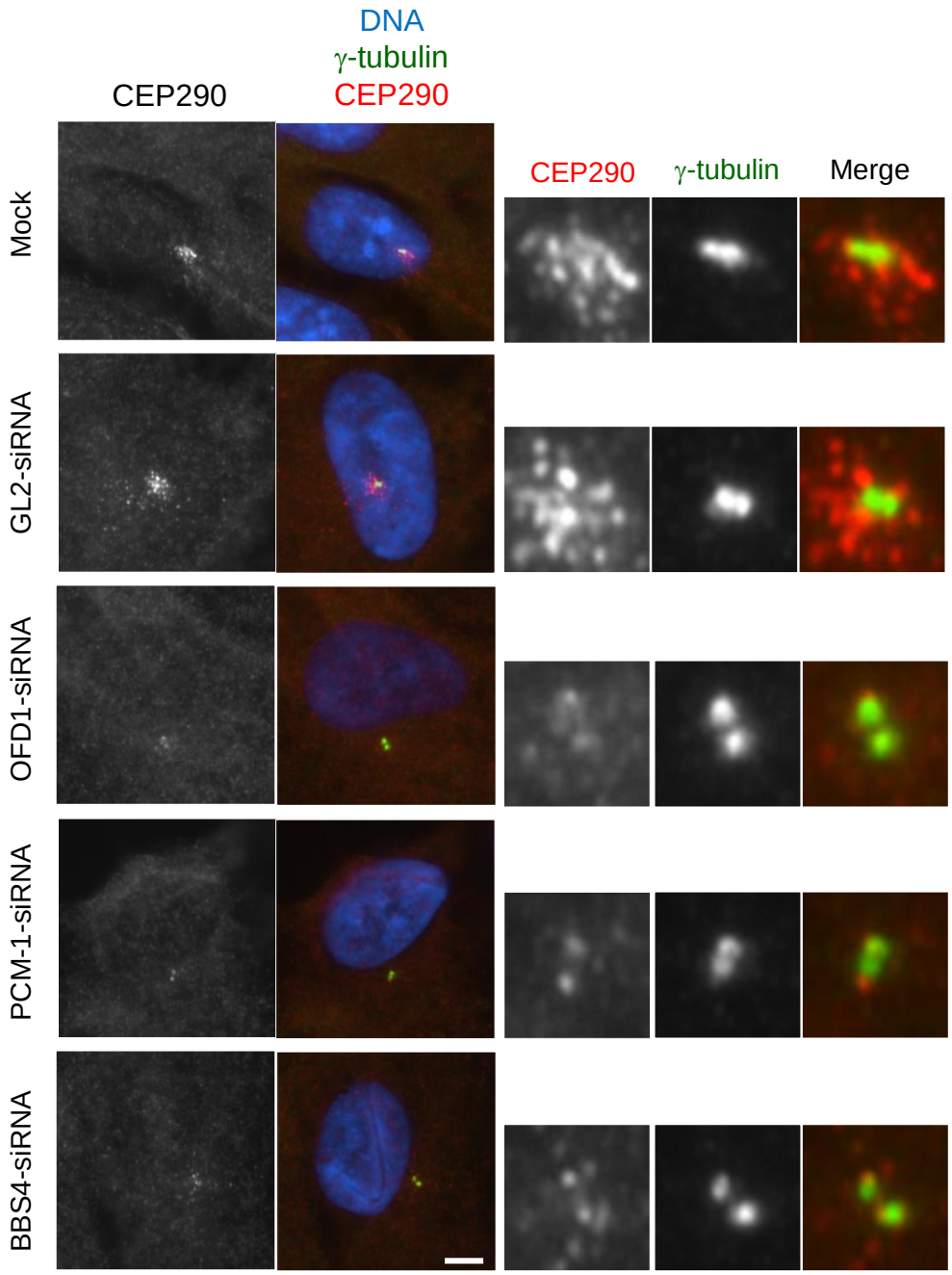

Figure 5.8 CEP290 localization to centriolar satellites is dependent upon OFD1, PCM-1 and BBS4

Mock, luciferase (GL2), OFD1, PCM-1 and BBS4 depleted hTERT-RPE1 cells were co-stained with antibodies against γ-tubulin (green in merge) and CEP290 (red in merge). DNA was stained with Hoechst 33258 (blue). Enlargements of the centrosome are shown. Scale bar, 5 µm.

OFD1 and CEP290 can be detected at the centrosome. While OFD1 localization to the centrosome is obvious in the absence of PCM-1, but not BBS4, CEP290 can be detected at the centrosome upon depletion of OFD1, PCM-1 or BBS4.

We next examined two other reported centriolar satellite proteins, pericentrin and Cep135 (Dammermann & Merdes 2002; Ohta et al. 2002). We had previously found that, unlike the ciliopathy disease proteins, these were primarily centrosomal in hTERT-RPE1 cells (Figure 3.5). Although localization and intensity of pericentrin was not altered in OFD1-depleted cells, the intensity of pericentrin at the centrosome was clearly reduced upon depletion of PCM-1, as previously reported (Dammermann & Merdes 2002), and BBS4 (Figure 5.9). In contrast, Cep135 localization and signal intensity in hTERT-RPE1 cells remained unaltered in cells depleted of OFD1, PCM-1 or BBS4 (Figure 5.10). Similarly, localization of the centrosomal protein γ-tubulin did not change in response to depletion of OFD1, PCM-1 or BBS4 (Figures 5.5 to 5.10).

The fact that for each protein analysed exposure times were set using the mock-treated sample and maintained equal for all other conditions makes them comparable. Therefore, although the successful knockdown of OFD1, PCM-1 and BBS4 proteins had been shown by Western blot analysis (Figure 5.1), we decided to use the images collected through immunofluorescence microscopy to confirm this. Measurement of the fluorescence signal intensity of each analyzed protein at the centrosomal and centriolar satellite area confirmed the successful knockdown of OFD1, PCM-1 and BBS4. The histogram in Figure 5.11 shows the knockdown of OFD1 and PCM-1 by approximately 95%, and 80% for BBS4. Also, these results also show the effect of the depletion of these centriolar satellite proteins on the fluorescence signal intensity of all the proteins analysed: OFD1, PCM-1, BBS4, CEP290, pericentrin, Cep135 and γ-tubulin (Figure 5.11). As expected, treatment with the non-specific siRNA against firefly luciferase (GL2) did not affect the intensity of the fluorescence signal of any of the analysed proteins. The histogram also

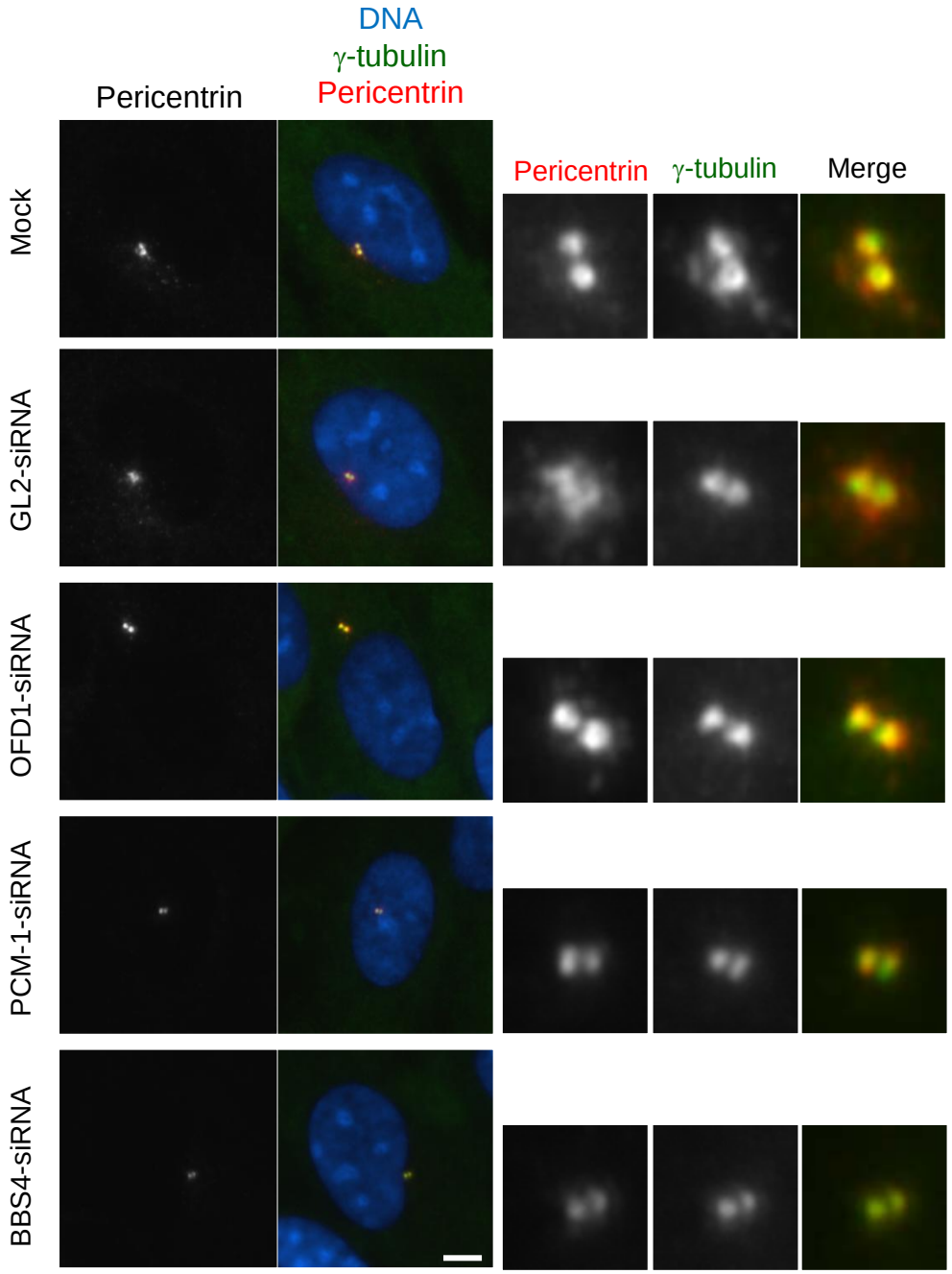

Figure 5.9 Pericentrin localization to the centrosome is dependent upon PCM-1 and BBS4

Mock, luciferase (GL2), OFD1, PCM-1 and BBS4 depleted hTERT-RPE1 cells were co-stained with antibodies against γ-tubulin (green in merge) and Pericentrin (red in merge). DNA was stained with Hoechst 33258. Enlargements of the centrosome are shown. Scale bar, 5 µm.

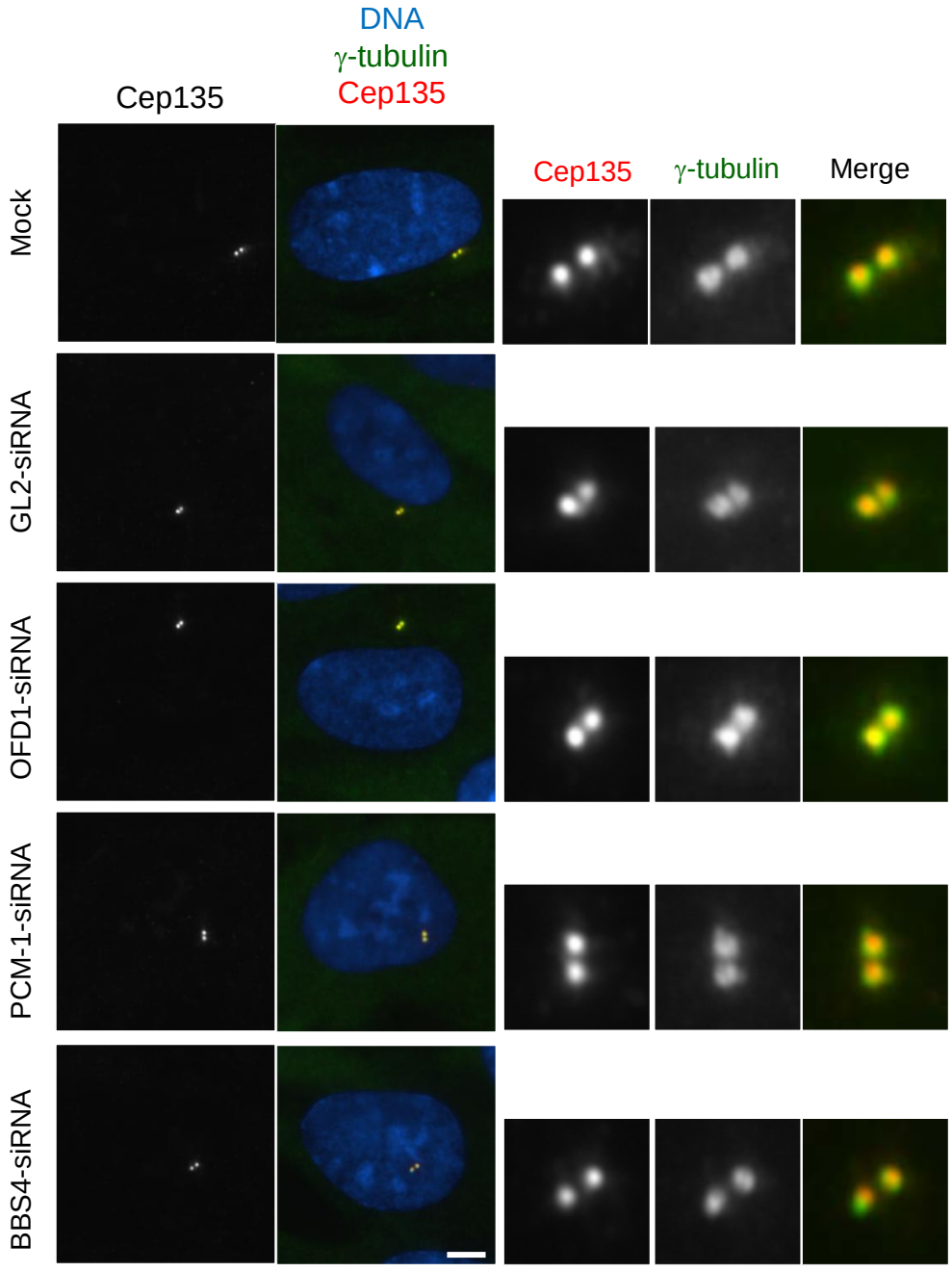

Figure 5.10 Cep135 localization to the centrosome is independent of OFD1, PCM-1 or BBS4

Mock, luciferase (GL2), OFD1, PCM-1 and BBS4 depleted hTERT-RPE1 cells were co-stained with antibodies against γ-tubulin (green in merge) and Cep135 (red in merge). DNA was stained with Hoechst 33258 (blue). Enlargements of the centrosome are shown. Scale bar, 5 µm.

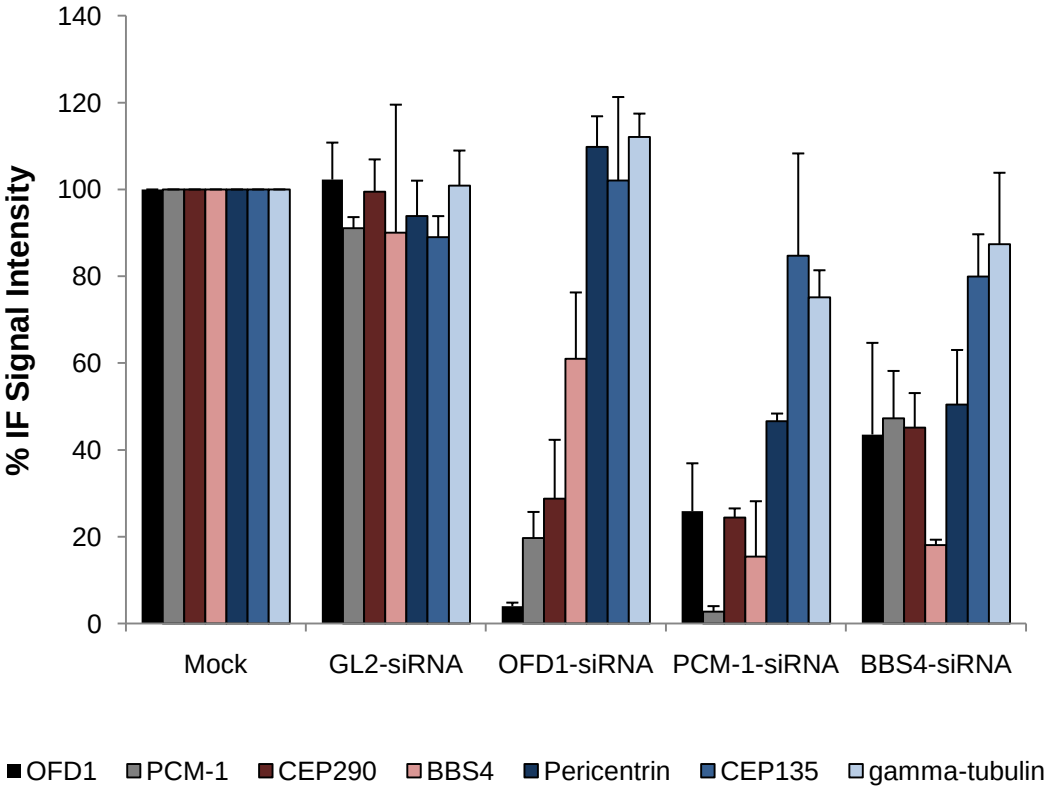

Figure 5.11 Intensity of immunofluorescence signal of centrosomal proteins after siRNA treatments

The total fluorescence intensities for the different antibodies was determined within a 2 micron square centered on the centrosome, and inclusive of the centriolar satellites, in cells treated with different siRNAs. The histogram presents the mean total intensities relative to that in the mock-treated sample (set at 100%). For each protein under each condition ten cells were imaged in two different experiments. Imaging was performed using a 100x objective and exposure times were set for each protein using the mock-treated sample and maintained equal for all other conditions. Error bars represent SD.

shows that whereas OFD1 depletion reduced PCM-1 and CEP290 proteins signal intensity at the centrosome and centriolar satellite area by about 70%, and BBS4 protein signal intensity by about 50%, it had no significant effect on the signal intensity of centrosomal proteins pericentrin, CEP135 or γ-tubulin. PCM-1 depletion, on the other hand, led to a more obvious reduction of centriolar satellite proteins signal intensity, approximately 80% for OFD1, CEP290 and BBS4, but also to a considerable drop on pericentrin signal intensity, about 50%. In response to BBS4 depletion, there was a reduction of about 50% in pericentrin signal intensity, and about 40% reduction in OFD1, CEP290 and PCM-1 proteins signal intensity. Despite not being easily detected by direct observation of the immunofluorescence microscopy images (Figures 5.5 to 5.10), both PCM-1 and BBS4 depletion also resulted in a small decrease (about 10-20%) in CEP135 and γ-tubulin signal intensity (Figure 5.11).

5.2.6 Functional interaction of Ofd1 and Bbs4 in zebrafish embryogenesis

Ofd1 is ubiquitously expressed in zebrafish embryos and, like human OFD1, it localizes to basal bodies and centrosomes (Ferrante et al. 2009). Given the striking co-localisation of OFD1, BBS4 and PCM-1 proteins in pericentriolar satellites, we used a zebrafish model to test biological effects of downregulation of these genes using antisense morpholinos (Ferrante et al. 2009). Specifically, we used this model not only to test ciliary function through observing heart primordium lateralization, but also to assess potential functional synergy between molecules by observing effects of combined administration of morpholinos directed against different protein. This experiment was undertaken by our colleagues, Dr. Leila Romio and Prof. Adrian Woolf at the ICH, London.

Heart laterality defects occurred in 1% of control embryos whereas administration of 4 ng of either Ofd1 (Spl6) morpholino or Bbs4 morpholino, produced defects in 20% and 50% embryos, respectively. When a lower dose (2 ng) of either morpholino was

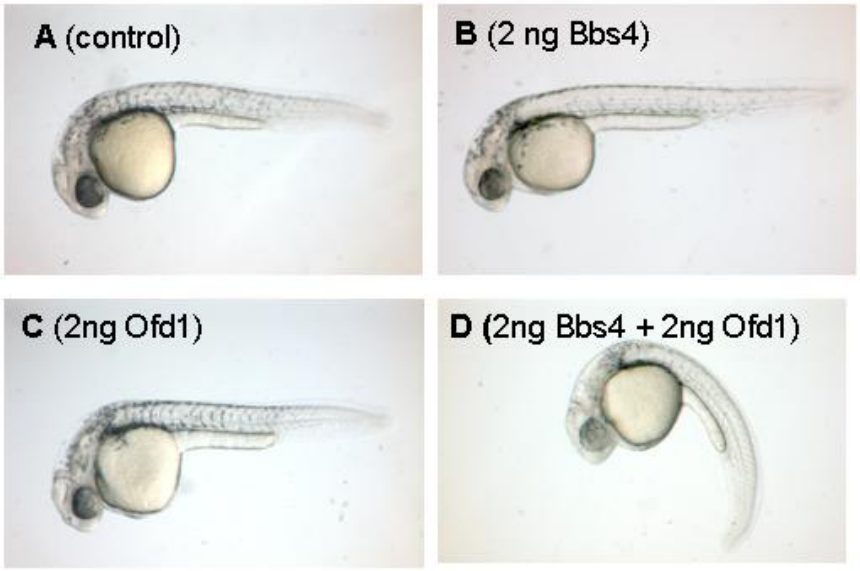

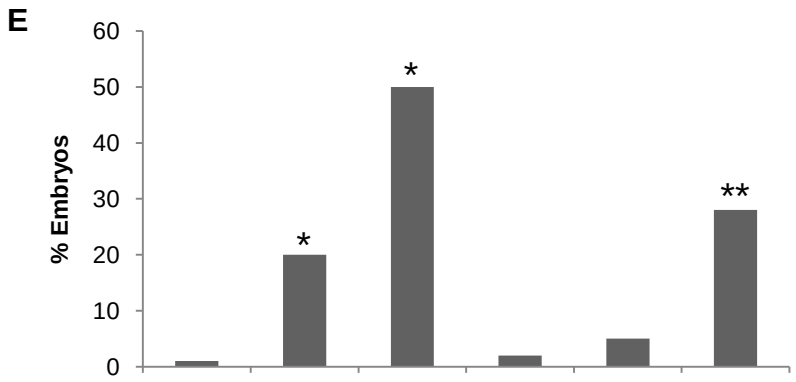

% Embryos	1%	20%	50%	2%	5%	28%
No. Events	1/95	6/30	7/14	1/48	2/40	24/85

Figure 5.12 Bbs4 and Ofd1 morpholinos synergize in disrupting body axis formation and laterality in zebrafish

Whole mount images of zebrafish embryos one day after fertilization. **(A)** Control. **(B)** 2 ng Bbs4 morpholino. **(C)** 2 ng Ofd1 morpholino. **(D)** 2 ng Bbs4 + 2 ng Ofd1 morpholino. Note that only the embryo administered with both Ofd1 and Bbs4 morpholinos exhibits a bent body axis. **(E)** Histogram indicates frequency of heart laterality defects in embryos treated with single or combined morpholinos as indicated. $p<0.001$ versus control (*), and $p<0.001$ versus effects from low dose morpholinos administered individually (**). Experiment undertaken by Dr. Leila Romio.

administered alone the frequency of laterality defects (Ofd1, 2%; Bbs4, 5%) was not significantly different from controls. Strikingly, however, co-administration of 2 ng of Ofd1 and 2 ng Bbb4 morpholinos led to laterality defects in 28% embryos (significantly different versus effects from low dose mopholinos administered individually) (Figure 5.12E). Moreover, abnormal body curvature of embryos, a phenotype characteristic of ciliopathies, was elicited by co-administration of these low dose morpholinos, whereas alone neither produced such an effect (Figure 5.12A to D). Similar experiments (data not shown) were attempted with PCM-1 morpholinos but these caused unspecific delays in early embryogenesis and thus could not be used to test effects on heart laterality and later phenotypes. These results support the hypothesis that OFD1 and BBS4 may cooperate *in vivo* in common molecular pathways.

5.3 DISCUSSION

Defects in primary cilia generation or function have been reported as the major cause of human diseases commonly referred to as ciliopathies (Satir et al. 2010). Consistent with OFD1 being included in this collection of diseases, we found that depletion of OFD1 through RNAi inhibited ciliogenesis in hTERT-RPE1 cells without affecting the cell cycle. Subsequent published studies have confirmed the requirement of OFD1 for primary cilia formation in hTERT-RPE1 and mouse embryonic stem cells (Graser et al. 2007; Corbit et al. 2008; Singla et al. 2010). Singla et al. (2010) have also confirmed our results showing that OFD1 did not affect the interphase microtubule organization or the mitotic spindle structures (Singla et al. 2010). Contrary to what has been previously reported, we did not detect loss of microtubule organization or G_1/S-phase arrest upon depletion of PCM-1 (Dammermann & Merdes 2002; Kim et al. 2004; Mikule et al. 2007). It is possible that these discrepancies result from the use of different cell lines, a less efficient knockdown in our study, or the presence of unknown off-target effects in some of these studies.

The unexpected colocalization of OFD1 with the ciliopathy associated proteins BBS4 and CEP290 at PCM-1-containing centriolar satellites (Chapter 4) prompted us to investigate how the absence of these proteins affected centriolar satellite proteins. Notably, we found that OFD1, PCM-1 and BBS4 are mutually dependent for localization at centriolar satellites. Depletion of OFD1, PCM-1 or BBS4 led to complete loss of CEP290, OFD1, PCM-1 and BBS4 pericentriolar aggregates from the vicinity of the centrosome. Remarkably, however, CEP290 and OFD1 exhibited a distinct behaviour from the remaining proteins. As previously described, CEP290 could be detected on the centrosome in cells depleted of PCM-1 (Kim et al. 2008), and an identical pattern was observed in cells depleted of OFD1 or BBS4. Similarly, whereas OFD1 disappeared in cells depleted of BBS4, in the absence of PCM-1, OFD1 was apparent at the centrosome. Furthermore, we confirmed that the centrosomal localization of pericentrin is PCM-1-dependent (Dammermann & Merdes 2002). However, similar to what was observed in CEP290-depleted cells (Kim et al. 2008), pericentrin protein levels were not altered in OFD1-depleted cells. This contrasts with the ~50% pericentrin signal intensity reduction seen in PCM-1- and BBS4-depleted cells.

Taken together with data published for PCM-1, BBS4 and CEP290 (Dammermann & Merdes 2002; Kim et al. 2004; Kim et al. 2008), these results suggest that removal of almost any centriolar satellite component may disrupt centriolar satellite organization. However, with respect to their centrosomal localization, these individual proteins revealed distinct responses when centriolar satellite organization was disturbed, suggesting a more intricate behaviour, and possibly different functions, at the centrosome. Indeed, these data are highly reminiscent of our localization studies in mitotic cells, where OFD1 and CEP290 were found to remain present at spindle poles but BBS4 and PCM-1 were not. This supports the notion that OFD1 and CEP290 may have specific centrosomal functions, perhaps related to mitosis. Although we and others (Singla et al. 2010) have not observed defects in mitosis in cells depleted of OFD1, a recent genome-wide study by the MitoCheck

consortium has identified OFD1 as essential for normal mitosis (Neumann et al. 2010).

It has been suggested that PCM-1 may serve as a carrier that associates with centrin, pericentrin, or ninein, and docks onto dynein-dynactin, thus serving as a mediator of the transport of centrosome components from the cytoplasm to the centrosome, along microtubules (Dammermann & Merdes 2002). Supporting this role for centriolar satellites as cargo carriers, BBS4 was found to bind to PCM-1 and it has been suggested that these proteins act together at centriolar satellites for protein recruitment (Kim et al. 2004). PCM-1 also interacts with CEP290, and together they are involved in the ciliary targeting of Rab8, a small GTPase that functionally interacts with the BBSome to promote ciliogenesis (Kim et al. 2008). Although PCM-1 was found to be dispensable for centriole formation and ciliogenesis in mouse multi-ciliated tracheal epithelial cells (MTEC) (Vladar & Stearns 2007), it is required for the formation of primary cilia (Mikule et al. 2007; Graser et al. 2007; Kim et al. 2008). Indeed, given its role in the recruitment of centrosomal proteins, it is not surprising that its depletion interferes with ciliogenesis. Still, PCM-1 has yet to be reported in association with ciliopathy. Nevertheless, removal of OFD1, BBS4 or CEP290 all lead to mislocalization of PCM-1 and other ciliopathy associated proteins, suggesting that removal of any satellite component destabilizes this structure. In addition, based on our zebrafish experiments, it appears that OFD1 and BBS4 functionally-synergise in terms of biological effects in the whole animal. These findings, together with the observations that OFD1 is required for the recruitment of Ift88 to the centrosome (Singla et al. 2010), suggest OFD1 may also be involved in the trafficking of other molecules to the centrosome, basal body or primary cilium.

Thus, centriolar satellites are critical assembly points for proteins implicated in human ciliopathies, and may function as large macromolecular assemblies that rely on protein-protein interactions for their integrity. Defects in each subunit result in the

dysfunction of the entire complex, and this could provide some explanation as to why the clinical spectrum of diseases such as OFD1 and the BBS disorders shows considerable overlap, for example featuring randomization of body axis asymmetry, polydactyly and renal cysts.

CHAPTER 6

STRUCTURE-FUNCTION STUDIES ON OFD1 REVEAL DOMAINS IMPORTANT FOR PCM-1 INTERACTION AND SATELLITE LOCALIZATION

CHAPTER 6 STRUCTURE-FUNCTION STUDIES ON OFD1 REVEAL DOMAINS IMPORTANT FOR PCM-1 INTERACTION AND SATELLITE LOCALIZATION

6.1 INTRODUCTION

Interactions between proteins are important determining factors in the control of many cellular processes. Therefore, knowledge of these interactions is crucial to understand how proteins function in biological systems and, ultimately, to improve our understanding of diseases and the development of new therapeutic avenues. There are a multitude of methods to detect protein interactions that differ in their sensitivity or specificity. Using the yeast two-hybrid system to screen a HeLa cDNA library with full-length OFD1 as a bait, Giorgio et al. (2007) found that OFD1 interacts with RuvBl1, a protein belonging to the AAA^+-family of ATPases and a component of the multiprotein nuclear complex, TIP60, via its coiled-coil domains. This interaction was confirmed by co-immunoprecipitation. Moreover, OFD1 was also found to interact with four other components of the same complex, raising the possibility that it may play direct roles in regulation of gene expression (Giorgio et al. 2007). A study on Leber congenital amaurosis (LCA), an inherited condition of very early-onset childhood blindness that is caused by retinal degeneration and which also belongs to the ciliopathy spectrum, identified OFD1 as an interacting partner of the *LCA5*-encoded protein, lebercilin. Again, this interaction was first identified in a yeast two-hybrid screen although this time using a retinal cDNA library and lebercilin as bait; this interaction was confirmed using both GST pull-down and co-immunoprecipitation assays (Coene et al. 2009).

Furthermore, the analysis of a protein's sequence can detect specific motifs, conserved regions of polypeptides that may form conserved structural entities, or domains. The presence of a conserved protein motif can provide some clue to function based on shared function of particular motifs. OFD1 protein contains an N-terminal Lis1 homology motif (LisH) and six predicted coiled-coil (CC) motifs

distributed within the much longer C-terminal region, as determined using SMART (http://smart.embl-heidelberg.de) (de Conciliis et al. 1998; Emes & Ponting 2001; Romio et al. 2003). Coiled-coils are bundles of long alpha-helices and are very common in centrosomal proteins, usually being associated with protein-protein interactions. The LisH motif has been identified in over 100 proteins, and is thought to be involved in cell migration, nucleokinesis and chromosome segregation. It has also been suggested that they can contribute to protein-protein interactions, dimerization, stability and/or localization (Emes & Ponting 2001; Gerlitz et al. 2005). The use of truncated constructs lacking selected regions of a protein allows the investigation of which regions of that protein are responsible or required for its localization or interactions. Indeed, it has been found that OFD1 is able to self-associate through its CC motifs, and that the fifth CC is necessary for OFD1 homotypic interactions (Giorgio et al. 2007). The coiled-coils are essential for localization of OFD1 to the centrosome (Romio et al. 2004), as well as for interaction with lebercilin (Coene et al. 2009) and RuvBl1 (Giorgio et al. 2007), and recruitment of Ift88 (Singla et al. 2010), a key component of the intraflagellar transport machinery. On the other hand, mutations in the LisH motif result in the reduction of OFD1 half-life and can mislocalize OFD1. Whereas overexpression of wild-type GFP-fused OFD1 resulted in cytoplasmic localization of the protein, expression of GFP-fused OFD1 with mutations in the LisH motif resulted in its localization to the nucleus and/or the Golgi apparatus. These observations therefore suggest that the LisH motif is essential for OFD1 stability and localization (Gerlitz et al. 2005).

Given the colocalization of OFD1 and PCM-1 to centriolar satellites and their mutual dependency for this association, we were particularly interested in investigating whether these two proteins were capable of interaction. Furthermore, we wished to uncover which regions of OFD1 were responsible for its localization to the centriolar satellites.

6.2 RESULTS

6.2.1 OFD1 and PCM-1 interact via their respective coiled-coil domains

To understand OFD1 protein function, it is crucial to identify proteins that interact with it. The potential interaction between OFD1 and PCM-1 suggested by their colocalization to the centriolar satellites and their mutual dependency for this localization was therefore examined through both immunoprecipitation and GST pull-down assays. For this purpose, Dr. Andreas Merdes (CNRS, Toulouse) kindly provided us with GFP-tagged chicken PCM-1 constructs encoding the full-length PCM-1 (PCM-1-FL-GFP, residues 1-1904), the coiled-coil-rich N-terminal domain (PCM-1-NTD-GFP, residues 1-1468) and the C-terminal non-coiled-coil domain (PCM-1-CTD-GFP, residues 1468-1904) (Dammermann & Merdes 2002). Furthermore, given the previously reported interaction between PCM-1 and BBS4 proteins , Prof. Philip L. Beales (ICH, UCL, London) kindly provided us with a GFP-tagged full-length BBS4 construct (GFP-BBS4, residues 1-519) (Figure 6.1).

We first performed an immunoprecipitation assay to assess if GFP-tagged full-length PCM-1 or BBS4 could precipitate endogenous OFD1, using GFP alone as a control. Following transfection of human embryonic kidney (HEK293) cells, we found that endogenous OFD1 could precipitate with GFP-tagged full-length PCM-1 but not GFP alone (Figure 6.2A and B). On the other hand, endogenous OFD1 was only very weakly detected in immunoprecipitates from extracts of cells expressing GST-tagged full-length BBS4, suggesting a much less robust interaction with BBS4 than with PCM-1 (Figure 6.2B). Moreover, our results also show that endogenous PCM-1 could precipitate with GFP-tagged full-length BBS4 and not GFP alone, thus confirming the previously reported interaction between PCM-1 and BBS4 (Kim et al. 2004). Interestingly, two bands were observed for OFD1 in the immunoprecipitated extracts. These are likely to reflect the full-length OFD1 and the version lacking exon

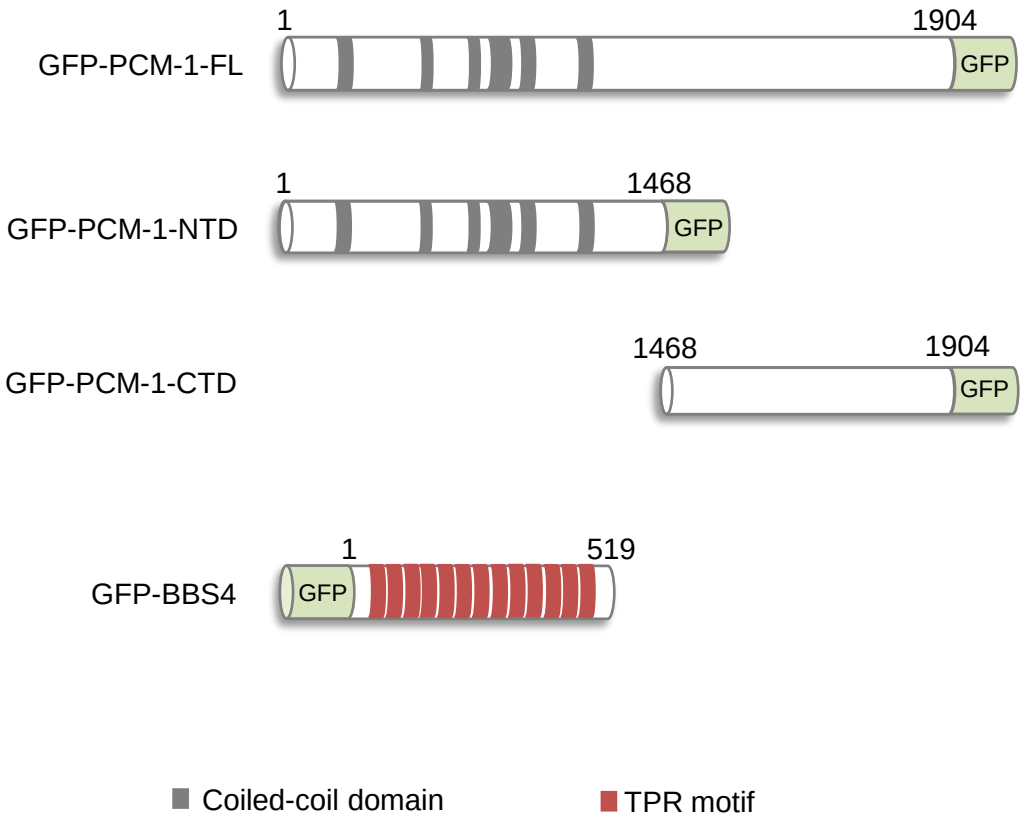

Figure 6.1 GFP-tagged PCM-1 and BBS4 constructs for mammalian expression

Schematic representation of GFP-tagged constructs encoding full-length chicken PCM-1 (PCM-1-FL-GFP), the N-terminus of PCM-1 (PCM-1-NTD-GFP), the C-terminus of PCM-1 (PCM-1-CTD-GFP) (all gifts from Dr. Andreas Merdes, Toulouse), and full-length BBS4 (GFP-BBS4; gift from Prof. Philip L. Beales, London), used for interaction studies. Grey bars represent predicted coiled-coil motifs and the red bars represent TPR motifs. Amino acids numbers are indicated.

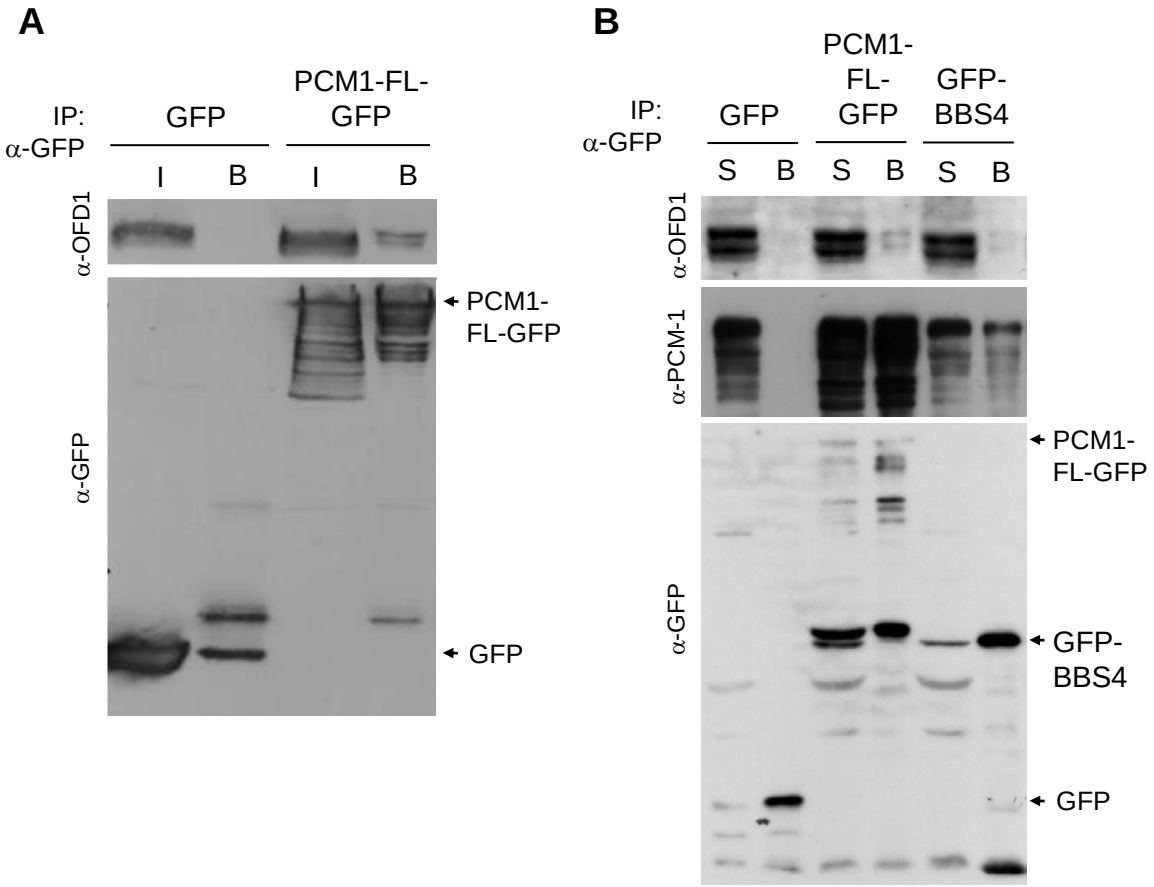

Figure 6.2 OFD1 interacts with PCM-1 and, more weakly, BBS4

(A) HEK293 cells were transfected with GFP alone or GFP-tagged full-length PCM-1 (PCM-1-FL-GFP). Cell lysates were immunoprecipitated with an anti-GFP antibody, and both the total lysates (input, I) and immunoprecipitates (bound, B) separated by SDS-PAGE and immunoblotted with antibodies against OFD1 and GFP. Arrows indicate the predicted molecular size of GFP alone (27 kDa) and PCM-1-FL-GFP (255 kDa). **(B)** HEK293 cells were transfected with GFP alone, GFP-tagged full-length PCM-1 (PCM-1-FL-GFP) or GFP-tagged full-length BBS4 (GFP-BBS4). Cell lysates were immunoprecipitated with an anti-GFP antibody, and both the unbound supernatant (S) and the GFP-bound material (B) were separated by SDS-PAGE and immunoblotted with antibodies against OFD1, PCM-1 and GFP. Arrows indicate the predicted molecular size of GFP alone (27 kDa), GFP-BBS4 (85 kDa) and PCM-1-FL-GFP (255 kDa).

10 (Coene et al. 2009), indicating that interaction with PCM-1 does not require the sequence encoded by exon 10 (Figure 6.2).

To define the regions of OFD1 and PCM-1 required for these interactions, we generated a series of GST-tagged OFD1 constructs in order to perfume GST pull-down assays using the GFP-tagged PCM-1 and BBS4 constructs mentioned above (Figure 6.1). To do this, we first generated GST-tagged constructs encoding the LisH motif-containing N-terminal domain (GST-OFD1-NTD, residues 3-132), the coiled-coil rich C-terminal domain (GST-OFD1-CTD, residues 145-1012), the last two coiled-coil domains (GST-OFD1-CC5-6, residues 601-1012) or the last coiled-coil domain (GST-OFD1-CC6, residues 765-1012) (Figure 6.3). Following optimization of expression in bacteria (data not shown), the soluble fraction was purified using glutathione-sepharose beads (Figure 6.4) and the peak elutions combined and dialysed to be used in GST pull-down assays.

Purified GST-tagged OFD1 proteins, or purified GST alone used as control, were mixed with extracts from HEK293 cells transfected with GFP-tagged full length BBS4, GFP-tagged full-length PCM-1 or, separately, the PCM-1 N-terminal domain encompassing its coiled-coils or C-terminal non-coiled-coil domain (Figure 6.1). Both full-length PCM-1 and the PCM-1 N-terminal domain interacted strongly with the C-terminal domain of OFD1 (residues 145-1012), but not the N-terminal region containing the LisH motif (residues 3-132) (Figure 6.5). Further truncation of the OFD1 coiled-coil region indicated that removal of the first four coiled-coils had no significant effect on the interaction, but the additional removal of the fifth coiled-coil led to its complete loss. In respect of BBS4, there was no binding of the GFP-tagged full-length BBS4 with the GST-tagged N- or C-terminal proteins in this experiment, suggesting that the weak BBS4 and OFD1 association detected by immunoprecipitation (Figure 6.2) is unlikely to be a direct one. GFP-tagged full-length BBS4 appears to weakly interact with the last coiled-coil of OFD1 (GST-OFD1-CC6, Figure 6.5). However, since it does not appear to interact with two other

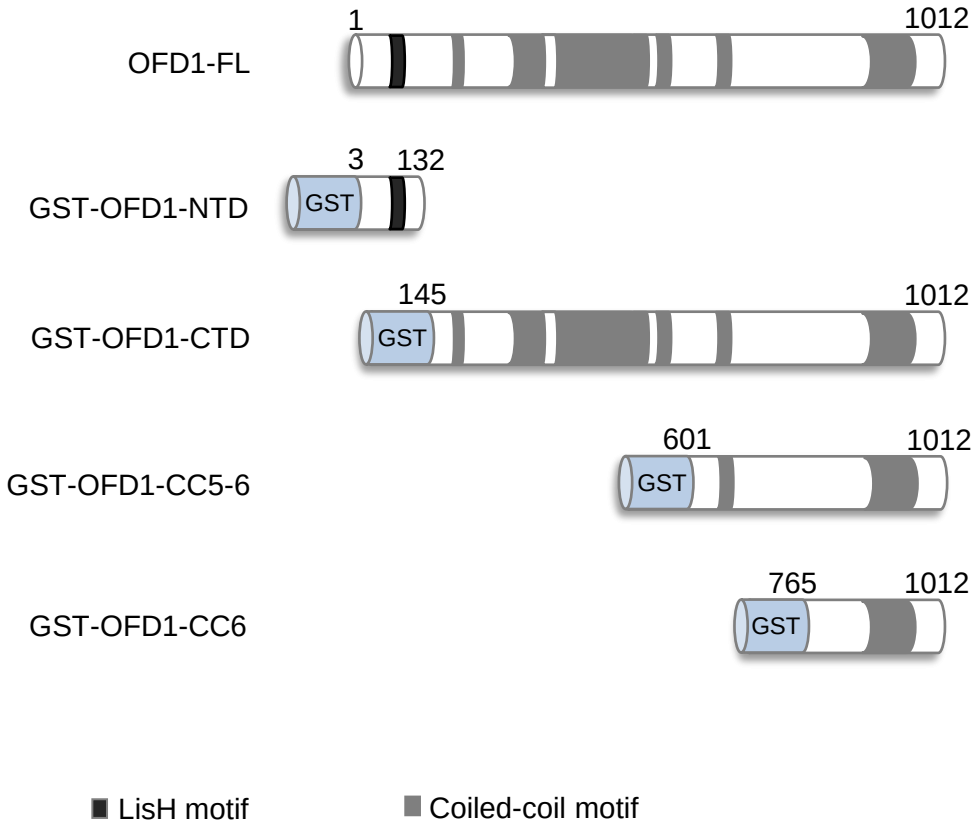

Figure 6.3 GST-tagged OFD1 constructs for bacterial expression
Schematic representation of OFD1 protein (OFD1-full-length) and of the truncated versions of OFD1 expressed as GST-tagged recombinant proteins for GST pull-down assays. These correspond to the N-terminus (OFD1-NTD), the C-terminus (OFD1-CTD), the C-terminus lacking the first four coiled-coil motifs (OFD1-CC5-6) and the C-terminus lacking the first five coiled-coil motifs (OFD1-CC6). The black box indicates the LisH motif and the grey boxes represent the coiled-coil motifs. Amino acids numbers are indicated.

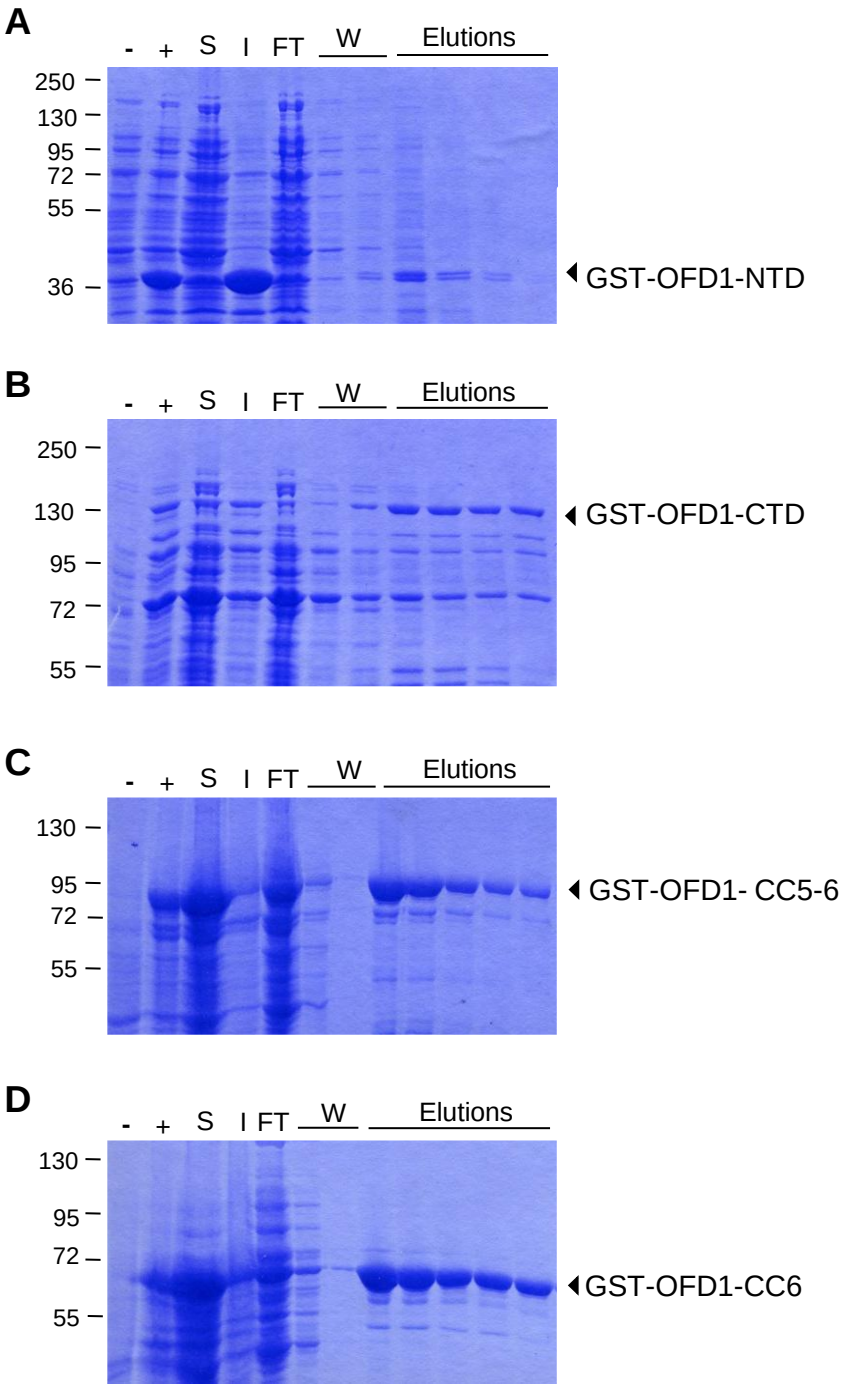

Figure 6.4 Expression and purification of GST-tagged OFD1 constructs
Expression and purification of the GST-tagged OFD1-NTD **(A)**, OFD1-CTD **(B)**, OFD1-CC5-6 **(C)** and OFD1-CC6 **(D)** recombinant proteins. The non-induced (-), induced (+), soluble (S), insoluble (I), flow-through (FT), washes (W) and elution fractions were analysed by SDS-PAGE with Coomasie Blue staining. Molecular weights (kDa) are indicated on the left of each panel. Black arrows indicate predicted molecular size of GST-OFD1-NTD (43 kDa), GST-OFD1-CTD (129 kDa), GST-OFD1-Δ1-601 (79 kDa) and GST-OFD1-Δ1-765 (60 kDa).

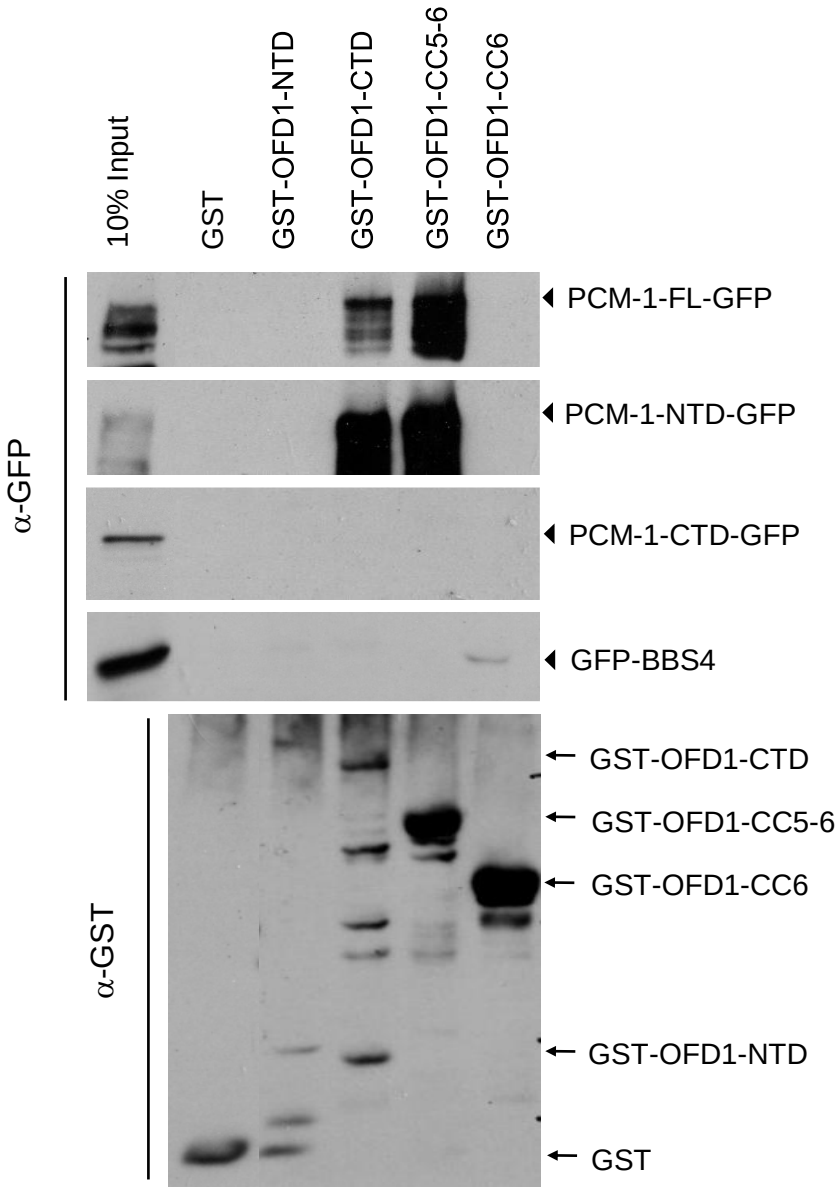

Figure 6.5 OFD1 and PCM-1 interact via their respective coiled-coil domains
Purified GST alone or GST-tagged OFD1 constructs as indicated were incubated with lysates prepared from HEK293 cells transiently transfected with PCM-1-GFP or GFP-BBS4 constructs. 10% of the input together with the GST-bound material were immunoblotted with an anti-GFP antibody. An immunoblot with anti-GST antibody shows the presence of the purified proteins in each fraction as indicated by the arrows.

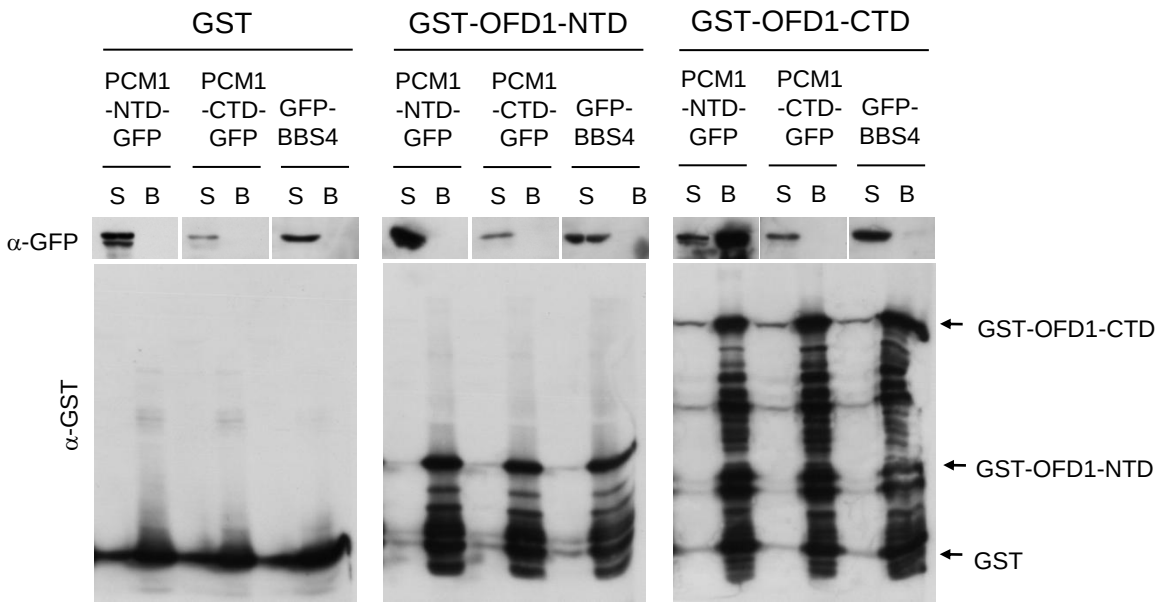

Figure 6.6 PCM-1 interacts with the C-terminal, but not N-terminal, domain of OFD1

Purified GST alone or GST-tagged OFD1-NTD or CTD constructs were incubated with lysates prepared from HEK293 cells transiently transfected with PCM-1-NTD-GFP, PCM-1-CTD-GFP or GFP-BBS4 constructs. Both the unbound supernatant (S) and the GST-bound material (B) were analysed by SDS-PAGE and immunoblotting with an anti-GFP antibody. An immunoblot with an anti-GST antibody shows the purified proteins in each fraction as indicated.

longer constructs containing this last coiled-coil motif (GST-OFD1-CTD and GST-OFD1-CC5-6), it remains unclear if there is a direct interaction between OFD1 and BBS4 (Figure 6.5). Although the GST-OFD1-NTD protein was present at lower amounts in this experiment, when analysed at equivalent amounts to the GST-OFD1-CTD, there was still no sign of interaction with the N- or C-terminal domains of PCM-1-GFP, or with GFP-BBS4 (Figure 6.6). We therefore conclude that the N-terminal coiled-coil domain of PCM-1 associates with residues 601-765 of OFD1 and that whilst OFD1 and BBS4 may weakly associate in cells, they are unlikely to interact directly.

6.2.2 The LisH-containing N-terminal domain is critical for OFD1 localization to centriolar satellites

Although previous work had shown that the C-terminal domain of OFD1 was required for its centrosomal localization (Romio et al. 2004), it did not distinguish between centriolar satellites and centrioles. We therefore decided to test the localization of different OFD1 truncation constructs. To do this, we generated a series of myc-tagged OFD1 constructs encoding the coiled-coil-rich C-terminal domain (Myc-OFD1-CTD, residues 145-1012), the last four coiled-coil domains (Myc-OFD1-CC3-6, residues 1-365), or the LisH motif-containing N-terminal region and the first coiled-coil domains (Myc-OFD1-NTD+CC1-4, residues 3-601) (Figure 6.7). We had also generated a few other myc-tagged OFD1 constructs encoding for different regions of the protein. However, we had difficulties with the expression of these constructs in cells. It is possible that, for some reason, the recombinant constructs were unstable as tagged fusion proteins or mRNAs.

As shown earlier, full-length OFD1 is primarily associated with centriolar satellites and only weakly present at the centrosome itself (Figures 3.3B, 3.4B and 3.5). Following transfection in hTERT-RPE1 cells, we confirmed that the OFD1 C-terminal domain encompassing all the coiled-coil motifs does indeed localize to the centrosome, as assessed using markers of the centrosome (γ-tubulin) and of the

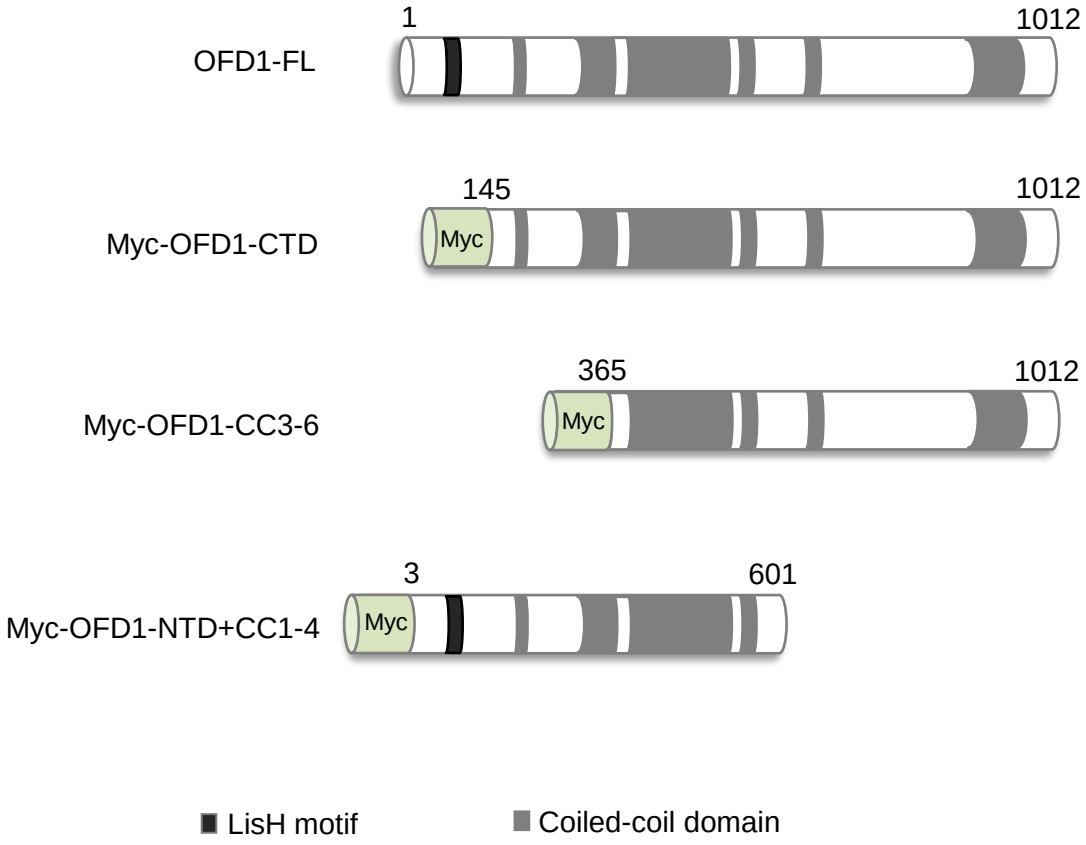

Figure 6.7 Myc-tagged OFD1 constructs for expression in mammalian cells
Schematic representation of Myc-tagged OFD1 deletion constructs encoding the full-length OFD1 (OFD1-FL), the C-terminus (OFD1-CTD), the C-terminus lacking the first two coiled-coil domains (OFD1-CC3-6) and the N-terminus lacking the last two coiled-coil domains (OFD1-CC1-4). Grey bars represent predicted coiled-coil motifs and the black bar represents the LisH motif. Amino acids numbers are indicated.

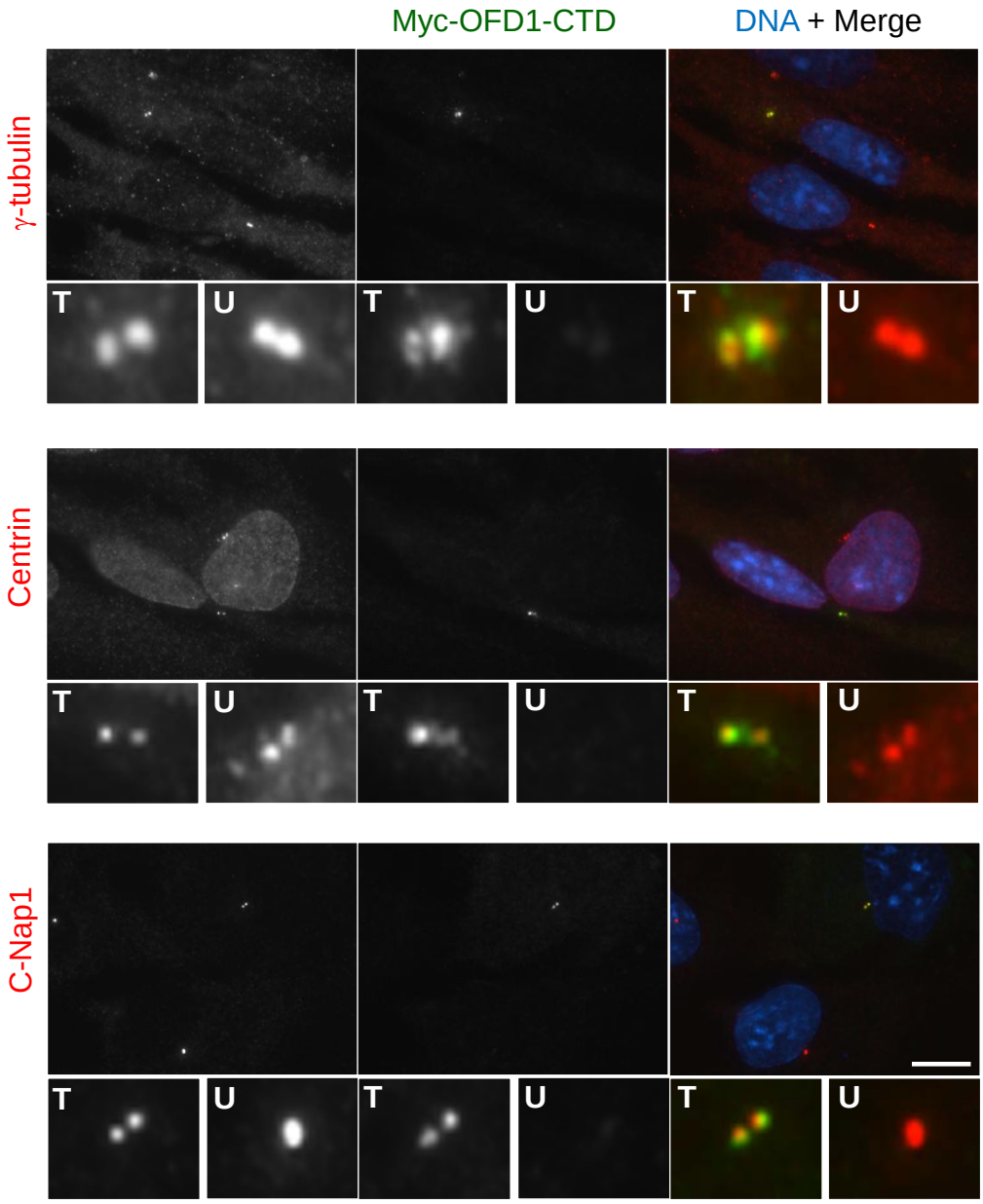

Figure 6.8 OFD1-CTD localizes to the centrosome
hTERT-RPE1 cells transiently transfected with Myc-OFD1-CTD were co-stained with antibodies against the Myc tag (greyscale and green in merge) to determine the localization of recombinant OFD1 protein, and with antibodies against the centrosomal marker γ-tubulin, or with antibodies against centrin or C-Nap1, markers of the distal and proximal ends of centrioles, respectively (greyscale and red in merge). DNA was stained with Hoechst 33258 (blue). Enlargements show centrosomal regions in transfected (T) and untransfected (U) cells. Scale bar, 10 µm.

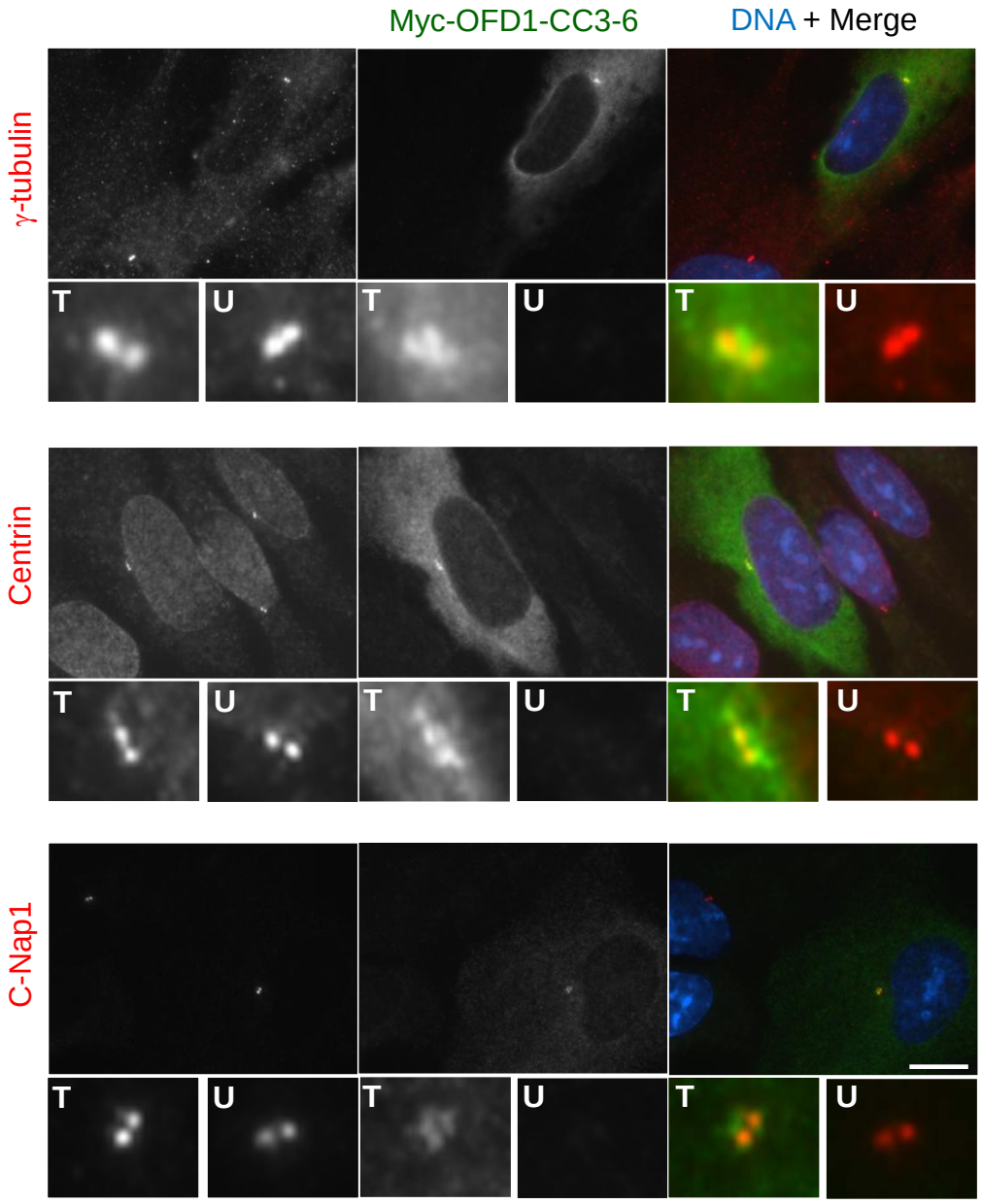

Figure 6.9 OFD1-CC3-6 weakly localizes to the centrosome
hTERT-RPE1 cells transiently transfected with Myc-OFD1-CC3-6 (residues 365-1012) were co-stained with antibodies against the Myc tag (greyscale and green in merge) to determine the localization of recombinant OFD1 protein, and with antibodies against the centrosomal marker γ-tubulin, or with antibodies against centrin or C-Nap1, markers of the distal and proximal ends of centrioles, respectively (greyscale and red in merge). DNA was stained with Hoechst 33258 (blue). Enlargements show centrosomal regions in transfected (T) and untransfected (U) cells. Scale bar, 10 µm.

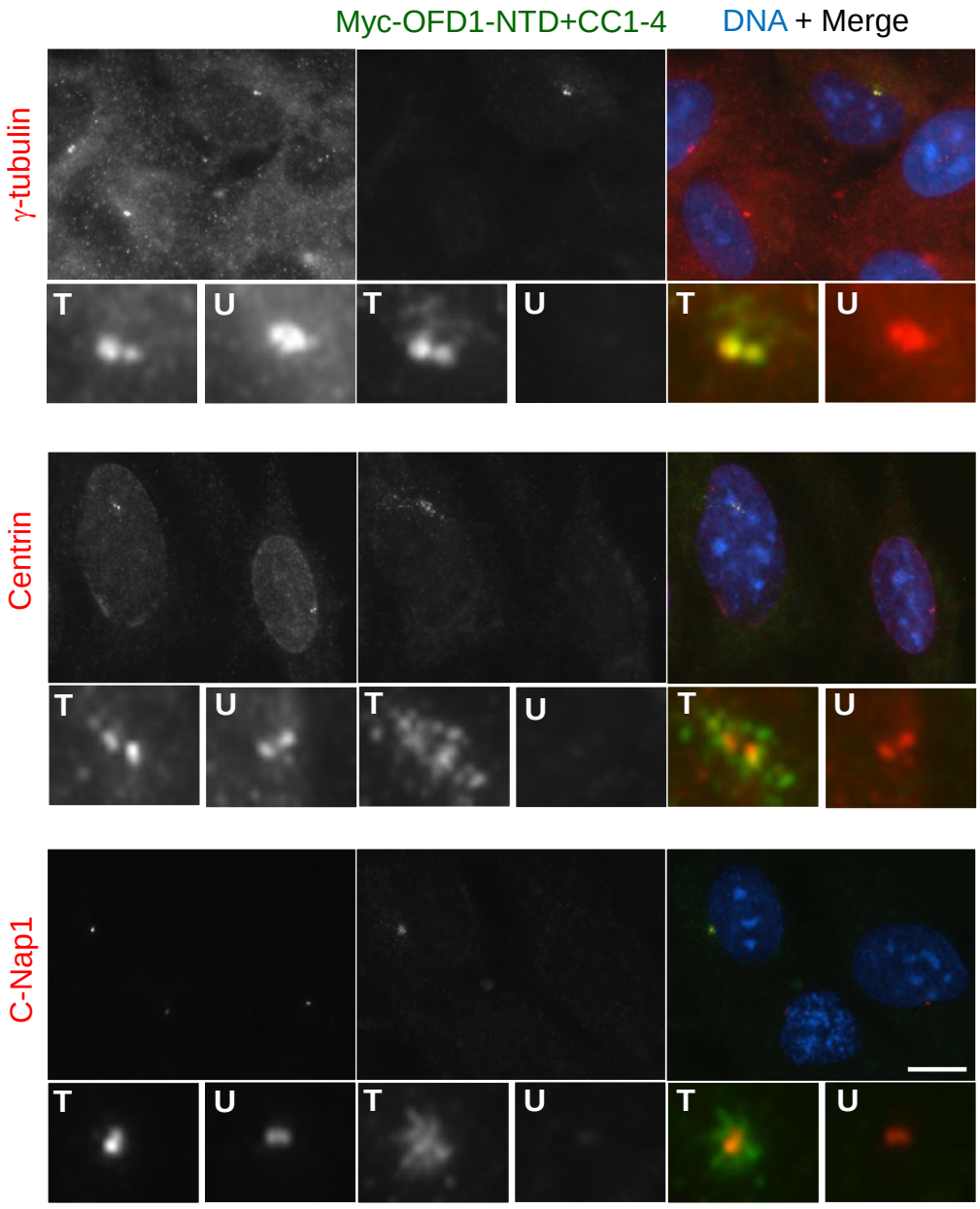

Figure 6.10 OFD1-NTD+CC1-4 localizes to centriolar satellites
hTERT-RPE1 cells transiently transfected with Myc-OFD1-NTD+CC1-4 (residues 3-601) were co-stained with antibodies against the Myc tag (greyscale and green in merge) to determine the localization of recombinant OFD1 protein, and with antibodies against the centrosomal marker γ-tubulin, or with antibodies against centrin or C-Nap1, markers of the distal and proximal ends of centrioles, respectively (greyscale and red in merge). DNA was stained with Hoechst 33258 (blue). Enlargements show centrosomal regions in transfected (T) and untransfected (U) cells. Scale bar, 10 µm.

distal (centrin) or proximal (C-Nap1) ends of the centrioles. Strikingly, however, no distinct pericentriolar aggregates were observed, indicating that this protein does not localize to centriolar satellites (Figure 6.8). Deletion of the first two coiled-coil domains from this construct, which already lacks the N-terminal LisH motif (OFD1-CC3-6), led to a weaker localization of the protein to the centrosome concomitant with a more obvious diffuse cytoplasmic distribution. Also, no centriolar satellite staining was apparent (Figure 6.9). In contrast, a protein containing the intact N-terminus and the first four coiled-coils, thus only lacking the last two coiled-coils (OFD1-NTD+CC1-4), specifically localized to centriolar satellites (Figure 6.10). Although the pericentriolar staining was not as strong as observed with full-length OFD1, this suggests that the LisH-containing N-terminal domain is critical for this localization. Unfortunately, a construct containing only the LisH-containing N-terminal domain could not be expressed in hTERT-RPE1 cells, most likely as a result of unstable mRNA or protein. This difficulty of expressing OFD1 constructs in cells may also explain the weak expression of the OFD1-NTD+CC1-4 construct.

6.2.3 The N-terminal domain of OFD1 is crucial for centriolar satellite integrity

Given the remarkably distinct localization of these truncated OFD1 constructs, we then examined the effect of their expression on the distribution of other satellite proteins. Specifically, we decided to look at PCM-1, a core centriolar satellite protein that we have shown to physically interact with OFD1 (see above), CEP290, a centrosomal and centriolar satellite protein that we have shown to behave in a similar fashion to OFD1 (Chapter 4 and 5), and pericentrin, a protein we have shown to be primarily centrosomal (Chapter 4) and not affected by OFD1 depletion (Chapter 5) in hTERT-RPE1 cells.

The OFD1-CTD protein that localized to centrosomes but not satellites, led to the redistribution of PCM-1 and CEP290 onto the centrosome at the expense of their localization to satellites (Figure 6.11). Even pericentrin became more intensively

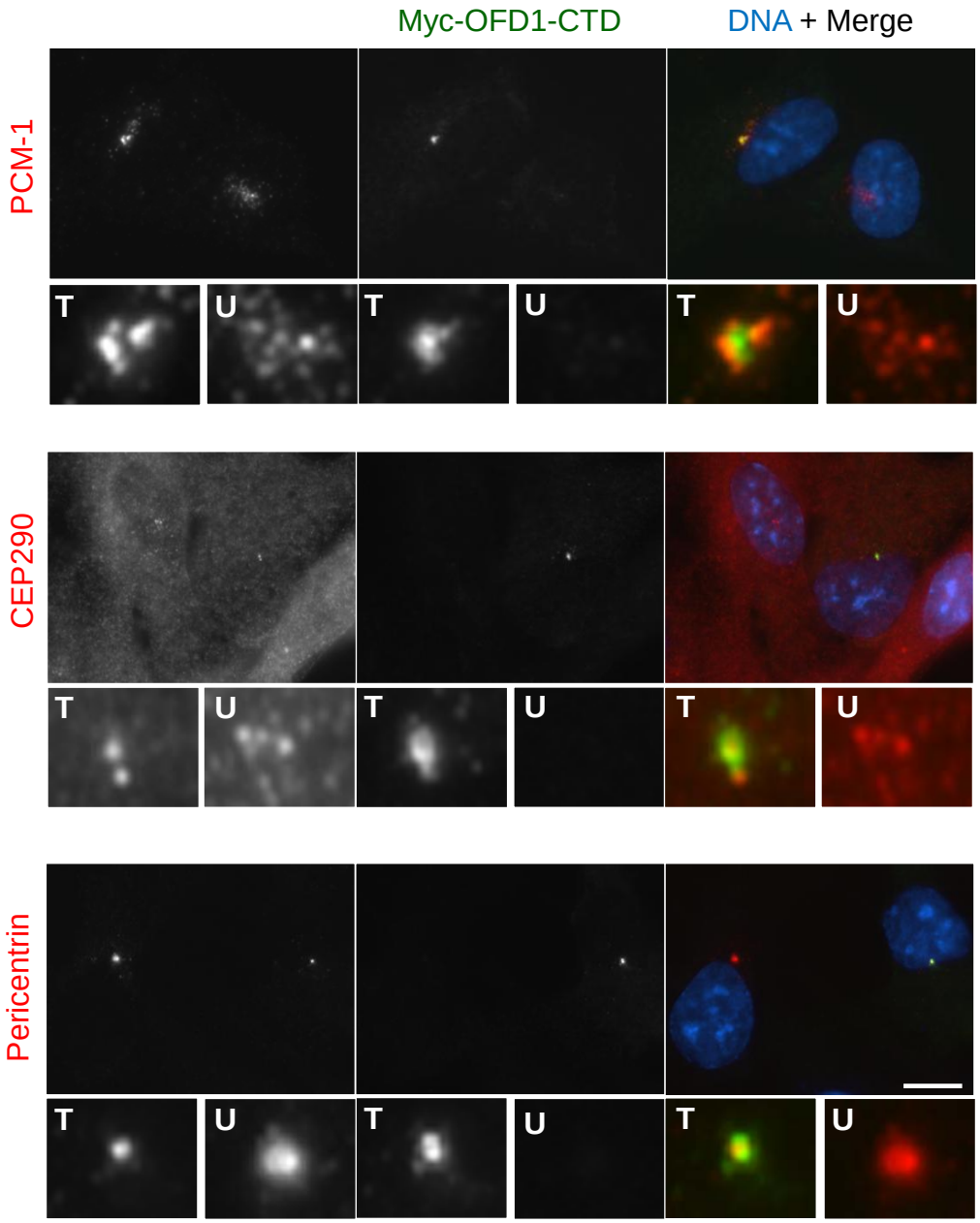

Figure 6.11 OFD1-CTD redistributes PCM-1 and CEP290 to the centrosome
hTERT-RPE1 cells transiently transfected with Myc-OFD1-CTD were co-stained with antibodies against the Myc tag (greyscale and green in merge) and with antibodies against the PCM-1, CEP290 or pericentrin (greyscale and red in merge). DNA was stained with Hoechst 33258 (blue). Enlargements show centrosomal regions in transfected (T) and untransfected (U) cells. Scale bar, 10 µm.

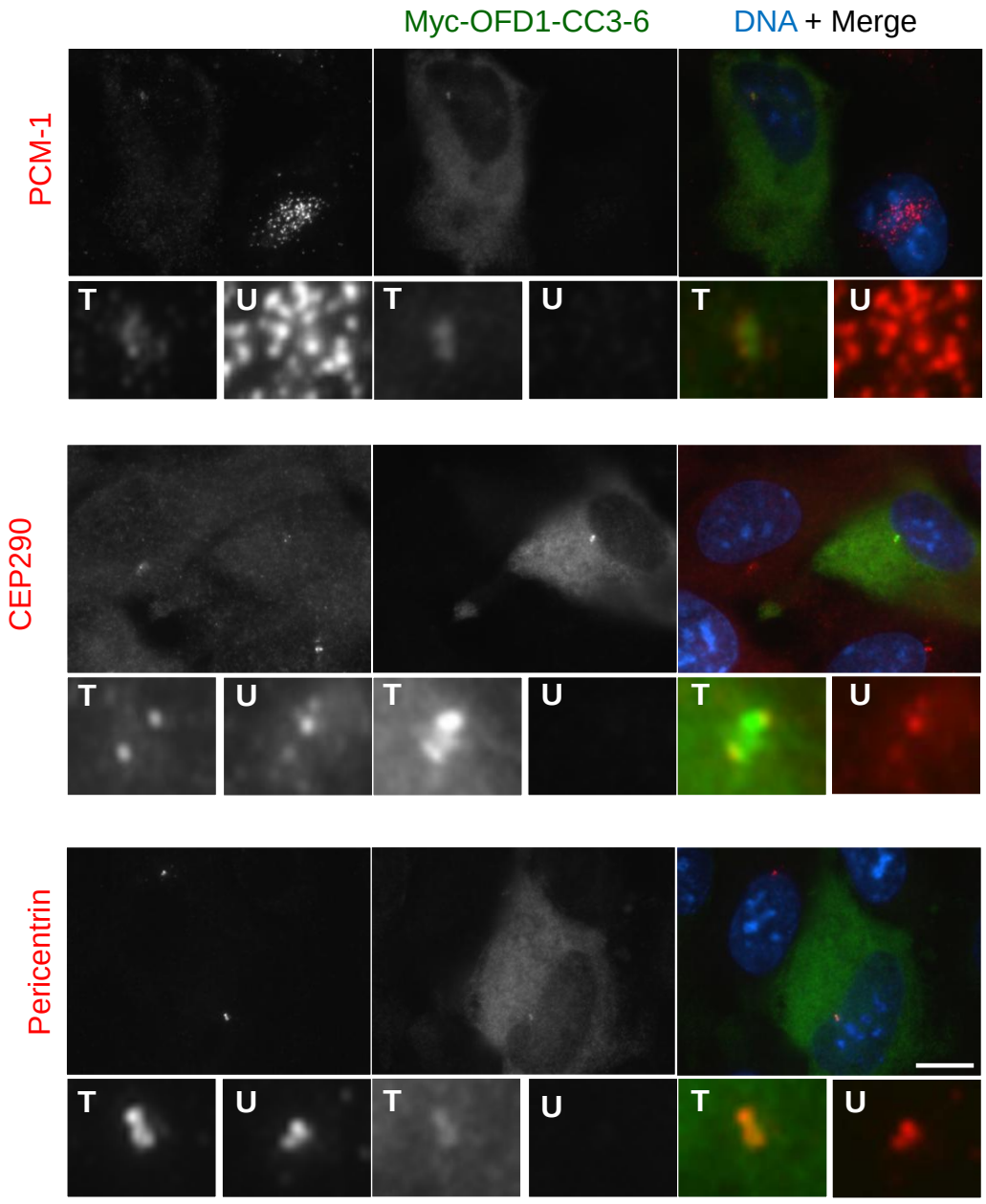

Figure 6.12 OFD1-CC3-6 leads to dispersal of PCM-1 and CEP290 satellites
hTERT-RPE1 cells transiently transfected with Myc-OFD1-CC3-6 (residues 365-1012) were co-stained with antibodies against the Myc tag (greyscale and green in merge) and with antibodies against the PCM-1, CEP290 or pericentrin (greyscale and red in merge). DNA was stained with Hoechst 33258 (blue). Enlargements show centrosomal regions in transfected (T) and untransfected (U) cells. Scale bar, 10 µm.

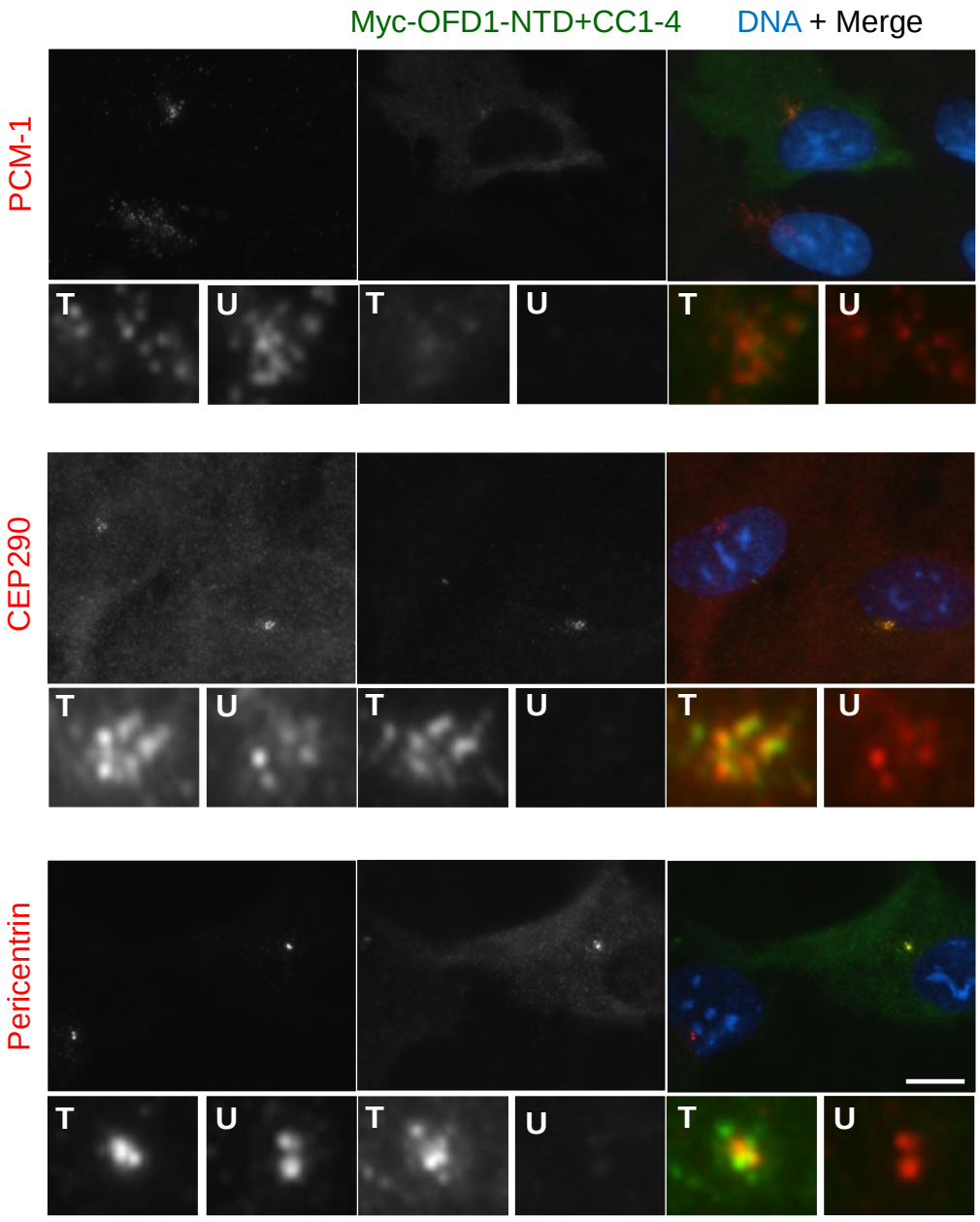

Figure 6.13 OFD1-NTD+CC1-4 does not affect localization of PCM-1 or CEP290 to centriolar satellites

hTERT-RPE1 cells transiently transfected with Myc-OFD1-NTD+CC1-4 (residues 3-601) were co-stained with antibodies against the Myc tag (greyscale and green in merge) and with antibodies against the PCM-1, CEP290 or pericentrin (greyscale and red in merge). DNA was stained with Hoechst 33258 (blue). Enlargements show centrosomal regions in transfected (T) and untransfected (U) cells. Scale bar, 10 µm.

A

Protein	Myc-tag		PCM-1		CEP290		Pericentrin	
Localization	c	s	c	s	c	s	c	s
Myc-OFD1-FL	-	+	-	+	-	+	+	-
Myc-OFD1-CTD	+	-	+	+	+	-	+	-
Myc-OFD1-CC3-6	+	-	-	-	+	-	+	-
Myc-OFD1-NTD+CC1-4	-	+	-	+	-	+	+	-

B

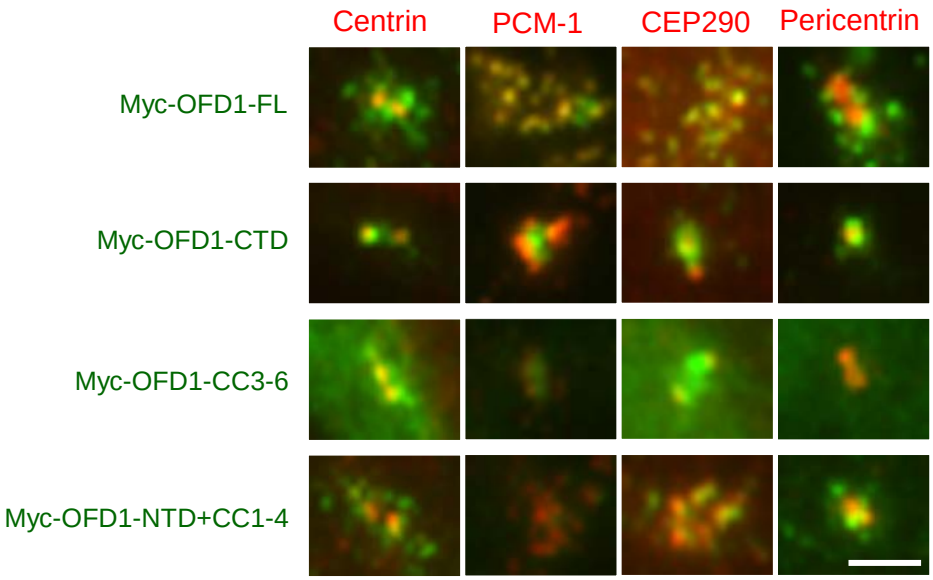

Figure 6.14 Localization of myc-OFD1 proteins, PCM-1, CEP290 and pericentrin
(A) The primary localization of the myc-OFD1 protein, PCM-1, CEP290 and Pericentrin in the presence of the different OFD1 constructs is indicated; c, centrosomes; s, centriolar satellites. **(B)** Representative images of the results shown in (A). hTERT-RPE1 cells transiently transfected with Myc-tagged OFD1 constructs were co-stained with antibodies against the Myc tag (green) and with antibodies against centrin, PCM-1, CEP290 or pericentrin (red). Scale bar, 2 µm.

concentrated on centrosomes in cells expressing this construct suggesting that, even though pericentrin is not easily detected on satellites in these cells, a fraction may be satellite-associated which becomes redistributed by this OFD1 construct (Figure 6.11). In contrast, in cells expressing the OFD1-CC3-6 protein that is only weakly centrosome-associated and diffusely cytoplasmic, PCM-1 and CEP290 containing satellites are dispersed, although CEP290 is still weakly detected on centrosomes (Figure 6.12). Pericentrin localization, on the other hand, was not affected by the expression of this construct. We interpret this to mean that both these C-terminal OFD1 constructs can bind to PCM-1 and CEP290 and disturb their localization to satellites, but the one lacking the first two coiled-coils is less efficient at centrosome targeting. Finally, expression of the OFD1-NTD+CC1-4 protein, which is still capable of localizing to satellites, does not obviously affect the localization of other satellite proteins (Figure 6.13). Together, these results, summarized in Figure 6.14, show that OFD1 constructs that themselves mislocalize cause mislocalization of other centriolar satellite components consistent with their interaction in cells (Figure 6.14).

6.3 DISCUSSION

Thus far, our description of the unexpected colocalization of the OFD1 syndrome protein with PCM-1 and the ciliopathy disease proteins BBS4 and CEP290 at centriolar satellites, together with the finding that these proteins are mutually dependent for the integrity of these structures, have led us to hypothesize that centriolar satellites are large molecular assemblies that depend on protein-protein interactions for their organization. Indeed, previous studies had shown that PCM-1 can directly interact with both ciliopathy disease proteins BBS4 (Kim et al. 2004) and CEP290 (Kim et al. 2008). In this study, we have now shown that PCM-1 can physically interact with another ciliopathy disease protein, OFD1, and that this interaction requires the regions encompassing the N-terminal coiled-coil domain of PCM-1 and at least the fifth coiled-coil motif of OFD1 implying the possibility of a direct coiled-coil interaction. On the other hand, both OFD1 and PCM-1 are able to

self-associate: PCM-1 is capable of oligomerization via its coiled-coil domains (Kubo & Tsukita 2003), and OFD1 is able to self-associate through its coiled-coil domains with its fifth coiled-coil necessary for OFD1 homotypic interactions (Giorgio et al. 2007). Whether this competes with PCM-1-OFD1 binding is not clear. In contrast, BBS4 interacts with the C-terminal non-coiled-coil region of PCM-1 (Kim et al. 2004). Hence, it is plausible that the weak interaction we detected between OFD1 and BBS4 in cells could be the result of PCM-1 bridging in the binding of OFD1 and BBS4.

Our interaction data is consistent with the consequences of expressing the C-terminal fragment of OFD1 containing the third to sixth coiled-coils, which led to mislocalization of PCM-1. This fragment also caused mislocalization of CEP290 pericentriolar granules suggesting either that OFD1 directly interacts with CEP290 through this region or it disturbs CEP290 via PCM-1. Indeed, CEP290 does coprecipitate with PCM-1, although the region of interaction was not mapped (Kim et al. 2008). Importantly, an N-terminal OFD1 fragment lacking the region required for PCM-1 interaction localized to pericentriolar granules indicating that association with PCM-1 is unlikely to be the primary mechanism for this localization and raising the prospect that the LisH motif may contribute to this targeting. To strengthen this hypothesis, a recent study has demonstrated that a functional LisH motif present in the newly identified centrosomal and centriolar satellite protein, FOR20, is necessary and sufficient for FOR20 pericentriolar satellite localization. This protein, related to FOP (FGFR1 Oncogene Partner) protein, and more distantly related to the N-terminus of OFD1 protein, is found only in ciliated organisms and its inhibition affects ciliogenesis (Sedjaï et al. 2010). Nevertheless, because the N-terminal fragment of OFD1 did not perfectly colocalize with PCM-1 or CEP290 at centriolar satellites, it is possible that the presence of the fifth coiled-coil is necessary to increase the stability of these structures. In line with our previous observation of two fractions of OFD1 with distinct dynamics and behaviour, these results show that distinct OFD1 domains contribute differently for the correct localization, and possibly

the function, of these fractions. Unfortunately, due to the difficulties of expression of OFD1 constructs mentioned above, we were not able to investigate more thoroughly the localization of OFD1 truncation constructs encoding for other regions of the protein or the effect of their expression on the distribution of other satellite proteins. This information would clearly better elucidate the potential function of each region of OFD1 protein. These difficulties also hindered additional co-immunoprecipitation experiments with transfected OFD1 constructs.

A recent study on OFD1 protein has found that LisH mutations blocked Ift88 recruitment and ciliogenesis (Singla et al. 2010). Although this study did not consider OFD1 at pericentriolar satellites, this is consistent with previous observations that perturbation of centriolar satellites affects the recruitment of proteins important for ciliogenesis (Dammermann & Merdes 2002; Kim et al. 2008). Together with our findings, this further supports our hypothesis that centriolar satellites function as assembly points for proteins implicated in human ciliopathies, and that defects in one of these subunits affect the integrity of the whole complex, thus offering some explanation as to why such different diseases show considerable phenotypic overlap.

CHAPTER 7

FINAL DISCUSSION

CHAPTER 7 FINAL DISCUSSION

7.1 Centriolar satellites: an assembly point for proteins implicated in human ciliopathies?

In this study, we show that the protein encoded by the OFD1 disease gene, mutated in oral-facial-digital syndrome type 1, localizes not only to centrosomes and basal bodies, but also to centriolar satellites. With BBS4 and CEP290 (Kim et al. 2004; Kim et al. 2008), OFD1 joins a growing list of ciliopathy associated genes known to encode proteins that localize to centriolar satellites. Remarkably, OFD1 colocalizes at these structures with BBS4 and CEP290, products of genes mutated in Bardet-Biedl syndrome and Joubert syndrome, respectively, as well as the known centriolar satellite component, PCM-1 (Kubo et al. 1999; Kubo & Tsukita 2003). OFD1, BBS4 and CEP290 all physically interact with PCM-1 (this study, (Kim et al. 2004; Kim et al. 2008)). Consistent with this, the localization of these ciliopathy proteins to centriolar satellites is dependent on PCM-1. Interestingly, however, depletion of OFD1, BBS4 or CEP290 also led to mislocalization of PCM-1, as well as other ciliopathy disease proteins. Thus, surprisingly, localization of all four of these proteins to centriolar satellites is mutually dependent. In addition, we show that interfering with microtubule dynamics, as well as expression of truncated OFD1 constructs, also results in the mislocalization of OFD1, BBS4, CEP290 and PCM-1 to centriolar satellites. Collectively, these observations suggest that removal of any centriolar satellite component destabilizes this structure. Thus, we propose that centriolar satellites are assembly points for proteins implicated in human ciliopathies, and that they function as large macromolecular complexes that rely on multiple protein-protein interactions for their integrity.

By physically linking components of a common molecular pathway, multisubunit protein complexes can limit non-specific interaction, increase the local concentration of components, and provide spatial control for their regulation by positioning them at

specific sites in proximity to downstream targets or upstream modulators. Because mutations in each subunit may result in the dysfunction of the entire complex, this hypothesis could explain the fact that mutations in many different genes give rise to a set of phenotypes associated with a particular ciliopathy. In support of this view, studies have identified the interaction between two Meckel-Gruber syndrome proteins, MKS1 and MKS3/meckelin, physical interactions between nephronophthisis proteins, including nephrocystin-1, nephrocystins-2/Inversin, nephrocystin-3, nephrocystin-4, and nephrocystin-2/CEP290, and a stable complex composed of seven highly conserved BBS proteins, the BBSome. In addition, there is evidence that proteins implicated in distinct ciliopathies may also interact in common molecular pathways (Nachury et al. 2007; Kim et al. 2008).

The organization of large protein complexes that can function as molecular scaffolds therefore relies on protein-protein interactions. Here, we show that the interaction between OFD1 and PCM-1 requires the regions encompassing the N-terminal coiled-coil domain of PCM-1 and at least the fifth coiled-coil motif of OFD1. PCM-1 is also capable of oligomerization via its coiled-coil region (Kubo et al. 1999), and OFD1 can self-associate through its coiled-coil domains with its fifth coiled-coil necessary for OFD1 homotypic interactions (Giorgio et al. 2007). However, whether this competes with binding between OFD1 and PCM-1, it is not clear. PCM-1 can also directly interact with two other ciliopathy disease proteins, BBS4 and CEP290 (Kim et al. 2004; Kim et al. 2008). Although the region of PCM-1-CEP290 interaction is not mapped (Kim et al. 2008), PCM-1 interacts with BBS4 via its non-coiled-coil region (Kim et al. 2004). Hence, PCM-1 could bridge binding of OFD1 and BBS4, as our results suggest that these two ciliopathy proteins do not directly interact. Interestingly, our interaction data is consistent with the effects of expressing a C-terminal fragment of OFD1 containing the third to sixth coiled-coil motifs, which resulted in PCM-1 mislocalization. Notably, this fragment also caused

mislocalization of CEP290, suggesting that OFD1 may directly interact with CEP290 through this region or, alternatively, that it disturbs CEP290 via PCM-1.

Given this collection of data, it is conceivable that PCM-1 may act as the central organizing subunit of a larger complex that relies on the presence of other proteins, including ciliopathy disease proteins OFD1, BBS4 and CEP290, for its stability and function. Moreover, based on our zebrafish experiments, it appears that OFD1 and BBS4 functionally-synergize in terms of biological effects in the whole animal, even if they do not directly interact at a protein-protein level. Together, these observations further support the hypothesis that ciliopathy associated proteins assemble as large complexes, providing some explanation as to why the clinical spectrum of diseases such as OFD1 and the BBS disorders show considerable overlap, for example featuring polydactyly and renal cysts. To test this hypothesis, we suggest the use of animal models. Previously, both mouse and zebrafish OFD1 knockout models (Ferrante et al. 2006; Ferrante et al. 2009) were shown to recapitulate the main features of the disease. We now suggest the use of animal knock-in mutant models to study the importance of these macromolecular assemblies of ciliopathy proteins in the normal embryonic development. Following careful determination of the amino acids that are crucial for the specific interaction between each centriolar satellite protein, we could investigate the biological effects of mutations in these residues in the whole animal. Particularly, the study of an OFD1 knock-in mutant with mutations that exclusively affect its interaction with PCM-1, would allow us to determine the role of this interaction and its importance in embryo development. Ultimately, this study could indicate how the perturbation of specific interactions can lead to different phenotypes or, perhaps, influence its severity.

7.2 OFD1 at centrioles: a distinct cellular role?

Our results show that there are at least two fractions of OFD1, one associated with centriolar satellites and one with centrioles, with distinct dynamics and behaviour

through the cell cycle. In untreated interphase hTERT-RPE1 cells, OFD1 does not strongly colocalize with core centrosomal markers such as centrin, Cep135 or γ-tubulin, suggesting that it primarily localizes at centriolar satellites. Interestingly, similar observations were reported for BBS4 and CEP290 (Kim et al. 2004; Kim et al. 2008). PCM-1, on the other hand, is exclusively localized to centriolar satellites and, upon progression through mitosis these disperse (Dammermann & Merdes 2002). During mitosis, both OFD1 and CEP290 become obviously associated with centrosomes at spindle poles, whereas BBS4 and PCM-1 do not. Following experimental disruption of centriolar satellites, the ciliopathy proteins also display distinct patterns in terms of centrosome localization. For example, under conditions that interfere with microtubule dynamics, OFD1 and CEP290 are both weakly detected on centrosomes, whereas BBS4 is not (this study, (Kim et al. 2004; Kim et al. 2008)). Also, upon depletion of OFD1, PCM-1 or BBS4, CEP290 can still be detected at the centrosome, despite loss of satellites. OFD1, however, is detected at centrosomes only upon depletion of PCM-1 but not depletion of BBS4. It would be interesting to test how depletion of CEP290 affects both centriolar and pericentriolar satellite fractions of OFD1. It has been reported that PCM-1 concentrates around centrosomes in the absence of CEP290 (Kim et al. 2008), although when CEP290 localization was disturbed in our experiments by either OFD1 or BBS4 depletion, there was no accumulation of PCM-1 at the centrosome. Nonetheless, under these conditions, CEP290 was not completely absent in the cell, as it remained at the centrosome. However puzzling, these observations indicate that ciliopathy disease proteins exhibit a much more complex dependency in terms of centrosomal localization. More importantly, they suggest that in many respects OFD1 and CEP290 display remarkably similar behaviour and might have additional functions at centrosomes that are not shared by PCM-1 and BBS4.

In this regard, we show that OFD1 localizes to the distal ends of centrioles during mitosis and near the base of each cilium generated in differentiated multiciliated

cells. Consistent with this, Singla et al. (2010) show localization of OFD1 to all centriole distal ends in murine embryonic stem cells, and demonstrate that OFD1 functions as a cap to stabilize microtubules and control length of centrioles. Moreover, this study reveals that OFD1 is also necessary for the formation of distal appendages and the recruitment of IFT88, two crucial processes for cilium formation (Singla et al. 2010). Indeed, OFD1 is required for primary cilia formation (this study, (Graser et al. 2007; Corbit et al. 2008; Singla et al. 2010). CEP290 is also centriolar throughout the cell cycle and, in ciliated cells it localizes to the distal end of the basal body near the base of the cilium (Tsang et al. 2008). Moreover, depletion of CEP290, although not having any effect on cell cycle progression, also reduces primary cilia formation. It is thought that this may result from defects in the migration of centrioles to the cell cortex and/or to the disrupted recruitment of Rab8 to the cilium, found to be dependent on CEP290 (Tsang et al. 2008). These findings show that OFD1 and CEP290 not only have similar dynamics, but also that these proteins might have analogous functions at the centrioles. This is intriguing in light of the observation that mutations in both proteins can cause JBTS (Coene et al. 2009). Importantly, as OFD1 and CEP290 do not entirely depend on centriolar satellites for their localization to the centrioles, it is plausible that these two fractions have separate functions in the cell. Also, there is the possibility that the relative fraction of each in the cell may vary with tissue and thus dictate how mutations in each protein affect the development or cellular homeostasis of the tissues.

Interestingly, CEP290 has been very recently identified at the transition zone, where it regulates the entry and exit of proteins to and from the cilium, respectively (Craige et al. 2010). Moreover, both OFD1 and CEP290 localize to the connecting cilium of photoreceptors, which is considered to be the orthologous structure of the transition zone (Coene et al. 2009; Craige et al. 2010). Again, it is plausible that the fraction of OFD1 detected at the base of the cilium may in fact localize to the transition zone where it may play analogous roles to CEP290.

Furthermore, although we and others (Singla et al. 2010) did not observe any obvious defects in centriole duplication, or cell cycle progression in cells depleted of OFD1, the fact that the protein is present on spindle poles may indicate an as yet unidentified role in mitosis. Indeed, it is noteworthy that OFD1 was identified as essential for mitosis in a recent genome-wide study by the MitoCheck consortium (Neumann et al. 2010).

7.3 OFD1 disease mutations: understanding their consequences in the context of centriolar satellites and centrosomes

Remarkably, analysis of mutations found in OFD1 patients reveals that most of the point mutations are represented by frameshifts that likely result in truncated versions of the protein which, in turn, probably lead to loss-of-function (Figure 7.1). Also, in some cases, the premature termination codon introduced due to frameshift mutations may result in nonsense mediated decay of the mutant mRNA, thus reducing the transcript levels. Interestingly, analysis of the two frameshift mutations in exon 21 of OFD1 described in an X-linked Joubert syndrome showed that these proteins retained the pericentriolar localization when compared to wild-type eCFP-tagged OFD1 constructs. In addition, the recombinant protein carrying the SGBS2-associated OFD1 mutation in exon 17 was localized diffusely throughout the cytoplasm but also showed clear concentration at both centrioles. On the other hand, OFD1 syndrome-associated mutant proteins carrying two different frameshift mutations in exon 16 showed similar scattering throughout the cytoplasm but also severely reduced concentration around the centrosome when compared to the wild-type (Coene et al. 2009). Combined with our results, these observations suggest that frameshift mutations resulting in truncated versions of OFD1 lacking the fifth coiled-coil motif, may interfere with PCM-1-OFD1 interaction and localization to centriolar satellites, thus resulting in OFD1 dysfunction defects. In contrast, because the two OFD1 mutations described to cosegregate with X-linked JBTS result in a

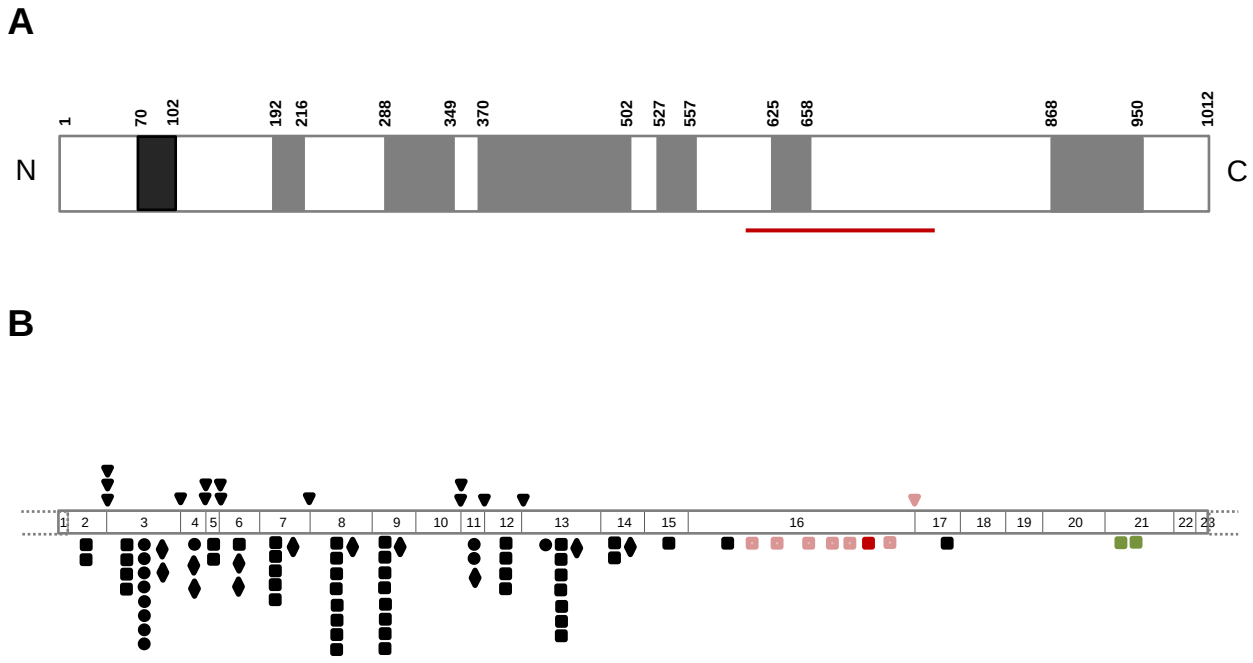

Figure 7.1 OFD1 mutations in the of context centriolar satellites and centrosomes

(A) Schematic representation of OFD1 protein. LisH (black) and coiled-coil (grey) motifs, as well as amino acid numbers, are indicated. The red line indicates the region in OFD1 (aa 601-765) that is essential for association with PCM-1, as assessed by our biochemical experiments; this critical region spans the fifth coiled-coil motif. **(B)** Schematic representation of OFD1 gene. The diagram depicts the 23 exons of OFD1 gene, and the positions of intron/exon boundaries are indicated by vertical bars. This is in scale so that the OFD1 protein domains shown above are aligned with their coding sequence below. All the point mutations identified to date in the literature are also shown (Ferrante et al. 2001; Rakkolainen et al. 2002; Romio et al. 2003; Thauvin-Robinet et al. 2006; Prattichizzo et al 2008; Budney et al. 2006; Coene et al. 2009). Point mutations are reported as frameshift (square); splice-site (triangle); nonsense (diamond); and missense (circle). Point mutations shown in red and pink are the mutations found within the region that encodes for the PCM-1-interacting region. The frameshift mutation in exon 16 depicted in red has been described in X-linked Simpson-Golabi-Behmed-like syndrome (Budney et al. 2006) and the frameshift mutations in exon 21 (green) have been described in X-linked Joubert syndrome (Coene et al. 2009). Diagram is adapted from Macca et al. (2009). Full description of mutations can be found in Macca et al. (2009).

longer OFD1 transcript that affects only the sixth coiled-coil, thus not affecting OFD1 pericentriolar localization or completely disrupting its interaction with lebercilin, it is plausible that their effects may be ascribed to the perturbation of OFD1 interaction with another yet unidentified protein (Figure 7.1).

Moreover, the majority of the missense mutations found in OFD1 patients affect highly conserved amino acids. In fact, most of the missense mutations fall within the LisH motif in the N-terminal domain of the protein, a highly conserved motif that we found is within the region necessary for localization of OFD1 protein to centriolar satellites. Any change in highly conserved amino acids is likely to result in dramatic change in the protein structure. Particularly, any change in the LisH motif can potentially have indirect effects on functions attributed to other parts of the protein. So, for example, it may disturb OFD1 interaction with PCM-1 through conformational changes in the protein structure. It is also possible that PCM-1 and OFD1 interaction requires OFD1 to be localized at satellites, and hence disruption of this localization somehow weakens the interaction. Taken together, these data suggest that differences in binding affinity of the OFD1 mutant protein to functionally interacting protein, such as PCM-1 or lebercilin, may account for the phenotypic variability observed in patients with OFD1, SGBS2 and X-linked JBTS. Notably, to our knowledge, PCM-1 mutations have not been associated with ciliopathies. Given its close relationship with proteins implicated in ciliopathies, we suggest that it may be fruitful to seek mutation of PCM-1 in patients with apparent ciliopathies who do not have defined mutation of other genes.

7.4 Ciliopathy proteins in a nutshell: a model for cellular trafficking

Not surprisingly, many ciliopathy disease genes are essential for primary cilia formation. Indeed, the pleiotropy and the genetic heterogeneity of ciliopathies may be attributed to the inherent complexity of the molecular mechanisms that underlie the formation and function of primary cilia. However, a specific function for centriolar

satellites in ciliogenesis remains elusive. Evidence suggests that satellites serve as mediators for the transport of proteins along microtubules to the centrosome or basal body. For example, the incorporation of centrin, pericentrin and ninein to the centrosome depends on PCM-1 (Dammermann & Merdes 2002). Moreover, centriolar satellite proteins, including BBS4 and CEP290, interact with microtubule-based motor protein subunits (Kim et al. 2004; Chang et al. 2006). This trafficking may serve to provide the machinery for basal body biogenesis, cilia extension or intraflagellar transport.

Indeed, the BBSome, a stable complex of seven highly conserved BBS proteins, is required for transport of Rab8 to the cilia where the small GTPase enables vesicle docking and fusion events essential to assemble the ciliary membrane (Nachury et al. 2007). Also, depletion of PCM-1 and CEP290 interferes with Rab8 translocation to the cilium (Kim et al. 2008). Because the BBSome promotes ciliogenesis without regulating centriolar satellite function, the current model predicts that the BBSome is transported to the basal body by centriolar satellites where it separates from these structures to perform its ciliogenic function at the basal body and/or inside the cilium. Furthermore, assembly of this PCM-1-BBSome complex requires normal levels of CEP290, suggesting that CEP290 complexes with PCM-1 and supports the assembly of large multisubunit PCM-1-BBSome complexes (Nachury et al. 2007; Kim et al. 2008). The existence of this complex of evolutionary conserved BBS proteins considerably simplified our perception of BBS, reducing the genetic complexity of BBS and providing an explanation for its genetic heterogeneity. As suggested by Nachury et al. (2007), this apparently complex mechanism of cytoplasmic transport of the BBSome by centriolar satellites presents advantages. By sequestering and shielding the BBSome in a complex with centriolar satellites, and only revealing it at the basal body, these structures can spatially limit BBSome activation to the proximity of the basal body.

Our findings have led us to hypothesize that centriolar satellites are themselves large protein assemblies that guarantee a precise and controlled delivery of specific proteins required for basal body biogenesis and/or cilia extension (Figure 7.2). Moreover, the integrity of such complexes depends on protein-protein interactions. Therefore, mutations that affect these interactions can result in the impairment or even collapse of the complex, disrupting the shuttling of key proteins to the function of the basal body and/or primary cilium, and thus resulting in ciliary dysfunction. Here, we propose that the ciliopathy associated proteins, including OFD1, CEP290 and BBS4, together with PCM-1, function as a stable complex in the same pathway. To help prove this hypothesis and further resolve the nature of this complex, it will be important to test how depletion of OFD1, BBS4, CEP290 or PCM-1, affects the properties of each component in the complex. This could be determined by examining the sedimentation property of each component in sucrose density gradient centrifugation or gel filtration. Other proteins may be part of, or transiently associate, with this complex. Indeed, a recent study has identified a new centriolar satellite protein, FOR20. Moreover, like OFD1, this protein contains a LisH motif that is necessary for its pericentriolar satellite localization (Sedjaï et al. 2010). Clearly, this protein is a likely candidate to also be part of this macromolecular complex. On the other hand, this proposed model does not exclude the possibility that some of its components may work in other complexes as well. In fact, the observation that, unlike PCM-1 (Dammermann & Merdes 2002), CEP290 (Kim et al. 2008) and OFD1 are not required for the recruitment of pericentrin to the centrosome or basal body indicates that the trafficking of this centrosomal protein depends on a different mechanism and perhaps a different complex of proteins. This model also provides a clue as to why some ciliopathy associated proteins, though required for ciliogenesis, have not been ascribed a direct role in centriole/basal body biogenesis, ciliary membrane biogenesis, intraflagellar transport or in ciliary signaling at the membrane.

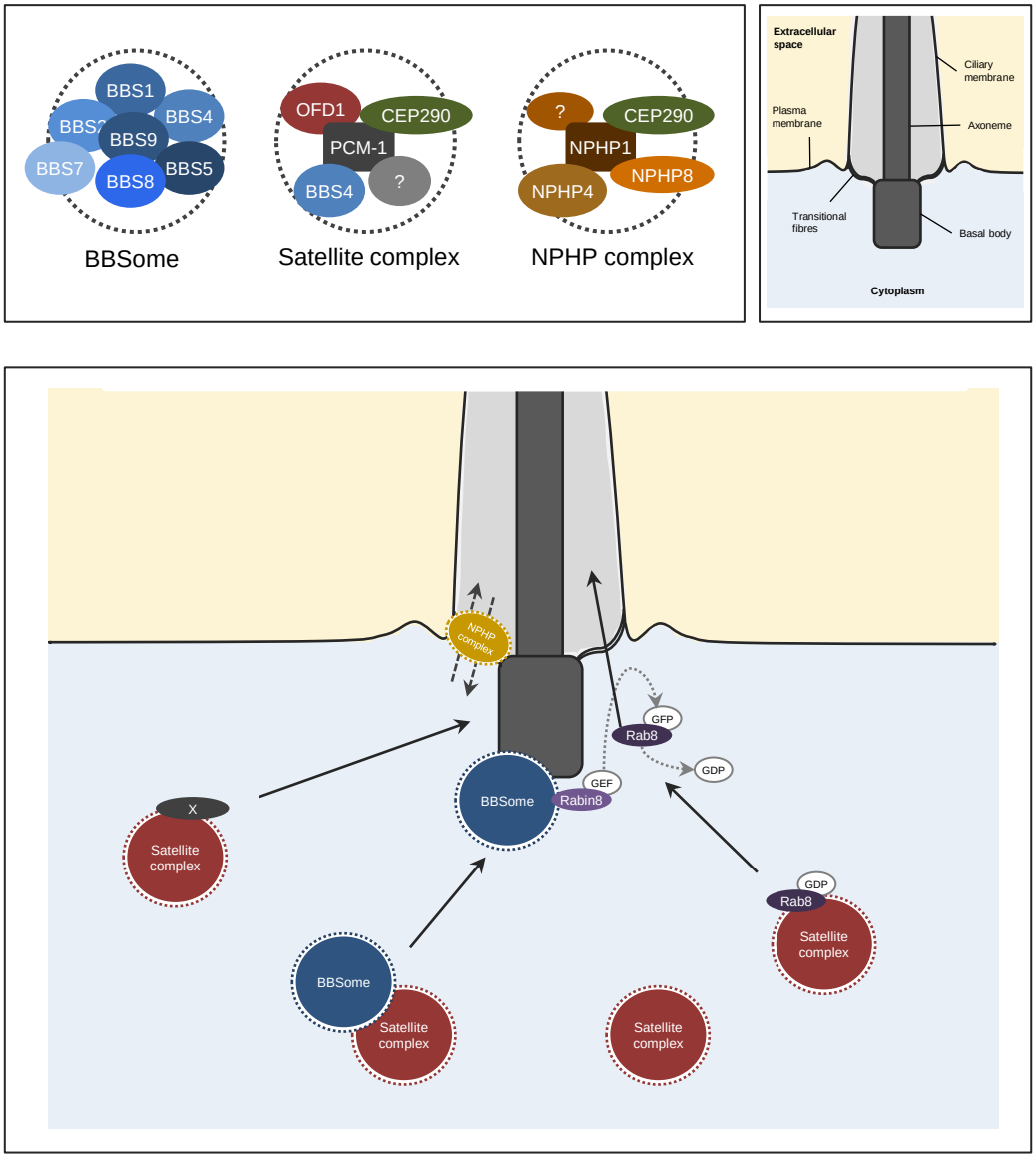

Figure 7.2 Ciliopathy proteins in a nutshell: a model for cellular trafficking
Diagram representing the proposed model in this thesis. The left hand top panel shows the composition of the previously described BBSome (Nachury et al. 2007), the proposed composition of the centriolar satellite complex (this study), and a potential composition of the recently proposed NPHP complex (Omran 2010). The right hand top panel shows a schematic representation of the primary cilium extending from a basal body and some of its associated structures. Bottom panel shows a diagram depicting the localization and function of the satellite complexes, as well as the BBSome and the NPHP complex.

Remarkably, a very recent discovery has unraveled a probable role for a complex of NPHP proteins at the ciliary transition zone. CEP290 was found to localize to the Y-shaped structures that bridge and connect the *C. reinhardtii* flagellar membrane to the outer doublet microtubules within the transition zone (Craige et al. 2010). More importantly, CEP290 is required to form the microtubule-membrane linkers that tether the flagellar membrane to the transition zone microtubules. Here, it is required for normal levels of polycystin 2 and BBS4 suggesting that CEP290 controls flagellar protein composition. Moreover, several studies have shown that other NPHP proteins also localize to the base of primary cilia, and that some of these have been found to interact with each other. Together, these observations suggest that NPHP proteins may have a gatekeeper-like functional role at the ciliary compartment border, also referred to the 'ciliary pore complex', controlling delivery and exit of proteins to and from the cilium, respectively (Craige et al. 2010; Omran 2010) (Figure 7.2).

Just as the BBSome yields an explanation for the molecular basis of BBS, and the NPHP model provides an explanation for the complex clinical phenotype in patients affected by *CEP290/NPHP6* mutations, the generalization of this model to different cilia in the human body offers a compelling explanation for the molecular basis of several ciliopathies, particularly OFD1, through the mistargeting of specific ciliary components important for the development and homeostasis of a specific organ.

In the future, identification of other ciliopathy associated proteins involved in this or similar complexes and associated proteins will be crucial for the understanding of the mechanisms underlying, and connecting, these seemingly distinct human disorders.

CHAPTER 8

BIBLIOGRAPHY

CHAPTER 8

BIBLIOGRAPHY

CHAPTER 8 BIBLIOGRAPHY

Adams, M., Smith, U. M., Logan, C. V., and Johnson, C. A. (2008) Recent advances in the molecular pathology, cell biology and genetics of ciliopathies. J. Med. Genet., 45(5), 257-267.

Badano, J. L., Teslovich, T. M., Katsanis, N., and Hopkins, J. (2005) The centrosome in human genetic disease. Nature Reviews Genetics, 6(March), 194-205.

Baker, K. and Beales, P. L. (2009) Making Sense of Cilia in Disease: The Human Ciliopathies. American Journal of Medical Genetics, 151C(4), 281 - 295.

Beales, P. L., Bland, E., Tobin, J. L., Bacchelli, C., Tuysuz, B., Hill, J., Rix, S., Pearson, C. G., Kai, M., Hartley, J., Johnson, C., Irving, M., Elcioglu, N., Winey, M., Tada, M., and Scambler, P. J. (2007) IFT80, which encodes a conserved intraflagellar transport protein, is mutated in Jeune asphyxiating thoracic dystrophy. Nature Genet., 39(6), 727-729.

Berbari, N. F., O'Connor, A. K., Haycraft, C. J., and Yoder, B. K. (2009) The primary cilium as a complex signaling center. Current biology, 19(13), R526-35.

Bettencourt-Dias, M. and Glover, D. M. (2007) Centrosome biogenesis and function: centrosomics brings new understanding. Nat. Rev. Mol. Cell Biol., 8(6), 451-463.

Boylan, J. P. and Wright, A. F. (2000) Identification of a novel protein interacting with RPGR. Human molecular genetics, 9(14), 2085-93.

Budny, B., Chen, W., Omran, H., Fliegauf, M., Tzschach, A., Wisniewska, M., Jensen, L. R., Raynaud, M., Shoichet, S. A., Badura, M., Lenzner, S., Latos-Bielenska, A., and Ropers, H.-H. (2006) A novel X-linked recessive mental retardation syndrome comprising macrocephaly and ciliary dysfunction is allelic to oral-facial-digital type I syndrome. Human genetics, 120(2), 171-8.

Campbell, T. N. and Choy, F. Y. M. (2005) RNA interference: past, present and future. Current issues in molecular biology, 7(1), 1-6.

Cardenas-Rodriguez, M. and Badano, J. L. (2009) Ciliary Biology: Understanding the Cellular and Genetic Basis of Human Ciliopathies. American Journal of Medical Genetics, 151C(4), 263 - 280.

Carvalho-Santos, Z., Machado, P., Branco, P., Tavares-Cadete, F., Rodrigues-Martins, A., Pereira-Leal, J. B., and Bettencourt-Dias, Mónica (2010) Stepwise evolution of the centriole-assembly pathway. Journal of cell science, 123(Pt 9), 1414-26.

Chang, B., Khanna, H., Hawes, N., Jimeno, D., He, S., Lillo, C., Parapuram, S. K., Cheng, H., Scott, A., Hurd, R. E., Sayer, A., Otto, E. A., Attanasio, M., Toole, J. F. O., Jin, G., Hildebrandt, F., Williams, D. S., and Heckenlively, J. R. (2006) In-frame deletion in a novel centrosomal/ciliary protein CEP290/ NPHP6 perturbs its interaction with RPGR and results in early-onset retinal degeneration in the rd16 mouse. Human Molecular Genetics, 15(11), 1847-1857.

Chilvers, M. A. and O'Callaghan, C. (2000) Local mucociliary defence mechanisms. Paediatric respiratory reviews, 1(1), 27-34.

Coene, K. L. M., Roepman, R., Doherty, D., Afroze, B., Kroes, H. Y., Letteboer, S. J. F., Ngu, L. H., Budny, B., Wijk, E. van, Gorden, N. T., Azhimi, M., Thauvin-Robinet, C., Veltman, J. A., Boink, M., Kleefstra, T., Cremers, F. P. M., Bokhoven, H. van, and Brouwer, A. P. M. de (2009) OFD1 is mutated in X-linked Joubert syndrome and interacts with LCA5-encoded lebercilin. American journal of human genetics, 85(4), 465-81.

Conciliis, L. de, Marchitiello, A., Wapenaar, M. C., Borsani, G., Giglio, S., Mariani, M., Consalez, G. G., Zuffardi, O, Franco, B, Ballabio, A., and Banfi, S. (1998) Characterization of Cxorf5 (71-7A), a novel human cDNA mapping to Xp22 and encoding a protein containing coiled-coil alpha-helical domains. Genomics, 51(2), 243-50.

Corbit, K. C., Shyer, A. E., Dowdle, W. E., Gaulden, J., Singla, V, and Reiter, J F (2008) Kif3a constrains b-catenin-dependent Wnt signalling through dual ciliary and non-ciliary mechanisms. Nat. Cell Biol., 10(1), 70-76.

Craige, B., Tsao, C.-C., Diener, D. R., Hou, Y., Lechtreck, K.-F., Rosenbaum, J. L., and Witman, G. B. (2010) CEP290 tethers flagellar transition zone microtubules to the membrane and regulates flagellar protein content. The Journal of cell biology, 190(5), 927-40.

Dabdoub, A. and Kelley, M. W. (2005) Planar cell polarity and a potential role for a Wnt morphogen gradient in stereociliary bundle orientation in the mammalian inner ear. Journal of neurobiology, 64(4), 446-57.

Dammermann, A. and Merdes, A (2002) Assembly of centrosomal proteins and microtubule organization depends on PCM-1. The Journal of cell biology, 159(2), 255-266.

Dawe, H. R., Farr, H., and Gull, K. (2007) Centriole/basal body morphogenesis and migration during ciliogenesis in animal cells. Journal of cell science, 120(Pt 1), 7-15.

Debec, A., Sullivan, W., and Bettencourt-Dias, M. (2010) Centrioles: active players or passengers during mitosis? Cellular and molecular life sciences, 67(13), 2173-94.

Deltas, C. and Papagregoriou, G. (2010) Cystic diseases of the kidney: molecular biology and genetics. Archives of pathology & laboratory medicine, 134(4), 569-82.

Doxsey, S. (2001) Re-evaluating centrosome function. Nat. Rev. Mol. Cell Biol., 2(September), 688-698.

Elbashir, S. M., Harborth, J., Lendeckel, W., Yalcin, A., Weber, K., and Tuschl, T. (2001) Duplexes of 21-nucleotide RNAs mediate RNA interference in cultured mammalian cells. Nature, 411(6836), 494-8.

Elbashir, S. M., Lendeckel, W., and Tuschl, T. (2001) RNA interference is mediated by 21- and 22-nucleotide RNAs. Genes & Development, 15(2), 188-200.

Eley, L., Yates, L. M., and Goodship, J. A. (2005) Cilia and disease. Current opinion in genetics & development, 15(3), 308-14.

Emes, R. D. and Ponting, C. P. (2001) A new sequence motif linking lissencephaly, Treacher Collins and oral-facial-digital type 1 syndromes, microtubule dynamics and cell migration. Human molecular genetics, 10(24), 2813-20.

Feather, S. A., Woolf, A S, Donnai, D, Malcolm, S, and Winter, R. M. (1997) The oral-facial-digital syndrome type 1 (OFD1), a cause of polycystic kidney disease and associated malformations, maps to Xp22.2-Xp22.3. Human molecular genetics, 6(7), 1163-7.

Ferrante, M. I., Giorgio, G., Feather, S. A., Bulfone, A., Wright, V., Ghiani, M., Selicorni, A., Gammaro, L., Scolari, F., and Woolf, A. S. (2001) Identification of the gene for oral-facial-digital type I syndrome. Am. J. Hum. Genet, 68, 569-576.

Ferrante, M. I., Zullo, A., Barra, A., Bimonte, S., Messaddeq, N., Studer, M., Dolle, P., and Franco, B. (2006) Oral-facial-digital type I protein is required for primary cilia formation and left-right axis specification. Nat. Genet., 38(1), 112-117.

Ferrante, M. I., Romio, L., Castro, S., Collins, J. E., Goulding, D. A., Stemple, D. L., Woolf, A. S., and Wilson, S. W. (2009) Convergent extension movements and ciliary function are mediated by ofd1, a zebrafish orthologue of the human oral-facial-digital type 1 syndrome gene. Human molecular genetics, 18(2), 289-303.

Fire, A., Xu, S., Montgomery, M. K., Kostas, S. A., Driver, S. E., and Mello, C. C. (1998) Potent and specific genetic interference by double-stranded RNA in *Caenorhabditis elegans*. Nature, 391(February), 806-811.

Fischer, E., Legue, E., Doyen, A., Nato, F., Nicolas, J.-F., Torres, V., Yaniv, M., and Pontoglio, M. (2006) Defective planar cell polarity in polycystic kidney disease. Nature genetics, 38(1), 21-3.

Fliegauf, M., Benzing, T., and Omran, H. (2007) When cilia go bad: cilia defects and ciliopathies. Nat. Rev. Mol. Cell Biol., 8(11), 880-893.

Gerdes, J., Liu, Y., Zaghloul, N. A., Leitch, C. C., Lawson, S. S., Kato, M., Beachy, P. A., Beales, P. L., DeMartino, G. N., Fisher, S., Badano, J. L., and Katsanis, N. (2007) Disruption of the basal body compromises proteasomal function and perturbs intracellular Wnt response. Nature Genet., 39(11), 1350-1360.

Gerlitz, G., Darhin, E., Giorgio, G., Franco, B., and Reiner, O. (2005) Novel Functional Features of the Lis-H Domain. Cell Cycle, 4(11), 1632-1640.

Germino, G. G. (2005) Linking cilia to Wnts. Nature genetics, 37(5), 455-7.

Giorgio, G., Alfieri, M., Prattichizzo, C., Zullo, A., Cairo, S., and Franco, B. (2007) Functional Characterization of the OFD1 Protein Reveals a Nuclear Localization and Physical Interaction with Subunits of a Chromatin Remodeling Complex. Molecular Biology of the Cell, 18(November), 4397- 4404.

Goetz, S. C. and Anderson, K. V. (2010) The primary cilium: a signalling centre during vertebrate development. Nature Reviews Genetics, 11(5), 331-344.

Graser, S., Stierhof, Y.-D., Lavoie, S. B., Gassner, O. S., Lamla, S., Le Clech, M., and Nigg, E. A. (2007) Cep164, a novel centriole appendage protein required for primary cilium formation. The Journal of cell biology, 179(2), 321-30.

Grimm, D. (2009) Small silencing RNAs: state-of-the-art. Advanced drug delivery reviews, 61(9), 672-703.

Guan, C., Ye, C., Yang, X., and Gao, J. (2010) A review of current large-scale mouse knockout efforts. Genesis, 48(2), 73-85.

Guay-Woodford, L. M. (2006) Renal cystic diseases: diverse phenotypes converge on the cilium/centrosome complex. Pediatric nephrology, 21, 1369-1376.

Hagiwara, H., Ohwada, N., and Takata, K. (2004) Cell Biology of Normal and Abnormal Ciliogenesis in the Ciliated Epithelium. International Review of Cytology, 234, 101-141.

Han, Y.-G. and Alvarez-Buylla, A. (2010) Role of primary cilia in brain development and cancer. Current opinion in neurobiology, 20(1), 58-67.

Hashimoto, M., Shinohara, K., Wang, J., Ikeuchi, S., Yoshiba, S., Meno, C., Nonaka, S., Takada, S., Hatta, K., Wynshaw-boris, A., and Hamada, H. (2010) Planar polarization of node cells determines the rotational axis of node cilia. Nature Cell Biology, 12(2), 170-176.

He, X. (2008) Cilia put a brake on wnt signalling. Nature Cell Biology, 10(1), 11-13.

Hildebrandt, F., Attanasio, M., and Otto, E. (2009) Nephronophthisis: Disease Mechanisms of a Ciliopathy. Journal of the American Society of Nephrology, 20, 23-35.

Hildebrandt, F. and Zhou, W. (2007) Nephronophthisis-associated ciliopathies. Journal of the American Society of Nephrology : JASN, 18(6), 1855-71.

Hirokawa, N., Tanaka, Y., Okada, Y., and Takeda, S. (2006) Nodal flow and the generation of left-right asymmetry. Cell, 125(1), 33-45.

Hirst, R. A., Rutman, A., Williams, G., and O'Callaghan, C. (2010) Ciliated air-liquid cultures as an aid to diagnostic testing of Primary Ciliary Dyskinesia (PCD). Chest (in press).

Hollander, A. I. den, Koenekoop, R. K., Yzer, S., Lopez, I., Arends, M. L., Voesenek, K. E. J., Zonneveld, M. N., Strom, T. M., Meitinger, T., Brunner, H. G., Hoyng, C. B., Den Born, L. I. van, Rohrschneider, K., and Cremers, F. P. M. (2006) Mutations in the CEP290 (NPHP6) gene are a frequent cause of Leber congenital amaurosis. American journal of human genetics, 79(3), 556-61.

Hoyer-Fender, S. (2010) Centriole maturation and transformation to basal body. Seminars in Cell and Developmental Biology, 21(2), 142-147.

Huang, S., Hirota, Y., and Sawamoto, K. (2009) Various facets of vertebrate cilia: motility, signaling, and role in adult neurogenesis. Proc Jpn. Acad., 85, 324-336.

Huelsken, J. (2002) The Wnt signalling pathway. Journal of Cell Science, 115(21), 3977-3978.

IHGSC (2004) Finishing the euchromatic sequence of the human genome. Nature, 431, 931-945.

IHGSC (2001) Initial sequencing and analysis of the human genome. Nature, 409(6822), 860-921.

Jenkins, P. M., McEwen, D. P., and Martens, J. R. (2009) Olfactory cilia: linking sensory cilia function and human disease. Chemical senses, 34(5), 451-64.

Jiang, J. and Hui, C.-C. (2008) Hedgehog Signaling in Development and Cancer. Developmental Cell, 15, 801-812.

Khodjakov, A, Rieder, C. L., Sluder, G., Cassels, G., Sibon, O., and Wang, C.-L. (2002) De novo formation of centrosomes in vertebrate cells arrested during S phase. The Journal of Cell Biology, 158(7), 1171-1181.

Kiefer, J. C. (2010) Primer and interviews: Diverse connections between primary cilia and Hedgehog signaling. Developmental dynamics, 239(4), 1255-62.

Kim, J., Krishnaswami, S. R., and Gleeson, J. G. (2008) CEP290 interacts with the centriolar satellite component PCM-1 and is required for Rab8 localization to the primary cilium. Human molecular genetics, 17(23), 3796-805.

Kim, J. C., Badano, J. L., Sibold, S., Esmail, M. A., Hill, J., Hoskins, B. E., Leitch, C. C., Venner, K., Ansley, S. J., Ross, A. J., Leroux, M. R., Katsanis, N., and Beales, P. L. (2004) The Bardet-Biedl protein BBS4 targets cargo to the pericentriolar region and is required for microtubule anchoring and cell cycle progression. Nature genetics, 36(5), 462-70.

Kubo, A, Sasaki, H., Yuba-Kubo, A., Tsukita, S, and Shiina, N. (1999) Centriolar satellites: molecular characterization, ATP-dependent movement toward centrioles and possible involvement in ciliogenesis. The Journal of cell biology, 147(5), 969-80.

Kubo, A. and Tsukita, S. (2003) Non-membranous granular organelle consisting of PCM1-1: subcellular distribution and cell-cycle-dependent assembly/dissassembly. Journal of cell science, 116, 919-928.

La Terra, S., English, C. N., Hergert, P., McEwen, B. F., Sluder, G., and Khodjakov, A. (2005) The de novo centriole assembly pathway in HeLa cells: cell cycle progression and centriole assembly/maturation. The Journal of cell biology, 168(5), 713-22.

Lancaster, M. A., Louie, C. M., Silhavy, J. L., Sintasath, L., DeCambre, M., Nigam, S. K., Willert, K., and Gleeson, J. G. (2009) Impaired Wnt–β-catenin signaling disrupts adult renal homeostasis and leads to cystic kidney ciliopathy. Nature Medicine, 15(9), 1046-1054.

Lee, J. H. and Gleeson, J. G. (2010) The role of primary cilia in neuronal function. Neurobiology of Disease, 38(2), 167-172.

Lehman, A. M., Eydoux, P., Doherty, D, Glass, I. A., Chitayat, D., Chung, B. Y. H., Langlois, S., Yong, S. L., Lowry, R. B., Hildebrandt, F., and Trnka, P. (2010) Co-occurrence of Joubert syndrome and Jeune asphyxiating thoracic dystrophy. American journal of medical genetics. Part A, 152A(6), 1411-9.

Leigh, M. W., Pittman, J. E., Carson, J. L., Ferkol, T. W., Dell, S. D., Davis, S. D., Knowles, Michael R., and Zariwala, M. A. (2009) Clinical and genetic aspects of primary ciliary dyskinesia/Kartagener syndrome. Genetics in Medicine, 11(7), 473-487.

Lieschke, G. J. and Currie, P. D. (2010) Animal models of human disease: zebrafish swim into view. Nature Reviews Genetics, 8(May 2007), 353-367.

Lindemann, C. B. and Lesich, K. A. (2010) Flagellar and ciliary beating: the proven and the possible. Journal of cell science, 123(Pt 4), 519-28.

Lüders, J. and Stearns, T. (2007) Microtubule-organizing centres: a re-evaluation. Molecular Cell Biology, 8(February), 161-167.

Macca, M. and Franco, B. (2009) The molecular basis of oral-facial-digital syndrome, type 1. American journal of medical genetics. Part C, Seminars in medical genetics, 151C(4), 318-25.

Mahjoub, M. R., Trapp, M. L., and Quarmby, L. M. (2005) NIMA-Related Kinases Defective in Murine Models of Polycystic Kidney Diseases Localize to Primary Cilia and. Journal of the American Society of Nephrology, 16, 3485-3489.

Mans, D. A., Voest, E. E., and Giles, R. H. (2008) All along the watchtower: is the cilium a tumor suppressor organelle? Biochimica et Biophysica Acta, 1786(2), 114-125.

Marshall, W. F. (2008) The cell biological basis of ciliary disease. J. Cell Biol., 180(1), 17-21.

Marshall, W. F. and Nonaka, S. (2006) Cilia: tuning in to the cell's antenna. Current biology : CB, 16(15), R604-14.

Meraldi, P., Lukas, J., Fry, A. M., Bartek, J., and Nigg, E. A .(1999) Centrosome duplication in mammalian somatic cells requires E2F and Cdk2-cyclin A. Nature cell biology, 1(2), 88-93.

Mikule, K., Delaval, B., Kaldis, P., Jurcyzk, A., Hergert, P., and Doxsey, S. (2007) Loss of centrosome integrity induces p38-p53-p21-dependent G1-S arrest. Nat. Cell Biol., 9(2), 160-170.

Moser, J. J., Fritzler, M. J., Ou, Y., and Rattner, J. B. (2009) The PCM-basal body/primary cilium coalition. Seminars in Cell and Developmental Biology, 21(2), 1-8.

Mosimann, C., Hausmann, G., and Basler, K. (2009) β-Catenin hits chromatin: regulation of Wnt targer gene activation. Nature Reviews Moleciular Cell Biology, 10(April), 276-286.

Müller, U. (2009) Cadherins and Mechanotransduction by Hair Cells. Curr Opin Cell Biol, 20(5), 557-566.

Nachury, M. V., Loktev, A. V., Zhang, Q., Westlake, C. J., Peränen, J., Merdes, A., Slusarski, D. C., Scheller, R. H., Bazan, J. F., Sheffield, V. C., and Jackson, P. K. (2007) A core complex of BBS proteins cooperates with the GTPase Rab8 to promote ciliary membrane biogenesis. Cell, 129(6), 1201-13.

Nayak, G. D., Ratnayaka, H. S. K., Goodyear, R. J., and Richardson, G. P. (2007) Development of the hair bundle and mechanotransduction. The International journal of developmental biology, 51(6-7), 597-608.

Neumann, B., Walter, T., Hériché, J.-K., Bulkescher, J., Erfle, H., Conrad, C., Rogers, P., Poser, I., Held, M., Liebel, U., Cetin, C., Sieckmann, F., Pau, G., Kabbe, R., Wünsche, A., Satagopam, V., Schmitz, M. H. A., Chapuis, C., Gerlich, D. W., Schneider, R., Eils, R., Huber, W., Peters, J.-M., Hyman, A. A., Durbin, R., Pepperkok, R., and Ellenberg, J. (2010) Phenotypic profiling of the human genome by time-lapse microscopy reveals cell division genes. Nature, 464(7289), 721-7.

Nigg, E. A. (2007) Centrosome duplication: of rules and licenses. Trends Cell Biol., 17(5), 215-221.

Nigg, E. A. and Raff, J. W. (2009) Centrioles, centrosomes, and cilia in health and disease. Cell, 139(4), 663-78.

Ohta, T., Essner, R., Ryu, J.-H., Palazzo, R. E., Uetake, Y., and Kuriyama, R. (2002) Characterization of Cep135, a novel coiled-coil centrosomal protein involved in microtubule organization in mammalian cells. The Journal of cell biology, 156(1), 87-99.

Omran, H. (2010) NPHP proteins: gatekeepers of the ciliary compartment. The Journal of cell biology, 190(5), 715-717.

Onori, P., Franchitto, A., Mancinelli, R., Carpino, G., Alavaro, D., Francis, H., Alpini, G., and Gaudio, E. (2010) Polycystic liver diseases. Dig Liver Dis, 42(4), 261-271.

O'Callaghan, C., Chilvers, M., Hogg, C., Bush, A., and Lucas, J. (2007) Diagnosing primary ciliary dyskinesia. Thorax, 62(8), 656-7.

Pan, J. and Snell, W. (2007) The primary cilium: keeper of the key to cell division. Cell, 129(7), 1255-7.

Parker, J. D. K., Hilton, L. K., Diener, D. R., Rasi, M. Q., Mahjoub, M. R., Rosenbaum, J. L., and Quarmby, L. M. (2010) Centrioles are freed from cilia by severing prior to mitosis. Cytoskeleton, 67(7), 425-30.

Pazour, G. J., Dickert, B. L., Vucica, Y., Seeley, E. S., Rosenbaum, J. L., Witman, G. B., and Cole, D. G. (2000) Chlamydomonas IFT88 and its mouse homologue, polycystic kidney disease gene tg737, are required for assembly of cilia and flagella. J. Cell. Biol, 151(3), 709-718.

Pedersen, L. B., Veland, I. R., Schrøder, J. M., and Christensen, S. T. (2008) Assembly of primary cilia. Developmental dynamics, 237(8), 1993-2006.

Piel, M., Meyer, P., Khodjakov, A., Rieder, C. L., and Bornens, M. (2000) The respective contributions of the mother and daughter centrioles to centrosome activity and behavior in vertebrate cells. The Journal of cell biology, 149(2), 317-30.

Plotnikova, O. V., Golemis, E. A., and Pugacheva, E. N. (2008) Cell cycle-dependent ciliogenesis and cancer. Cancer research, 68(7), 2058-61.

Prattichizzo, C., Macca, M., Novelli, V., Giorgio, G., Barra, A., and Franco, B. (2008) Mutational spectrum of the oral-facial-digital type I syndrome: a study on a large collection of patients. Human mutation, 29(10), 1237-46.

Prosser, S. L., Straatman, K. R., and Fry, A. M. (2009) Molecular Dissection of the Centrosome Overduplication Pathway in S-phase-arrested Cells. Molecular and Cellular Biology, 29(7), 1760-1773.

Pugacheva, E. N., Jablonski, S. A., Hartman, T. R., Henske, E. P., and Golemis, E. A. (2007) HEF1-dependent Aurora A activation induces disassembly of the primary cilium. Cell, 129(7), 1351-63.

Quarmby, L. M. and Parker, J. D. K. (2005) Cilia and the cell cycle? Journal of Cell Biology, 169(5), 707-710.

Rakkolainen, A., Ala-Mello, S., Kristo, P., Orpana, A., and Jarvela, I. (2002) Four novel mutations in the OFD1 (Cxorf5) gene in Finnish patients with oral-facial-digital syndrome 1. Journal of Medical Genetics, 39(4), 292-296.

Ramamurthy, V. and Cayouette, M. (2009) Development and disease of the photoreceptor cilium. Clinical Genetics, 76(2), 137-145.

Rida, P. C. G. and Chen, P. (2009) Line up and listen: Planar cell polarity regulation in the mammalian inner ear. Seminars in Cell and Developmental Biology, 20(8), 1-8.

Robert, A., Margall-Ducos, G., Guidotti, J.-E., Brégerie, O., Celati, C., Bréchot, C., and Desdouets, C. (2007) The intraflagellar transport component IFT88/polaris is a centrosomal protein regulating G1-S transition in non-ciliated cells. Journal of Cell Science, 120, 628-637.

Romio, L., Wright, V., Price, K., Winyard, P. J. D., Donnai, D., Porteous, M. E., Franco, B., Giorgio, G., Malcolm, S., Woolf, A. S., and Feather, S. A. (2003) OFD1, the Gene Mutated in Oral-Facial-Digital Syndrome Type 1, Is Expressed in the Metanephros and in Human Embryonic Renal Mesenchymal Cells. Journal of the American Society of Nephrology, 14(3), 680-689.

Romio, L., Fry, A. M., Winyard, P. J. D., Malcolm, S., Woolf, A. S., and Feather, S. A. (2004) OFD1 is a centrosomal/basal body protein expressed during mesenchymal-epithelial transition in human nephrogenesis. Journal of the American Society of Nephrology : JASN, 15(10), 2556-68.

Ross, A. J., May-Simera, H., Eichers, E. R., Kai, M., Hill, J., Jagger, D. J., Leitch, C. C., Chapple, J. P., Munro, P. M., Fisher, S., Tan, P. L., Phillips, H. M., Leroux, M. R., Henderson, D. J., Murdoch, J. N., Copp, A. J., Eliot, M.-M., Lupski, J. R., Kemp, D. T., Dollfus, H., Tada, M., Katsanis, N., Forge, A., and Beales, P. L. (2005) Disruption of Bardet-Biedl syndrome ciliary proteins perturbs planar cell polarity in vertebrates. Nature genetics, 37(10), 1135-40.

Roy, S. (2009) The motile cilium in development and disease: emerging new insights. BioEssays, 31(7), 694-9.

Saal, S., Faivre, L., Aral, B., Gigot, N, Toutain, A., Van Maldergem, L., Destree, A., Maystadt, I., Cosyns, J.-P., Jouk, P.-S., Loeys, B., Chauveau, D., Bieth, E., Layet, V., Mathieu, M., Lespinasse, J., Teebi, A., Franco, B., Gautier, E., Binquet, C., Masurel-Paulet, A, Mousson, C., Gouyon, J.-B., Huet, F., and Thauvin-Robinet, C. (2009) Renal insufficiency, a frequent complication with age in oral-facial-digital syndrome type I. Clinical genetics, 77(3), 258-65.

Salomon, R., Saunier, S., and Niaudet, P. (2009) Nephronophthisis. Pediatric nephrology (Berlin, Germany), 24(12), 2333-44.

Satir, P. (2008) Primary cilia: integral to development and disease. Developmental dynamics: an official publication of the American Association of Anatomists, 237(8), 1953-4.

Satir, P. and Christensen, S. T. (2008) Structure and function of mammalian cilia. Histochemistry and cell biology, 129(6), 687-93.

Satir, P. and Christensen, S. T. (2007) Overview of structure and function of mammalian cilia. Annual review of physiology, 69, 377-400.

Satir, P., Pedersen, L. B., and Christensen, S. T. (2010) The primary cilium at a glance. Journal of cell science, 123(Pt 4), 499-503.

Schatten, H. (2008) The mammalian centrosome and its functional significance. Histochemistry and Cell Biology, 129, 667-686.

Schrøder, J. M., Schneider, L., Christensen, S. T., and Pedersen, L. B. (2007) EB1 is required for primary cilia assembly in fibroblasts. Current biology : CB, 17(13), 1134-9.

Schwander, M., Kachar, B., and Müller, U. (2010) Review series: The cell biology of hearing. The Journal of cell biology, 190(1), 9-20.

Sedjaï, F., Acquaviva, C., Chevrier, V., Chauvin, J.-P., Coppin, E., Aouane, A., Coulier, F., Tolun, A., Pierres, M., Birnbaum, D., and Rosnet, O. (2010) Control of ciliogenesis by FOR20, a novel centrosome and pericentriolar satellite protein. Journal of cell science, 123(Pt 14), 2391-401.

Seeley, E. S. and Nachury, M. V. (2010) The perennial organelle: assembly and disassembly of the primary cilium. Journal of cell science, 123(Pt 4), 511-8.

Silverman, M. A. and Leroux, M. R. (2009) Intraflagellar transport and the generation of dynamic, structurally and functionally diverse cilia. Trends in Cell Biology, 1-11.

Simms, R. J., Eley, L., and Sayer, J. A. (2009) Nephronophthisis. European Journal of Human Genetics, 17, 406-416.

Simons, M., Gloy, J., Ganner, A., Bullerkotte, A., Bashkurov, M., Kro, C., Schermer, B., Benzing, T., Cabello, O. A., Jenny, A., Mlodzik, M., Polok, B., Driever, W., Obara, T., and Walz, G. (2005) Inversin, the gene product mutated in nephronophthisis type II, functions as a molecular switch between Wnt signaling pathways. Nature Genetics, 37(5), 537-543.

Simons, M. and Mlodzik, M. (2008) Planar Cell Polarity Signaling: From Fly Development to Human Disease. Annual Review of Genetics, 42(August), 1-24.

Singla, V., Romaguera-Ros, M., Garcia-Verdugo, J. M., and Reiter, J. F. (2010) Ofd1, a human disease gene, regulates the length and distal structure of centrioles. Developmental cell, 18(3), 410-24.

Spektor, A., Tsang, W. Y., Khoo, D., and Dynlacht, B. D. (2007) Cep97 and CP110 suppress a cilia assembly program. Cell, 130(4), 678-90.

Stannard, W. A., Chilvers, M. A., Rutman, A. R., Williams, C. D., and O'Callaghan, C. (2010) Diagnostic testing of patients suspected of primary ciliary dyskinesia. American journal of respiratory and critical care medicine, 181(4), 307-14.

Temiyasathit, S. and Jacobs, C. R. (2010) Osteocyte primary cilium and its role in bone mechanotransduction. Annals of the New York Academy of Sciences, 1192(1), 422-8.

Thauvin-Robinet, C., Cossée, M., Cormier-Daire, V., Van Maldergem, L., Toutain, A., Alembik, Y., Bieth, E., Layet, V., Parent, P., David, A., Goldenberg, A., Mortier, G., Héron, D., Sagot, P., Bouvier, A. M., Huet, F, Cusin, V., Donzel, A., Devys, D., Teyssier, J. R., and Faivre, L. (2006) Clinical, molecular, and genotype-phenotype correlation studies from 25 cases of oral-facial-digital syndrome type 1: a French and Belgian collaborative study. Journal of medical genetics, 43(1), 54-61.

Thauvin-Robinet, C., Callier, P., Franco, B., Zuffardi, O., Payet, M., Aral, B., Gigot, N., Donzel, A., Mosca-Boidron, A.-L., Masurel-Paulet, A., Huet, F., Teyssier, J.-R., Mugneret, F., and Faivre, L. (2009) Search for genomic imbalances in a cohort of 20 patients with oral-facial-digital syndromes negative for mutations and large rearrangements in the OFD1 gene. American journal of medical genetics. Part A, 149A(8), 1846-9.

Thauvin-Robinet, C., Franco, B., Saugier-Veber, P., and Aral, B. (2008) Genomic Deletions of OFD1 Account for 23% of Oral-facial-digital Type 1 Syndrome After Negative DNA Sequencing. Human Mutation, 29(May), 320-329.

Tobin, J. L. and Beales, P. L. (2009) The nonmotile ciliopathies. Genetics in medicine, 11(6), 386-402.

Toriello, H. V. (2009a) Are the oral-facial-digital syndromes ciliopathies? American journal of medical genetics. Part A, 149A(5), 1089-95.

Toriello, H. V. (2009b) Cilia and the Ciliopathies: An Introduction. American Journal of Medical Genetics, 151C, 261 - 262.

Tsang, W. Y., Bossard, C., Khanna, H., Peränen, J., Swaroop, A., Malhotra, V., and Dynlacht, B. D. (2008) CP110 suppresses primary cilia formation through its interaction with CEP290, a protein deficient in human ciliary disease. Developmental cell, 15(2), 187-97.

Urbani, L. and Stearns, T. (1999) The centrosome. Current Biology, 9(9), 315-317.

Varjosalo, M. and Taipale, J. (2008) Hedgehog: functions and mechanisms. Genes & Development, 22, 2454-2472.

Veland, I. R., Awan, A., Pedersen, L. B., Yoder, Bradley K, and Christensen, S. T. (2009) Primary cilia and signaling pathways in mammalian development, health and disease. Nephron. Physiology, 111(3), p39-53.

Vlacque, O. E., Cevik, S., and Kaplan, O. I. (2008) Intraflagellar transport: from molecular characterisation to mechanism. Frontiers in Bioscience, 13, 2633-2652.

Vladar, E. K. and Stearns, T. (2007) Molecular characterization of centriole assembly in ciliated epithelial cells. J. Cell Biol, 178(1), 31-42.

Wong, S. Y. and Reiter, J. F. (2008) The Primary Cilium: at the crossroads of mammalian hedgehog signaling. Curr Top Dev Biol, 85(March), 225-260.

Wright, A. F., Chakarova, C. F., Abd El-Aziz, M. M., and Bhattacharya, S. S. (2010) Photoreceptor degeneration: genetic and mechanistic dissection of a complex trait. Nature reviews. Genetics, 11(4), 273-284.

Wu, J. and Mlodzik, M. (2009) A quest for the mechanism regulating global planar cell polarity of tissues. Trends in Cell Biology, 1-11.

Yoder, B. K. (2007) Role of primary cilia in the pathogenesis of polycystic kidney disease. J. Am. Soc. Nephrol., 18, 1381-1388.

Zariwala, M. A., Knowles, M. R., and Omran, H. (2007) Genetic defects in ciliary structure and function. Annual review of physiology, 69, 423-50.

Zhang, Q., Taulman, P. D., and Yoder, B. K. (2004) Cystic kidney diseases: all roads lead to the cilium. Physiology, 19, 225-30.

Zhou, J. (2009) Polycystins and Primary Cilia: Primers for Cell Cycle Progression. Annual Review of Physiology, 71, 83-113.

Zyss, D. and Gergely, F. (2009) Centrosome function in cancer: guilty or innocent? Trends in Cell Biology, 19(7), 334-46.